UNIVERSITA' DEGLI STUDI DI PADOVA

SEDE AMMINISTRATIVA: UNIVERSITÀ DEGLI STUDI DI PADOVA
DIPARTIMENTO DI PEDIATRIA

SCUOLA DI DOTTORATO DI RICERCA IN MEDICINA DELLO SVILUPPO E SCIENZE DELLA PROGRAMMAZIONE – INDIRIZZO MALATTIE RARE – XX CICLO

TESI DI DOTTORATO

Genetic bases and experimental models for the study of inherited metabolic diseases

Direttore della Scuola : Ch.mo Prof. Giuseppe Basso
Supervisore : Dr. Leonardo Salviati

Dottoranda : Eva Trevisson

ANNO ACCADEMICO 2007-2008

CONTENTS

ABBREVIATIONS

ASA = argininosuccinic acid
ASL = argininosuccinate lyase
ASS = argininosuccinate synthetase
bp = base pair
CNS= Central nervous system
CoQ= Coenzyme Q10 or ubiquinone
COX = Cytochrome *c* oxidase
CPS = carbamoyl phosphate synthetase I
CS = Citrate synthase
CSF = Cerebrospinal fluid
DIC = Differential interference contrast microscopy
$DMQH_2$ = 5-demethoxyubiquinol
ESTs = expressed sequence tags
ETS = Avian erythroblastosis virus homolog
4-HB = 4-hydroxybenzoic acid
$FADH_2$ = Flavin adenine dinucleotide, reduced form
FCS = fetal calf serum
GUS = β-glucuronidase
HHB = polyprenyl-4-hydroxybenzoic acid
Hif-1 = Hypoxia inducible factor 1
HSF = heat shock factor
IEM = Inborn errors of metabolism
IMS = Intermembrane space
IPTG = isopropyl-β-D-thiogalactopyranoside
kb = kilobase
kDal = kilo Dalton
MIM = Mitochondrial inner membrane
MOM = Mitochondrial outer membrane
MRC = Mitochondrial respiratory chain
mtDNA = Mitochondrial deoxyribonucleic acid
nDNA = Nuclear deoxyribonucleic acid
NADH = β-Nicotinamide adenine dinucleotide, reduced form
NO = nitroxide
NOS = nitric oxide synthetase
NRF1 = nuclear respiratory factor 1
NS = nephrotic syndrome
nt = nucleotide
OCT = ornithine transcarbamylase
PNS = Peripheral nervous system
RACE = rapid amplification of cDNA ends
RNAi = RNA interference
RQ-PCR = real-time polymerase chain reaction
RRFs = Ragged-red-fibers
SDH= Succinate dehydrogenase
SP1 = Specific protein 1

SRE = sterol regulatory element
STAT = signal transducers and activators of transcription
UCDs = urea cycle defects

SUMMARY

Inherited metabolic diseases are genetic disorders caused by the alteration of a specific metabolic reaction, and account for an important proportion of illness in pediatric patients.

We focused on the study of the genetic bases of two main types of metabolic disorders, mitochondrial diseases and urea cycle defects.

Mitochondrial disorders represent a heterogeneous group of disease due to defects in the mitochondrial respiratory chain (MRC), which affect tissues with high energetic requirements and whose etiology often remains elusive. In this work, we report the characterization of novel genes that are potentially involved in mitochondrial respiratory chain defects: we identified three novel COX-assembly genes required for Cytochrome *c* Oxidase (COX) biogenesis (*hCOX16*, *hCOX18* and *hCOX19*), the fourth complex of MRC.

hCOX16, hCOX18 and *hCOX19* encode ancillary proteins that are not part of COX holoenzyme, but are necessary for its maturation and for the synthesis and transport of the prosthetic groups and metal cofactors. Particularly, we demonstrated that silencing of *COX16* in HeLa cells causes a decrease in COX activity and a reduction in the levels of COX II subunits. *COX19*, as the previously identified *COX17*, is involved in the transfer of copper ions from the cytosol to the mitochondrial intermembrane space. These genes represent new candidates to be screened in patients with isolated COX deficiencies without mutations in other known COX-assembly genes. In fact, except for few cases due to mitochondrial DNA mutations, most of these forms are transmitted as recessive traits, underlying a defect in a nuclear gene.

In order to study the pathogenesis of isolated COX deficiency, one of the most common MRC defects in infancy, we modeled this disorder in *Caenorhabditis elegans* by knocking-down the expression of *COX19* and *COX17*. We showed that this multicellular experimental model present the cardinal signs of COX deficiency, including lactic acidosis and a COX-dependent decrease in respiration; moreover, in the case of *COX17*, the phenotype can be rescued with copper. These findings, together with previous reports of COX deficiencies complementation with copper,

open a new possible therapeutical approach for this group of disorders, which are still without an effective treatment, and indicate that *C.elegans* represents a good organism for the study of their pathogenesis and for drug screening.

We then focused on primary CoQ deficiency, a mitochondrial disorder due to defects in one of the genes required for the biosynthesis of this electron carrier, which represents the only mitochondrial disease that can be effectively treated. We studied the genetic bases of this disorder in a family, who presents with a severe encephalopathy and a nephrotic syndrome and found the first molecular defect responsible for this disease, a mutation in the *COQ2* gene, required for the second step of ubiquinone biosynthesis. We characterized this gene and the biochemical phenotype of patients' fibroblasts, showing that pathogenesis involves both a defect in bioenergetics and in pyrimidine metabolism. Furthermore, in order to prove the pathogenetic role of the novel homozygous mutation found in the family, we modeled it in *Saccharomyces cerevisiae* and performed a functional complementation, showing that this system is sufficiently sensitive to study the pathogenicity of *COQ2* mutations.

Since CoQ biosynthetic pathway is not fully understood in humans and given its implications in human diseases, we characterized two other genes required for Coenzyme Q10 (CoQ) biosynthesis (*hCOQ4* and *hCOQ5*). The polypeptides encoded by these two genes show a conserved role compared to *Saccharomyces cerevisiae* and could be involved in other forms of primary CoQ deficiency. Notably, finding the molecular defect of this disorder has an important prognostic significance, allowing the distinction between primary forms, which respond dramatically to ubiquinone supplementation, and secondary ones, whose prognosis is not favorable.

In the last section of this work, we studied a cohort of patients affected by argininosuccinic aciduria, an urea cycle defect caused by mutation in argininosuccinate lyase gene. We performed a mutational screening using a protocol that relies exclusively on genomic DNA and identified mutations in all kindreds analysed. Most of mutations were novel and we developed distinct systems to prove their pathogenicity. For the two splice site mutations we used a hybrid-minigene assay, confirming that they effectively cause an aberrant splicing with exon skipping. For the missense mutations, we performed molecular modeling to predict their

consequences on the enzyme structure, and measured ASL activity in patients' erythrocytes.

In order to confirm the pathogenesis of the missense mutations, we developed a functional complementation assay using a mutant *S.cerevisiae* strain with a deletion in the yeast homologue of the *ASL* gene, which is auxotrophic for arginine. This strain was transformed with constructs carrying one of the missense mutations and growth in the absence of arginine was used as a marker of functional complementation. We found that the mutations can be divided into three classes based on their different growth. We also performed an intragenic complementation assay, confirming that Q286R is a high-frequenting complementing allele and demonstrating a new high activity complementing allele, R182Q. We establish some genotype-phenotype correlations.

Finally, we characterized the molecular defect of a patient with a hypomyelinating disorder, Pelizaeus-Merzbacher disease. We found a homozygous deletion in the *GJA12* gene, encoding a protein which is highly expressed in oligodendrocytes.

SOMMARIO

Le Malattie Metaboliche Ereditarie sono disordini genetici provocati da alterazioni in una specifica reazione metabolica e complessivamente rappresentano un'importante causa di malattia in età pediatrica.

Ci siamo focalizzati sullo studio delle basi genetiche di due principali tipi di disordini metabolici, le malattie mitocondriali e i difetti del ciclo dell'urea.

Le malattie mitocondriali rappresentano un gruppo eterogeneo di disordini dovuti a difetti nella catena respiratoria mitocondriale (MRC), che colpiscono tessuti ad alta richiesta energetica e la cui eziologia è spesso ignota. In questo lavoro, abbiamo caratterizzato nuovi geni potenzialmente implicati nei difetti della MRC, in particolare abbiamo identificato tre nuovi "COX-assembly genes" che risultano indispensabili per la biogenesi della citocromo *c* ossidasi (COX), il quarto complesso della MRC.

hCOX16, hCOX18 and *hCOX19* codificano proteine che non fanno parte dell'oloenzima COX, ma sono necessarie per la sua maturazione e per la sintesi e il trasporto dei gruppi prostetici e dei cofattori metallici.

In particolare, abbiamo dimostrato che il silenziamento genico di *hCOX16* in cellule HeLa causa una riduzione sia dell'attività della citocromo *c* ossidasi, sia dei livelli della subunità COX II. *hCOX19* invece, come il gene precedentemente identificato *COX17*, è coinvolto nel trasferimento del rame dal citosol allo spazio intermembrana, un cofattore metallico che partecipa alla formazione dei centri redox della COX ed è indispensabile per la sua funzione. Questi geni rappresentano nuovi candidati da analizzare in pazienti .con deficit isolato di COX senza mutazioni in altri COX-assembly genes conosciuti. Infatti, ad eccezione di qualche raro caso descritto di mutazioni del DNA mitocondriale, la maggior parte di queste forme sono trasmesse come tratti autosomici recessivi, indicando un difetto in un gene nucleare.

Allo scopo di studiare la patogenesi del deficit isolato di COX, uno dei difetti più comuni della MRC nella prima infanzia, abbiamo utilizzato come modello sperimentale *Caenorhabditis elegans*. Il silenziamento di *COX17* e *COX19* nel nematode conferisce un fenotipo caratterizzato dai segni principali del deficit di COX, tra cui l'acidosi lattica e una riduzione COX-dipendente della respirazione

mitocondriale; inoltre, nel caso di *COX17*, il fenotipo può essere corretto con la supplementazione di rame. Questi risultati, assieme alla precedente descrizione di complementazione di deficit di COX con il rame, aprono una nuova prospettiva terapeutica per questo gruppo di disordini che sono ancora senza un trattamento efficace, e indicano che *C.elegans* rappresenta un buon organismo modello per lo studio della loro patogenesi e per lo screening di farmaci.

Ci siamo poi focalizzati sulla deficienza primitiva di Coenzima Q10 (o ubiquinone), un altro disordine mitocondriale dovuto a difetti in uno dei geni richiesti per la biosintesi di questo trasportatore di elettroni, che rappresenta attualmente l'unica patologia mitocondriale che può essere efficacemente trattata.

Abbiamo studiato le basi genetiche di questo disordine in una famiglia affetta da severa encefalopatia e sindrome nefrosica e trovato il primo difetto molecolare responsabile di questa patologia, una mutazione nel gene *COQ2*, richiesto per il secondo step della biosintesi dell'ubiquinone. Abbiamo caratterizzato questo gene ed il fenotipo biochimico dei fibroblasti dei pazienti, dimostrando che la patogenesi coinvolge non solo un difetto bioenergetico, ma anche nel metabolismo delle pirimidine. Inoltre, per dimostrare il ruolo patogenetico della nuova mutazione omozigote riscontrata nella famiglia, abbiamo messo a punto un sistema di complementazione funzionale in *Saccharomyces cerevisiae* e dimostrato che questo sistema è sufficientemente sensibile per studiare la patogenicità delle mutazioni in *COQ2*.

Poichè la via metabolica per la biosintesi del coenzima Q10 è ancora scarsamente caratterizzata nell'uomo, e date le sue implicazioni in patologia umana, abbiamo caratterizzato gli omologhe umani di altri due geni che nel lievito sono indispensabili per la sintesi di questo trasportatore elettronico (*hCOQ4* and *hCOQ5*). I prodotti proteici codificati da questi geni hanno una funzione conservata nell'evoluzione, dato che sono in grado di complementare ceppi mutanti di lievito con delezioni dei corrispondenti omologhi. Rappresentano pertanto geni candidati da analizzare nel caso di deficit primario di Coenzima Q10. Individuare il difetto molecolare in questo disordine, oltre a definire la diagnosi eziologia e consentire un'adeguata consulenza genetica, ha un importante risvolto prognostico, in quanto consente di differenziare le forme primarie che rispondono drammaticamente alla somministrazione di ubiquinone, e quelle secondarie, dovute a difetti in geni non correlati alla biosintesi del coenzima Q10, la cui prognosi non è così favorevole.

Nell'ultima parte di questo lavoro, abbiamo studiato una coorte di pazienti affetti da aciduria argininosuccinica, un difetto del ciclo dell'urea dovuto a mutazioni nel gene che codifica l'argininosuccinato liasi. Abbiamo condotto l'analisi molecolare utilizzando un protocollo basato esclusivamente sul DNA genomico ed identificato mutazioni in tutti i pazienti. Abbiamo quindi sviluppato distinti sistemi per provare la loro patogenicità. Per le mutazioni di splicing abbiamo utilizzato un sistema basato su un minigene ibrido e confermato che le nuove varianti di sequenza causano effettivamente uno splicing aberrante con exon skipping. .Le mutazioni missenso sono state validate con vari sistemi: per predire le conseguenze sulla struttura dell'enzima abbiamo valutato il grado di conservazione dei residui mutati ed eseguito il modeling molecolare; inoltre abbiamo misurato l'attività enzimatica negli eritrociti dei pazienti. Per confermare la patogenicità delle mutazioni missenso, abbiamo sviluppato un saggio di complementazione funzionale, utilizzando un ceppo mutante di *S.cerevisiae* con una delezione nel gene di lievito omologo all'*ASL* umano, che è auxotrofico per l'arginina. Questo ceppo è stato trasformato con costrutti recanti una delle mutazioni missenso e la crescita in assenza di arginina è stata utilizzata come marker di complementazione funzionale. In base alla diversa crescita dei trasformanti, le mutazioni possono essere distinte in tre classi. Abbiamo eseguito un saggio di complementazione intragenica, confermando che Q286R è un allele ad alta frequenza di complementazione e dimostrando che R182Q è un nuovo allele ad alta attività di complementazione. Abbiamo inoltre stabilito alcune correlazioni genotipo-fenotipo.

Infine, abbiamo caratterizzato il difetto molecolare di un paziente affetto da un disordine ipomielinizzante, la malattia di Pelizaeus-Merzbacher, riportando una delezione omozigote nel gene *GJA12*, che codifica una proteina altamente espressa negli oligodendrociti.

SECTION I

INTRODUCTION

Inborn errors of metabolism (IEM) are genetic disorders that are caused by alteration of a specific biochemical reaction. Although individually rare, IEM collectively account for a significant proportion of illness, particularly in children; they can be pleiotropic and can involve virtually any organ or system.

The history of human biochemical genetics began at the turn of the twentieth century, when Sir Archibald Garrod initiated the studies on alkaptonuria (Garrod et al 1907) and developed the concept that certain diseases of lifelong duration arise because an enzyme governing a single metabolic step is reduced in activity or completely missing.

The relation between gene and enzyme attained clear definition in the “one gene-one enzyme” theory, first stated by Beadle in 1945 (Beadle et al 1950). This concept had immediate explanatory potential for the IEM described by Garrod: it appeared that inherited diseases were produced by loss-of-function mutations in genes encoding enzymes. However, it was not until 1948 that the Gibson demonstrated the first enzyme defect in a human genetic disease: the deficiency of a NADH-dependent enzyme required for methemoglobin reduction in recessive methemoglobinemia (Gibson 1948). It became soon clear that IEM were caused by mutant genes that produce abnormal proteins whose functional activity were altered.

Recombinant DNA revolution has transformed the study of human genetics, allowing identification of many human disease genes through linkage analysis and positional cloning (McCurdy 1971, Collins 1990); moreover, the molecular methods have also made possible the discovery of novel disease mechanisms, such as uniparental disomy.

Although IEM have traditionally been regarded as Mendelian traits caused by single-gene mutations, it has now become clear that environment interactions and genetic modifiers account for their complex pathogenesis and their phenotypic variability.

Reductive strategies, focusing on specific genes or proteins, resulted in much of the remarkable progress in genetic research in the last two decades of the nineteenth century; yet, the current challenge is to understand how defects on one or few genes disrupt normal development and physiological homeostasis to produce genetic diseases. The study of the pathogenesis of genetic disorders requires an integrative approach and is

likely to depend heavily on the use of animal models. In fact modeling a human genetic disease in an experimental model is extremely valuable for a variety of uses: first, it can facilitate the identification of genes responsible for monogenic and multifactorial disorders, and for these latter it can help to distinguish among genetic and environmental contributions to complex traits; a second use is to elucidate the pathogenesis of specific disorders, providing an excellent alternative experimental system in the case low disease frequency and genetic heterogeneity; finally, development of treatments for genetic diseases must rely on the use of animal models.

1. MITOCHONDRIA and RESPIRATORY CHAIN

Mitochondria are intracellular organelles ubiquitous in eukaryotes and essential for survival. Their primary function is to support aerobic respiration and to provide energy substrates (such as ATP) for intracellular metabolic pathways. Beyond their critical function in cellular bioenergetics, mitochondria have also been shown to play a pivotal role in the life cycle of the cell, being key players in signaling, particularly in programmed cell death (Bernardi et al 1999), in calcium homeostasis (Rizzuto et al 1999) and thermogenesis (Echtay et al 2002). They host several metabolic pathways, including the Krebs cycle, fatty acids β-oxidation, lipid and cholesterol synthesis, and oxidative phosphorylation. The final result is ATP generation through a series of biochemical and biophysical (chemiosmotic) events.

Mitochondrial respiratory chain (MRC) is composed of four enzymatic multisubunit complexes (I to IV, fig 1) and two electron transporters, cytochrome *c* and ubiquinone (coenzyme Q10 or CoQ).

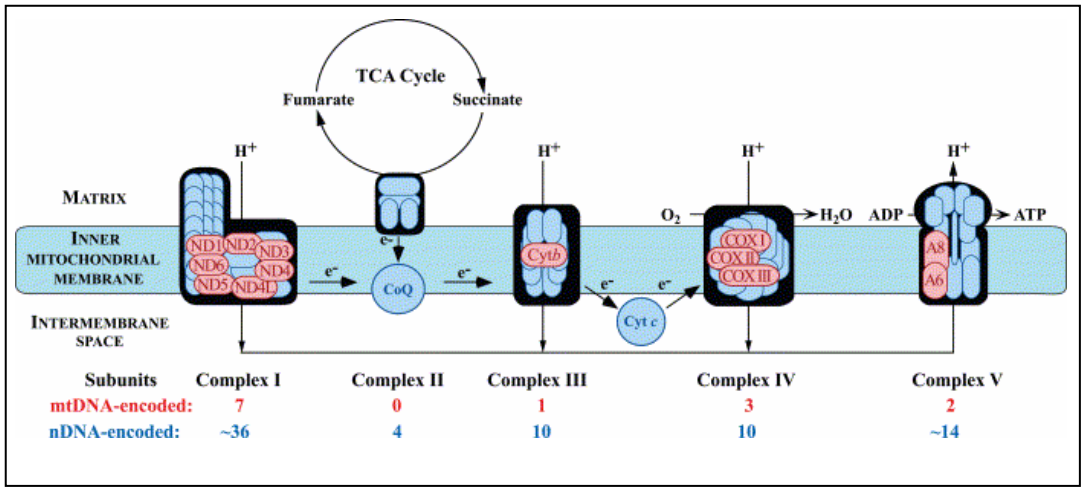

Fig. 1 Schematic representation of the mitochondrial respiratory chain, with the four complexes and ATPase embedded in the mitochondrial inner membrane. The mtDNA and nDNA-encoded subunits are indicated in red and blue, respectively (adapted from DiMauro, 2004).

Acetyl-Coenzyme A derived from pyruvate or fatty acids oxidation is oxidized through the Krebs cycle producing high-energy electrons (in the form of NADH and $FADH_2$). The reducing equivalents are transported through the four complexes and reoxidized to form water; the resulting energy is used to generate an electrochemical gradient by

pumping protons across the mitochondrial inner membrane (MIM). Finally, ATP synthase (complex V) acts like a rotary engine by synthesizing ATP as protons flow back into the mitochondrial matrix (MM) (Yoshida et al, 2001).

Mitochondria are composed of hundreds of different proteins. What makes these organelles unique and fascinating it‘s the fact that they are relics of independent bacteria-like intruders that took permanent residence in our cells over a billion years ago (Searcy 2003). As such, they are double-membrane and their proteome depends on two different genomes: mitochondrial DNA (mtDNA) encodes only thirteen subunits of the MRC and the RNA genes (22 tRNAs and 2 rRNAs) necessary for the organelle expression machinery; yet, the great majority of proteins required for mitochondrial function are encoded by the nuclear genome (nDNA), synthesized in the cytosol and imported into the organelles through a complex system that is highly conserved across species (Milenkovic et al, 2007). nDNA-encoded proteins are necessary for most mitochondria functions, such as mtDNA replication and maintenance, its transcription and translation machineries, protein import system and correct assembly of MRC holoenzymes. Therefore, an adequate cross-talk between both genomes is essential for proper mitochondrial function (Garesse et al, 2001).

1.1 Mitochondrial Diseases

Although mitochondrial diseases are defined restrictively as disorders due to defects in MRC (DiMauro 2004a), deficiencies in almost all mitochondrial biochemical pathways, transport systems and other mitochondrial proteins, not involved in bioenergetics, have been reported (Munnich and Rustin, 2001). They are relatively common diseases, as several epidemiologic studies from Northern Europe have documented (Chinnery et al, 2001).

Their clinical presentation is extremely heterogeneous because of the ubiquitous nature of mitochondria and the dual genetic control of the respiratory chain: mitochondrial disorders can be multisystemic, or confined to a single tissue.

1.1.1 Genetic aspects of Mitochondrial Respiratory chain defects

Although some acquired forms of primitive mitochondrial disorders have been reported (Dalakas et al 1990), most are genetic; they can be sporadic or transmitted by mendelian

or maternal inheritance. The former are usually inherited as autosomal or X-linked recessive traits, being caused by mutations in nuclear genes; they tend to present earlier in life and affect more family members with a homogeneous phenotype. The protein products encoded by the affected nuclear genes can be grouped into three categories: structural components of the respiratory chain, factors influencing the structural integrity or the copy number of mitochondrial DNA (intergenomic signaling), and proteins which control the formation, assembly and turnover of the respiratory complexes (Zeviani et al, 1999).

By contrast, the latter have usually a later onset and are due to mutations in mtDNA; they have a highly heterogenic clinical picture and their presentation vary within members of the same family. Since all zygotic mitochondria derive from the oocyte (Schon 2000), these forms are strictly maternal inherited. Mitochondrial inheritance displays another unusual feature, due to the fact that cells contain many mtDNA copies: *heteroplasmy*, which refers to the coexistence of a mixed population of normal and mutant mitochondrial genomes in tissues form patients. A corollary of heteroplasmy is the *threshold effect*: phenotypic expression of the disease will vary from tissue to tissue according to the relative dependence of each organ on oxidative metabolism and will rely on the relative proportions of mutant and wild type mtDNA. Another important feature of mitochondrial genetics is *mitotic segregation*: mutational load can change from one generation to the next (due to the random distribution of mitochondria during cell division) and, with time, it can either surpass or fall below the pathogenetic threshold, explaining the high variable clinical course of these diseases. Mitotic segregation has also another important consequence: unlike nuclear genetic mosaicism, which must arise post-zigotically, mitochondrial heteroplasmy can be directly transmitted from the mother to the child through a heteroplasmic oocyte. In such case, the proportion of abnormal mtDNA molecules can vary remarkable in different generations. Phenotype-genotype correlations are very hard to establish.

1.1.2 Clinical picture and diagnosis

Genetic defects of oxidative phosphorylation account for a variety of clinical symptoms, in both childhood and adulthood. Since most organs and tissues depend mainly on aerobic metabolism, respiratory chain deficiency can theoretically give rise to any symptom, in any organ or tissue and at any age. Yet, tissues with high energetic

requirements, such as muscle, myocardial and CNS, are usually the most severely affected (Munnich and Rustin, 2001). Each of these organs can be singly affected (isolated myopathies, cardiomyopathies, encephalopathies) or as part of combined syndromes (such as cardioencephalomyopathies). The complexity of biochemical and genetic features of MRC explains the high variability and heterogeneity of the clinical pictures of these diseases. Nevertheless, there are some "typical" symptoms that can suggest the diagnosis (table 1). Diagnosis of a MRC deficiency is difficult initially when only one symptom is present, and easier when additional, seemingly unrelated, symptoms are observed.

Table 1. Phenotypic expression of mitochondrial diseases (adapted from Zeviani and Di Donato 2004).

CNS	Epilepsy and seizures Ataxia Myoclonus Psychomotor delay and regression Hemiparesis and emianopsia Cortical blindness Headache Dystonia Stroke-like episodes Bilateral lesions of basal ganglia at BMI
PNS	Peripheral sensory-motor neuropathy
MUSCLE	Exercise intolerance Myopathy Ophtalmoplegia Blepharoptosis
EYE and EAR	Pigmentary retinopathy Optic atrophy Cataract Sensorineural deafness
HEART	Cardiomyopathy Cardiac conduction defects
BLOOD	Pancytopenia Sideroblastic anemia
ENDOCRINE SYSTEM	Diabetes Exocrine pancreas dysfunction Hypoparathyroidism Multiple endocrinopathy Short stature
GASTROINTESTINAL SYSTEM	Nausea Vomiting Hepatopathy Intestinal pseudo-obstruction
KIDNEY	Nephropathy Fanconi syndrome
METABOLISM	Lactic acidosis
MUSCULAR BIOPSY	Ragged red fibers

Laboratory tests useful for diagnosis of MRC defects include measurements of serum lactic acid, pyruvate, ketonic bodies and of their molar ratios, which reflect cytoplasmatic and oxidative mitochondrial metabolism. An increase in serum lactic acid is a typical finding. While a disturbance of the Krebs cycle or of pyruvate metabolism causes a proportional increase in both pyruvate and lactate, an increase in their ratio is highly suggestive of a MRC defect. If plasma redox state is not altered, the same parameters should be measured in the cerebrospinal fluid (CSF). However, it has to be noted that lactic acid is not an absolute requisite for diagnosis, and a negative test does not exclude a MRC defect.

Magnetic proton resonance spectroscopy is a not invasive technique that can be used to determine CSF concentrations of lactate, ATP, ADP, phosphate and phosphocreatine, although detectable alterations are not specific for MRC defects.

Brain MRI is fundamental for diagnosis of these disorders, allowing detecting characteristic patterns, as stroke-like lesions (MELAS), bilateral signal hyperintensities in the basal ganglia and brain stem (Leigh syndrome).

In the absence of clear genotype-phenotype correlations and in front of the large number of possibly involved genes, morphological and biochemical analyses on muscle biopsies or other tissues are still the cornerstones of the diagnosis of this condition. Morphological examination can reveal ragged-red-fibers (RRFs), which represent sign of massive mitochondrial proliferation or lipid accumulations; SDH and COX histochemical stainings are routinely performed, allowing to obtain information about enzymatic activity and on the tissue pattern of the defect. For example, a COX defect caused by a nuclear mutation has a diffuse pattern, while mtDNA mutations are often characterized by scattered COX-negative and COX-positive fibers.

By using spectrophotometric assays, it is possible to measure the activity of the following MRC complexes (DiMauro et al 1987): NADH dehydrogenase (Complex I, EC 1.6.5.3); Succinate dehydrogenase (Complex II, EC 1.3.5.1); Ubiquinone-Cytochrome *c* oxidoreductase (Complex III, EC 1.10.2.2); Cytochrome *c* oxidase (Complex IV, EC 1.9.3.1); and citrate synthase (CS, EC 4.1.3.7), a matrix enzyme of the Krebs cycle, used as normalization control. Measurement of Complex III is often substituted by combined assays of Complexes I+III (NADH-cytochrome c reductase) II+III (succinate-cytochrome c reductase), which allow to reveal also CoQ biosynthetic defects. Biochemical profile data give useful diagnostic clues: isolated defects of Complex I, III or IV suggest mitochondrial or nuclear mutations of individual subunits or ancillary factors, whereas

Complex II defects must be due to a nuclear mutation, since mtDNA does not encode for any SDH subunits; a combined defect can suggest a mtDNA mutations affecting mitochondrial synthesis *in toto* (large scale deletions, depletions, tRNA mutations).

The information gathered from clinical phenotype, family history, and all reported diagnostic tests should orient on the priority of different genetic tests and on which molecular defects to screen for. This is particularly important not only for an adequate genetic counseling, but also for a rational therapeutic approach.

2. UREA CYCLE

The urea cycle is the primary mechanism by which excess nitrogen that is generated by endogenous protein catabolism or exogenous protein intake is detoxified and excreted as urea; moreover, urea cycle includes several of the biochemical reactions required for the *de novo* synthesis of arginine (Brusilov and Horwich 2001). Five enzyme are involved in urea cycle, the individual reactions catalyzed by each enzyme are depicted in figure 2.

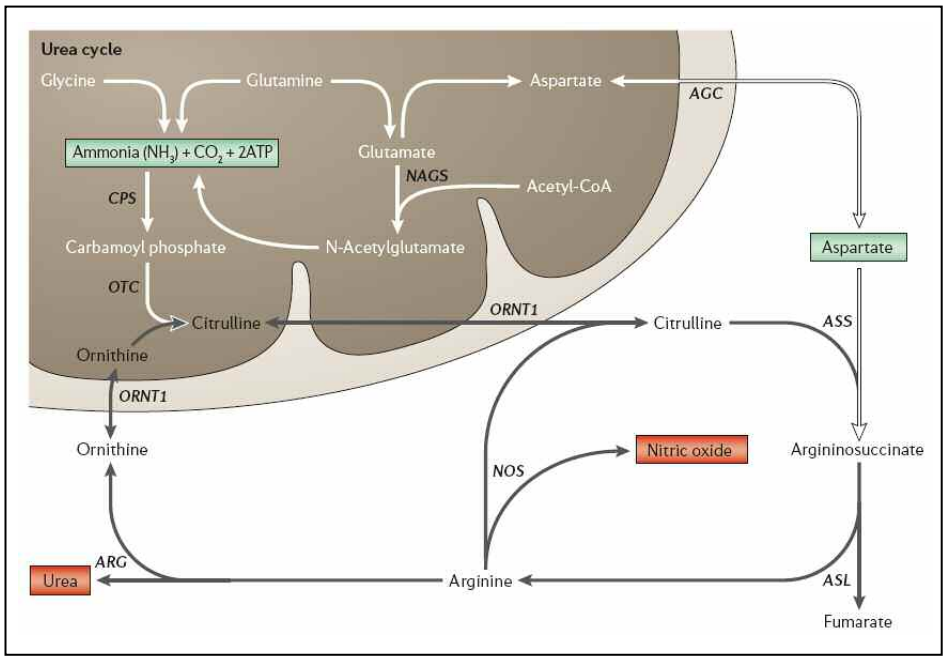

Fig. 2 Urea cycle enzymes generate urea from nitrogen, which is donated from ammonia and aspartate. Embedded within the urea cycle is the arginine–citrulline cycle, which produces nitric oxide (adapted from Lanpher et al 2006).

The first two enzymes of the cycle, carbamoyl phosphate synthetase I (CPS, EC 6.3.4.16) and ornithine transcarbamylase (OCT, EC 2.1.3.3), are mitochondrial matrix enzymes expressed almost exclusively in the liver. This tissue-dependent expression localizes urea synthesis to this organ (Raijman 1974). Citrulline, the product of the OCT reaction, is exported out of the mitochondria to the cytosol by facilitated diffusion through an ornithine/cytrulline antiporter (Indiveri et al 1992). The three remaining enzymes, argininosuccinate synthetase (ASS, EC 6.3.4.5), argininosuccinate lyase (ASL, EC 4.3.2.1), and arginase (EC 3.5.3.1), are cytosolic and, unlike CPS and OCT enzymes, are expressed in a wider range of tissues. In mammalian tissues where urea synthesis does not occur, and in nonureotelic organisms, the primary role of these enzymes is the biosynthesis of arginine from cytrulline and aspartate (Paulus 1983). Arginine production

in nonhepatic tissues is important not only for protein synthesis but also for nitric oxide (NO) production, a key signaling molecule, which is produced by the conversion of arginine to citrulline by nitric oxide synthetase (NOS) (Lane and Gross 1999). ASS and ASL, in conjunction with NOS form the cytrulline-NO or arginine-cytrulline cycle, and hence provide the cell with a continuous source of cellular arginine for NO production (fig.2).

2.1 Urea Cycle Defects

Classical urea cycle defects (UCDs) are caused by enzymatic deficiencies in this pathway and have a total prevalence of at least 1/30.000.

Disease-causing mutations have been identified in all enzymes and transporters involved in urea-cycle and arginine-cytrulline cycle (fig.2). Deficiencies of ornithine transcarbamilase (OTC, MIM# 311250), carbamyl phosphate synthetase (CPS, MIM# 237300), argininosuccinate synthetase (ASS, MIM# 215700) and argininosuccinate lyase (ASL, MIM# 207900) display a heterogeneous clinical presentation; however, patients with null activity in proximal urea-cycle enzyme present classically in the neonatal period with severe hyperammonaemia leading to lethargy, hypothermia, apnea and coma, while in patients with residual enzyme activity symptoms appear later, during childhood or adulthood, and range from cycling vomiting to psychiatric disorders (Msall et al 1984). Arginase deficiency (ARG1, OMIM 215700) is characterized by a clinical picture consisting of progressive spastic quadriplegia and mental retardation, but hyperammonaemia never occurs as severely as in the other forms.

UCDs are inherited as autosomal recessive traits, except for OTC deficiency, which is an X-linked disorder.

Loss of urea cycle enzymes leads to the accumulation of ammonia upstream of the enzymatic block and deficiency of arginine downstream (except in the case of arginase deficiency). The pathogenesis of these disorders is largely related to ammonia, which exerts its major toxic effects on CNS. However, patients have also other clinical features, such as primary liver dysfunction (mostly seen in patients affected by argininosuccinic aciduria). The phenotypic differences among the UCDs underline the importance of urea-cycle intermediates in other metabolic pathways: some clinical features that are not directly related to hyperammonaemia could depend on alteration in NO synthesis (Maher et al 2003).

2.2 Diagnostic and therapeutic approach of UCDs

Diagnosis of UCDs is indicated initially by elevated ammonia levels in the absence of significant metabolic acidosis (Hill et al 1974); alterations of plasma amino acids profile allow to find out the specific enzymatic defects. While this approach can identify null-activity patients, it can result unreliable for detecting carriers or partial-activity patients, since metabolite pools are often normal in the absence of stress. Thus, the definitive diagnosis can be done through direct enzyme assay on fibroblasts or erythrocytes; yet, enzymatic activities do not necessarily correlate with phenotypic severities. Finally, molecular diagnosis can be achieved by sequencing of urea-cycle genes, which has also an important role in prenatal diagnosis for fetuses at risk and genetic counseling for carriers.

UCDs therapeutic strategies aim at limiting exogenous and endogenous sources of the nitrogen-containing compounds and at activating other pathways of waste nitrogen synthesis and excretion. This is achieved with restriction of dietary protein intake and by preventing catabolic stress that stimulates amino acids mobilization from muscle. The alternative-pathway therapy makes use of scavenger molecules, such as sodium benzoate or sodium phenylbutyrate, which bind glycine and glutamate (key nitrogen donors to the urea cycle), favoring their renal excretion. In patients deficient in ASS and ASL diet is also supplemented with arginine.

SECTION II

GENERAL AIMS OF THE WORK

During my PhD program, I followed distinct research lines in order to investigate the molecular bases of two main types of metabolic diseases: mitochondrial disorders, discussed in section III and IV, and urea cycle defects, described in section V.

Among mitochondrial diseases, I focused on the characterization of novel genes involved in isolated cytochrome *c* oxidase deficiency and in ubiquinone defects and on the study of their genetic bases. In collaboration with the groups at Columbia University, New York, and at Universidad Pablo de Olavide, Sevilla, we have studied a family affected by coenzyme Q deficiency and reported the first mutation in a gene involved in ubiquinone biosynthesis. Moreover, I visited the laboratory of Prof. Navas at the University Pablo de Olavide in Sevilla where I developed an animal model of COX deficiency to unveil the pathogenetic mechanisms of this disorder and to search for new potential therapeutic strategies.

In the second part, I performed a mutational screening on a cohort of Italian patients affected by argininosuccinic aciduria and I developed distinct functional systems to confirm the pathogenicity of mutations and to study potential genotype-phenotype correlations.

Finally, in appendix I report the genetic characterization of a family affected by Pelizaeus-Merzbacher disease, a hypomyelinating disorder.

SECTION III

ISOLATED CYTOCHROME c OXIDASE DEFICIENCY

3. CYTOCHROME *c* OXIDASE

Cytochrome c oxidase (COX) (EC 1.9.3.1) or complex IV, is the terminal enzyme of the MRC and catalyzes the transfer of reducing equivalent from cytochrome *c* to oxygen, reducing the latter to water; energy generated by this reaction is used to pump protons across the MIM (Michel et al 1998). COX is active as a dimer and most of the information regarding its dimeric structure was obtained by crystallographic resolution of the bovine heart enzyme (Tsukihara et al 1995), showing that the cytochrome *c* binding site (two molecules of cytochrome *c* bind to the dimer in a cooperative way) is located in a cleft at the interface between the two monomers. Each COX monomer comprises 13 subunits and a number of prosthetic groups that contribute to redox center formation: two heme groups (*a* and *a3*), three copper ions (two in the Cu_A site and one in Cu_B site), a zinc ion and a magnesium ion (fig.3).

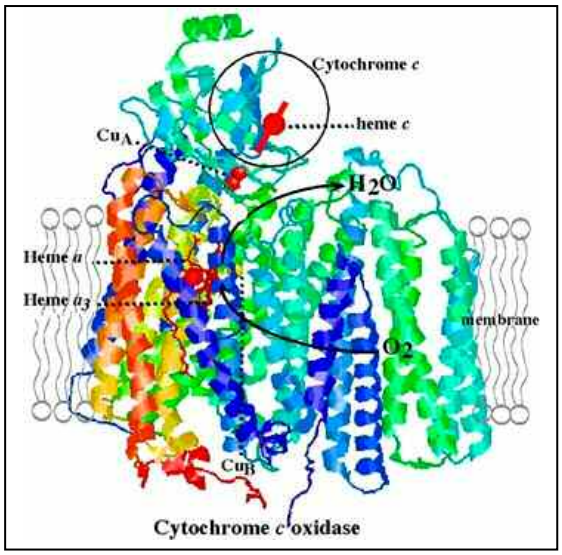

Fig. 3 Tridimensional structure of the bovine heart cytochrome *c* oxidase. The multisubunit complex is embedded in the MIM. The prosthetic groups and the substrate are indicated.

The biogenesis of COX requires the interplay of two genomes. The three larger subunits (COX I, COX II, and COX III) are encoded by mtDNA, are embedded in the MIM, forming the catalytic core of the enzyme, and contain the prosthetic groups.

The ten smaller COX subunits (COX IV, Va, Vb, VIa, VIb, VIc, VIIa, VIIb, VIIc according Kadenbach nomenclature 1983) are encoded by nDNA, and have regulatory and structural functions. Two of them (VIa and VIIa) have tissue-specific isoforms.
The two heme moieties are found in subunit I, which contains also the Cu_B site (with one only copper atom), while the binuclear Cu_A site is located on subunit II; additionally, the magnesium ion occupies the cleft formed by COX I and II, and the zinc ion is found near Vb subunit. COX III does not contain prosthetic groups and seems not to be involved in proton pumping, indicating that its role could be regulatory or structural (Tsukihara et al 1995).
The Cu_A active site accepts electrons from cytochrome *c* and rapidly reduces heme *a*. From heme *a*, electrons are transferred intramolecularly to the heme *a3*-Cu_B binuclear center, where molecular oxygen binds to be reduced (Babcock and Wikstrom 1992). For each electron transferred, two protons are pumped across the MIM.

3.1 COX assembly genes

COX assembly is a complex multi-step process, which is tightly controlled in a nuclear-mitochondrial coordinated fashion and requires the assistance of a large number of assembly factors acting at several levels. These proteins are encoded by some nuclear genes, called COX-assembly genes, identified and characterized from study of yeast respiratory-deficient *pet* mutant strains (Tzagoloff and Dieckmann, 1990). They control the folding and maturation of the different polypeptides and their insertion into the MIM, the synthesis of prosthetic groups, and the delivery and insertion of the metal cofactors into the holoenzyme.
Analysis of the human enzyme by blue-Native electrophoresis, after exposition of human cells to inhibitors of mitochondrial and cytoplasmatic protein synthesis, has shown that COX biogenesis occurs in a sequential process (Nijtmans et al 1998). These studies allowed defining a possible model of COX assembly with three different intermediates that probably represent rate-limiting steps in the process. The first assembly intermediate S1 contains only CoxIp, the second intermediate S2 is possibly formed by CoxIp, CoxIVp and perhaps CoxVap, while the third one S3 contains all of the subunits except subunits VIa and VIIb, the addition of which concludes the formation of the holoenzyme (fig.4).

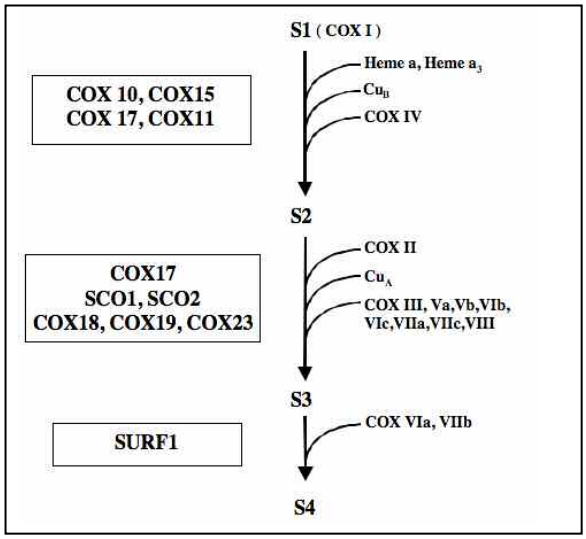

Fig. 4 Schematic representation of COX assembly (modified from Nijtmans et al 1998). S1-S3 referred to the three intermediates of the complex, S4 to the holoenzyme. The prosthetic groups and the structural subunits that are progressively added are reported on the right; in the boxes on the left, the COX-assembly genes that are supposed to be involved in each step are indicated.

Studies performed with yeast mutants have shown that the COX assembly process is conserved between yeast and human. Screens of nuclear respiratory-deficient mutants have revealed the existence of at least 30 nuclear genes coding for factors other than structural subunits, which selectively affect expression of this respiratory complex in yeast (Tzagoloff and Dieckmann 1990; McEwen et al 1986). By contrast, in humans the information is still incomplete and less than ten counterparts have been identified and characterized thus far. In table 2, some of the yeast COX-assembly genes and their *C.elegans* and human homologues are reported.

3.2 Copper-binding proteins involved COX assembly

The insertion of copper into COX is an essential requirement for both its catalytic activity and its assembly. Copper is a trace metal and represents an essential cofactor of key enzymes in the cell, but its reactivity with dioxygen may lead to toxicity (Valentine et al 1998). For this reason, free aqueous-copper ions are virtually absent in the cytoplasm, due to an instant association of imported copper with chaperones, scavengers and other proteins.

Mitochondria have their own copper transport and distribution network, with COX and its associated copper-binding factors as probably the only known proteinaceous endpoints.

Table 2. Yeast, human and nematode COX assembly genes (in parenthesis the systematic gene name is indicated). For COX-assembly genes involved in human COX deficiency, the clinical phenotype is reported.

S.cerevisiae	C.elegans	Human	Locus	Function	Phenotype
SHY1 (YGR112W)	*Sft-1* (H06I04.2)	*SURF1*	9q34	Stability of assembly intermediate subcomplex S3	Classical Leigh Syndrome (Tiranti et al 1998; Zhu et al 1998)
SCO1 (YBR037C)	*Sco-1* (C01F1.2)	*SCO1*	17p13.1	Copper transport to Cu_A site of COX II	Hepato-encephalomyopathy (Valnot et al. 2000a)
SCO2 (YBR024W)	-	*SCO2*	22q13.33	Copper transport to Cu_A site of COX II	Fatal infantile cardio-encephalomyopathy Hypertrophic cardiomyopathy (Papadopoulou et al. 1999 Jaksch et al. 2001) Spinal muscular atrophy (Salviati et al. 2002a)
COX10 (YPL172C)	*Cox-10* (Y46G5A.2)	*COX10*	17p12	Heme A farnesyltransferase	Anemia, Leigh Syndrome, sensorineural deafness (Valnot et al. 2000b) Fatal infantile hypertrophic cardiomyopathy (Antonicka et al 2003a)
COX15 (YER141W)	*Cox-15* (T06D8.5)	*COX15*	10q24	Heme hydroxylase	Hypertrophic cardiomyopathy (Antonicka et al. 2003b)
PET309 (YLR067C)	(C04E6.11)	*LRPPRC*	2p21	Stability and processing of Cox1p	Saguenay – Lac. St. Jean form of Leigh syndrome (LSFC) (Mootha et al. 2003)
COX11 (YPL132W)	*Cox-11* (JC8.5)	*COX11*	17q22	Copper transport to Cu_B site of COX I	-
COX17 (YLL009C)	*Cox-17* (F40G9.2)	*COX17*	3q13.33	Copper cytosolic transporter	-
COX19 (YLL018C-A)	*Cox-19* (F45H11.5)	Our sequence	See text	Putative copper cytosolic transporter	-
COX23 (YHR116W)	-	Our sequence	See text	Putative copper cytosolic transporter	-
COX18 (YGR062C)	*Cox-18* (Y55F3AR.1)	Our sequence	See text	Membrane insertion of COX II	-

Several proteins participate in copper metabolism. Metal ions enter the cell through CTR1, a specific plasma membrane importer, which gives them to specific high affinity copper chaperones necessary for the trafficking within cells. Among these chaperones, CCS protein donates copper to the anti-oxidant enzyme Cu,Zn-superoxide dismutase (SOD1), while Cox17 transports it to the IMS (Glerum et al 1996; Balamurugan and

Schaffner 2006). In yeast, at least other two genes, COX19 and COX23, encode soluble protein involved in copper trafficking to mitochondria (Barros et al 2004; Rigby et al 2007). Copper is then transferred to Cox11, which inserts it into the Cu_B site on subunit Cox1p (Hiser et al 2000), but it is also transferred to the Sco1 and Sco2 proteins, which insert it into the Cu_A site on subunit Cox2p (Horng et al 2004). Cox17 and Cox23 share structural and functional properties, since yCOX23 can complement $yCO17^{null}$ mutants (Barros et al 2004). To date, there are no data on the functional relationships between Cox19p and Cox17p or Cox23p. A proposed model for copper delivery to COX is depicted in fig.5.

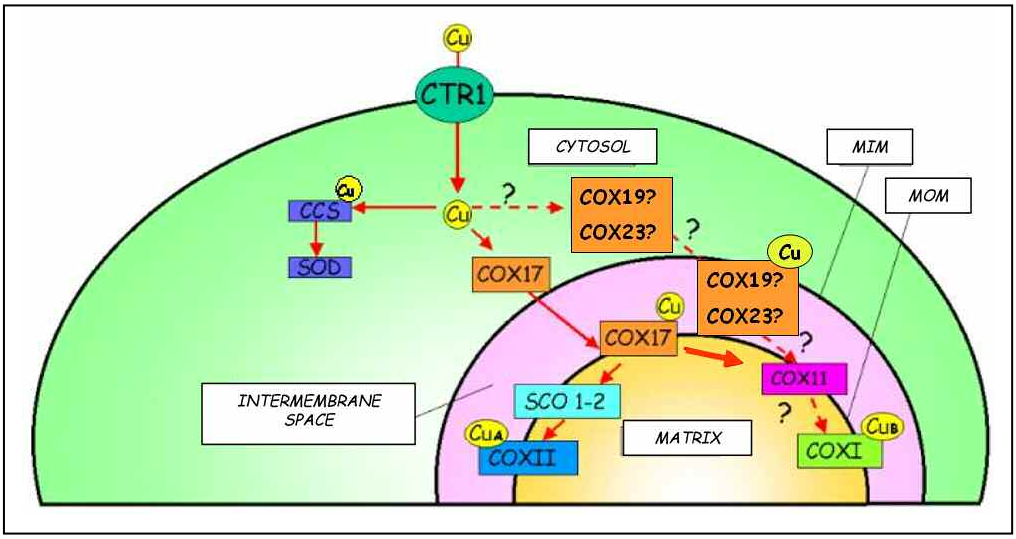

Fig.5. Representation of copper transport in eukaryotes.

3.3 Isolated COX deficiency

COX deficiency is a relatively common biochemical finding and can present as an isolated defect or as part of combined MRC defects. In this case it is due to large-scale rearrangements of mtDNA or to mutations in genes encoding the mitochondrial tRNAs (Zeviani and Di Donato 2004).

Isolated COX deficiency account for the largest proportion of specific defects associated with the MRC in infancy (Robinson 2000). The clinical presentations are variable, ranging from hypertrophic cardiomyopathy to Leigh syndrome, which is the most common form of these defects (Van Coster et al 1991). Leigh syndrome patients have widely varying clinical courses; in most patients, the disease presents early in life and

death occurs during the first decade of life (Robinson et al. 1987). Other clinical manifestations include psychomotor retardation and developmental delay, ataxia, ophthalmoplegia, hypotonia, myopathy, hypertrophic cardiomyopathy, Saguenay Lac San Jean Syndrome and lactic acidosis (table 2). COX deficiencies that are not associated with Leigh syndrome present with a variety of clinical phenotypes, which include some or all of the above symptoms.

Although these disorders have been characterized biochemically, in most cases their etiologic diagnosis remains elusive. They can have two different genetic origins (mtDNA and nDNA). Mutations in the three mtDNA genes cause only a minority of human COX deficiencies (Shoubridge 2001), whereas the majority of these forms are inherited as autosomal recessive traits, thus underlying a defect in a nuclear gene. However, the cDNA sequencing for all of the nuclear-encoded subunits from a large number of patients with COX deficiencies has revealed no mutations (DiMauro and De Vivo 1996; Adams et al. 1997). These data had suggested that most COX deficiencies might originate from decreased stability or failure to complete assembly of the holoenzyme (Glerum et al. 1988).

To date, pathogenic mutations have been identified in six COX assembly genes, *SURF1*, *SCO1*, *SCO2*, *COX10*, *COX15*, and *LRPPRC* (table 2), with all of these discoveries facilitated by the previous identification of the homologous genes in yeast. These result in a variety of clinical phenotypes. However, a substantial number of human COX deficiencies whose etiologies is still unknown remains and other, as yet unidentified, genes must be involved.

4. SPECIFIC AIM

Our aim was to study the genetic bases and the pathogenetic mechanisms of isolated COX deficiency. Particularly, we focused on the identification of new COX-assembly genes and we modeled this disorder on *Caenorhabditis elegans*, a multicellular experimental organism.

5. RESULTS AND DISCUSSION

5.1 Identification and cloning of *hCOX16, hCOX18* and *hCOX19*

We identified the human homologues of *yCOX16*, *yCOX18* and *yCOX19*, three *S.cerevisiae* genes involved in the biogenesis of MRC complexes. The human gene sequences were identified through the ‘‘cyber-screening’’ method described by Petruzzella et al. (1998). In brief, using as probes the amino acidic sequences of the yeast proteins (Carlson et al 2003; Souza et al 2000; Nobrega et al 2002), we screened the GenBank database by the tBLASTn algorithm (www.ncbi.nlm.nih.gov/blast) (Woodsmall and Benson 1993) and found several human ESTs showing regions of significant homology with the yeast genes. We aligned these ESTs and obtained an initial contig, which was again used as a probe for the tBLASTn software to identify ESTs overlapping with the 5’ or 3’ ends of our sequences. We repeated this operation until we obtained the complete coding region of each of the three genes. This information allowed us to design a set of oligonucleotides for the amplification by RT-PCR of the entire coding region of the three genes. PCR products were cloned in both the pCRIITOPO cloning vector and sequencing of single clones confirmed our *in silico* predictions.

We then aligned the obtained sequences with those of human genomic DNA to establish their chromosomal localization, which are reported in table 3. Their protein sequences were subsequently aligned with those of the corresponding *S.cerevisiae* homologues and with proteins of other species identified with a similar bioinformatic procedure (Table 3; fig.6).

Table 3. Structure of *hCOX16, hCOX18* and *hCOX19* and of their protein products.

Gene name	Locus (size)	Exon number	ORF (nt)	Predicted protein MW	Yeast homologue	Homology* with yeast homologue
hCOX16	14q24.1 (35 kb)	4	318	12.9 kDal	yCOX16 (YJL003W)	28% identity 54% similarity
hCOX18	4q21.1 (25 kb)	7[a]	999	37.1 kDal	yCOX18 (YGR062C)	25% identity 45% similarity
hCOX19	7p22.3 (12 kb)	3	270	10.4 kDal	yCOX19 (YLL018C-A)	40% identity 60% similarity

[a] The last exon of *hCOX18* encodes only the 3’ untranslated region (3’UTR).
* The degree of homology was calculated by using the BLASTp algorithm.
MW=molecular weight; kDal=kilo Dalton

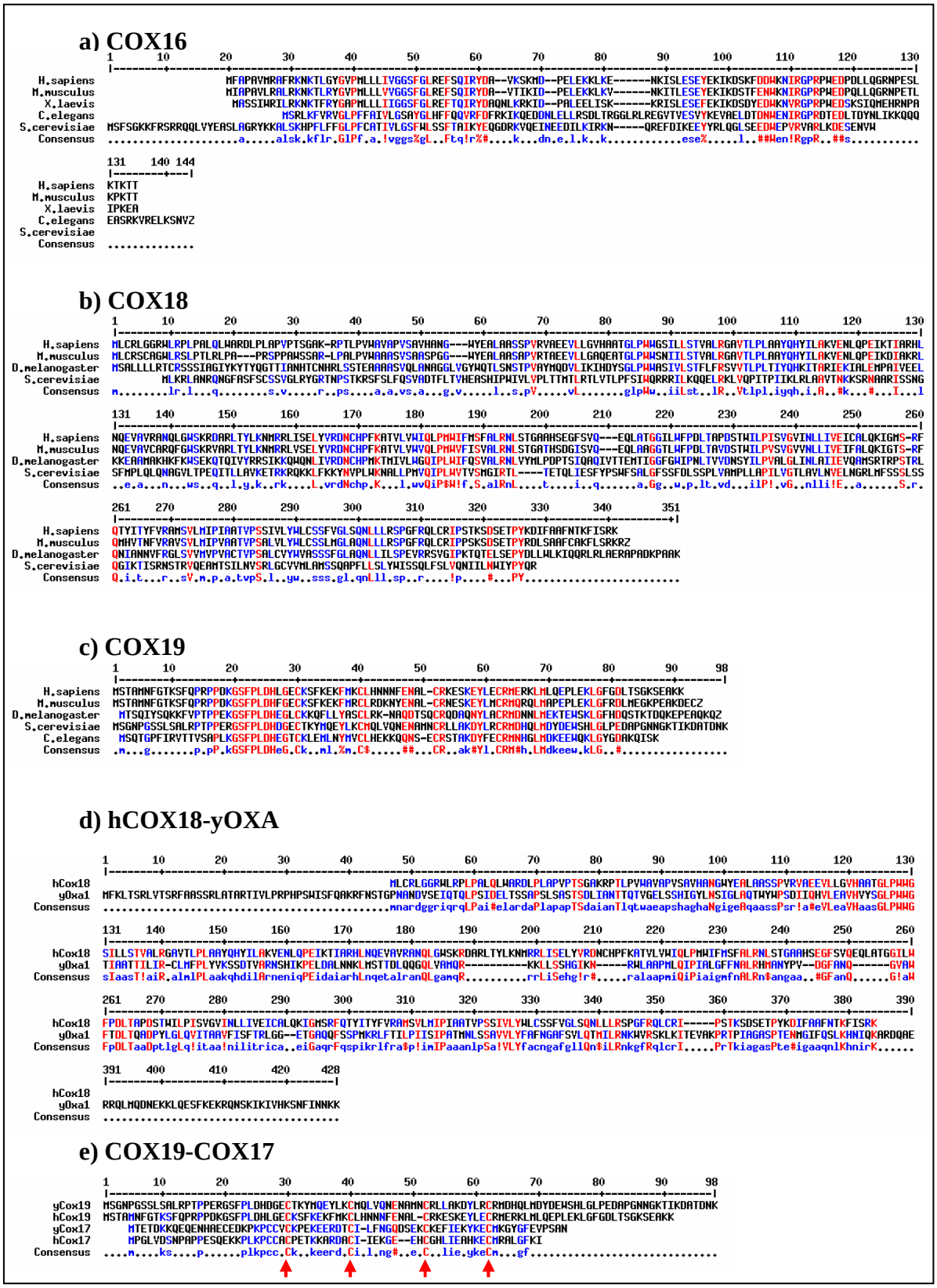

Fig 6. Alignment of Cox16p (a), Cox18p (b) and Cox19p (c) sequences in different species. In (d), hCox18p is aligned with yOxa1p; in (e) arrows indicate the four cystein residues which are conserved in Cox19p and in Cox17p. Sequence alignments were performed by using Multalin software (http://prodes.toulouse.inra.fr/multalin/multalin.html).

hCox18p has also discreet homology with Oxa1p (fig.3d), which is located in the MIM, and is involved in the integration of both mtDNA- and nDNA-encoded proteins into the MIM (Preuss et al. 2005).

The protein product of *hCOX19* has a greater homology with its yeast counterpart than hCox18p or hCox16p and its structure is similar to that of hCox17p (Glerum et al 1996), another protein involved in COX biogenesis that participates in copper transport into the mitochondrial intermembrane space (IMS) (fig.3e).

The predicted subcellular localization of the three proteins was analyzed by employing three specific software (PREDOTAR, PSORT, and MITOPROT): all suggested a mitochondrial localization in the inner membrane for hCox16p and hCox18p and a cytosolic localization for hCox19p, which does not appear to contain a mitochondrial importation signal.

We employed the SOSUI software (Hirokawa et al 1998) to predict the hydropathy profile for the three proteins.

hCox16p reveals one possible transmembrane domain, similar to that of yCox16p, with the N terminus facing the matrix side and the conserved C terminal domain in the IMS; hCox19p instead is a hydrophilic protein, without any region compatible with transmembrane domains. yCox18p is predicted to contain four transmembrane domains (Souza et al 2000), however *in silico* analysis produced conflicting results, with some programs predicting a five transmembrane helixes model, and others a four helix model. For hCox18p, only one software predicted a five-helix model, while the other programs favored a four-helix structure. Prediction software gave consistent results on the first three transmembrane domains, but was discordant about the fourth and fifth helixes, located at the C-terminus of the protein, that theoretically should be separated only by a short loop of two or three amino acids. We therefore aligned hCox18p with yOxa1p (fig.3d), whose transmembrane topology has been determined experimentally and contains five transmembrane domains with the C-terminus located in the mitochondrial matrix (Herrmann et al 1997). The first three transmembrane domains of yOxa1p match those predicted in hCox18p by computer analysis, while the fourth and fifth domains correspond to the fourth predicted domain of hCox18p. Despite the contradictory data obtained from our computer analyses, we favor a five helix model for hCox18p for two main reasons: because in all members of this family thus far characterized, including the bacterial proteins (Sääf et al 1998), the portion of the molecule with the translocase activity has five transmembrane domains, and because in a four helix model the

positively charged C-terminus of the protein would be located in the IMS, thereby contradicting the so-called ‘‘positive inside rule’’ (von Heijne 1989; Boyd et al 1990) of the MIM proteins. We believe that the closely spaced fourth and fifth transmembrane helixes (they appear to be separated only by a short loop of just two or three amino acids) are identified as a single transmembrane domain by topology prediction software. In fact, similar problems were reported with the computer analysis of bacterial and yOxa1p membrane topology (Sääf et al 1998). Figure 7 depicts a possible model of hCox18p membrane topology based on these data.

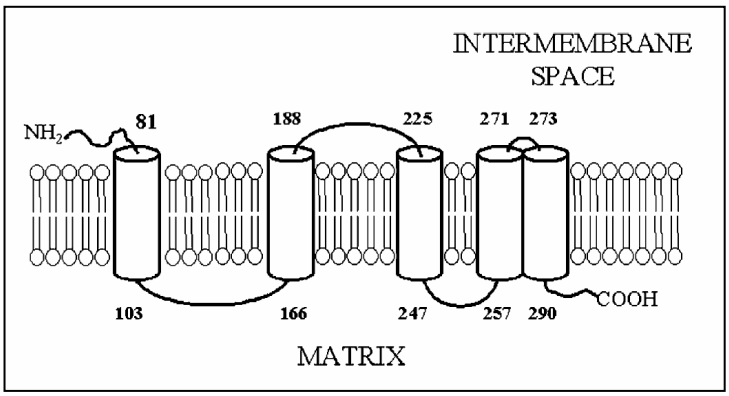

Fig. 7. Putative membrane topology of hCox18p. The numbers indicate the amino acid residues that limit the transmembrane segments.

5.2 Expression analysis and characterization of the transcripts

In order to explore by Northern blot analysis the pattern of tissue expression of the three genes and to gain information about the approximate size of the transcripts, we used the cloned cDNAs to synthesize ^{32}P labeled probes as described (Rezzonico et al 1998). Probes were hybridized at 42°C in 50% formamide with a pre-made multiple-tissue Northern blot (Clontech), containing 2 µg per lane of poly(A)+ RNA from eight human tissues, according to the manufacturer’s protocol. Autoradiographs were quantified by densitometric scanning using a laser densitometer equipped with ImageQuant software (Molecular Dynamics). The same blot was rehybridized with a β-actin probe (provided by the manufacturer) to monitor the quality and quantity of RNA samples. The three genes are expressed in all tissue analyzed and present more transcripts (fig. 8); moreover, they appeared to be transcribed at very low levels compared to β actin.

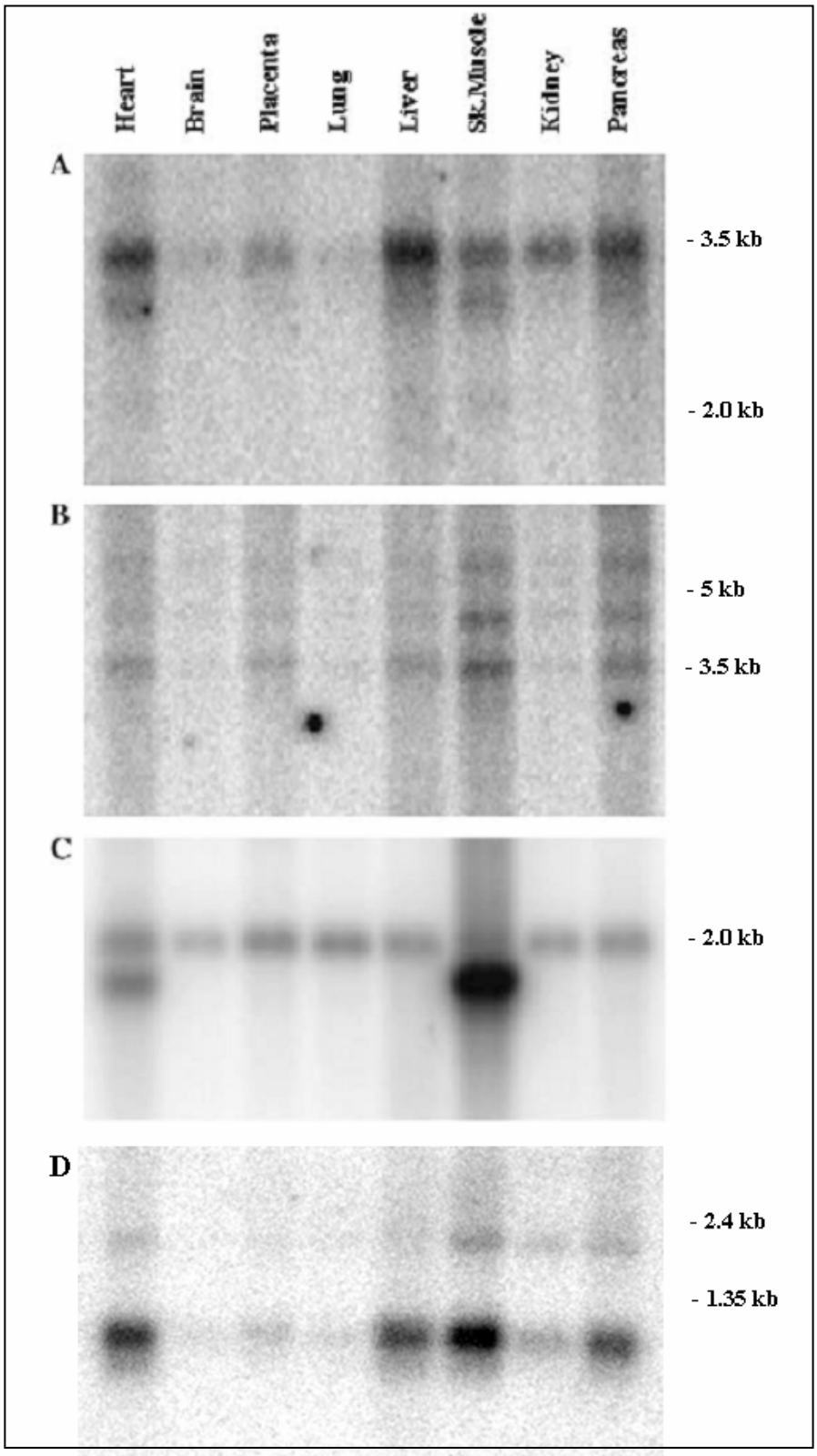

Fig. 8. Northern blot analysis of *hCOX18*, *hCOX19* and *hCOX16* expression. (A) Membrane hybridized with hCOX18 probe and exposed for 3 days and visualized as described in text. (B) hCOX19 probe, exposed for 4 days. (C) β-Actin probe, exposed for 2 h. (D) Membrane hybridized with hCOX16 probe. Note that in heart and skeletal muscle two different transcripts of β-actin (1.8 and 2.0 kb long) are normally present.

hCOX16 displays a main transcript of 0.9 kb, which shows the higher levels of expression in heart, muscle, liver and pancreas, and another longer transcript of about 1.7 kb (fig.8D). *hCOX18* is present predominantly as a transcript of about 3.5 kb, although the blot showed also some fainter signals corresponding to shorter mRNAs. Its expression is ubiquitous, with higher levels in liver and heart (fig.8A). This suggests a possible role of *hCOX18* in the pathogenesis of those forms of COX deficiency associated with liver and heart involvement. *hCOX19* is present in different transcripts, the smallest of which is of about 3.6 kb. Higher molecular weight transcripts are about 4.6 and 6 kb. Also this gene is expressed ubiquitously, but *hCOX19* mRNA is most abundant in skeletal muscle (fig.8B). This is in accordance with the high metabolic requirements of this tissue.

To characterize the structure of these transcripts, we employed a rapid amplification of cDNA ends (RACE) protocol using the Gene Racer kit (Invitrogen) according to the manufacturer's guidelines. Briefly, for 5' RACE total RNA was initially treated with DNAse to eliminate traces of genomic DNA from the fibroblasts RNA preparation. RNA was treated with calf intestinal phosphatase to dephosphorylate partially degraded mRNA. The 3-methyl-guanosine cap of full-length mRNA was then removed by treatment with tobacco acid phosphatase, and a synthetic RNA oligonucleotide provided by the manufacturer was ligated at the 5'end of the mRNA. This procedure selects for full-length mRNA because partially degraded RNA molecules are not ligated to the synthetic oligonucleotide. The mRNA was retrotranscribed using the modified oligo(dT) nucleotides provided in the kit and aliquots of the reaction were used for PCR amplification of the transcript extremities. The amplification was carried out with a nested PCR protocol using the conditions recommended by the manufacturer. Finally, PCR products were cloned into pCR4TOPO vector (Invitrogen) and at least 20 single clones were sequenced for each gene.

Sequencing of the cloned RACE products indicated that in *hCOX16*, the 5' untranslated region (5'UTR) extends for different lengths upstream to the ATG starting codon, showing at least three different transcription initiating sites: the main one is located 144 nt upstream to the ATG starting codon, while the others extend respectively 96 and 180 nt upstream to the ATG.

In *hCOX18*, the 5'UTR region extends 106 bp upstream of the ATG triplet at the beginning of the coding region, with a second, less frequent, transcription start site located 53 bases upstream to the ATG. *hCOX19* instead shows one only transcription origin, located 40 bp upstream to ATG triplet.

To characterize the 3' region, we used the approximate size information obtained from Northern blots to design specific primers on the 3'UTR of the gene. For *hCOX16*, we confirmed Northern blot data, revealing the presence of two transcripts, a longer one, with a 3'UTR of 1251 nt and a shorter one with a 3'UTR of 472 nt (with the exclusion of the poly(A) sequence).

Also for *hCOX18*, we proved the presence of two types of transcripts. The 3406 nt long transcript is more abundant, whereas the shorter 2027 nt one is present at much lower levels. We could not identify any other transcript in fibroblasts. We established by 3'RACE that *hCOX19* transcript is 3602 nt long, while, in contrast to Northern blot data, we could not detect longer mRNAs. Interestingly, the 3'UTR region contains a second potential ORF that encodes a predicted 158 aa hypothetical protein. The latter, however, does not show homology with any known protein, and this ORF is not present in the murine COX19 transcript. We believe that this second ORF is not actually translated into protein.

Sequences of the transcripts were submitted to the GenBank database.

In all cDNAs, the poly(A) is preceded by a canonical AATAAA polyadenylation consensus. Both *hCOX16* and *hCOX18* show two different transcripts, which differ only in the length of the 3'UTR. This region is important for modulation of nucleo-cytoplasmic mRNA transport, translation efficiency, subcellular localization, and message stability (Mignone et al 2005). Other COX-assembly genes, such as *hCOX11* and *hCOX15*, exhibit a similar phenomenon (Petruzzella et al 1998), but its physiological significance is still unclear.

5.3 Intracellular localization

To study the subcellular localization of the three COX-assembly factors, we generated GFP-fusion proteins. COX18-GFP was construct by cloning a 5'-*COX18* 210 bp fragment (cut with SacI and ScaI), containing the putative mitochondrial importation signal sequence and the first conserved portion of the gene, into pEGFPN1; the whole coding regions of *COX16* and *COX19*, lacking the termination codon and amplified with primers containing appropriate recognition sites (SacI and BamHI for COX19, HindIII and SacI for COX16) were cloned into the same vector digested in a similar way. We used the COX18-GFP vector to transfect human HEK293 cells. Forty-eight hours after transfection, cells were incubated with TMRM, a mitochondrial specific fluorescent dye

that exploits the membrane potential of these organelles. Cells were visualized using a Nikon Video Confocal microscope. The GFP fluorescence pattern (fig.9A) was compared with TMRM (fig.9B): as shown in figure 9C, there is perfect overlap between the two patterns, confirming that Cox18p is indeed a mitochondrial protein.

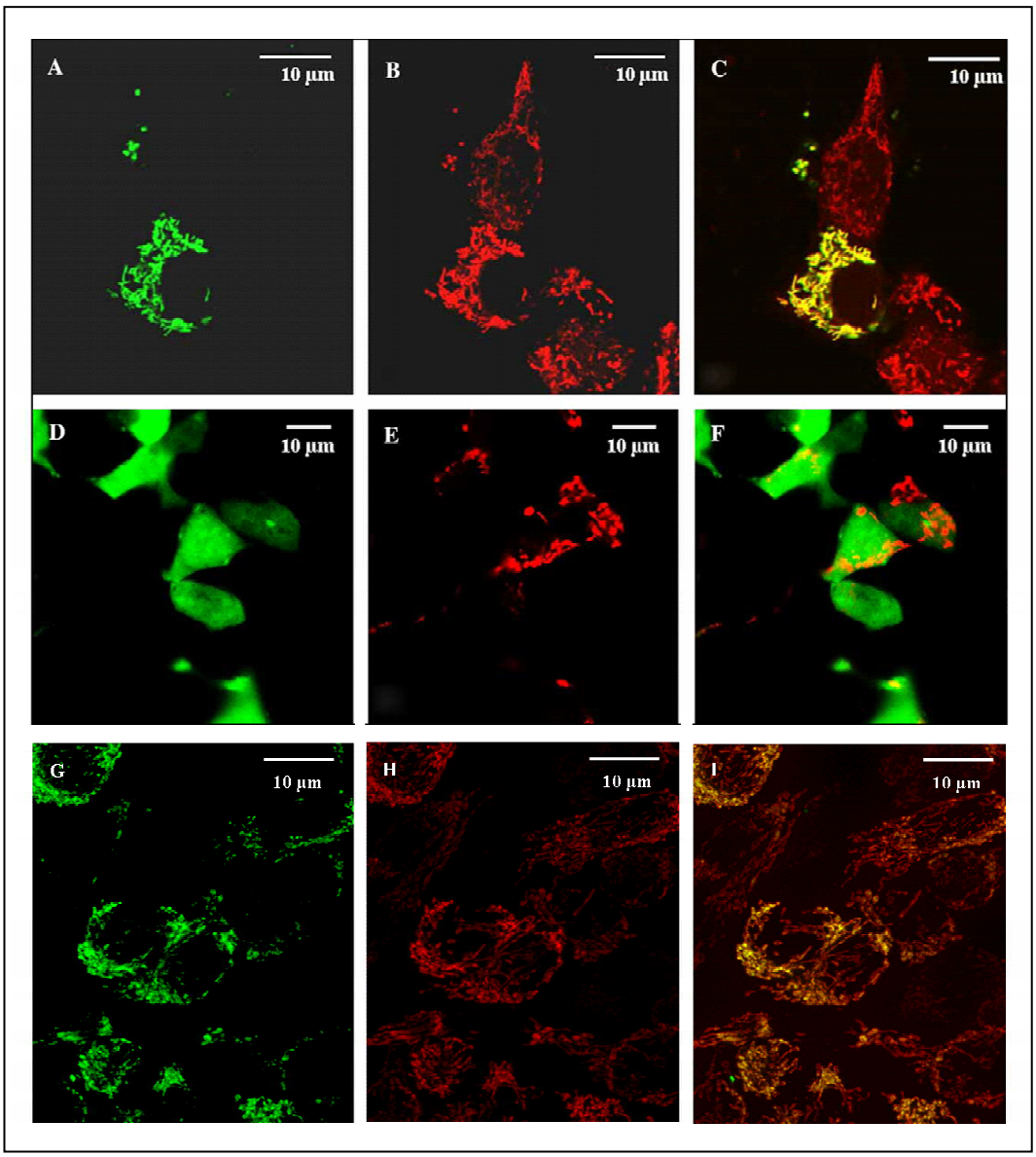

Fig. 9. Localization of COX18-GFP and COX19-GFP in HEK293 cells and of and COX16-Ha in HeLa cells. (A) COX18-GFP, (B) TMRM, (C) Superimposition of the previous images; (D) COX19-GFP, (E) mtRFP, (F) superimposition of the previous images; (G) COX16-HA, (H) mtRFP, (I) superimposition of the previous images.

We repeated a similar experiment with a COX19-GFP-fusion protein: COX19-GFP was co-transfected with a plasmid expressing red fluorescent protein linked to the mitochondrial importation sequence of COX VIII (mtRFP) In the microscope, it is evident that COX19-GFP fluorescent pattern (fig.9D), unlike that of mtRFP (fig.9E), is diffuse, and resembles the fluorescence pattern of a purely cytosolic protein. We are aware that GFP may alter mitochondrial targeting, but our observations are in agreement with experimental data obtained in yeast, in fact yCox19p is located mainly in the cytosol, although it has access to the IMS (Nobrega et al 2002). We will perform more detailed studies as soon as an anti-Cox19 antibody becomes available.

For *hCOX16,* we cotransfected HeLa cells with COX16-GFP and mtRFP; the fusion protein showed a cytoplasmatic localization, in contrast to the yeast data. We reasoned that the steric hindrance of GFP could have interfered with the correct importation of such a small protein in the MIM. Therefore, we generated the expression vector COX16-HA-pEGFPN1, in which the full-length cDNA of *hCOX16,* lacking the stop codon, had been cloned in frame with the HA epitope (hemagglutinin protein of human influenza virus) and repeated the transfection. HeLa stably expressing mtRFP (fig.9H) were immunostained with an anti-HA antibody (Covance) (fig.9G), and with a secondary antibody FITC-conjugated: as it is shown in figure 9I, there is a perfect overlapping between the two fluorescence patterns, confirming the mitochondrial localization of Cox16p.

5.4 Functional characterization

5.4.1 *hCOX18*

hCox18p presents significant homology with proteins belonging to the Alb3/Oxa1/YidC family, which is very ancient phylogenetically and comprises proteins that mediate the correct membrane insertion of several classes of transmembrane proteins. Particularly, Cox18p is similar to Oxa1p, a protein located in the MIM, which is found in yeast and in humans, where it is involved in the insertion into MIM of several proteins, synthesized in the cytosol or in mitochondria (Szyrach et al 2003; Petruzzella et al 1998). hCox18p present significant amino acid identity with the corresponding yeast polypeptides (fig.6D) and reveal highly conserved functional domains. In addition, we demonstrated that it is targeted to mitochondria, as is its yeast homologue. These data strongly suggest that the human gene product shares similar functions with their yeast homologues. Recently, it

has been demonstrated that the human gene fulfills a Cox-18-like function (Gaisne and Bonnefoy 2006): a hybrid gene, carrying the 5' region of *yCOX18* fused with *hCOX18* sequence, when expressed in yeast *cox18* mutants strains, it is able to functional complement them, restoring respiration and thus the growth in glycerol.

Since yCox18p is required for the insertion into the MIM of the C-terminal tail of the mtDNA-encoded Cox2p subunit (Saracco and Fox 2002), hCox18p should be involved in the intermediate phase of COX assembly (formation of subcomplex S3). $COX18^{null}$ yeast exhibits isolated COX deficiency with normal activities of other RC complexes (Souza et al 2000), but it is not yet clear whether this protein is required for the insertion into the MIM of components of other mitochondrial metabolic pathways.

5.4.2 *hCOX16*

Like most COX assembly factors characterized to date, Cox16p is an integral component of the MIM, however, there are no clues about its function. In yeast, Cox16p does not appear to be involved in maturation of subunit 2, copper recruitment, or heme A biosynthesis and it does not shown any functional domains homologous to any known protein family (Carlson et al 2003).

To further characterize *hCOX16* function, we performed a silencing experiment by employing RNA interference technology in HeLa cells. Small interference RNA duplexes (siRNAs) were used to target the *hCOX16* gene: a 21-nucleotide siRNA oligonucleotide for COX16 silencing and a non-silencing control siRNA (NS-siRNA, designed for *Thermotoga maritime* and used as a negative siRNA control for transfection) were chemically synthesized by Qiagen.

HeLa cells were transfected using the Amaxa cell optimization kit R, following the manufacturer guidelines. Briefly, the cells, 80% confluent, were resuspended in the Nucleofector R solution obtaining 100 μL of cell suspension at a density of $1\text{-}2\times10^6$/mL. After siRNAs addition (at a final concentration of 20 nM), cells were transfected with the Amaxa Nucleofector apparatus, and immediately transferred into 6-well plates containing 37ºC pre-warmed culture medium. Transfected cells were incubated for 48 hours and then three aliquots for each sample were used for RNA and proteins extraction and for biochemical assay. The level of silencing was measured by real-time PCR: cDNAs were synthesized by using SuperScript™ II Reverse Transcriptase (Invitrogen). Primers for PCR reaction were designed specifically for *hCOX16* gene with the assistance of the

Primer Express 1.0 software, while the control primers were designed according to the beta-glucoronidase (GUS) gene. Quantitative SYBR Green RT-PCR was performed with an ABI Prism 7700 Sequence Detector. COX16 transcript levels were reduced to less than of 30%, compared to those of the housekeeping gene GUS (fig.10A).

We then checked the biochemical phenotype of these cells by measuring COX and CS activities as described (Salviati et al 2002b): biochemical data revealed a 50% decrease in COX activity in COX16-silenced cells compared to controls (fig.10B), suggesting that this protein is involved in COX maturation.

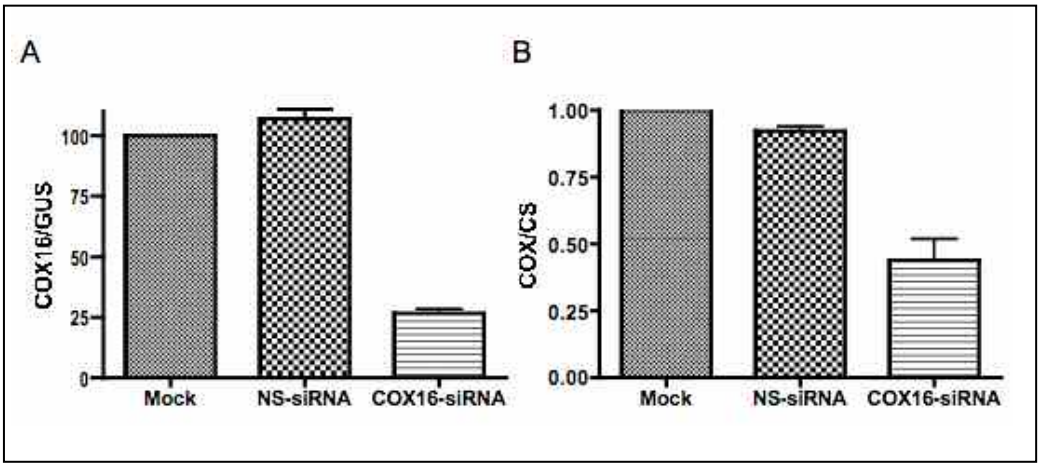

Fig. 10. (A) RQ-PCR of RNA from HeLa cells: ratio between levels of COX16 and GUS transcripts. (B) COX activity is expressed as % of controls and is normalized to CS activity and to protein content. Mock=cells transfected without siRNA addition; NS-siRNA=non-silencing siRNA negative control; COX16-siRNA=siRNA targeting specifically COX16. Data correspond to the average of the measures of three different experiments.

The biochemical hallmarks of a failure to complete COX assembly include a general loss or decrease in steady-state levels of the mitochondrially encoded subunits (Glerum and Tzagoloff 1997), as a result of degradation by intramitochondrial proteases (Rep and Grivell 1996). In fact, $COX16^{null}$ yeast strains are respiratory deficient due to a specific loss of COX activity and, as in other COX assembly-defective mutants, the steady state concentrations of subunits I, II and III are very low (Carlson et al 2003). Thus, we checked by Western blot the levels of Cox II protein: proteins extracted from COX16-silenced and NS-siRNA cells were resolved by SDS polyacrylamide gel electrophoresis and transferred electrophoretically to nitrocellulose membrane. A monoclonal mouse anti-COX II antibody (Molecular Probes), followed by peroxidase-labeled goat anti-

mouse secondary antibody allowed detection by enhanced chemiluminescence (Amersham Pharmacia Biosciences). Protein levels were normalized by stripping blot and reprobing it with a mouse antibody against the mitochondrial protein OPA1 (BD Biosciences). The relative amounts of protein were quantified from films using the BioRad Gel Doc 1000 image analysis system and Molecular Analyst software (BioRad Laboratories).

As shown in figure 11, the levels of this mtDNA-encoded subunit are reduced to 30% in COX16-silenced cells compared to non-silenced control cells.

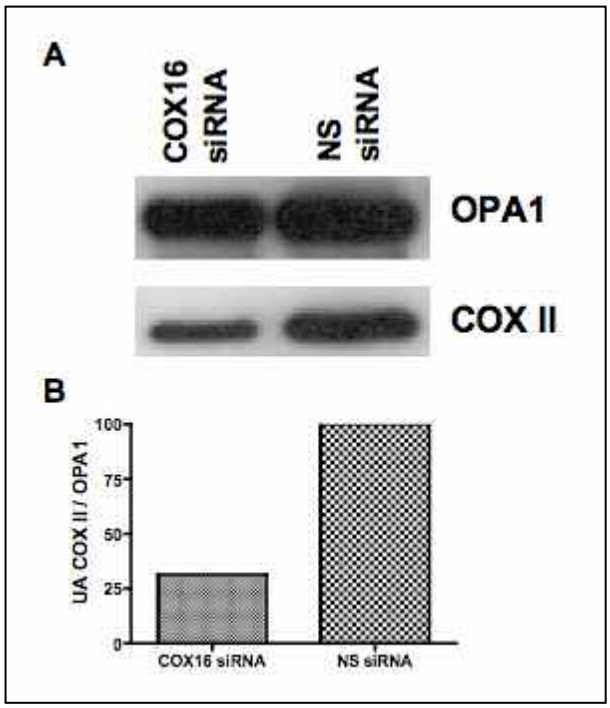

Fig. 11. (A) Western blot analysis of COX16 silenced (COX16-siRNA) and control non-silenced (NS-siRNA) HeLa cell lysates. (B) Relative amounts of COX II proteins: COX II levels were quantified by densitometry and normalized to OPA1 levels.

All these data confirmed that *hCOX16*, like its yeast homologue, encodes a mitochondrial protein which is essential for COX assembly and consequently for its function. However, the precise role of this small membrane protein of the MIM is still unclear and further studies are required to unveil its function.

5.4.3 *hCOX19*

hCox19p presents an even higher homology with the corresponding yeast polypeptides than both hCox16p and hCox18p and, like its yeast homologue, is a mainly cytosolic protein. Cox19p is very similar to another previously known COX-assembly gene, COX17, encoding a small soluble protein involved in copper transport to the MIM (Glerum et al. 1996; Beers et al. 1997; Arnesano et al. 2005). Similarly to Cox17p, Cox19p is soluble and shows the same subcellular localization in the cytosol and in the IMS. Moreover, it displays four highly conserved cystein residues, which align with a series of cysteines in Cox17p (fig.6e); these residues are arranged in a twin CX9C sequence motif that adopts a helical hairpin in Cox17 and have been shown to be required for copper binding, making it likely that also Cox19p is involved in metal transport (Nobrega et al 2002). Although the exact function of Cox19p in yeast is still unknown, it also resembles Cox17 in its ability to coordinate Cu(I). In fact, recombinant Cox19 binds 1 mol eq of Cu(I) per monomer, it exists as a dimeric protein and cysteine residues that are critical for Cu(I) coordination are important also for in vivo Cox19 function (Rigby et al 2007). Taken together, all these data support the hypothesis that Cox19p acts as a copper chaperone.

To further characterize Cox19p function, we developed a knockdown model to analyze the defective phenotype and to identify the role of this protein in COX assembly. We chose as experimental organism the free-living nematode *Caenorhabditis elegans*. In fact, yeast does not represent a useful model to study the function of *COX19*, since unlike *COX17*, the human gene cannot complement yeast COX19^{null} strains, although the two orthologues have a high degree of homology (Salviati, unpublished results). *C.elegans* instead displays a conserved orthologue; moreover, it is a more complex, multicellular organisms that may better reproduce the situation in human and allow gaining insight into the mechanisms at the basis of COX deficiency.

Nematodes have been introduced as experimental organisms in 1965 by Sydney Brenner (Brenner, 1974) and since then, they have been used extensively as a powerful genetic system. In fact, they have a number of experimental advantages: they are easy to maintain (the worm reproduces rapidly and prolifically, with a life cycle of three days and a short generation time) and are amenable to genetic analysis, with the availability of a large mutant collection (Kaletta and Hengartner 2006).

These organisms are ideal candidates as models for mitochondrial diseases, which affect basic processes that are conserved throughout evolution. Structure and bioenergetics of the nematode MRC are very similar to those of mammalian MRC. Mitochondrial dysfunction can often present in a tissue-specific fashion, affecting those tissues with the highest demand for MRC-generated ATP; *C.elegans* is a sophisticated multicellular animal: the adult hermaphrodite has only 959 cells, but they are organized in distinct tissues, including muscle and nervous system.

The worm has been already successfully used as a model for mitochondrial disease: Grad et al. (2005) showed that nematode strains with complex I mutations exhibit characteristic features of human mitochondrial disease, including decreased rates of respiration and lactic acidosis, demonstrating how central mechanisms of pathogenesis in mitochondrial dysfunction can be disclosed with this simple model.

5.4.3.1 Knockdown of *COX19* in *C.elegans* by RNA interference

We developed a transient knockdown model of COX19 deficiency by RNA interference (RNAi) technology. This technique exploits small siRNA that can be easily delivered to nematodes either by direct cellular microinjection, soaking animals into a concentrated double-stranded RNA (dsRNA) solution, or by feeding animals with dsRNA-containing food (Timmons 2006).

RNA interference (RNAi) was carried out as described previously (Timmons et al 2001; Kamath et al 2001). Full-length genomic or cDNA fragments (250-1000 bp length), homologue to *hCOX19* gene, were amplified with specific primers carrying adequate restriction sites and cloned into the bacterial expression vector pL4440 (Firelab vector, Addgene) that carries two promoters for T7 RNA polymerase facing each other. These constructs were then transformed into HT115DE3 (see table I in appendix II), a tetracycline-resistant *E.coli* strain that is deficient in Rnase III and can express T7 RNA polymerase from an IPTG-inducible promoter, in order to produce high quantities of specific dsRNA fragments. These engineered bacteria are able to induce a strong and gene-specific interference when fed to *C.elegans*.

Since silencing efficiency is affected by many influencing factors, such as worm strain, incubation temperature and IPTG induction, we employed as control worms feeding with bacteria transformed with the pLT61.1 vector (FireLab, Addgene), a pL4440-derived plasmid carrying the unc-22 gene, which is required for a proper movement of the worm.

Silencing of unc-22 confers a visible phenotype and was used as control of dsRNA expression.

Bacteria lawns were prepared by adding 75 µl of a saturated overnight culture to a 3.5 cm nematode growth medium (NMG) plate containing 1 mM IPTG, ampicillin 100 µg/ml and tetracycline 13 µg/ml. The plates were incubated overnight at 37°C to induce expression of T7 RNA polymerase from the IPTG-inducible promoter.

To obtain COX19-silenced nematode populations, we started feeding with transformed *E.coli* cells and we performed all the following experiments after at least three generations.

5.4.3.2 Phenotypic characterization of COX19-silenced worms

We performed a thorough characterization of the silenced worms. Since growth, reproduction and aging are biological processes that depend on the integrity and function of the MRC, at first we measured brood size and lifespan to characterize the phenotype in RNA-interfered nematodes.

Brood size was determined as described by Stiernagle (1999), using the wild-type N2 Bristol strain (see tab I in appendix II). In brief, a population of decontaminated synchronized animals was prepared, L1 larva were plated on RNAi plates and grown for one generation. Individual L4 animals were put on separate plates, incubated at 20°C and monitored daily during egg laying; nematodes were transferred every day to fresh plates to keep them separate from their progeny. Plates with eggs were incubated an additional 24 hours to allow hatching and larvae counted. This continued until adult animals no longer laid eggs. As shown in figure 12A, COX-19-silenced worms (expressing dsRNA specific for both genomic or cDNA) display a significant decrease in reproductive capabilities.

For lifespan measurements, FER-15 strain was used (see tab I in appendix II), a temperature-sensitive mutant strain, which is sterile at 25°C. Synchronized L1 larva were transferred on RNAi plates and grown for one generation at 20°C. Gravid adults were allowed to lay eggs on unseeded plates for 6 h at 20 C. Once hatched, L1 animals were transferred to separate plates and incubated at 25°C. About 120 worms for each RNAi population were grown onto RNAi NGM plates and monitored daily for survival. Alive worms proportion was estimated by reaction upon physical contact with a platinum wire and scored as dead when they no longer responded to gentle prodding on the head. Dead

worms were removed from the plate by aspiration. Survival curves are shown in figure 12B and 12C and were compared using the logrank test. COX-19 silenced nematodes exhibit an increase in longevity when compared to worms fed on bacteria transformed with the empty vector. The difference is statistically significant, with p values lower than 0,0001.

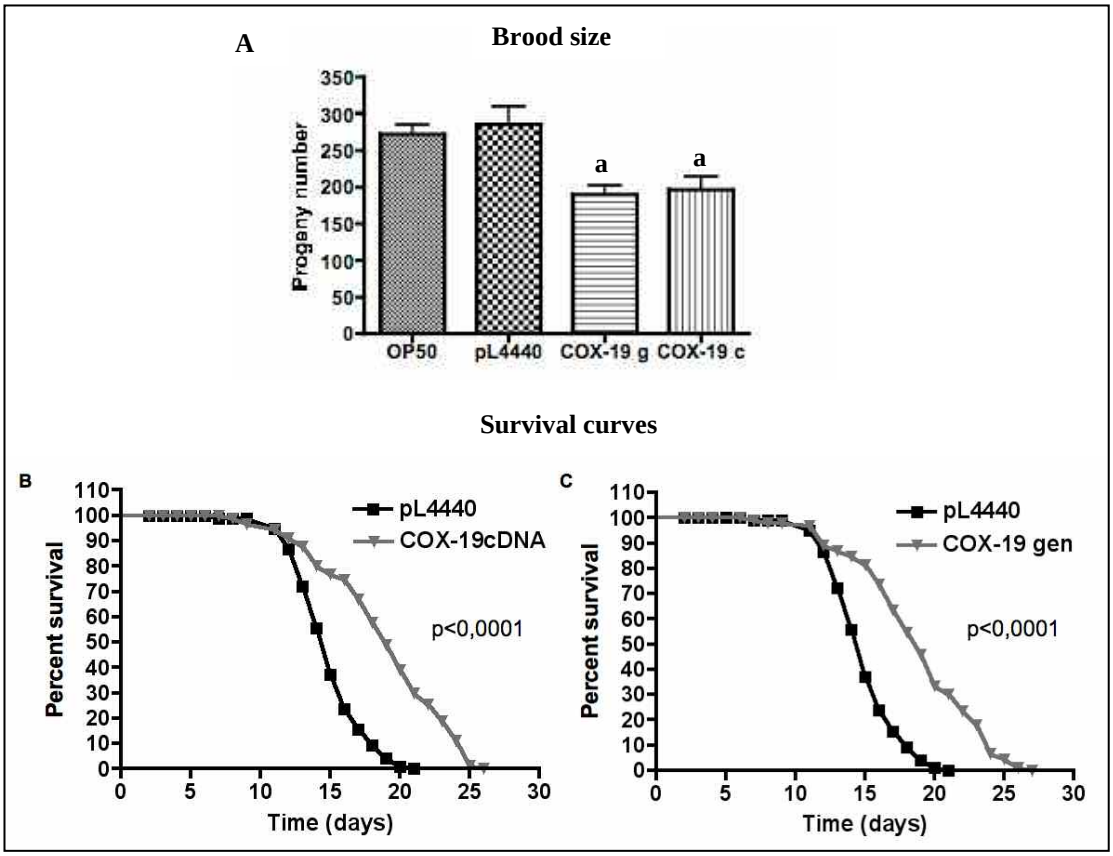

Fig. 12. (A) Brood size measurements. Values are the average of 24 broods counted. OP50 = worms fed on OP50 E.coli bacteria (the routinely used food source); all the other animals were fed on HT115DE3 bacteria transformed with the empty vector (pL4440), COX-19 genomic (COX-19 g) or COX19 cDNA (COX-19 c) pL4440-derived plasmids. Data were compared using a Mann-Whitney test (a = statistically significant, with a p<0,05). Lifespan measurements: survival curve of nematodes fed on bacteria expressing cDNA (B) or genomic of COX-19 (C) were compared with that of worms fed on bacteria transformed with the empty vector. Values are the averages of 120 animals.

Interestingly, COX-19 silencing in worms confers a phenotype similar to that of a large class of mutant with disruptions in genes essential for the function of MRC, the so-called *Mit* mutants, many of which are long-lived and less fertile (Rea et al 2007; Tsang et al 2001). The phenomenon of life extension caused by loss of critical genes is still controversial and has not found a comprehensive explanation. Since many studies suggest a connection between increased oxidative stress and aging (Muller et al 2007), the oxidative stress theory states that reduced reactive oxygen species (ROS) production

would decrease extraneous cellular damage. Nevertheless, other findings demonstrated that there is almost no alteration in the degree of oxidative damage occurring in some long-lived mit mutants (as atp-3 *Mit*, Dillin et al 2002). According to the "mitochondrial threshold effect theory", cells have the ability to counter reduction in MRC function up to a certain threshold but after this point, cell viability is compromised. *Mit* mutant animals would operate their mitochondria at a level somewhere below normal but above that which results in pathology. It is likely that they manage this feat by actively invoking processes that directly compensate for their altered MRC function. These same processes would be responsible for their increased lifespan.

5.4.3.3 Biochemical characterization of COX19-silenced worms

In order to confirm that the reported phenotype was effectively due to an effect of COX-19 loss of function on MRC, we characterized the biochemical phenotype.

Nematodes were grown in liquid culture as described, using S medium and concentrated bacteria stocks as food source (Lewis and Fleming, 1995). In this experiment, we used the RRF-3 strain, a mutant strain showing an increased sensitivity to RNAi (see tab I in appendix II). Worms in liquid medium were grown at 200 r.p.m. in a rotary shaker at 20ºC. Overnight saturated LB-grown *E. coli* bacteria cultures were used to make a concentrated pellet of bacteria, worms were monitored daily and concentrated bacteria were added when food supply was depleted. Once the culture was saturated, nematodes were harvested and alive worms were collected with the sucrose flotation method (Johnstone, 1999). *C.elegans* mitochondria purification was performed as previously described (Grad et al. 2005) and, after determination of protein content, purified mitochondria fraction was directly used to measure mitochondrial activities. Enzymatic activities of individual MRC complexes were measured spectrophotometrically as previously described (Larsen and Clarke, 2002), using 25–50 μg of disrupted mitochondrial protein.

COX-19 silenced worms display a decrease in COX activity (normalized to both CS activity and protein content) (fig.13A). We checked by Western blot the levels of a mtDNA-encoded COX subunit: worm mitochondrial protein were separated on a 12.5% SDS-PAGE and blot as above. Membrane was stained with a mouse monoclonal antibody against human COX I, stripped and reprobed with a goat serum against nematode clk-1, a mitochondrial protein. The relative amounts of protein were quantified as above. As

shown in figure 13B and 13D, COX I levels are decreased of about three times compared to the control, suggesting that COX defect is due to a failure in enzyme maturation.

Impaired complex IV-dependent respiration will lead to blockage in electron transport, favoring the reduction of pyruvate to lactate. We therefore measured lactate concentration in controls and silenced-animals, starting from liquid RRF-3 cultures incubated at 20°C. Animals were harvested and aliquots counted to determine the approximate worm concentrations of cultures (approximately 1.0 10^6 animals); after repeated washing, proteins were precipitated with 5% trichloroacetic acid. Worms were then sonicated on ice and the obtained lysate was centrifuged to pellet precipitate and debris. The supernatant was neutralized with 5 N KOH and clarified with a second centrifugation. Lactate concentrations were measured using Randox diagnostics kits (Randox). We found a marked increase in lactate concentrations in the COX19-silenced nematodes compared with controls (fig.13C).

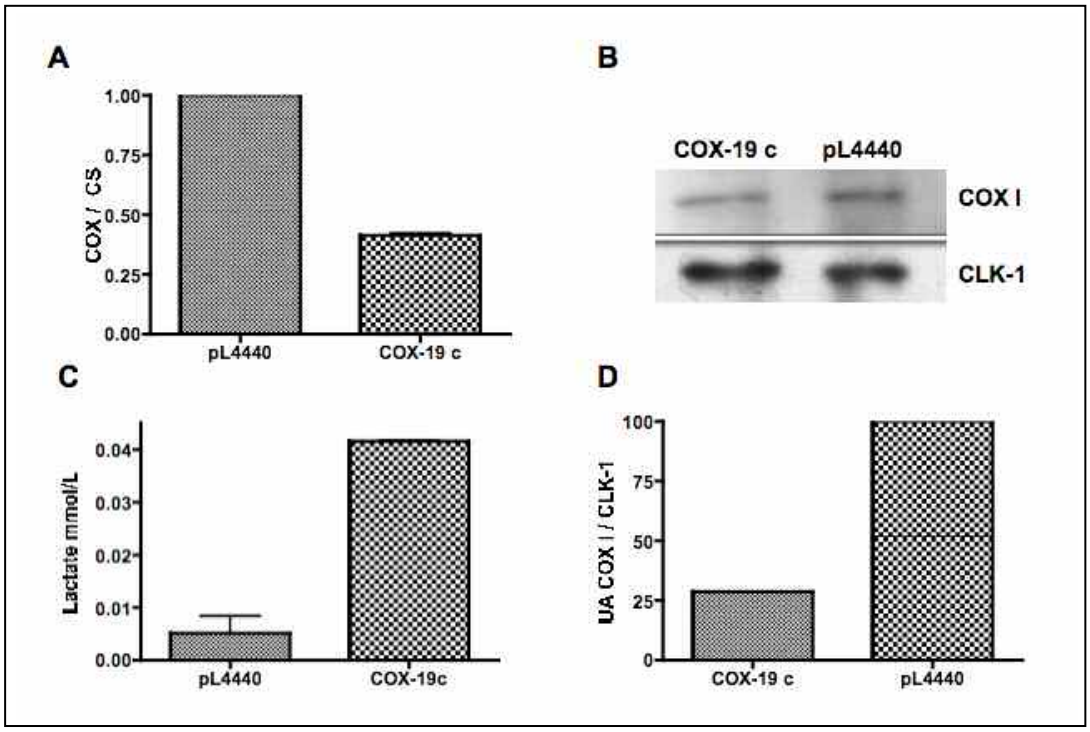

Fig. 13. (A) COX activity in COX-19 cDNA-silenced nematodes and controls fed on bacteria with the empty vector. Activity is expressed as % of controls and is normalized to CS activity and protein content. (B) Western blot analysis of mitochondrial proteins from COX-19 silenced animals and controls (pL4440) (D) Relative amounts of COX I proteins: COX I levels were quantified by densitometry and normalized to CLK-1 levels. (C) Lactate measurements in COX-19-silenced worms and in control pL4440; values are expressed in mmol/L.

Interestingly, COX19-silenced nematodes displayed features that parallel those elicited by mutations in other COX-assembly genes, such as lactic acidosis and decreased COX-dependent mitochondrial respiration.

These result confirm the value of *C.elegans* to study isolated COX deficiency and underline how in the absence of a loss-of-function mutant model, it is possible to create a phenocopy through RNAi.

5.4.3.4 Double knockdown of COX-19 and COX-17

RNAi in worms allowed the rapid silencing of either single genes or gene pools. Hence, we decided to explore the consequences of a double knockdown affecting two COX-assembly genes involved in the same pathway: copper delivery to COX. At this purpose, we amplified COX-17 cDNA sequence and cloned it into pL4440, as described above. This plasmid was transformed in HT115DE3 bacteria. Two overnight bacterial cultures, expressing dsRNA specific for COX-19 and COX-17, were grown. Before plating on NMG plates, the two saturated cultures were mixed in a 1:1 ratio. We started silencing experiments with RRF-3 strain and we performed a fertility assay on the double-silenced animals as described above. As reported in figure 14, unlike COX-19 silenced worms, whose decreased brood size is comparable with the first experiment performed with N2 (fig.12a), COX-17 silenced animals display an almost total loss of reproductive capabilities. The double-silenced animals show a less pronounced effect, probably because the simultaneous knockdown of two genes causes a lower efficiency of silencing.

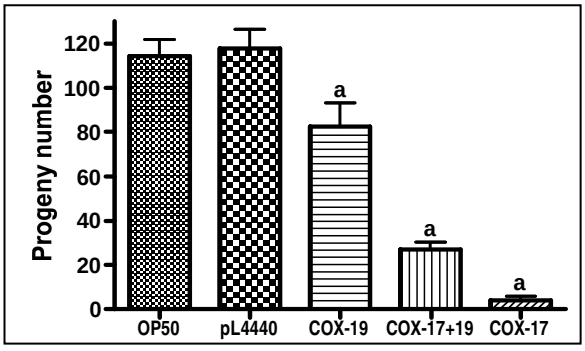

Fig. 14. Brood size measurements. Values are the average of 24 broods counted. Legend as in fig.12A (COX17+19 = double silencing of the two genes, see text for details). Data were compared using a Mann-Whitney test (a = statistically significant, p < 0,05).

While performing this experiment at the binocular dissecting microscope, we realized that COX-17 silenced nematodes carried morphologic abnormalities and appeared smaller compared to the controls. So, we performed a morphologic analysis. Worms were synchronized and L1 individuals were put on separated plates. 72 hours after hatching, worms were prepared and mounted as described by Sulston (Sulston et al 1983): animals were anesthetized with sodium azide 25 mM, mounted on glass pads, and examined them under a Leica Sp2 confocal microscope equipped with differential interference contrast (Nomarski) optics. While control animals (fed on bacteria transformed with the empty vector) reached the adult stage, as pointed out by the size of about 1,2 mm (fig.15A) and by the completed gonadal development, silenced worms displayed a developmental delay, and remained at the L2 larval stage three days after hatching (fig.15B).

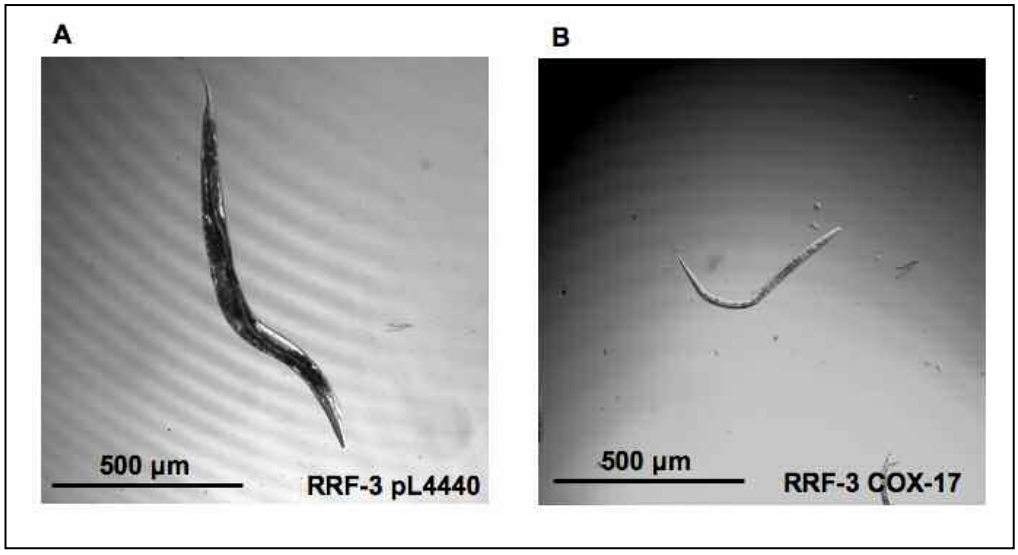

Fig. 15 DIC photographs of control (A) and COX-17 silenced worms (B) cultured at 20°C, 72 hours after hatching. Silenced worms display a developmental delay, and remain at the L2 larval stage 3 days after hatching.

5.4.3.5 Copper rescue experiments

Since COX17 have been shown to be involved in copper transport, we performed experiments with copper, in order to investigate whether its supplementation in the culture medium could rescue the developmental delay phenotype. In fact, several studies have shown that copper supplementation can bypass defects in genes of the Cu delivery pathway (Mattatall et al. 2000; Glerum et al. 1996; Rae et al. 1999, Salviati et. al 2002b).

For copper rescue experiments, NMG solution was supplemented with different volumes of $CuSO_4$ solution just prior to its being poured, in order to obtain plates with the following $CuSO_4$ final concentrations: 25 µM or 50 µM or 100 µM. Bacteria expressing dsRNA were then plated and allowed growing overnight at 37°C. Individual L1 animals were transferred to single plates and observed with a binocular dissecting microscope 72 hours after hatching (fig.16).

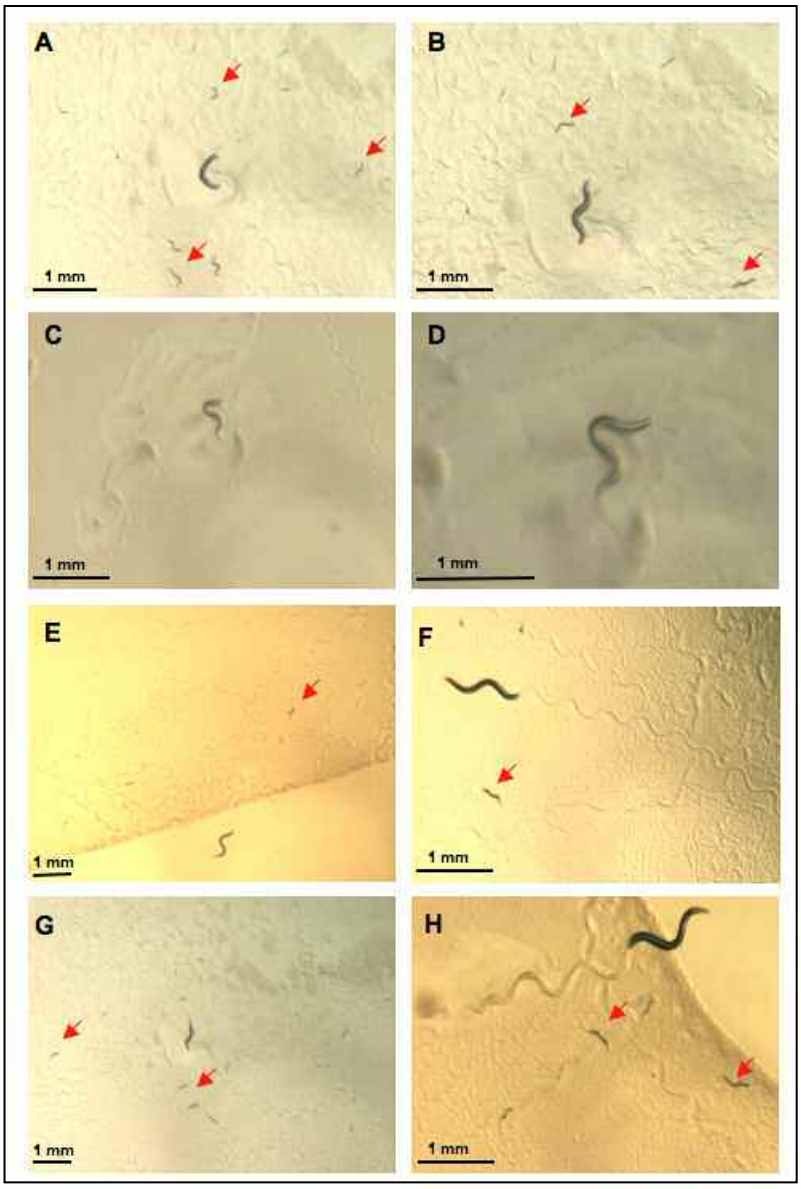

Fig. 16 Photographs at the binocular dissecting microscope of RRF-3 nematodes cultured at 20°C, 72 hours after hatching. Control animals fed on pL4440-transformed bacteria (A and B); COX-17 silenced worms (C and D); COX-17 silenced worms cultured on NMG plates supplemented with 25 µM (E and F) or 100 µM (G and H). Red arrows indicate larva.

Unlike controls fed with pL4440-transformed bacteria (fig.16A and B), no progeny could be detected in plates of cox-17 silenced animals after three days from hatching (fig.16C and D) which retained size and morphologic features characteristic of larval stage; in plates supplemented with 25 μM of copper sulphate some larva could be observed (fig.16E and F), while in presence of 100 μM the brood size was comparable to control animals (fig.16G and H), suggesting that the silenced animals in the presence of copper could reach the adult stage and become fertile.

We examined the same worms under the confocal microscopy as above.

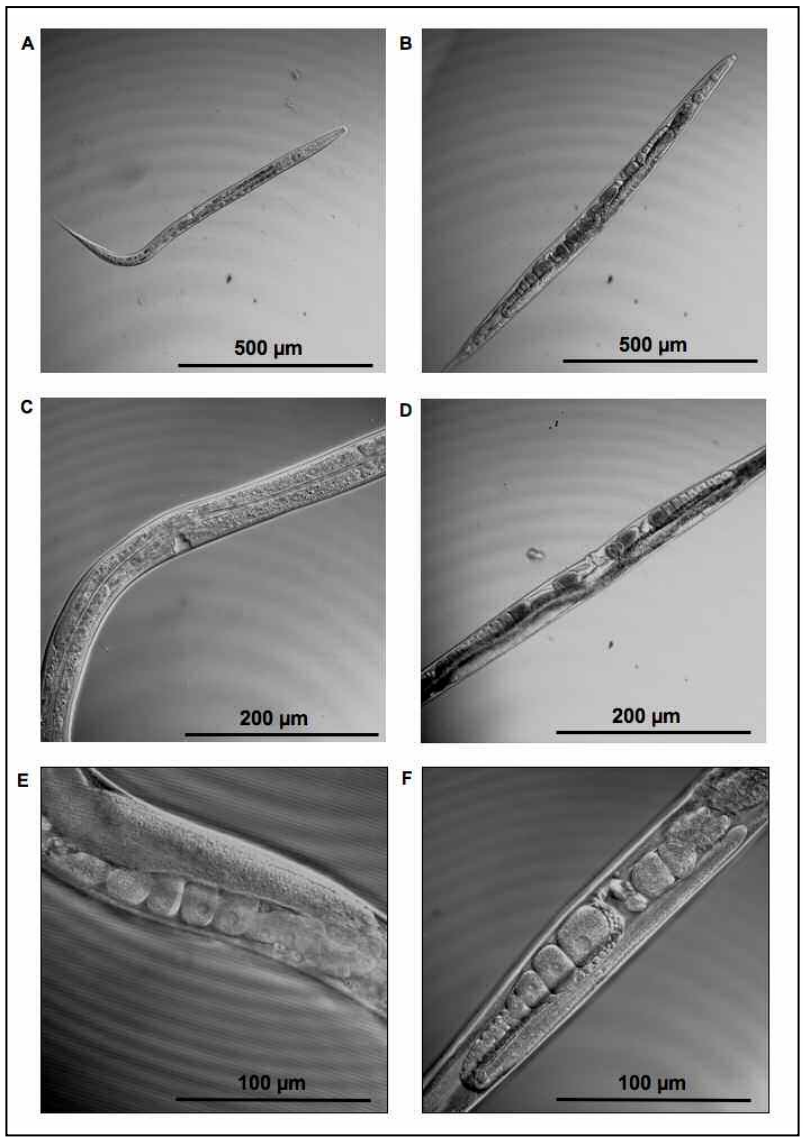

Fig. 17 Nomarski photographs of COX-17-silenced animals grown in normal NMG medium (A) or in medium supplemented with 100 μM $CuSO_4$ (B) 72 hours after hatching. In (C) and (D) magnifications of corresponding reproductive apparatus are reported, showing impaired vulva and gonadal development in COX-17 silenced worms (C), which is rescued in presence of copper (D). In panel (F) gonadal apparatus of a COX-17 silenced worm in presence of 100 μM $CuSO_4$ displays the same morphological features of an adult control animal (E).

Morphological examination confirmed that COX-17-silenced nematodes showed a developmental delay (fig.17A), with impairment in vulva and gonadal apparatus (fig.17C); these abnormalities are completely rescued in the presence of copper: the animals fully develop reaching the adult stage (fig.17B), vulva (fig.17D) and reproductive apparatus (fig.17F) are comparable to wild-type worms (fig.17E).

6. CONCLUSIONS

COX biogenesis is a complex process involving several genes, many of which remain unidentified. Our experiments provide preliminary data on three novel human COX-assembly genes and underscore the complexity of COX-assembly process in humans. *hCOX16*, *hCOX18* and *hCOX19* represent attractive candidates to be screened in patients with isolated COX deficiency without mutations in other known COX-assembly genes. In fact, the etiology of this disease in most cases remains unidentified and reaching a definitive molecular diagnosis allows not only rational genetic counseling, but also prenatal diagnosis.

Moreover, we developed a *C.elegans* knockdown model of isolated COX deficiency by RNAi, in order to disclose the pathogenetic mechanisms of this disorder. We observed that COX-19 silenced worms display COX deficiency (both of biochemical activity and protein content) and lactic acidosis, recapitulating the phenotype observed in patients with mutations in COX assembly genes. In fact, lactic acidosis resulting from impaired utilization of pyruvate by the citric acid cycle, increased glycogen utilization, and increased glycolytic activity, is a hallmark of complex VI dysfunction and of mitochondrial disease in general (DiMauro et al, 2004b).

COX-19 silenced animals have a decrease in reproductive capabilities (as measured by their brood sizes) and an increase in lifespan, similarly to the phenotype of worms mutated in other genes involved in the biogenesis of the mitochondrial respiratory chain (*Mit* mutants). In fact, oogenesis requires the synthesis of large numbers of copies of mitochondrial DNA as well as the storage of maternally-derived products needed to support embryonic and early larval development (Tsang et al 2002, 2003). It is not surprising that a normally functioning MRC is needed for reproductive fitness. The phenotype is even stronger by silencing COX-17, another COX-assembly gene which acts as a copper chaperone for COX, and can be rescued by supplementing nematode growth media with copper sulphate.

To our knowledge, only experiments with complex I defects and ubiquinone biosynthesis had been carried out in *C.elegans* to date. These preliminary data suggest that *C.elegans*, although it represents a lower metazoan model of mammalian COX defects, can be successfully used as a model to investigate the molecular mechanisms of pathogenesis of isolated COX deficiency. Furthermore, it constitutes a useful biological tool for drug screening in COX deficiency forms due to copper-chaperone genes defects, such as SCO1 and SCO2, providing important insights on the role of copper supplementation as

therapeutic approach. The possibility to test the efficacy of copper to bypass a genetic defect opens new potential therapeutical applications for these severe forms of mitochondrial diseases, which are still without an effective treatment. Finally, the same technique could be applied to other COX assembly genes, in order to obtain simple, yet more sophisticated than yeast, models of COX deficiency.

SECTION IV

UBIQUINONE DEFICIENCY

7. COENZYME Q

Coenzyme Q (CoQ) or ubiquinone (2,3-dimethoxi-5-methyl-6-decaisoprenyl-1,4 benzoquinone in humans) is a membrane-bound small lipophilic molecule located in the MIM, where it functions in redox chemistry. It is composed of a redox active benzoquinone acid ring and a lipophilic polyisoprenoid tail (fig.18). Its small size and lipophilic properties allow CoQ to freely diffuse in the double-layer of the MIM. In fact, it is an essential component of the MRC, acting as electron shuttle between flavine-linked dehydrogenases (complexes I and II) and complex III (Brandt and Trumpower 1994).

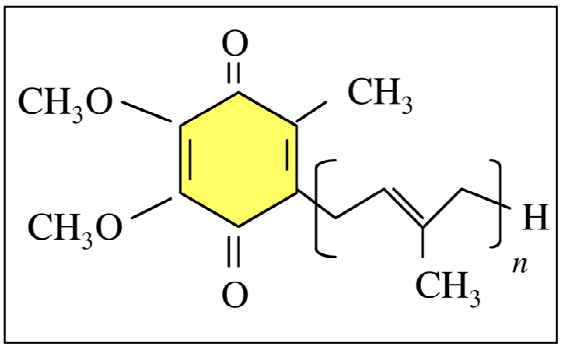

Fig.18 Structure of Coenzyme Q. *n* designs the length of the polyisoprenoid chain that varies in different species (10 in *H.sapiens*, 6 in *S.cerevisiae*, 9 in *C.elegans*)

CoQ is involved in a number of aspects of cellular metabolism: it acts as a chain-breaking antioxidant of lipid-peroxyl radicals, representing the only lipophilic antioxidant synthesized in all aerobic eukaryotes; it plays a role in stabilizing the bc1 complex (Santos-Ocana et al 2002), and participates in extra-mitochondrial electron transport chains of lysosomal and plasma membranes; (Turunen et al 2004; Littarru and Tiano 2007). Moreover, it is involved in regulation of mitochondrial permeability transition pore (Fontaine et al 1998) and it is required for the activation of mitochondrial uncoupling proteins (Echtay et al , 2000).

7.1 Coenzyme Q biosynthesis

Although the physiological significance of CoQ is extensively investigated in eukaryotes, its biosynthesis, which consists of multiple enzymatic steps, has not been fully characterized. Current knowledge about the CoQ biosynthetic pathway in eukaryotes is mostly derived from characterization of CoQ-deficient mutant strains of *S.cerevisiae* (Tran et al 2007): so far, nine complementation groups of CoQ (*coq1* through *coq9*) and a partially respiratory deficient mutant (*coq10*) have been identified (Tzagoloff and Dieckmann 1990; Barros et al 2005). Cells generally rely on *de novo* synthesis of CoQ, which starts with formation of a hydroxybenzoic acid head group and a lipophilic polyisoprenoid tail, that are finally condensed. The benzoquinone ring is synthesized from tyrosine, an essential amino acid in mammals, which is converted into 4-hydroxybenzoic acid (4-HB); dimethylallyl diphosphate and isoprenyl diphosphate are the precursors for the synthesis of the polyisoprenic side chain and derive from a series of reactions which are common to cholesterol and dolichol biosynthesis (fig.19).

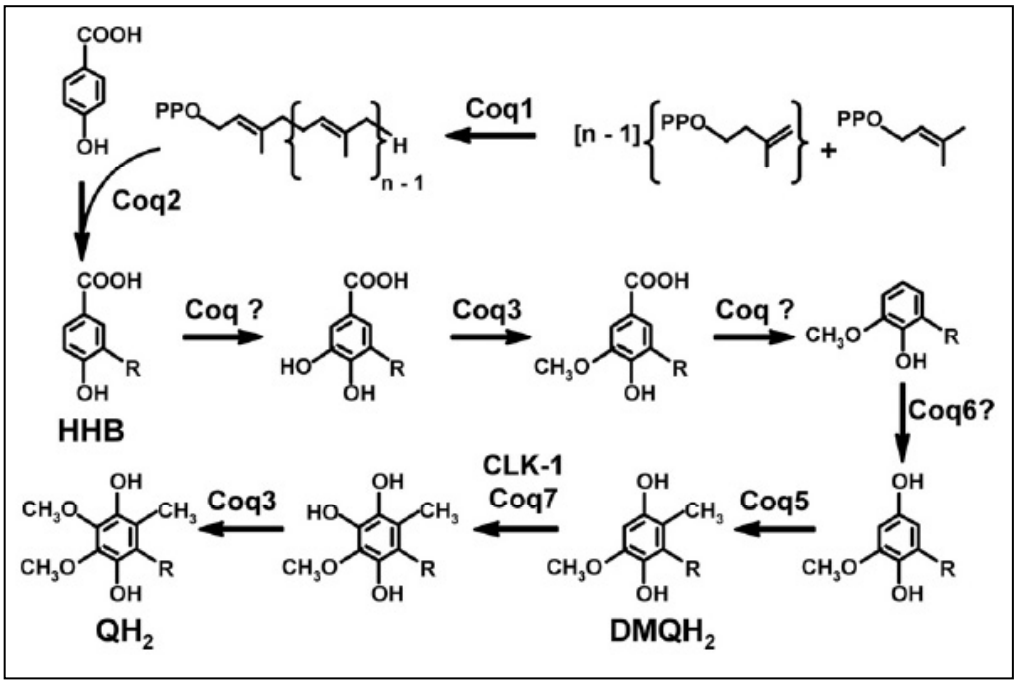

Fig.19 CoQ biosynthetic pathway in eukaryotes (from Tran et al 2007).

Polyprenyl diphosphate synthase (*coq1*) is the first enzyme of the biosynthetic pathway, which assembles the polyisoprenoid tail and is responsible for determining the number of isoprene units that varies in different species (fig.18); next, *para*-hydroxybenzoate-polyprenyl transferase (*coq2*) catalyzes the formation of a covalent bond between the benzoquinone head group and the tail, producing the first intermediate: 4-hydroxy-3-polyprenyl benzoic acid (HHB). The structure of the aromatic ring is then modified through a series of reactions (hydroxylation, decarboxylation, *O* and *C*-methylation,), which are required to generate the fully substitute hydroquinone. Yet, the order of these reactions is speculative, as only few of the intermediates are known (such as 5-demethoxyubiquinol $DMQH_2$).

Previous genetic and biochemical data have provided numerous lines of evidence that Coq polypeptides and the CoQ intermediates generated by these proteins are arranged in a CoQ biosynthetic complex (Gin and Clarke 2005; Tran et al 2007), which would allow a coordinative regulation of components and enhance catalytic efficiency. A proposed model for this multi-subunit complex, in which Coq2 serves as anchor to the MIM is depicted in figure 20 and its putative components are reported in table 4.

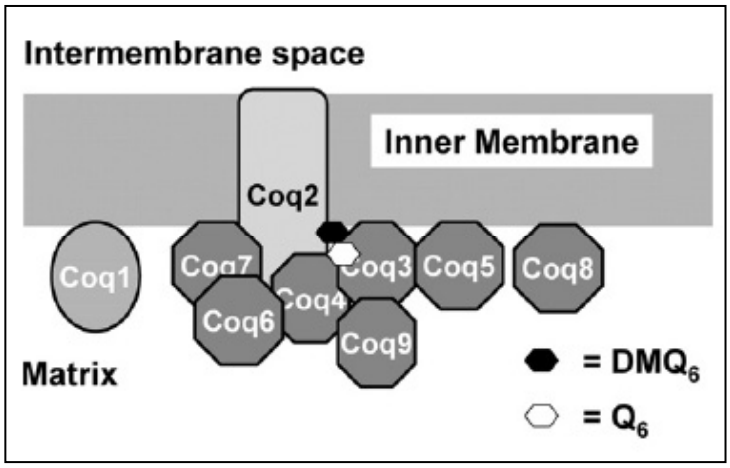

Fig.20 A model of the mitochondrial Q biosynthetic protein complex in *S. cerevisiae*. The putative complex includes Coq3, Coq4, Coq5, Coq6, Coq7 and Coq9 (that are peripherally associated with MIM), Coq2 (a spanning integral membrane) and, among lipid components, the intermediate DMQ6 and the final product Q6 (from Tran et al 2007).

All the enzymes required for CoQ biosynthesis are encoded by nuclear genes and are highly conserved among species. Mammalian homologues have been identified via sequence homology. In table 4, the main characteristics of the ten yeast coq proteins required for CoQ biosynthesis and of their human homologues are depicted.

For some of the human genes (*coq2*, *coq3* and *coq7*), it has been demonstrated a conserved enzymatic role, based on the ability of functionally complement the corresponding yeast mutant strain (Forsgren et al 2004; Jonassen and Clarke, 2000; Vajo et al 1999). Polyprenyl diphosphate synthase (*coq1*) in humans is a heterotetramer of two subunits, *PDSS1* and *PDSS2*, while in yeast functions as homo-oligomers. Expression of both human subunits in deleted yeast strains restores CoQ production (Saiki et al 2005). In humans, there are not available data about *coq4*, *coq5*, *coq6*, *coq8*, *coq9* and the recently identified *coq10*.

Table 4. Characteristics of the ten genes involved in CoQ biosynthesis in *S.cerevisiae* and of their human homologues.
(* NCBI Blastp score > 150. ** Blastp score > 200. # Blastp score > 50;
[a]There are two human homologues for coq10).

Yeast gene	Mitochondria localization	Component of Q biosynthetic complex	Complementation of yeast mutants by human homolog	Human homologue
coq1	Peripheral i.m. matrix side	Unknown	Yes	PDSS1/PDSS2
coq2	Integral i.m. matrix side	Yes	Yes	COQ2
coq3	Peripheral i.m. matrix side	Yes	Yes	COQ3
coq4	Peripheral i.m. matrix side	Yes	Unknown	NP_057119*
coq5	Peripheral i.m. matrix side	Yes	Unknown	CAI46073**
coq6	Peripheral i.m. matrix side	Yes	Unknown	NP_872282**
coq7/cat5	Peripheral i.m. matrix side	Yes	Yes	Clk-1/COQ7
coq8/abc1	Peripheral i.m. matrix side	Unknown	Unknown	Adck-1–Adck5
coq9	Peripheral i.m. matrix side	Yes	Unknown	AAH54340#
coq10	Integral i.m.	Unknown	Unknown	NP_653177*[a] NP_079423*[a]

7.2 Coenzyme Q10 deficiency

Coenzyme Q deficiency (MIM #607426) is a rare autosomal recessive disease, described for the first time in 1989 (Ogasahara et al 1989). This disorders is due to a defect in the biosynthetic pathway of CoQ and, unlike most MRC defects, for which there is no effective therapy, is treatable; in fact patients respond well to oral CoQ supplementation. This makes early diagnosis of critical importance in the management of these patients.

Traditionally, CoQ deficiency has been classified in three major clinical phenotypes:

1. a myopatic form (Ogasahara et al 1989; Boitier et al 1998; Lalani et al 2005) which is characterized by recurrent myoglobinuria, exercise intolerance, and also CNS involvement (with seizures, ataxia or mental retardation);

2. a childhood-onset ataxia (Musumeci et al 2001; Lamperti et al 2003), which is dominated by ataxia and cerebellar atrophy, with varying involvement of the CNS, muscle and peripheral nerve;

3. a third multisystemic infantile variant, described thus so far in six families (Rötig et al 2000; Rahman et al 2001; Salviati et al 2005; Quinzii et al 2006; Lopez et al 2006; Mollet et al 2007) which manifests with encephalomyopathy and renal involvement.

In the first two variants the onset is in infancy or early childhood and the progression is relatively slow; CoQ defect is apparently confined to neuromuscular tissue, while fibroblasts and lymphoblastoid cells show normal or only moderately decreased levels of ubiquinone. The third form instead manifests very early in infancy and is associated with a generalized CoQ deficiency, in which ubiquinone levels are markedly reduced both in muscle and in fibroblasts or lymphoblastoid cells.

Recently, a distinction between primary and secondary CoQ defects has been proposed: primary forms are due to defects in the CoQ biosynthetic pathway, whereas secondary deficiencies involve genes unrelated to CoQ biosynthesis (DiMauro et al 2007). Primary defects have been associated with the earliest and most severe variant of CoQ deficiency: the multisystemic infantile form.

Although >30 patients have been described with CoQ deficiency, the genetic bases of this disorder are largely unknown and in most patients the etiologic diagnosis remains elusive. Since in humans CoQ is almost completely synthesized endogenously, it has been assumed that these diverse syndromes are all due to primary CoQ deficiency, and the different clinical phenotypes have been attributed to blocks at different levels in the biosynthetic pathway of ubiquinone.

So far, the molecular defects have been identified in only three families. In the first family, our group, in collaboration with the Columbia University of New York, has identified a homozygous missense mutation in *COQ2* gene in two siblings with infantile encephalomyopathy and nephrotic syndrome (Salviati et al 2005, Quinzii et al 2006). In the second family, Lòpez et al (2006) reported the identification of compound heterozygous mutations in the *PDSS2* gene in a patient with severe Leigh syndrome, nephrotic syndrome and CoQ deficiency in muscle and fibroblasts. Finally, Mollet et al

(2007) described two unrelated families with the multisystemic variant carrying mutations respectively in the *PDSS1* gene and in the *COQ2* gene.

The documentation of mutations in CoQ synthetic genes confirms the existence of primary CoQ deficiency. In fact, *PDSS1* and *PDSS2* encode the two subunits of decaprenyl diphosphate synthase and *COQ2* encodes PHB-polyprenyl transferase, the first two enzymes of the CoQ biosynthetic pathway.

In secondary forms, etiology is unknown in most cases. Yet, recently a homozygous mutation was identified in the aprataxin gene, *APTX* (MIM #606350), which is known to cause ataxia and oculomotor apraxia 1 (AOA1 [MIM #208920]), in three siblings and a cousin with cerebellar ataxia and CoQ deficiency (Quinzii et al 2005); moreover, Aeby et al (2007) described a patient who presented a cardiofaciocutaneous syndrome, confirmed by the presence of a pathogenic R257Q *BRAF* gene mutation, together with a muscular CoQ10 deficiency.

All these findings supports the hypothesis that both the myopatic and ataxic forms are genetically heterogeneous entities in which CoQ deficiency can be secondary, while primary CoQ deficiency is a clinical homogeneous variant due to mutations in one of the genes required for ubiquinone biosynthesis (DiMauro et al 2007).

Identification of the molecular causes of the CoQ deficiency allows early and accurate diagnosis and the differentiation between primary and secondary forms; this is particularly critical because patients with primary defects respond dramatically to replacement therapy, while prognosis for patients with secondary forms is less favorable.

8. SPECIFIC AIM

Since in humans CoQ biosynthesis is still poor characterized and given the importance of identifying molecular bases of primary CoQ deficiency, our aims were the study of the molecular defect in a family affected by ubiquinone deficiency and the characterization of other unknown human homologues of yeast coq genes.

9. RESULTS AND DISCUSSION

9.1 A family with CoQ deficiency

We reported a 33-month-old boy (patient 1) with infantile encephalomyopathy, nephropathy, and deficiency of CoQ. The disease appeared to be an autosomal recessive trait because the patient's parents were first cousins and his 9-mo-old sister with nephropathy also had CoQ deficiency in fibroblasts. The proband presented with a severe nephrotic syndrome, which was resistant to steroids and a renal biopsy showed focal and segmental glomerulosclerosis.

At age 18 months he manifested end stage renal failure and he required peritoneal dialysis; he developed a progressive encephalomyopathy, with hypotonia, mild psychomotor delay, optic atrophy, psychomotor regression, tremor, and new-onset status epilepticus with focal electroencephalogram abnormalities predominantly in the left occipital region. Brain MRI showed cerebellar atrophy, mild diffuse cerebral atrophy, and stroke-like lesions in the left cingulate cortex and subcortical area. Blood and cerebrospinal fluid lactate levels were normal. A muscle biopsy revealed myofibers with excessive SDH staining but no RRFs or COX-deficient fibers. Respiratory chain enzyme activities and CoQ content in muscle extracts and fibroblasts were measured as described (DiMauro et al 1987; Musumeci et al 2001) and are reported in table 5: decreased activities of complexes I+III and II+III (whereas other complexes had normal activities), are associated with a reduction in CoQ concentration both in skeletal muscle and in fibroblasts.

Table 5. Respiratory chain enzyme activities in muscle extracts and CoQ content measured in both fibroblasts and muscle of patient 1.

Assay	Control mean ±SD	Patient
complexes I+III (µmol/min/g fresh tissue)	1.02 ± 0.38	0.38
complexes II+III (µmol/min/g fresh tissue)	0.70 ± 0.23	0.22
CoQ in skeletal muscle (µg/g fresh tissue)	32.1 ± 6.7	12
CoQ in fibroblasts (ng/mg protein)	105 ± 14	19

The patient started oral supplementation of ubiquinone (300 mg/day) and, after 8 months of therapy, the neurological manifestations improved dramatically, while there was no improvement in renal function. In fact, renal damage had progressed beyond the possibility of recovery (end stage failure) when therapy was initiated.

The 9-month-old sister (patient 2), born after an uneventful pregnancy, did not show any clinical or laboratory abnormalities. Her parents allowed a skin biopsy to establish fibroblasts culture, and CoQ levels were severely reduced (18 ng/mg protein). The sister developed a typical nephrotic syndrome (NS) immediately after the diagnosis; a kidney biopsy was performed showing a histological picture of minimal change and pedicle fusion and a very high number of mitochondria in the podocytes on electron microscopy (fig.21).

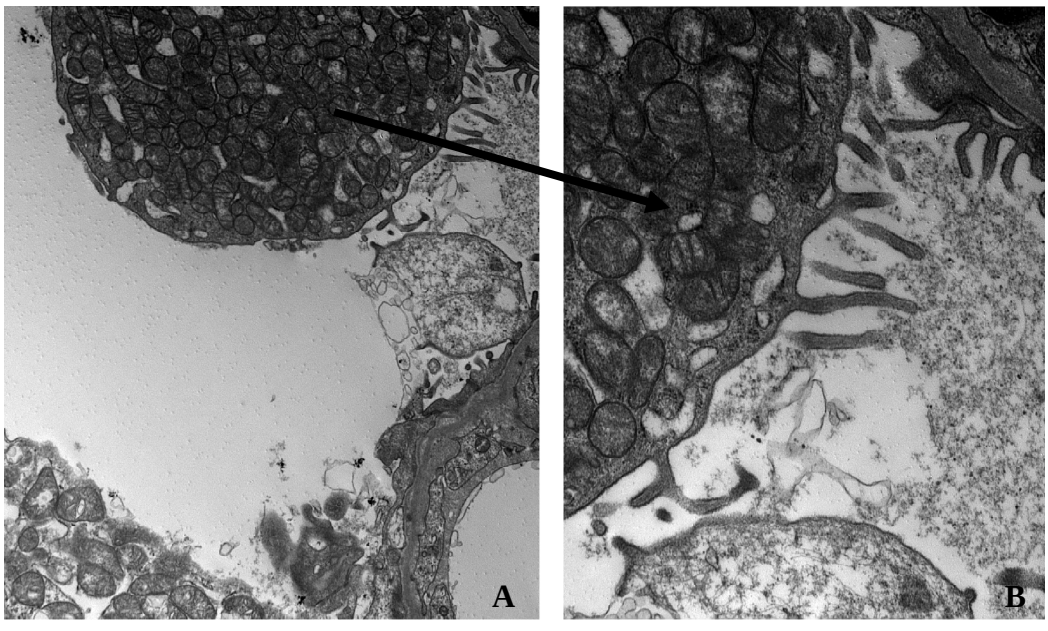

Fig.21 (A) Electron microscopy photograph showing podocytes with the cytoplasm completely occupied by mitochondria and hyperplasia of the podocyte villae. (B) Detailed view of the mitochondria, some of which appear dysmorphic with a reduced number of crests.

She was immediately treated with high-dose CoQ10 (30 mg/kg/day) with resolution of the NS in 20 days. Proteinuria persisted in the range of 0.5-1 g/day for 12 months and then almost completely resolved. After a follow-up of 30 months her renal function is normal, proteinuria is 0.22 g/day and has no neurological symptoms (fig.22).

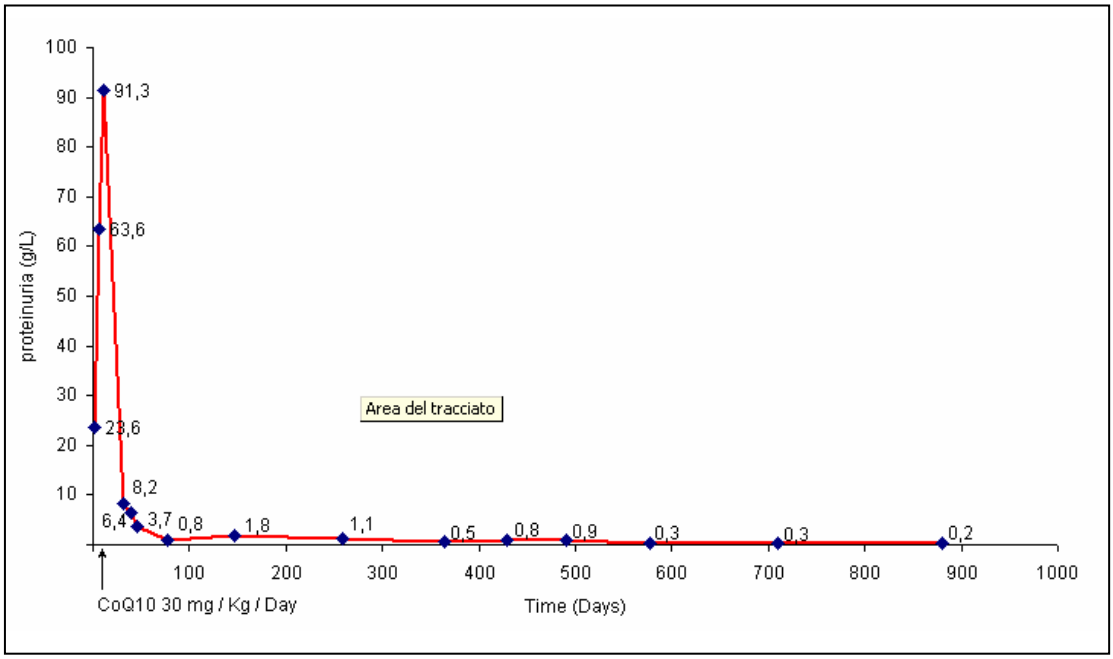

Fig.22 Time course of proteinuria of patient 2 after treatment with CoQ.

9.1.1 Effects of CoQ and uridine on patients' fibroblasts.

To confirm the consequences of reduced levels of CoQ on MRC, we measured the combined activities of complexes I+III and II+III (whose activity depends on CoQ) in fibroblasts of both patients. We then supplemented the medium with CoQ, since it has been proved that ubiquinone added to human cells reaches the MIM and acts on the MRC (Marbois et al 2005): fibroblasts, cultured in DMEM with 20% FCS, were incubated for 24 hours with serum-solubilized CoQ at a final concentration of 10 μM. As shown in table 6, enzymatic activities were decrease, but both complexes I+III and II+III activities were significantly increased after long-term incubation with CoQ.

Table 6. Effect of supplementation of CoQ10 on the CoQ-dependent mitochondrial complexes activities in human fibroblasts.
(*Activities are expressed as nmol/min/mg protein; [1]Significant versus no addition, $p<0,05$)
(P1= patient 1; P2 = patient 2).

Samples	Complex I+III*		Complex II+III*	
	No addition	10 μM CoQ10	No addition	10 μM coQ10
Control	410±36	445±27	3.5±0.23	3.8±0.41
P1	248±25	386±44[1]	1.7±0.02	3.6±0.12[1]
P2	301±37	480±56[1]	1.9±0.07	3.1±0.15[1]

These results support the cause of mitochondrial dysfunction on the deficiency and would explain the positive effects after the treatment of deficient patients with CoQ (Salviati et al 2005; Artuch et al 2006).

Patients' fibroblasts display slow rates of growth. To assess whether this phenotype was due to CoQ deficiency, we seeded 100 ± 20 cells/cm^2 and grown them in DMEM containing 20% FCS, supplemented with CoQ. CoQ supplementation significantly increases the growth of these cells (fig.23A). CoQ is required also for biosynthesis of pyrimidine nucleotides, being an essential co-factor of dihydro-orotate dehydrogenase, a MIM enzyme (Jones 1980). Thus, we incubated CoQ-deficient fibroblasts with uridine, showing that growth was also increased compared to control and fibroblasts from a patient with mitochondrial encephalomyopathy but without CoQ deficiency (fig.23B).

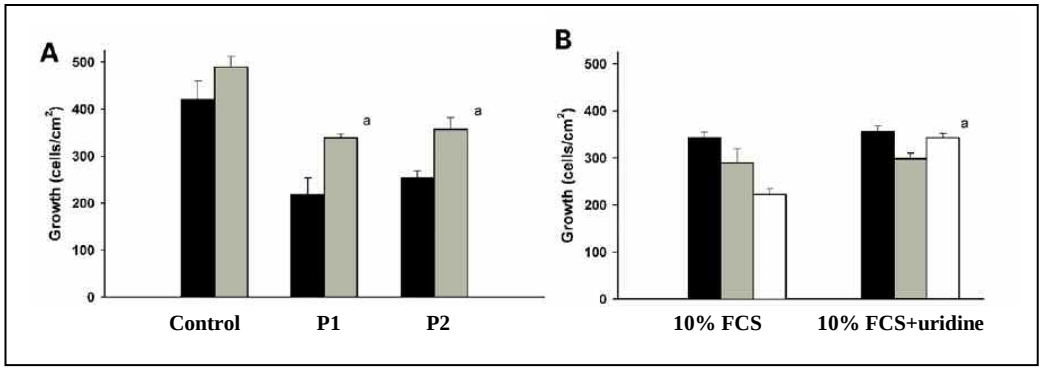

Fig.23 (A) Addition of CoQ to culture media induced significant increases of growth of fibroblasts of patients 1 and 2 (P1 and P2) harboring the *COQ2* mutation compared to control cells. Black bars: no CoQ. Grey bars: plus 10 µM CoQ.
a: Significant vs. no addition ($p \leq 0.01$).
(B) Growth of fibroblasts in media containing 10% FCS supplemented with 10 µM uridine. Black bars: control fibroblasts; grey bars: fibroblasts from a patient with MRC deficiency but normal concentration of CoQ; white bars: fibroblasts harboring *COQ2* mutation (patient 2). a: Significant vs. no addition of uridine ($p<0.05$).
Data were analyzed by using a two-way ANOVA with Tukey's post-hoc test.

Surprisingly, the effect of uridine addition was even more pronounced than that of CoQ, suggesting that this phenotype is largely due to an insufficient supply of nucleotides, rather than to a reduction in ATP production; yet, the lower efficiency of CoQ in rescuing the growth-deficient phenotype is probably due to a lower incorporation in cells (Turunnen et al 2004). Taken together, these data indicate that the pathogenicity of CoQ deficiency is related not only to a defect in bioenergetics, but also to an important impairment of pyrimidine metabolism.

9.1.2 Genetic analysis and biochemical assay

Since patients' parents were first cousins, we performed homozygosity mapping as described (Quinzii et al 2006), analyzing the chromosomal loci for eight human coq genes (*COQ1-COQ8*): three loci revealed homozygosity in the patients: chromosomes 14q24 (COQ6), 12q24 (COQ5) and 4q21 (COQ2). The three candidate genes were sequenced and only one missense mutation was found in COQ2: a homozygous A>G transition at nucleotide 890, which changes amino acid 297 from an aromatic residue (tyrosine), localized in a putative high conserved transmembrane domain of the Coq2 protein, to a polar uncharged cysteine (fig.24). The mutation was heterozygous in both parents and absent in DNA from 100 healthy controls (tested by RFLP analysis, using AflII restriction digestion of PCR-amplified DNA fragments).

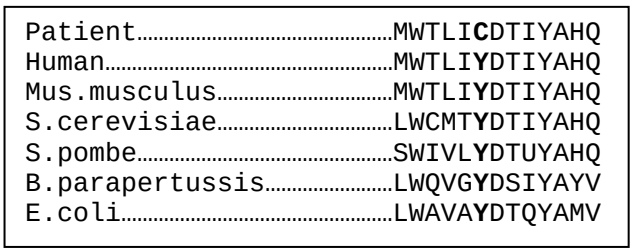

Fig.24 Evolutionary conservation of COQ2. Human amino acid 297 is normally tyrosine (Y). The A>G transition at nucleotide 890 changes amino acid 297 to cysteine.

Enzymatic activity of COQ2 was tested through measurement of incorporation of both the radiolabelled substrates in CoQ (para-hydroxybenzoate [^{14}C-PHB] and decaprenyl pyrophosphate [^{3}H decaprenyl-PP] as described (Quinzii et al 2006; Kalen et al 1990), revealing a marked decrease of radiolabelled CoQ levels in fibroblasts of patient 1 (22% of control means for the first assay and 36% of control means for the second one).

The high degree of conservation of tyrosine 297, the absence of the G>A890 transition of *COQ2* in 100 unrelated controls and the significantly reduced rate of radiolabelled PHB and decaprenyl-PP into CoQ in patient fibroblasts suggest that the mutation exerts its pathogenic effect by blocking ubiquinone biosynthesis.

This is the first molecular cause of primary CoQ deficiency and the first mutation identified in a CoQ biosynthesis gene.

9.1.3 Characterization of human *COQ2*

COQ2 encodes for Para-Hydroxybenzoate-Polyprenyl Transferase, which catalyses the condensation of PHB with the all-trans polyisoprenoid chain, the second step in CoQ biosynthesis (fig.19). This gene, which has been cloned and sequenced in different species, shows a high degree of sequence homology: all the homologues contain six potential membrane-spanning domains and an N-terminal mitochondrial leader sequence. Human *COQ2* cDNA (accession number #AJ621061) has been isolated from a muscle and liver cDNA library and, when expressed in yeast Coq-2 null mutant cells, rescues the growth of this yeast strain in the absence of a non-fermentable carbon source and restores CoQ biosynthesis (Forsgren et al 2004).

The reported human sequence cDNA contains an ORF of 1263 nt, encoding a protein of 421 amino acids, and is composed of seven exons. Interestingly, it shows four different in frame ATG initiation codons in exon 1 (the sequence reported by Forsgren et al starts from ATG number 1). The third ATG produces a transcript of similar length to the yeast gene (fig.25).

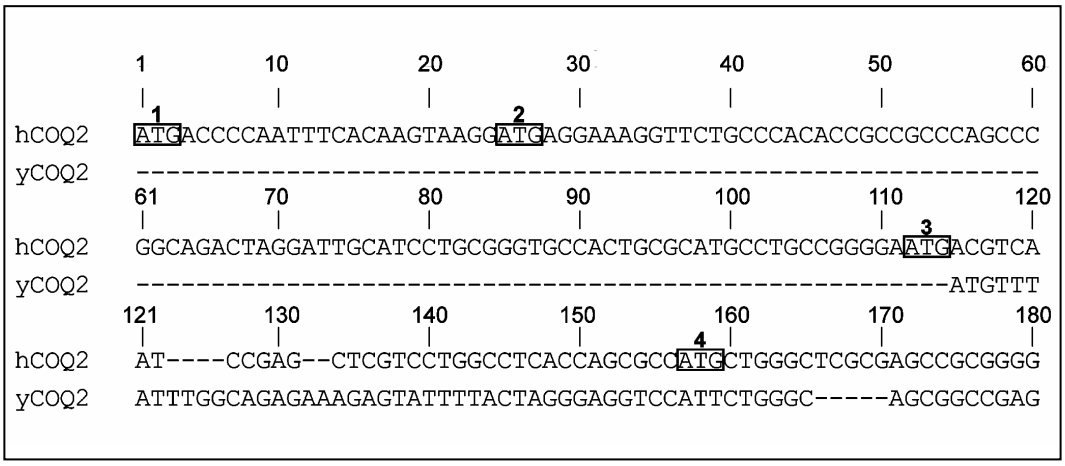

Fig.25 Comparison of 5' end of human and yeast *COQ2* gene showing the four initiation codons (ATG). The initiation ATG in yeast gene corresponds to the 3rd ATG in human gene.

We cloned *hCOQ2* as a hybrid molecule, in a two-step protocol similarly to what has been described (Forsgren et al 2004), due to difficulties in amplifying the 5' region of the mRNA: the 3'-portion was amplified from cDNA and subcloned in the pCRIITOPO vector, while the 5'-sequence corresponding to each of the four ATG was amplified from genomic DNA and sub-cloned in the same vector.

To characterize the 5' region of human *COQ2* gene, the cDNA sequence of the gene was used as probe to identify human expressed sequence tags (ESTs) with significant homology to the *COQ2* transcripts through the tBLASTn software (http://www.ncbi.nlm.nih.gov/BLAST/Blast). As reported by Forsgren et al, several Genbank ESTs predict all the exons in the cDNA except for exon 1: we could not find any EST corresponding to the first 111 nt at the 5' end of exon 1. By aligning the human protein with other mammalian COQ2 proteins, we found that the N-terminus of the reported sequence did not show any homology with other mammalian COQ2 proteins.

The 5' extremity of COQ2 mRNA was characterized by a RACE (rapid amplification of cDNA ends) protocol using the Gene Racer kit (Invitrogen) as above (see §5.2). The PCR products were cloned in pCR2.1TOPO and 10 clones were sequenced with the appropriate primers. 90 further colonies were analyzed on a sequencing gel to determine the exact length of the cloned product (table 7).

Table 7. Different initiation sites of *hCOQ2* identified through 5'RACE.

Transcript initiation site	% of transcripts	Starting ATG codon
-31	79%	(atg4)
-40	12%	(atg3)
-25	3%	(atg4)
-37	2%	(atg4)
-21	2%	(atg4)
-52	1%	(atg4)

These data show that in fibroblasts the most represented *COQ2* transcripts include only ATG4, while there are some rare variants including also ATG3. We didn't find any evidence of neither ATG1, nor ATG2 transcripts in fibroblasts. We then amplified fibroblasts cDNA using a fixed primer within exon 2 of the gene, distal to the predicted targeting sequence, and several primers located upstream of the fourth ATG. Genomic DNA and cDNA from HeLa expressing hCOQ2-ATG1 were amplified as controls. None of the detected PCR products included the first two reported ATG (fig.26).

To confirm the physiological relevance of these mRNAs, we cloned the 5'region of each of the four transcripts in frame with GFP into the pEGFPN1 vector; expression vectors initiating at ATG1 or ATG2 were constructed by cloning a fragment amplified from genomic DNA into the SacI site of the pEGFP-N1-COQ2-ATG4.

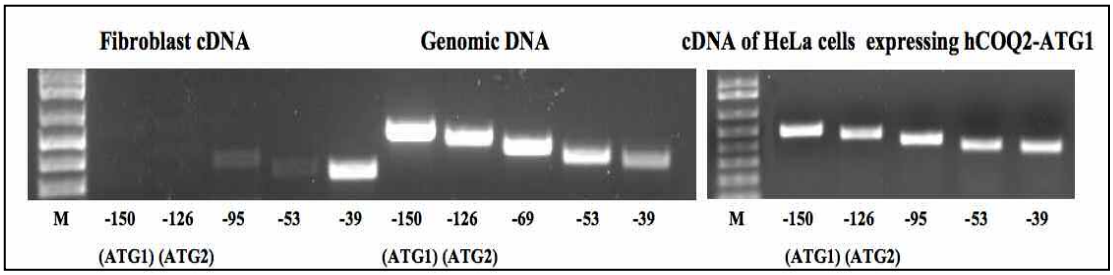

Fig. 26. RT-PCR of COQ2 from fibroblasts, using the same reverse primer on exon 2 and different forward primers upstream to the forth ATG. The numbers indicate nucleotides from ATG 4 (with A as nucleotide 1). Genomic DNA and cDNA from HeLa expressing hCOQ2 ATG1 were amplified as controls.

We then transfected HeLa cells stably expressing mtRFP (fig.27). Each of the four GFP fusion proteins localizes to mitochondria, indicating that all the pre-sequences are functionally equivalent.

Our data indicate that the most representative transcript is the one initiating at the forth ATG. The actual initiation codon still remains elusive; however, analysis of *COQ2* in other mammalians species, such as rat and dog, shows that they contain only one possible ATG initiation codon (corresponding to the human forth ATG).

We are currently constructing an adenoviral vector to transduce patients' fibroblasts, in order to confirm that ATG4 is sufficient for Coq2p activity.

9.1.4 Functional complementation in *Saccharomyces cerevisiae*

To prove the pathogenicity of Y297C mutation, we performed functional complementation in *S.cerevisiae*, using the deleted strain BY4741Δcoq2 (see table I in appendix II).

At first, we checked whether the human *COQ2* gene could complement the yeast null mutant strain. Yeast *COQ2* (*yCOQ2*) and wild-type human *COQ2* (*hCOQ2*) cDNA sequences, initiating from the four different ATG, were subcloned in pYES2.1 with a *GAL* promoter and transformed into the coq2 null mutant strain. Transformations were performed with the PEG-Lithium acetate method (Gietz and Woods 2006).

Growth on glycerol, a non-fermentable carbon source (YPG medium), was determined as marker of functional complementation.

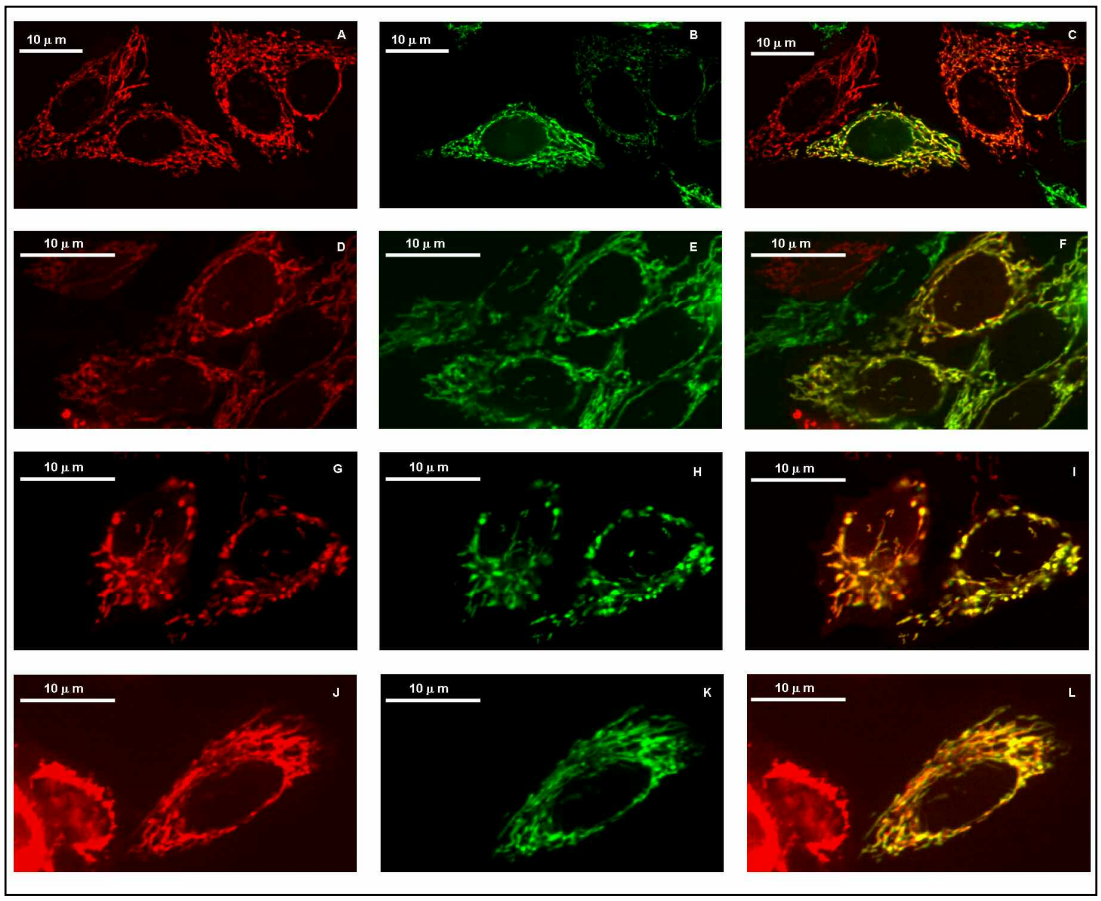

Fig. 27. Localization of COQ2-GFP in HeLa cells stably expressing mtRFP (A, D, G, J); COQ2-GFP starting from ATG1 (B), ATG2 (E), ATG3 (H) and ATG4 (K) Superimposition of the previous images (C,F, I, L).

Increased growth in glycerol was observed when either yCOQ2 or ATG3-initiating *hCOQ2* was expressed in BY4741Δcoq2, lower growth was observed with cDNA initiated at the first or second ATG, while no growth was detected with *hCOQ2* starting from the fourth ATG (fig. 28).

We observed complementation with constructs initiating from each of the first three ATG, achieving the highest complementation efficiency with ATG number 3 (the more similar to the yeast mitochondrial importation pre-sequence); yet, we did not observe complementation with the ATG number 4. This apparently disagrees with our data on human COQ2 expression, where the most abundant transcript is that starting from the forth ATG. One possible explanation is that yeast cells require a critical signal for mitochondrial importation, located between the third and forth ATG. It has been shown that leader sequences are characteristically species-specific (Dolezal et al 2006), thus

hCOQ2 ATG 4 could prevent the heterologous polypeptide to be correctly imported into mitochondria.

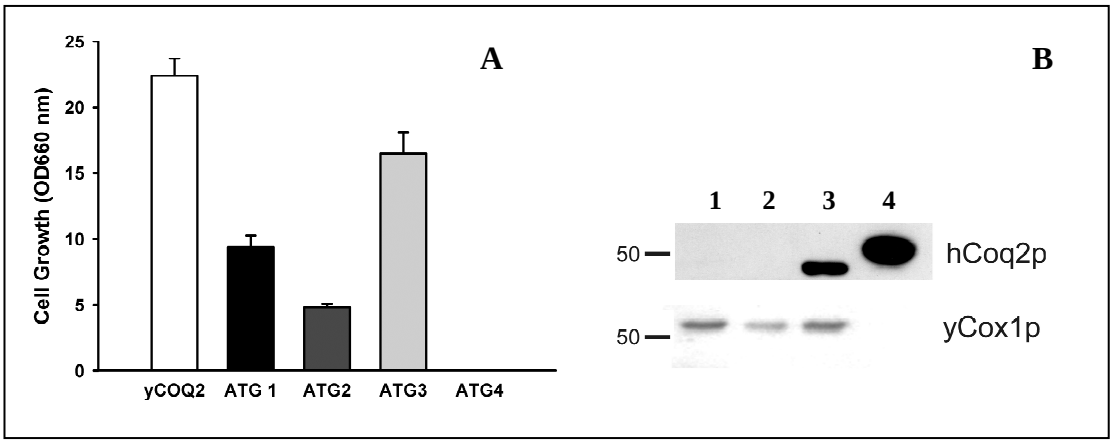

Fig. 28 (A) Culture densities of coq2 yeast strain transformed with clones of homologous yeast wild-type cDNA, and the heterologous human cDNAs starting from the four initiation codons. These cells were grown for 120 h in non-fermentable carbon source media (YPG). (B) Western blot with a polyclonal antibody against human Coq2 peptide. Mitochondria isolated from wild-type (lane 1), coq2null (lane 2) yeast strains, from BY4741 coq2:hCOQ2 (ATG3), and from HeLa cells (lane 4).

We performed a mitochondrial immunolocalization of hCoq2p (3rd ATG) with a polyclonal antibody against the human Coq2 peptide (Agrisera, Sweden). The same membrane was probed with an antibody against yCox1p (Molecular Probes), a protein with known mitochondrial localization. hCoq2 (3rdATG) protein was not detected in either wild-type yeast or coq2 null strain, but it was present in mitochondria of Δcoq2::*hCOQ2* and HeLa cells (with a different molecular weight, probably related to a different processing of the precursor polypeptide in yeast) (fig.28B).

To determine whether the Y297C mutation in *hCOQ2* gene caused a loss of function of the encoded protein, we modeled this mutation on the yeast orthologue (c.783A>G, equivalent to the human c.890A>G transition) by site-directed mutagenesis. We performed complementation assay, transforming Δcoq2 strain with the pYES2.1 vector containing the wild-type yeast and human *COQ2* cDNA, and the corresponding mutant sequences.

Cells expressing the mutant yeast gene displayed a lower growth rate in YPG than those expressing the wild-type gene (fig.29A), demonstrating that functional complementation is sufficiently sensitive to study the effect of a missense mutation in a CoQ biosynthetic gene. Additionally, transformation of Δcoq2 yeast strain with mutated *hCOQ2* showed a

considerably lower respiration-dependent growth than with wild-type *hCOQ2*, which was, however, still significantly increased compared with the deleted strain (fig.29B).

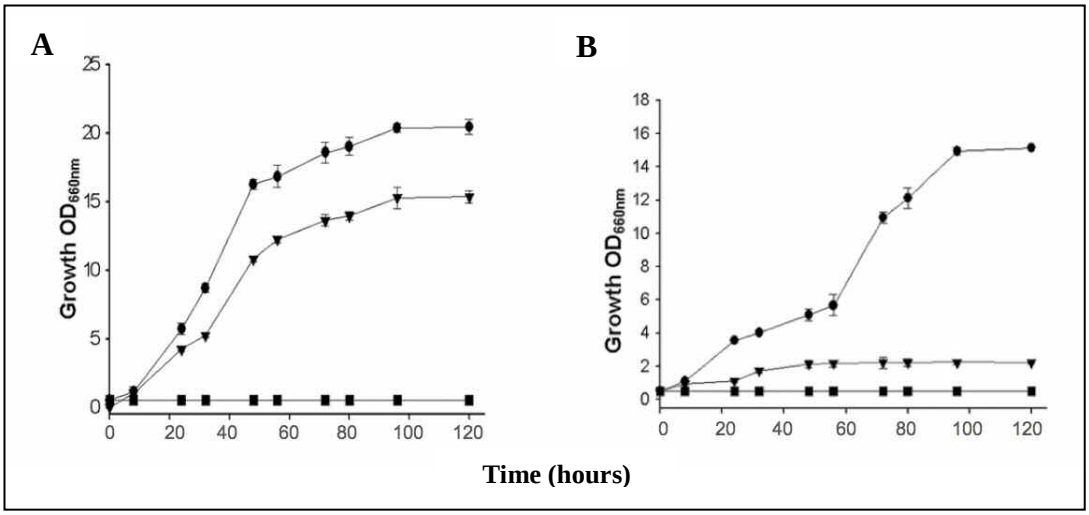

Fig. 29 (A) Growth curves of the Δcoq2 yeast strain (squares), and of this strain transformed with: wild-type yCOQ2 (circles) or c.783 A.G mutated yCOQ2 (triangles). (B) Growth of the Δcoq2 yeast strain (squares) transformed with wild-type (circles) or mutant (triangles) *hCOQ2*.

We then checked the effects on CoQ biosynthesis in the different transformed strains. Mitochondrial purification, lipid extraction and HPLC-ECD quinone separation was performed as described (Padilla et al 2004). Growth results correlated with the content of Coenzyme Q6 (CoQ6) in the different transformed strains (Table 8).

Table 8. Content in CoQ6 and Demetoxy-CoQ6 in yeast strains after 120 h growing in YPG.
(Values are expressed as ng/mg protein ± SD; ND = not detectable)

Strain	CoQ6	Demetoxy-CoQ6	CoQ6/DMQ6 Ratio
BY4741	1448±20	122±10	11.86
BY4741Δcoq2	ND	ND	-
BY4741Δcoq2:hCOQ2	842±12	73±4	11.52
BY4741Δcoq2:hCOQ2 (890G>A)	92±3	42±9	2.19
BY4741Δcoq2:yCOQ2	1309±45	110±18	11.90
BY4741Δcoq2:yCOQ2 (783A>G)	774±70	230±25	3.36

The expression of yCOQ2 caused an accumulation of CoQ6 in transformed yeasts in the range of the wild-type strain, and strains harboring yCOQ2 (c.783 A>G) attained CoQ levels 59% of wild type. These results demonstrate the deleterious effect of the mutation on the Coq2 protein, which, however, apparently retains some residual enzymatic activity. The expression of wild-type *hCOQ2* gene increased CoQ6 levels to 64% of control, while expression of the mutated sequence produced CoQ6 levels that were only 11% of transformed cells with the human wild-type allele.

Analysis of demetoxy-Q6 (DMQ) levels, an intermediate of coenzyme Q biosynthesis that is synthesized by reactions downstream of Coq2p, showed an increase of DMQ relative to CoQ6, in strains transformed with the mutated genes (Table 8), indicating an inhibition of the biosynthetic process also downstream of CoQ2p. This phenomenon can be explained by the fact that enzymes that catalyze CoQ biosynthesis are thought to function in a multisubunit complex (Tran et al 2007): the mutation in Coq2p would interfere not only with the enzymatic function, but probably affecting the whole complex, impairing also some downstream reactions.

Both yeast and human mutated genes failed to fully complement Δcoq2 deleted strain; nevertheless, these transformed strains can grow on YPG and accumulate some amount of CoQ6, indicating that mutated proteins still retain some enzymatic activity These observations suggest that residual *COQ2* function is probably essential for embryogenesis and may explain why the patients did not present symptoms of the disease until 1 year of age.

9.2 Characterization of *hCOQ4* and *hCOQ5*

We characterized the human homologues of *yCOQ4* and yCOQ5, two yeast genes required for CoQ biosynthesis in *Saccharomyces cerevisiae*. These genes represent novel candidates to be screened in patients with primary CoQ deficiency.

9.2.1 Identification and cloning

The human genes *COQ4* and *COQ5* were identified through the "cyber-screening" method described above (see §5.1). The deduced sequences were used to design PCR primers to amplify the human *COQ4* and *COQ5* cDNA from total fibroblasts cDNA. PCR products were cloned in both the pCRIITOPO cloning vector and pYES2.1V5His yeast expression vector (Invitrogen). Individual clones were sequenced with internal primers confirming the *in-silico* predictions. The cDNA sequences were aligned with human genomic DNA to determine the chromosomal localizations of the genes.

Human *COQ4* spans a region of about 12 kb on chromosome 9q34.13, and comprises seven exons. Individual exons were amplified from genomic DNA and sequenced. We found single nucleotide polymorphisms: c.149 G>C (G50A) and c.534 G>C (G178G). The cDNA contains an open reading frame (ORF) of 795 bp that encodes a predicted 265 amino acid protein.

Human *COQ5* is located on chromosome 12q24.31, spanning a region of about 30 kb. It is composed of seven exons transcribed into an mRNA with a coding sequence of 981 nucleotides (227 amino acids). Sequencing of individual exons did not reveal any common polymorphism. We found no evidence of *COQ4* or *COQ5* pseudogenes.

In figure 30, hCoq4p and hCoq5p are aligned with homologue proteins of other species identified with a similar procedure; hCoq4 shows 39% identity and 55% similarity with the *S.cerevisiae* orthologue (yCoq4p), whereas Coq5p shares 45% identity and 60% similarity with the yeast protein (yCoq5p).

PREDOTAR (Small et al 2004) and MITOPROT (Claros 1995) software predict a mitochondrial localization for both Coq4p and Coq5p proteins, with a cleavage consensus site at proline 22 and at tryptophan 17, respectively. The hydropathy profile calculated with the SOSUI software (Hirokawa et al 1998) suggests that both polypeptides are soluble protein.

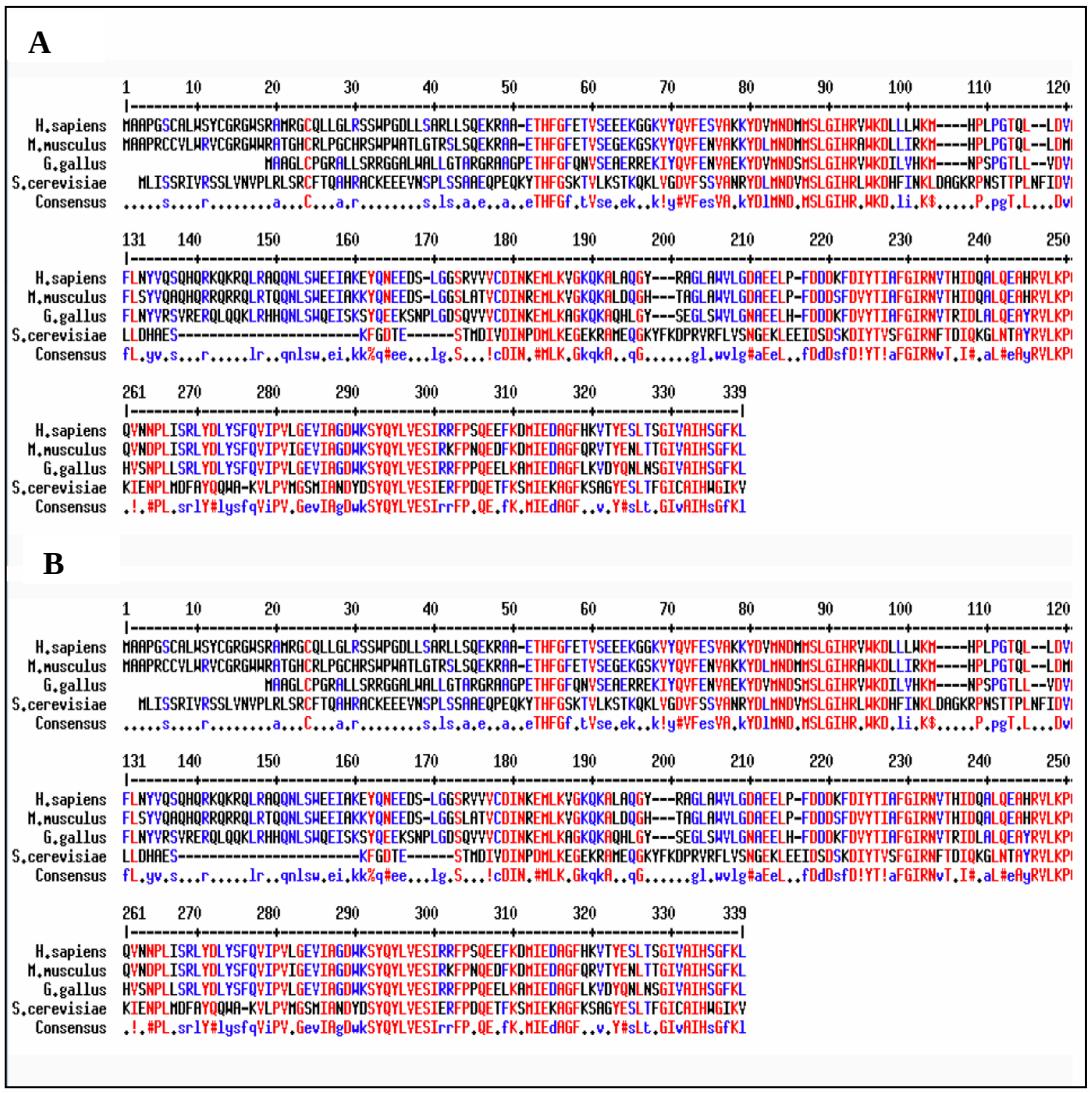

Fig.30 Alignment of Coq4p (A) and Coq5p (B) sequences in different species. Sequence alignments were performed as above (§ 9.1.3, fig.25)

9.2.2 Expression analysis and characterization of the transcripts

Human *COQ4* and *COQ5* expression patterns were assessed by Northern Blot using as a probe an EcoRI digested fragment of pCRIITOPO-COQ4 or pCRIITOPO-COQ5, which were radiolabelled as above (see §5.2).

Both *hCOQ4* and *hCOQ5* are expressed in all human tissues analysed, and were detected as bands of respectively 1.3-1.4 kb and 1.5 kb in the blot (figure 31). Higher expression levels are found in lung, liver, pancreas and colon for *hCOQ4* and placenta, liver, lung, brain and skeletal muscle for *hCOQ5*, whereas beta actin expression is constant in all lanes (data not shown).

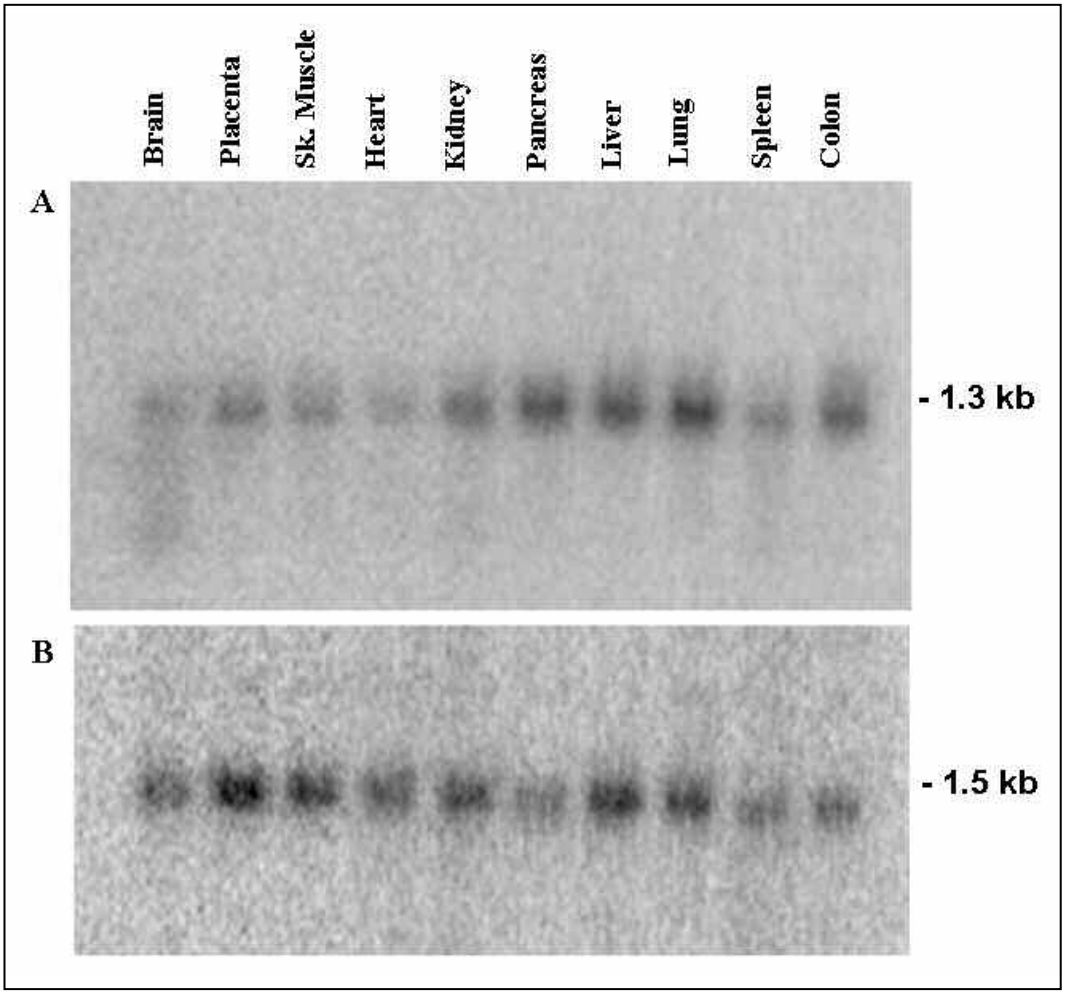

Fig. 31 Northern blot analysis of *hCOQ4* and *hCOQ5* expression. (A) Membrane hybridized with hCOQ4 probe and exposed overnight and visualized as described in text. (B) hCOQ5 probe, exposed overnight.

To characterize transcripts structures and reinforce expression data, we performed a 5' and 3' RACE experiment using the Gene Racer kit as described above.

For *COQ4*, 3' RACE confirmed that the 3' untranslated region (3'UTR) extends for 425 nt after the TGA stop codon and the polyA sequence is preceded by a canonical AATAAA consensus signal; 5' RACE detected multiple transcripts initiating at nucleotide position -333 (in respect to the ATG), -251, -85, and -23 (Figure 32). This phenomenon has been reported in other genes involved in MRC biogenesis (see §5.2). The northern blot detects a single band in each tissue, but the sensitivity of the method is not sufficient to discriminate between individual transcripts. We found also a fifth transcription initiation site located within the short intron 1 of the gene, 141 nucleotides downstream of the ATG (19 nucleotides upstream of the isoform 2 ATG).

The resulting transcript is predicted to encode a shorter protein, which lacks the initial 24 amino acids on the N-terminus (isoform 2). Structure of the 5' region of the gene is depicted in figure 32. Re-analysis of the EST database detected several EST corresponding to isoform 2.

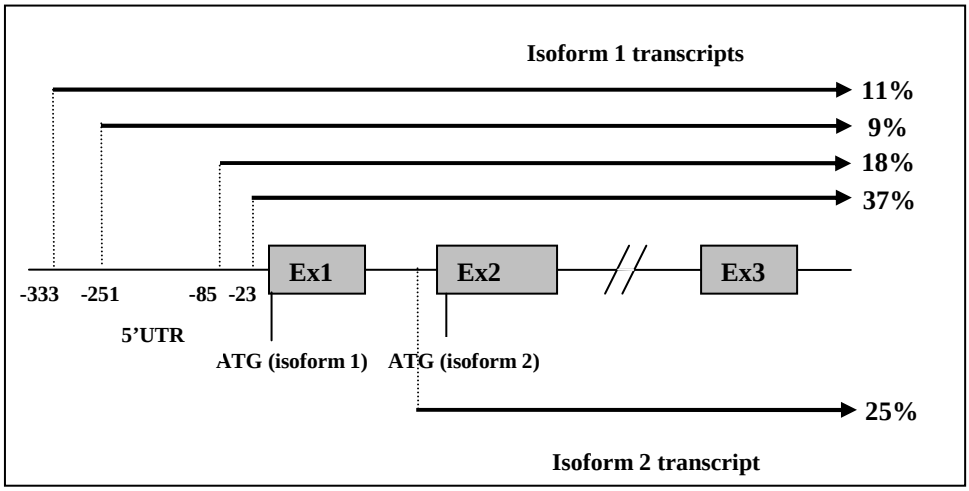

Fig. 32 Structure of the *COQ4* 5' region with the different transcription initiation sites detected by RACE experiments. The percentages indicate the relative abundance of each individual transcript (a total of 100 colonies were analysed).

For *COQ5*, 5' RACE detected a unique transcription starting site at nucleotide position -14 (in respect to the ATG), while the 3'UTR extends for 504 nt after the TAA stop codon and the polyA sequence is preceded by a non canonical consensus signal (AATCAA).

Analysis of the promoter region of *COQ4* reveals the absence of a classical TATA box, and consensus binding sites for several transcription factors, either ubiquitous, like SP1, but also for factors related to respiratory metabolism such as nuclear respiratory factor 1 (NRF1) and hypoxia inducible factor (Hif-1). Interestingly several consensus elements are located between exon 1 and exon 2 and may account for the transcription of isoform 2 mRNA.

Coq5 promoter region shows the presence of two classical TATA box sites, one SRE box site (sterol regulatory element) and consensus-binding regions for ubiquitous factors, like STAT (signal transducers and activators of transcription), ETS (ubiquitous transcription factor GA-binding proteins) and HSF (heat-shock factor); as reported for *COQ4*, also in *COQ5* promoters there are binding sites for transcription factors controlling aerobic metabolism, such as nuclear respiratory factor 1 (NRF1).

The human *COQ4* and *COQ5* transcripts were detected in all tissues tested, but the patterns of expression are different from each other and from that of *COQ2*, which has

relatively higher expression levels in skeletal muscle and in the heart (Forsgren et al 2004); in fact, while *COQ4* is more expressed in liver, lung, and pancreas, *COQ5* shows the highest expression levels in placenta, liver and brain. Interestingly, these data on expression patterns of human COQ genes seem to indicate the existence of different regulatory pathways for at least three of them. This observation is reinforced by the fact that, *hCOQ5* presents only one transcription starting site, differently from *hCOQ2* and *hCOQ4*.

9.2.3 Intracellular localization

To study the subcellular localization of human Coq4p isoforms and Coq5p, the cDNAs devoid of the stop codon were cloned into pEGFPN1 to generate COQ4-GFP and COQ5-GFP fusion proteins, which were used to transfect human HeLa cells stably expressing mitochondrially targeted red fluorescent protein (mtRFP). The GFP fluorescence pattern was compared with mtRFP, as reported above (see §5.3).

As shown in figure 33, in the case of *COQ4* isoform 1 (panel C) and *COQ5* (panel L), there is a perfect overlap between the two patterns, confirming that Coq4p isoform 1 and Coq5p are targeted to mitochondria. Coq4p Isoform 2 instead is localized mainly to the cytosol (fig.33, panel F), and to some extent also to the nucleus, but not to mitochondria. Its pattern resembles that of native GFP, which is localized both to the cytosol and the nucleus (fig.33, panel I).

The role of the human Coq4p isoform 2 is puzzling. The predicted protein lacks the mitochondrial importation sequence, and is localized to the cytosol (the fluorescence visible in nuclei is likely due to a nuclear localization signal present in GFP, see figure 33, panel H). Mitochondrial importation is essential for CoQ synthesis, and other human COQ gene products, such as Coq2p, are localized only to mitochondria, therefore the existence of an extramitochondrial CoQ biosynthetic pathway seems unlikely. One possible explanation is that if isoform 2 has any biological role, it could be a regulatory function, binding nascent Coq polypeptides in the cytosol. Further experiments are required to address this issue. However, it should be noted that in the mouse, despite a similar genomic organization, we found no evidence of a second COQ4 transcript, and there is no equivalent ATG initiation codon for a shorter protein isoform.

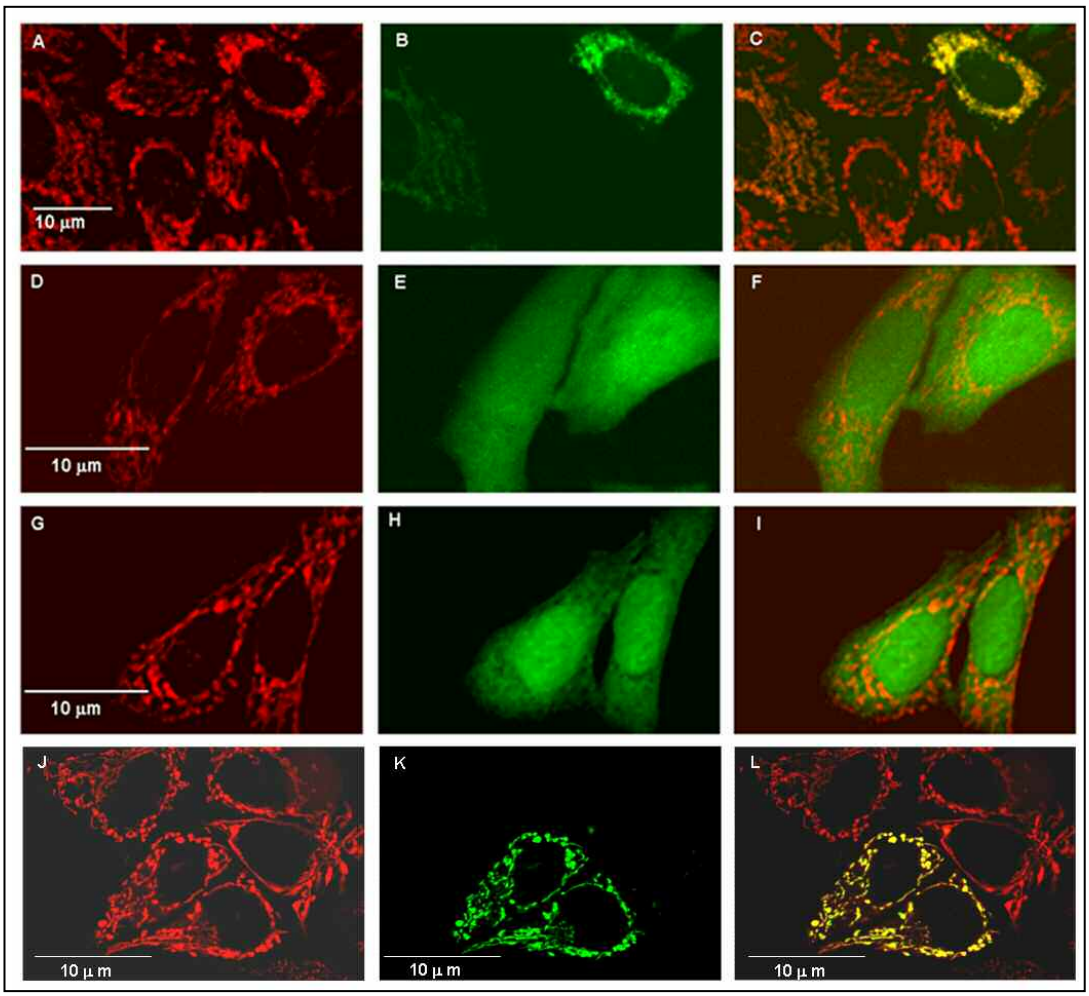

Fig. 33. Localization of COQ4-GFP and of COQ5-GFP: HeLa cells stably expressing mtRFP (A, D, G, J) were transfected with plasmids expressing Isoform 1 COQ4-GFP (B), Isoform 2 COQ4-GFP (E), GFP (H) or COQ5-GFP (K). C, F, I, L represent superimposition of the previous images.

9.2.4 Functional complementation in *S.cerevisiae*

As for other yeast coq mutants, $COQ4^{null}$ and COQ^{5null} *S. cerevisiae* are non-respiring, hence they are unable to grow on non-fermentable carbon sources and cannot synthesize CoQ6 (Tran et al 2007). We transformed the strains harboring a full deletion of the *COQ4* and *COQ5* gene (BY4741 Δcoq4; BY4741Δcoq5, see table I in appendix II), with the pYES2.1-V5His vector containing the full-length human and yeast COQ4 or COQ5 cDNAs, or with an empty vector. Transformations were performed as described above (see §9.1.4). Cells were grown in SD-URA 2% galactose 16 hours at 30ºC with shaking

to express the recombinant genes. These cultures were used to inoculate liquid YPG media (fig.34 panels A, B).

For COQ4, we also measured CoQ6 content in the transformants. Mitochondrial samples from wild type cells (BY4741), COQ4 mutant cells harboring the human genes (ΔCOQ4:hCOQ4) and the yeast gene (ΔCOQ4:yCOQ4) grown in YPG were subjected to lipid extraction and HPLC-ECD quinone separation and quantification as above (see §9.1.4) (fig.34 panels C).

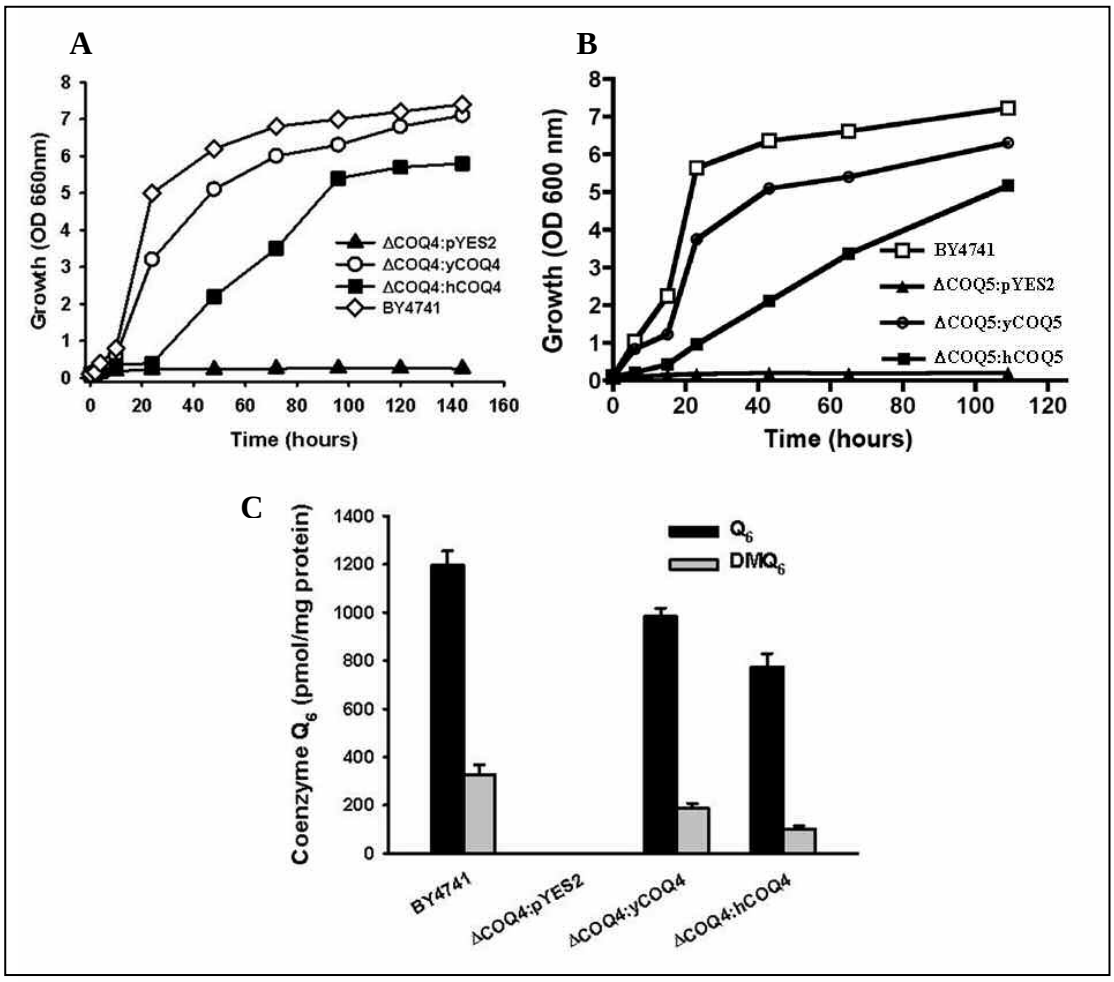

Fig. 34 (A) (B) Wild-type cells (BY4741) and COQ4 or COQ5 mutant cells harbouring the human *COQ4* or *COQ5* genes (ΔCOQ4:hCOQ4; ΔCOQ5:hCOQ5) and the yeast COQ4 or COQ5 genes (ΔCOQ4:yCOQ4; ΔCOQ5:yCOQ5) were grown in SD–URA 2% galactose and cultures at 0.1 U OD 660nm/mL were inoculated into liquid YPG medium. Growth was monitored measuring the OD at 660 nm. Data correspond to the average of three measures. (C) Mitochondrial samples from wild type cells (BY4741) and COQ4 mutant cells transformed with the human *COQ4* and the yeast *COQ4* genes grown in YPG were subjected to lipid extraction and HPLC-ECD quinone separation and quantification as reported in the text. Data corresponds to the average ± SD of at least three determinations.

The growth data indicate that human *COQ4* and *COQ5* genes can efficiently rescue the yeast mutants, normalizing the growth in $COQ4^{null}$ and $COQ5^{null}$ strains and, in the case of *COQ4*, also CoQ6 content (fig.34).

Both human *COQ4* and *COQ5* genes are highly similar to their yeast counterpart, and, when expressed from a multicopy plasmid, they can effectively complement the corresponding null mutant *S.cerevisiae* strains. Interestingly, with *COQ4*, the high efficiency of complementation is demonstrated by the fact that levels of demetoxy-coenzyme Q6 (DMQ6) detected in complemented strains are similar to the wild type. High levels of DMQ6 (compared to total CoQ) suggest a poorly functioning biosynthetic pathway (López-Martín et al 2007).

In yeast, Coq4p is essential for the metabolism of CoQ, and its deletion completely abolishes CoQ biosynthesis; moreover, growth on a non-fermentable carbon source of the $COQ4^{null}$ mutant strain causes an up-regulation of COQ4 mRNA levels, consistent with its role in Q biosynthesis (Belogrudov et al 2001). Yet, its exact function is still unclear. Although Coq4p could be involved in one of the yet-to-be-characterized biosynthetic steps, its protein sequence does not share homology with protein domains or motifs with known enzymatic activity. In yeast, it is reported to be associated with other COQ gene products forming a multienzyme complex (Tran et al 2007) It is possible that Coq4p has a structural role in the putative Q biosynthetic complex (see fig.20 §7.1).

In *S.cerevisiae COQ5* encodes a C-methyltransferase (2-methoxy-6-polyprenyl-1,4-benzoquinone methyltransferase) , which catalyzes the only C-methylation step in the CoQ biosynthetic pathway, generating the 2-methoxy-5-methyl-6-polyprenyl-1,4-benzoquinone intermediate (Baba et al 2004). COQ5 mutant strains are respiratory deficient but their growth in non-fermentable carbon source can be restored to near wild-type level by adding coenzyme Q6 (Tzagoloff and Dieckmann, 1990). The open reading frame harbors four sequence motifs present in a large family of AdoMet-dependent methyltransferase enzymes (Katz et al 2003). *hCOQ5* has a highly conserved sequence compared to the *S.cerevisiae* gene, displays the same mitochondrial localization and it is able to complement the yeast null mutant strain. All these data strongly suggest that the two homologues act in the same step in the Q biosynthetic pathway.

10. CONCLUSIONS

CoQ biosynthesis in human is still not fully understood. Its importance is related to the recent identification of patients affected by ubiquinone deficiencies, which represent the only form of mitochondrial diseases that can be efficiently treated.

We studied a family affected by primary CoQ biosynthesis, with a multisystemic clinical phenotype involving CNS and kidney. The older patient responded well to ubiquinone administration, showing a dramatic improvement in neurological symptoms; yet his renal function did not improve since it had already reached the end-stage renal failure; by contrast, his younger sister started CoQ oral therapy very early, when she displayed a steroid-resistant nephrotic syndrome and showed a complete regression of proteinuria.

We studied the molecular bases of CoQ defect and reported the first mutation in a CoQ biosynthetic gene (*COQ2*). We analyzed the pathogenicity of the novel sequence variance, using a yeast functional complementation system and demonstrated that *COQ2* mutations can be modeled on *S.cerevisiae* to verify whether they affect the enzymatic activity of the polypeptide.

Finally we characterized *hCOQ4* and *hCOQ5*, two novel human genes required for CoQ biosynthesis. By employing functional complementation assay, we proved that yeast might be a useful model to assess the pathogenicity of eventual *COQ4* and *COQ5* mutations.

Although, to date, no mutations has been detected in *hCOQ4* and *hCOQ5* sequences, both genes may represent novel candidate for mutational screening in CoQ deficient patients. After the identification of molecular defects in three of the ten genes required for CoQ biosynthesis, it is possible that defects in the other seven genes will cause a similar early-onset encephalomyopathy.

SECTION V

ARGININOSUCCINIC ACIDURIA

11. ASAuria

Argininosuccinic aciduria (ASAuria; MIM# 207900) is an autosomal recessive disorder of the urea cycle, caused by deficiency of argininosuccinate lyase (ASL; EC 4.3.2.1; MIM# 608310). It was first recorded in the late 1950s (Allan et al. 1958), it is transmitted as an autosomal-recessive trait and occurs with an incidence of approximately 1:70,000 live births, being the second most frequent UCDs after citrullinemia (Levy et al. 1980).

ASL defect leads to the accumulation of argininosuccinic acid (ASA) in body fluids and severe hyperammonaemia.

ASAuria displays considerable clinical heterogeneity, which is manifested by variations in the age of onset and the severity of symptoms. Patients may present at any age, but onset is typically in the neonatal period or in infancy. The acute neonatal form is characterized by severe symptoms: poor feeding, vomiting, tachypnea, life-threatening hyperammonaemic crises, lethargy, hypothermia and seizures, with subsequent progression to coma and death, if untreated; the late-onset variant is milder and typically the main symptom is psychomotor retardation, which can be associated with vomiting, failure to thrive, irritability and behavioral problems. ASAuria has two distinguishing features: severe hepatomegaly, which is common later in the course of the disease, and trichorexis nodosa, a hair abnormality typical of the late-onset form. Biliary calculosis has been reported in many patients with the subacute form.

Laboratory tests reveal hyperammonaemia, a mild increase of hepatic enzymes and citrulline (lower than in the case of citrullinemia), aspecific increase of plasmatic glutamine and alanine and high levels of argininosuccinic acid in plasma and urine (which can be found also in cerebrospinal fluid).

The diagnosis is made by measuring plasma levels of ammonia, ASA, and its anhydrides. Plasma amino acid analysis, measured by automated quantitative column chromatography, provides sufficient information to make a confident diagnosis of ASAuria. The analysis is definitive and unambiguous, and assays of ASL enzyme activity

in erythrocytes or cultured fibroblasts are usually not required (Brusilov and Horwich, 2001).

Kleijer et al (2002) reported five patients presenting with relatively mild clinical symptoms, variable age of onset, marked argininosuccinic aciduria and severe, but not complete, deficiency of argininosuccinate lyase. [^{14}C] Citrulline incorporation into proteins, which is completely blocked in classical argininosuccinic aciduria, was only partially reduced in fibroblasts of these patients. Nevertheless, at present, the biochemical basis for this clinical heterogeneity is unclear, as in other studies it has been shown that there is only a partial correlation between the clinical phenotype and residual ASL activity in cultured fibroblasts and other tissues (McInnes et al 1984; Walker et al 1990; Brusilow et al, 2001; Sampaleanu et al 2001).

Prenatal diagnosis can be performed with two reliable biochemical techniques: determination of ASL activity in the villi by [^{14}C] citrulline incorporation into proteins (preferably done by chorionic villus sampling in the 12th week and), or alternatively by measurement of ASA in the amniotic fluid (amniocentesis is done in the 15-16th week) (Brusilov and Horwich 2001; Kleijer ate al 2002). However, genetic analysis should be considered the method of choice.

As for other UCDs, the goal of the therapy is to provide a diet sufficient in proteins, arginine and energy to promote growth and development, while avoiding the metabolic perturbations caused by hyperammonaemia (Scaglia et al 2004). The clinical outcome is unsatisfactory in many cases, in fact a mild to moderate psychomotor retardation is a common finding also in patients with an adequate metabolic control. However, asymptomatic individuals, diagnosed in routine urine tests, have been reported (Applegarth et al. 1975; Brusilow and Horwich 2001); moreover it has been shown that asymptomatic children suffering from ASAuria, detected during neonatal screening programs and treated, result in normal intellectual and psychomotor development in long-term follow-up (Widhalm et al 1992).

11.1 The argininosuccinate lyase enzyme

Argininosuccinate lyase (ASL) is a cytosolic enzyme, which catalyzes the cleavage of argininosuccinate into arginine and fumarate, an essential step in the urea cycle (fig.35). The enzyme's primary physiological role is in the liver, where it is predominantly expressed and functions in the urea cycle for the disposal of ingested nitrogen. Yet, it’s

expressed in virtually all tissues, particularly in kidney and brain. Since neither of these organs is capable of ureagenesis, it is presumed that it plays an important role in the synthesis of arginine from citrulline (Yu and Howell 2000).

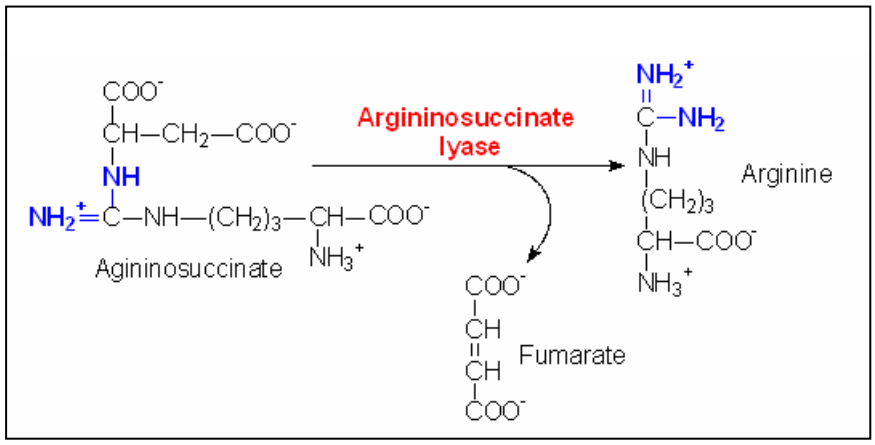

Fig.35 Reaction catalyzed by the argininosuccinic lyase enzyme.

The ASL protein consists of 464 amino acids with a predicted molecular weight of about 52 kDal (O'Brien et al. 1986). ASL belongs to a superfamily of homotetrameric enzymes that have homologous parts, catalyze similar cleavages and include δ crystallin, class II fumarase, aspartase, adenylosuccinase lyase, and 3-carboxy-cis,cis-muconate lactonizing enzyme. These enzymes all have similar three-dimensional structures and catalyze β-elimination reactions involving the cleavage of a carbon-oxygen or carbon-nitrogen bond with the formation of fumarate as one of the products. Particularly, there are three regions of highly conserved residues, denoted C1, C2, and C3 that are spatially distant from each other in the monomer but cluster together in the tetramer to form a multisubunit active site, in which the three regions are each contributed by a different monomer (Yu and Howell 2000; Sampaleanu et al 2001) (fig.36). Among these homotetrameric enzymes, ASL is strictly connected to δ-crystallins, structural proteins of vertebrate lens, sharing up to 71% of identity. Particularly, δ2 crystallins of duck and chicken have significant ASL enzyme activity; it has been speculated that they have been evolutionary recruited to the lens in birds via gene duplication and subsequent specialization, where they function as structural components (Barbosa et al 1991a; Piatigorsky et al. 1988).

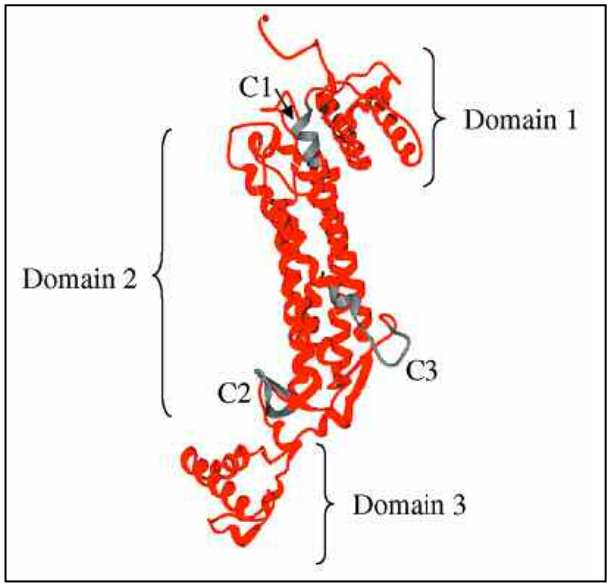

Fig.36 Structure of ASL: schematic diagram of the three-dimensional topology of the ASL monomer. The three structural domains are indicated, and the conserved amino acid regions C1, C2, and C3 are shown in gray (adapted from Sampaleanu et al 2001).

ASL is active in the cytosol as a homotetramer and its x-ray crystal structure has been determined (Turner et al 1997). Every monomer has a secondary structure, which is predominantly α-helical and consists of three distinct structural domains (fig.36). Domains 1 and 3 have a similar overall topology and consist of two helix-turn-helix motifs arranged mutually perpendicular to each other. Domain 2 consists of nine helical segments, five of which form a central five-helix bundle with an up-down-up-down-up topology. Three of the five helices of the central five-helix bundle participate in the association of two monomers. Two pairs of closely associated monomers interact to form the tetramer (Sampalenau et al, 2001).

11.2 The *ASL* gene

The human *ASL* gene is approximately 17 kb in length, is comprised of 17 exons (the first, exon 0, codes only for the 5'UTR), and is located on chromosome 7cen–q11.2 (Naylor et al 1978; Linnebank et al 2002). Exon size spans from 53 bp (exon 8) to 195 bp (exon), while intron size is comprised between 80 bp (IVS6) and 5.7 kb (IVS1). The presence of another partial sequence on chromosome 22q11.2 (*ΨASL1*) was assumed to be a pseudogene (O'Brien et al., 1986; Linnebank et al., 2002). It spreads over 88.4 kb,

shares 88% of homology with the *ASL* gene and it seems to be a regular gene with a promoter region, a poly-A signal and 11 exons containing a typical initial exon and a terminal exon; its function is still unknown.

11.3 Intragenic Complementation

ASL defects display substantial clinic heterogeneity (Brusilov and Horwich 2001), and to explain some of the cases with milder phenotypes the theory of intragenic complementation has been proposed (McInnes et al, 1984; Walker et al, 1997; Howell et al, 1998). In fact, ASL is a homotetramer and in microorganisms, interallelic complementation has been found to be almost universal at loci coding for homomultimeric proteins. The accurate prediction of genotype-phenotype correlations in ASAuria requires a complete understanding of the mechanisms by which this phenomenon can occur.

Intragenic complementation takes place when particular combinations of mutant alleles at a given locus produce a less severe phenotype than the same alleles do in the homozygous state, or in the presence of noncomplementing alleles: a partially functional hybrid protein is produced from the two distinct types of mutant subunits, neither of which individually has appreciable enzymatic activity. The molecular symmetry of the ASL protein dictates that when active-site mutant monomers combine randomly, at least one active site will contain no mutations at all (fig.37). It is these “wild-type” active sites in the hybrid proteins that are responsible for the partial recovery of enzymatic activity observed during intragenic complementation.

Complementation phenotypes do not arise with all mutant alleles, and the complementing ones can be distinguished in two types: (i) frequent complementers, that participate in the majority of complementation events (as Q286R), and (ii) high activity complementers, in which complementation is associated with a relatively high level of restoration of ASL activity (as D87G). Additionally, interallelic complementation can occur through the interaction of unstable non-active site mutant subunits (affecting the thermodynamic stability of the protein, as M360T and A398D) and stable monomers (Q286R), leading to the formation of a more stable heterotetrameric protein with partial recovery of catalytic activity (Yu et al 2001).

Although interallelic complementation of ASL polypeptides has been proposed as an important feature for modulating enzyme activity, Linnebank et al (2002) did not observe

major impact of this phenomenon on the biochemical phenotype of a large series of patients; in fact a residual enzymatic activity has been found in homozygous patients (excluding complementation), whereas some patients with the late-onset phenotype and heterozygous compound mutations revealed absent enzyme activity. It seems rather that interallelic complementation at the *ASL* locus involves some specific mutant alleles, such as Q286R and D87G.

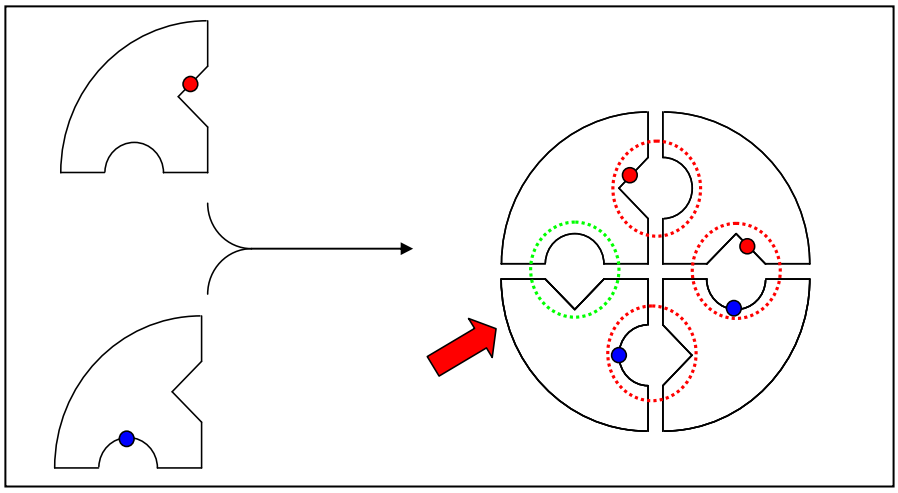

Fig.37 Schematic representation of intragenic complementation: mutant subunits of ASL enzyme, each possessing distinct amino acid substitutions that render the homomutant proteins inactive, interact to form heteromutant multimers possessing partial activity. Blue and red circles represent two different active-site mutations; dotted green and red lines indicate active and inactive multi-subunit catalytic site.

12. SPECIFIC AIM

Although the *ASL* gene was cloned 20 years ago (O'Brien et al. 1986), the molecular defects have so far been investigated in only a few patients, and the number of reported mutations is still quite small compared to other UCDs, like OCT deficiency, revealing a considerable allelic heterogeneity.

The aim of this study was to analyze the mutational spectrum of *ASL* in a cohort of Italian patients with ASAuria, employing a diagnostic test that relies exclusively on genomic DNA. Moreover, we aimed at developing a functional system to validate missense and splicing mutations and to study potential genotype-phenotype correlations.

13. RESULTS AND DISCUSSION

13.1 Identification of a novel *ASL* pseudogene

Unlike all previous reports that relied essentially on cDNA analysis (and genomic DNA was used only to validate cDNA results (Walker et al. 1990; Barbosa et al. 1991b; Linnebank et al. 2002; Kleijer et al. 2002), we developed a protocol based exclusively on genomic DNA analysis. This approach has several advantages over cDNA analysis in terms of sample handling and availability, and it overcomes the possible mRNA degradation associated with some frameshift or splicing mutations (Linnebank et al., 2002); yet, it is mandatory to assure that specific primers avoid regions of homology between the gene of interest and its pseudogenes.

We used a protocol modified from the one reported by Linnebank et al (2002). When testing the PCR primer pair designed to amplify exon 3 (located in introns 2 and introns 3), we realized that PCR amplification yielded two different products of the same size: the first corresponded to the correct *ASL* exon 3 and its intronic boundaries, while the other displayed multiple single nucleotide changes compared to the reported *ASL* sequence, a result compatible with the simultaneous amplification of a gene and its pseudogene.

We performed a BLAST search against the whole human genome using as probe the genomic sequence surrounding *ASL* exon 3, and retrieved three different sequences: *ASL* exon 3 (100% identity), the reported *ASL* pseudogene on chromosome 22—*ψASL1*— (88% identity), and a third sequence (90% identity), which however showed 100% identity with the second PCR fragment we had obtained. We have denominated this locus *ψASL2*. The *ψASL2* region comprises 561 nucleotides and is located on chromosome 7 about 3Mb upstream of the *ASL* gene (nucleotides 589296–589857 of genomic sequence NT_007758.11), close to the centromere.

We believe that *ψASL2* was not detected by the bioinformatic analysis of Linnebank et al. (2002) probably because at the time information on centromeric regions was still largely incomplete.

We checked whether *ψASL2* is actively transcribed, as reported for *ψASL1* (Linnebank et al 2002), but we found no evidence of expressed sequence tags (ESTs) transcribed from the *ψASL2* locus; we then analyzed by RT-PCR pseudogene expression using primers specific for *ψASL2* that amplify a 66-bp fragment corresponding to a portion of *ψASL2*

homologous to *ASL* exon 3. A control amplification was conducted on genomic DNA. We could not detect any *ψASL2* expression in primary fibroblasts, peripheral blood cells, and HeLa cells (fig.38). We repeated a similar bioinformatic analysis for the entire *ASL* gene and we did not detect other pseudogenes. The sequence of *ψASL2* was submitted to Genbank (Accession # DQ679421).

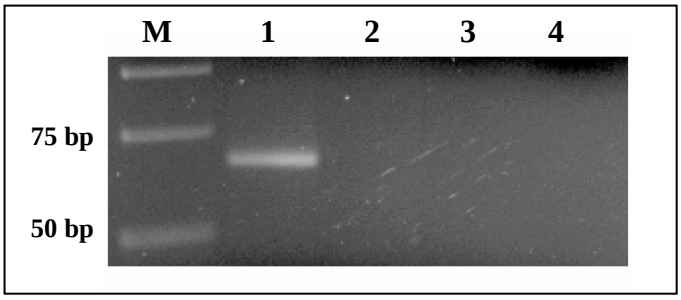

Fig.38 *ΨASL2* expression analysis: RT-PCR with primers specific for *ΨASL2*. M = molecular marker; lane 1 = genomic DNA; lane 2 = primary fibroblasts; lane 3 = peripheral lymphocytes; lane 4 = HeLa cells.

The identification of the novel *ψASL2* was critical to design primers that specifically amplified *ASL*, avoiding the region of homology between, *ψASL1* and *ψASL2*.

13.2 Mutation analysis in patients

We studied 15 patients from 13 different Italian kindreds (see table 9 for clinical features), with hyperammonaemia and elevated ASA levels. The diagnosis of ASAuria was based on both clinical and biochemical criteria, and was established by the quantification of plasma ASA by amino acid chromatography, levels of serum ammonia, and determination of urinary orotic acid, during the acute phase of the disease.

The entire coding region of the *ASL* gene was amplified from patients genomic DNA; primer pairs and PCR conditions are described in Trevisson et al 2007. PCR fragments were purified and sequenced using the ABI PRISM 3100 automated sequencer (Applied Biosystems). The presence of each mutation was confirmed on a second PCR product.

Table 9. Clinical features of patients.

Patient	Clinical phenotype				Biochemical phenotype
	Subtype	**Age at diagnosis**	**Presenting symptoms**	**Outcome (age)**	**Laboratory tests**
1	Neonatal onset	5d	Coma, hyperammonaemia	MR, alive (3 y)	NH_3 = 850 ug/dl ASA>1000 µmol/L
2	Neonatal onset	6d	Coma, hyperammonaemia	MR, dead (10 y)	NH_3 = 1200 ug/dl ASA>1000 µmol/L
3	Neonatal onset	4d	Coma, hyperammonaemia	MR, alive (9 y)	NH_3 = 2000 ug/dl ASA>700 µmol/L
4	Neonatal onset	7d	Coma, hyperammonaemia	MR, alive (15 y)	NH_3 = 1800 ug/dl ASA>1000 µmol/L
5a	Late onset	4y	MR	MR, alive (24 y)	NH_3 = 120 ug/dl ASA>300 µmol/L
5b	Late onset	2y	MR	MR, alive (21 y)	NH_3 = 90 ug/dl ASA>300 µmol/L
6	Neonatal onset	2d	Coma, hyperammonaemia	MR, alive (9 y)	NH_3 = 950 ug/dl ASA>1200 µmol/L
7	Neonatal onset	2d	Coma, hyperammonaemia	MR, alive (2 y)	NH_3 = 450 ug/dl ASA>600 µmol/L
8a	Late onset	3y	Seizures	Seizures, alive (4 y)	NH_3 =120 ug/dl ASA>300 µmol/L
8b	Late onset	6mo	Failure to thrive, vomiting	Normal, (18 mo)	NH_3 =60 ug/dl ASA>300 µmol/L
9	Neonatal onset	6d	Coma, hyperammonaemia	MR, alive (18 y)	NH_3=2000 ug/dl ASA>1000 µmol/L
10	Neonatal onset	7d	Coma, hyperammonaemia	alive (1 y)	NH_3 = 400 ug/dl ASA>500 µmol/L
11	Late onset	13y	MR	alive (14y)	NH_3 = 110 ug/dl ASA>300 µmol/L
12	Late onset	7d	Failure to thrive, vomiting	alive (1y)	NH_3 = 100 ug/dl ASA>300 µmol/L
13	Neonatal onset	2d	Coma, hyperammonaemia	alive (6mo)	NA

(MR=mental retardation; NH_3 : n.v. 20-70 ug/dl; ASA = argininosuccinic acid; y=years; mo=months; d=days; NA=not available)

All novel missense mutations were validated by PCR-RFLP analysis: PCR products were digested overnight with the appropriate restriction nuclease and for mutations that did not alter natural restriction sites, we designed appropriate mismatched PCR primers in order to create novel nuclease recognition sequences in the mutant alleles (Trevisson et al 2007). Fragments containing insertions/deletions were subcloned in the pCRIITOPO vector (Invitrogen, Carlsbad, CA; www.invitrogen.com) and individual colonies were sequenced as described (Salviati et al. 2004). The presence of the mutations was confirmed in the parents DNA.

We detected pathogenic mutations in all kindreds (table 10). Homozygous mutations were detected in three kindreds, while all other patients were compound heterozygotes.

Table 10. Mutations and ASL activity in patients.

Patients	Mutation			ASL activity[d]
	Location	**DNA (analyzed)**	**Amino acid change**	
1	Exon 11	c.[857A>G][a]	p.[286Q>R][a]	<5%
	Exon 11	c.[857A>G]	p.[286Q>R]	
2	Intron 6	c.[IVS6+2T>G]	p.[E150_S175del?]*	ND
	Exon 15	c.[1145T>G]	p.[382M>R]	
3	Intron 6	c.[IVS6+2T>G]	p. [E150_S175del?]*	<5%
	Exon 8	c.[637C>T]	p.[213R>X]	
4	Exon 7	c.[532G>A][b]	p.[178V>M][b]	<2% (in fibroblasts)
	Exon 7	c.[557G>A]	p.[186R>Q]	
5a[e]	Exon 2	c.[91G>A]	p.[31D>N]	ND
	Exon 2	c.[91G>A]	p.[31D>N]	
5b[e]	Exon 2	c.[91G>A]	p.[31D>N]	ND
	Exon 2	c.[91G>A]	p.[31D>N]	
6	Exon 8	c.[584_585delAT]	p.[N195fsX233]	<5%
	Intron 8	c.[IVS8-1G>A]	p.[E219_V239del?]*	
7	Exon 4	c.[338G>A]	p.[113R>Q]	<5%
	Exon 9	c.[706C>T]	p.[236R>W]	
8a[e]	Exon 7	c.[551_552delCT]	p.[184S>X]	ND
	Exon 13	c.[1003G>T]	p.[335V>L]	
8b[e]	Exon 7	c.[551_552delCT]	p.[184S>X]	<9%
	Exon 13	c.[1003G>T]	p.[335V>L]	
9	Exon 7	c.[551_552delCT]	p.[184S>X]	<5%
	Exon 10	c.[793_795delACCinsT]	p.[265T>X]	<2% (in fibroblasts)
10	Exon 7	c.[544C>T]	p.[182R>X]	ND
	Exon 16	c.[1366C>T]	p.[456R>W]	
11[e]	Exon 7	c.[545G>A]	p.[182R>Q][c]	ND
	Exon 11	c.[890G>A]	p.[297R>Q]	
12[e]	Exon 7	c.[532G>A]	p.[178V>M][b]	ND
	Exon 11	c.[839delG]	p.[T279fsX283]	
13	Exon 3	c.[217G>A]	p.[73E>K]	ND
	Exon 3	c.[217G>A]	p.[73E>K]	

The reference *ASL* cDNA sequence used was GenBank accession NM_001024943.1. For DNA numbering, nucleotide +1 is the A of the ATG initiation codon (codon+1).
*Predicted effect on protein according to the minigene functional assay
[a] Mutation previously reported by Barbosa *et al.* 1991; Walker *et al.* 1997; Sampaleanu *et al.* 2001; Linnebank *et al.* 2002.
[b] Mutation previously reported by Kleijer *et al.* 2002; Linnebank *et al.* 2002.
[c] Mutation previously reported by Linnebank *et al*. 2002.
[d] ASL activity in is expressed as a percentage of normal controls (7.771.2 nmol/hr/mg hemoglobin). In Patient 9, activity was determined both in skin fibroblasts and erythrocytes, while in Patient 4 activity was determined only in fibroblasts (courtesy of Dr.W.J. Kleijer).
ND, not determined.
[e] Patients with late onset phenotype.

We found a total of 20 mutations, only three of which were previously reported: Q286R, V178M and R182Q (Barbosa et al., 1991b; Walker et al., 1997; Sampaleanu et al., 2001; Kleijer et al., 2002; Linnebank et al., 2002). Among the 17 novel mutations we found 13 single-nucleotide changes (nine missense, two nonsense, and two splicing) and four small insertion/deletions. Only the c.524+2T>G, the c.549_550delCT and V178M mutations were found in two different kindreds.

We also found a novel intronic sequence variant located in intron 1 of the gene (c.12+105C>T). Allelic frequencies are similar to those found in 100 healthy controls (41% T/T, 46% T/C, and 13% C/C), which correspond to the Hardy-Weinberg equilibrium.

Previous studies have reported marked heterogeneity of ASL mutations in European patients (Linnebank et al. 2002), while Arabic patients have a common (Q354X) allele (Al-Sayed et al. 2005). We did not find a common "Italian" mutation, most patients were compound heterozygous for different alleles, and the homozygous mutations were found in two families in whom we suspect consanguinity (Q286R, E73K), and in another from Sardinia island (D31N), where a founder effect has been reported for many other genetic diseases.

Mutations were scattered throughout the gene (fig.39); however, we confirm that exon 7 seems to be a mutational hotspot (Linnebank et al. 2002); in fact, 5 of the 20 mutations we found were located in this region.

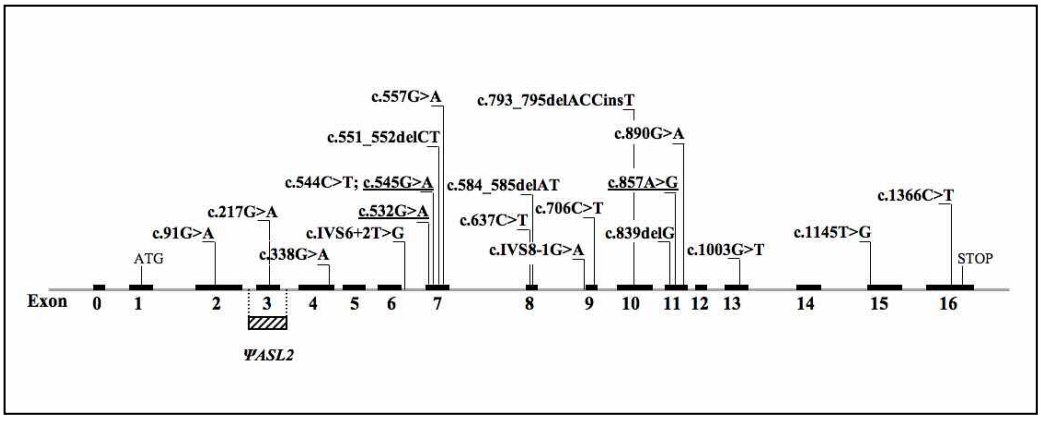

Fig.39 Representation of the human ASL gene. Exons are shown as black boxes. The region homologous to the *ΨASL2* pseudogene is depicted below as a striped box. Mutations are identified throughout the length of the gene. Previously reported mutations are underlined.

Two mutations (R113Q and R182X) involve codons 113 and 182 that have been found affected by a different mutational event (R113W and R182Q) (Linnebank et al. 2000,

2002). In all cases a transition has occurred. However, analysis of the sequences flanking these codons did not reveal any peculiar motif that could explain the particular susceptibility of these codons to mutational events.

13.3 Validation of mutations

Of the 17 novel mutations, the four small insertions/deletions and the two nonsense mutations are predicted to cause premature stop codons. We believe their pathogenicity is obvious. We proved that the splicing mutations cause an aberrant splicing using a functional splicing assay that employed a hybrid minigene. The pathogenicity of missense mutations was suggested by the high degree of conservation of the mutated residues, their absence in 100 control alleles and molecular modeling data; for some patients, blood samples were available and we could measure ASL biochemical activity. Furthermore, we developed a yeast functional system to validate missense mutations and to verify intragenic complementation.

13.3.1 Analysis of splice-site mutations

To prove the pathogenicity of the two intronic mutations detected in our patients, we tested their effect with a functional splicing assay, based on the use of hybrid minigenes, since no patients' RNA was available for our studies.

Both mutations affect nucleotides (positions +2 and -1 in respect to the corresponding exon) that are critical for exon recognition by the spliceosomal machinery (Cartegni et al. 2002).

The two hybrid minigene constructs were generated using as a backbone the pEGFP-N1 vector (Clontech, Mountain View, CA) with the 5' region of the human *COQ2* gene cloned in the BglII-PstI sites (pEGFP-COQ2). This construct was selected because it had convenient restriction sites.

To generate 5-6-7 and 8-9-10 minigenes, the wild type and mutated genomic DNA from the patient was amplified using primers containing appropriate restriction sites for subsequent cloning; PCR products, comprising the exon adjacent to the mutation, and part of the upstream and downstream exons, were cloned in pEGFP-COQ2. For 5-6-7 minigene, an additional cloning step was required to remove part of intron 5. The structure of both hybrid minigene constructs is depicted in figure 40. In both cases the

resulting inserts (if correctly spliced) were designed to be in-frame with *COQ2* and GFP. The correctness of plasmid clones was confirmed by direct sequencing.

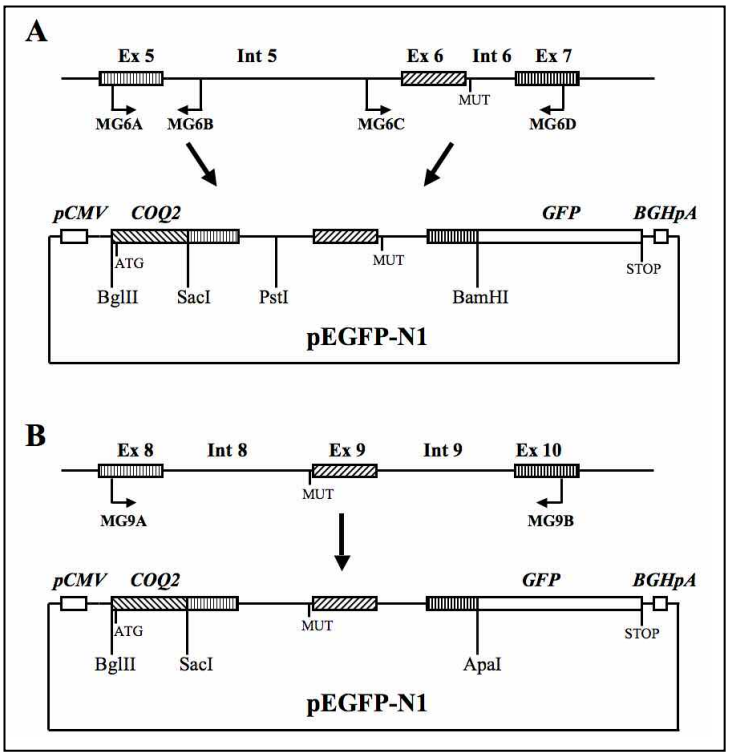

Fig.40 Schematic representation of the minigene constructs.
pCMV = CMV promoter, BGHpA = bovine growth hormone polyadenylation signal sequence, MUT indicates the position of the mutation to be tested.

Each wild type and mutant minigene plasmid constructs was transfected into HeLa cells and RNA was extracted after 48 hours and retrotranscribed. To avoid interference from endogenous *ASL* mRNA, cDNA was amplified with primers specific for plasmid sequences flanking the minigene.

RT-PCR analysis of mRNA expressed by the exon 5-6-7 minigenes transfected into HeLa cells revealed that the wild-type transcripts are correctly spliced, while transcripts carrying the c.524+2T>G mutation display skipping of exon 6 (fig.41A).

The same experiment was repeated for the exon 8-9-10 minigene. In this case the splicing of the hybrid minigene was less efficient, showing some degree of exon skipping also in the wild-type minigene (fig.41B). It should be noted, however, that a variable degree of skipping occurs physiologically for various exons of the ASL transcript during maturation (Linnebank et al. 2000). Nevertheless, no transcripts containing exon 9 were expressed from the mutated construct (fig.41C).

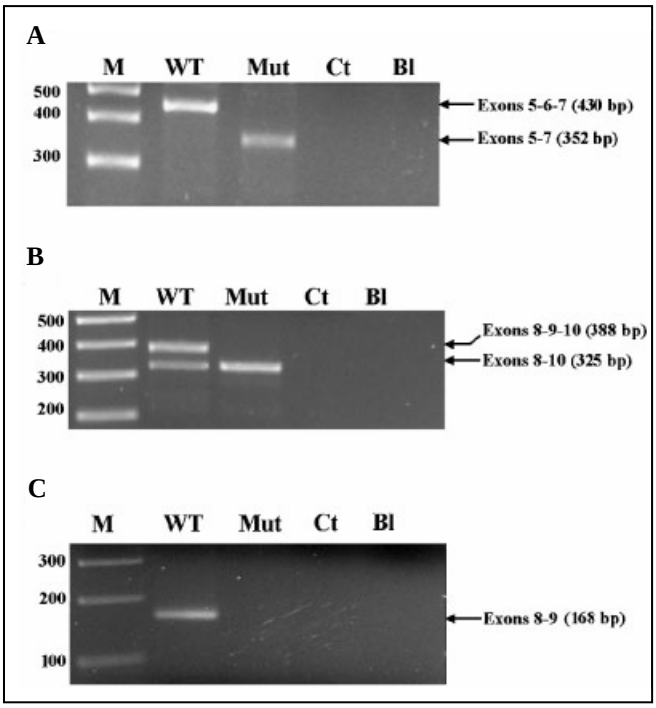

Fig.41 RT-PCR analysis of the Exon 5-6-7 minigene (A) and 8-9-10 minigene (B) expressed in HeLa cells; (C) RT-PCR of the Exon 8-9-10 minigene with primers specific for exon 9, showing exon skipping. M= molecular marker, WT= wild type construct, Mut= mutant construct, Ct=control cell line transfected with pEGFP-N1, Bl= blank control.

The transcripts from the mutant minigenes display aberrant splicing with exon skipping, and we could not detect the correctly spliced mRNA, which in contrast is expressed by the wild type constructs. Even though we cannot be certain that our model exactly reproduces the in vivo situation, our data indicate that the two mutations have a severe effect on mRNA maturation; moreover, other reported splicing mutations in the *ASL* gene cause similar exon skipping (Linnebank et al. 2002). In both cases exon skipping maintains the reading frame of the transcript and causes a deletion of 26 (exon 6) or 21 (exon 9) amino acids in critical regions of the protein: transfected cells were examined by fluorescent microscopy, but only faint fluorescence was detected for either wild-type and mutated minigenes, indicating that expression levels of mature transcripts were low.

13.3.2 Analysis of missense mutations

Specific PCR-RFLP analysis showed that all missense mutations were absent in 100 control alleles. We performed sequence alignment of ASL protein sequences in different species using the Multalin software (version 5.4.1, http://www-archbac.u-psud.fr/genomics/multalin.html): all novel missense mutations affect highly conserved residues of the protein (Table 11).

13.3.2.1 Biochemical analysis

We analyzed ASL activity in erythrocytes of 10 healthy controls and six patients using the method of Bastone et al (1990), which measures the production of ornithine, using a Jeol JLC 500/V amino acid analyzer (Jeol Ltd., Tokyo, Japan). All samples were processed immediately after collection. Activity is expressed as nmol/hr/mg hemoglobin (table 10).

In patients 4 and 9, ASL activity had been previously determined in Dr. W.J. Kleijer's laboratory (Department of Clinical Genetics, Erasmus University Medical Center, Rotterdam, The Netherlands) by [^{14}C] citrulline incorporation in primary skin fibroblasts.

ASL activity was very low (<5% of controls) in all patients, except in Patient 8b, who had a relatively higher residual activity (about 9% of controls) and displayed the late-onset phenotype. In Patient 9, ASL activity had previously been measured in fibroblasts with a similar result. In Patient 4, activity has been determined only in fibroblasts and was also low (<2% of controls).

13.3.2.2 Molecular modeling

To predict the possible consequences of individual missense mutations, we have analyzed the three-dimensional structure of the enzyme.

All images were generated by using Pymol (DeLano Scientific LLC; Palo Alto, CA; http://pymol.sourceforge.net) as reported previously (Pagano et al. 2004). The structures utilized as templates for modeling were the human ASL protein (pdb code 1AOS) and Duck Delta Crystallin (pdb code 1TJW), an orthologue of ASL, which is the only one crystallized as a tetramer with its substrate. The calculation of the electrostatic surface

charges was performed with the APBS software (Baker et al. 2001) and visualized by using Pymol.

Table 11: Alignment of the region encompassing the missense mutations in various species.

D31N

Patient	ASIAY**N**RHLWEVD
H.sapiens	ASIAY**D**RHLWEVD
M.musculus	SSISY**D**RHLWNVD
X.laevis	CSVNY**D**QRMWSAD
C.reinhardtii	ESLPF**D**KRLWAED
S.cerevisiae	ASLPY**D**YKMYKAD
B.subtilis	ASISF**D**QNLVAED

E73K

Patient	DKVAE**K**WAQGTFK
H.sapiens	DKVAE**E**WAQGTFK
M.musculus	DKVAE**E**WAQGTFK
X.laevis	DKIHD**E**WSSGTFV
C.reinhardtii	AKVAE**E**WKAGAFV
S.cerevisiae	AEIKK**E**WDADKFV
B.subtilis	NTLLQKAEEGALE

R113Q

Patient	HTGRS**Q**NDQVVTD
H.sapiens	HTGRS**R**NDQVVTD
M.musculus	HTGRS**R**NDQVVTD
X.laevis	HTGRS**R**NDQVVTD
C.reinhardtii	HTGRS**R**NDQVATD
S.cerevisiae	HTGRS**R**NDQVVTD
B.subtilis	HTGRS**R**NDQVATD

R186Q

Patient	TRDSE**Q**LLEVRKR
H.sapiens	TRDSE**R**LLEVRKR
M.musculus	TRDSE**R**LLEVQKR
X.laevis	SRDAE**R**LGEVKKR
C.reinhardtii	QRDDM**R**LRDLLPR
S.cerevisiae	TEDYK**R**LGQILHR
B.subtilis	ERDKE**R**FQDSMKR

R456W

Patient	QIRQV**W**ALLQAQQ
H.sapiens	QIRQV**R**ALLQAQQ
M.musculus	QIRQV**R**ALLQAQE
X.laevis	QIEQL**R**TWMKTHR
C.reinhardtii	QVQKM**R**TYLAAEG
S.cerevisiae	QLDNLKSQLN
B.subtilis	ALEKAKACVAAGV

R236W

Patient	DATSE**W**DFVAEFL
H.sapiens	DATSE**R**DFVAEFL
M.musculus	DATSE**R**DFVAEFL
X.laevis	DATSE**R**DFIAEFL
C.reinhardtii	DAVSD**R**DFVIETV
S.cerevisiae	VAVSD**R**DFIVELM
B.subtilis	DGVSD**R**DFILEFL

R297Q

Patient	SLELI**Q**SKAGRVF
H.sapiens	SLELI**R**SKAGRVF
M.musculus	SLELI**R**SKAGRVF
X.laevis	SLELI**R**GKTGRVF
C.reinhardtii	ALELI**R**GKGGRVQ
S.cerevisiae	SLELL**R**GKSGRVF
B.subtilis	MAELI**R**GKTGRVY

V335L

Patient	EAVFE**L**SDTMSAV
H.sapiens	EAVFE**V**SDTMSAV
M.musculus	EAVFE**V**SDTMIAV
X.laevis	EAMFD**V**YDTVCAV
C.reinhardtii	ELLFDTVDTVHDV
S.cerevisiae	EPLFDCLTTVEHS
B.subtilis	EGMFDTVKTVEGS

M382R

Patient	LVRKG**R**PFRQAHE
H.sapiens	LVRKG**M**PFRQAHE
M.musculus	LVRKG**M**PFRQAHE
X.laevis	LVRKG**M**PFRQAHG
C.reinhardtii	LVRKGVPFRETHH
S.cerevisiae	LVRKGVPFRETHH
B.subtilis	LAKKG**M**PFREAHE

ASL is active as a homotetramer (fig.42A) and each monomer is composed of three main domains (see §11.1, fig.36).

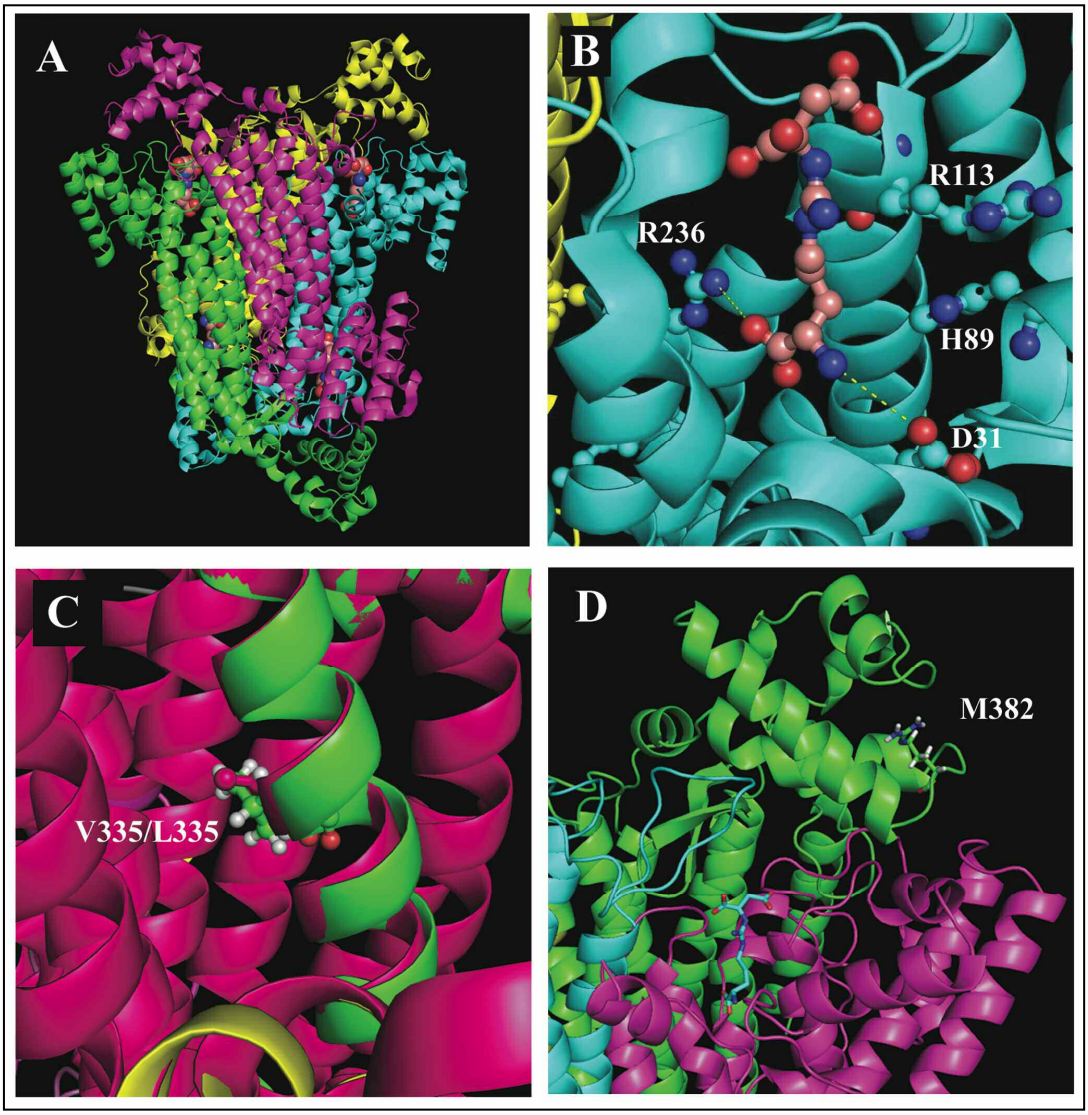

Fig.42 Analysis of the effect of missense mutations on the structure of ASL. A) Representation of the active ASL tetramer. Individual monomers have different colors. B) Active site of the enzyme with aspartate 31, arginine 113, and arginine 236 and the ASA substrate. Arginine 113 interacts with histidine 89, which is actively involved in the catalytic process. C) Superimposition of the normal structure (magenta) with the calculated structure of the subunit carrying the V335L mutation (green). D) Representation of methionine 382 in the third domain of the enzyme.

Aspartate 31, arginine 113, and arginine 236 are conserved throughout evolution, are located within the active site of the enzyme, and interact with the substrate (fig.42B), Arginine 113 interacts also with histidine 89, which is directly involved in the catalytic process (Abu-Abed et al. 1997; Sampaleanu et al. 2001). Mutations in these highly conserved residues are likely to have a severe impact on the catalytic function

of the protein. Interestingly, a different mutation at codon 113 has already been reported (R113W) (Linnebank et al. 2000).

Arginine 186, together with arginine 182 and histidine 252, forms a positively charged pocket on the surface of the protein, which interacts with the negatively charged aspartate 237 residue located on the adjacent monomer (fig.423A). We calculated the distribution of surface charges in the wild-type protein, and in the protein modeled with the R186Q mutation. As seen in figure 43B and 43C, the presence of a glutamine at position 186 completely alters charge distribution, abolishing the positively-charged pocket essential for the interaction with aspartate 237. As the catalytic site is formed by three different monomers (Sampaleanu et al. 2001), it is likely that a faulty interaction between monomers impairs the catalytic properties of the mutated enzyme. Moreover, aspartate 237 is in contact with arginine 236, which, as was discussed above, is part of the catalytic site.

Valine 335 is located in one of the five alpha-helical segments that form a helical bundle within the central domain of the protein, which is critical for the association of monomers. As seen in figure 42C, the larger steric hindrance of leucine displaces the alpha helix and probably impairs the correct folding of the enzyme. Valine is conserved in higher eukaryotes, while lower organisms have threonine or cysteine in this position, both residues with a smaller steric hindrance than leucine (Table 11).

Methionine 382 is located on the third domain of the protein (fig.42D). Analysis of ASL structure did not provide us with an obvious explanation for the pathogenicity of the M382R mutation. Methionine 382 is conserved in higher eukaryotes, while simpler organisms have a valine in this position (table 11). It is possible that the substitution of a hydrophobic amino acid with a positively charged arginine alters the stability of this domain, however more detailed structural and functional analyses are needed to clarify this issue.

R456W mutation involves a conserved arginine in the terminal alpha helix of the protein. It is conserved in all higher eukaryotes, while in lower organisms is replaced by lysine, another basic amino acid with a similar size (table 11). Substitution with tryptophan is predicted to cause a displacement of this alpha helix (fig.43D and 43F) and to shift the position of glutamine 454. This residue is important for dimerization because it forms a hydrophobic pocket that tightly interacts with leucine 227 located on the adjacent subunit (fig.43E). Both these amino acids are also highly conserved.

Modeling data suggest that this interaction is impaired in the mutated protein (fig.42F).

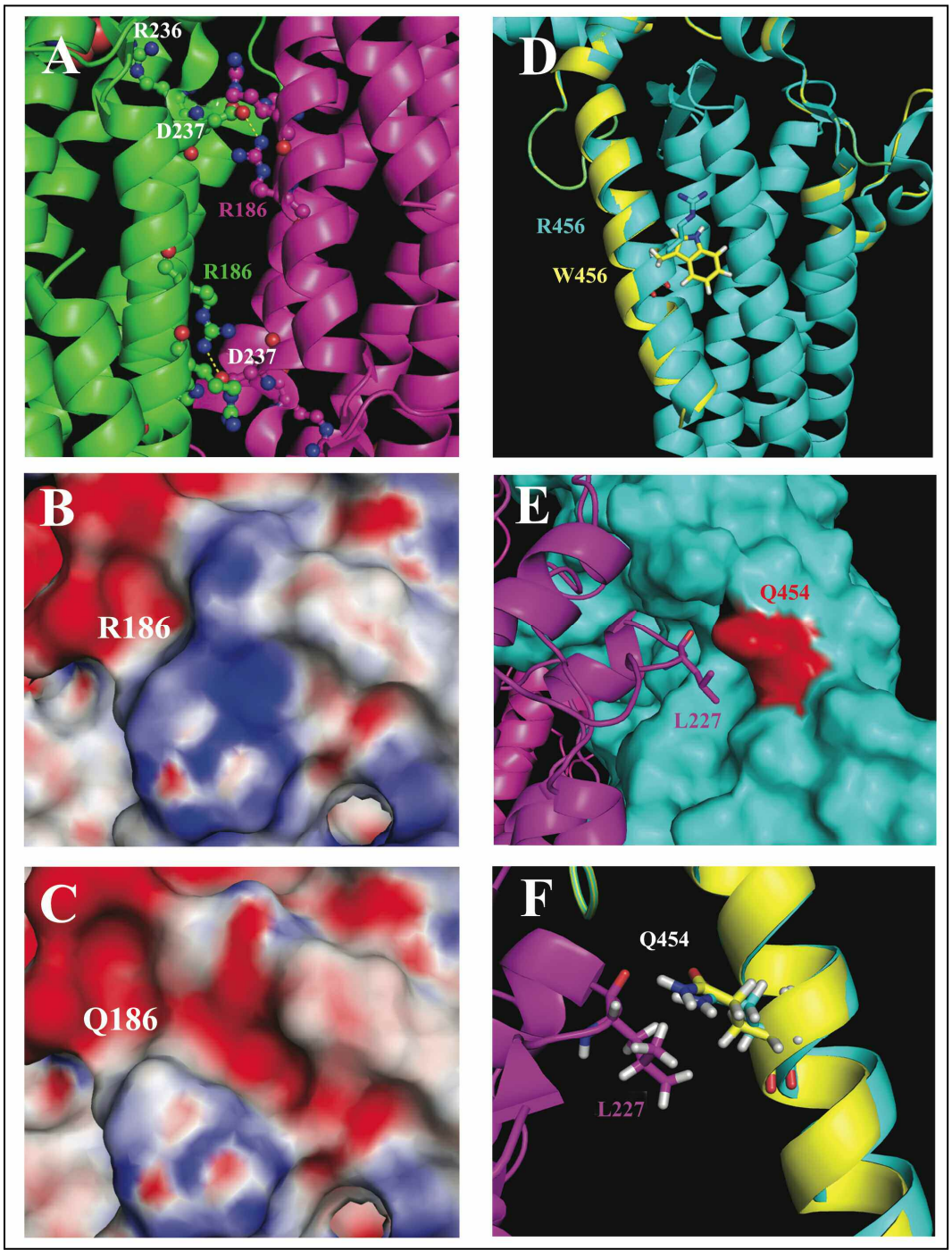

Fig.43 (A) Representation of arginine 186 and aspartate 237 involved in the interaction of two adjacent subunits. (B,C) Calculated surface charge surrounding residue 186 in the wild type (B) and in the protein with the R186Q mutation (C). In blue the negatively charged regions, in red the positively charged regions. D) Structure of the terminal domain in the wild type protein (cyan) superimposed to the calculated structure of the R456W mutant (yellow). R456 and W456 are depicted. E) Interaction between glutamine 454 and leucine 227 on the adjacent monomer. F) Position of glutamine 454 in the wild type (cyan) and in the R456W mutant (yellow).

We did not perform modeling for the two last mutations, E73k and R297Q; yet, both are highly conserved in eukaryotes (table 11).

Biochemical data are available only for four of the nine novel missense mutations, showing marked reduction of ASL activity in all cases. Nevertheless, all missense mutations were absent in 100 control alleles, affect highly conserved residues of the protein, and molecular modeling data (even though they represent only computer predictions) indicate that the involved amino acids are located in critical sites of the enzyme. Moreover, the D31N and the V335L mutations segregate with the phenotype in the two affected sibling pairs. Taken together, these data strongly argue in favor of the pathogenicity of these mutations.

13.3.2.3 Functional complementation in *Saccharomyces cerevisiae*

In order to prove the pathogenicity of the novel missense mutations and to unveil potential genotype-phenotype correlations among the ASL mutational spectrum, we developed a functional complementation assay in *S.cerevisiae*. This single-cell eukaryote represents an excellent experimental system, because it is amenable to genetic analysis (yeast readily takes up, recombines, and expresses foreign DNA) and stably exists in both the haploid and diploid state with a fast generation time. Thus, two haploid strains of opposite mating type can fuse to form a diploid strain, allowing for intragenic complementation assays and haplo-insufficiency analysis.

The *ASL* gene is highly conserved throughout evolution: the human protein shares the 56% of identity with the corresponding yeast homologue ARG4 (O'Brien et al 1986). Moreover, expression of duck δ2-crystallin protein can restore the growth of a yeast strain deficient for argininosuccinate lyase activity (Barbosa et al 1991a).

At first, we checked whether the human *ASL* gene could complement the yeast null mutant strain BY4741ΔARG4 ($ARG4^{null}$ or Y00981, see table I in appendix II), which is deficient for argininosuccinate lyase activity and consequently auxotrophic for arginine. cDNA sequences of the human and the yeast homologues were sub-cloned into the yeast expression vector pYES2.1, under the control of a *GAL* promoter for the inducible expression of the inserted gene (Invitrogen, Carlsbad, CA; www.invitrogen.com). These two constructs or the empty vector were transformed into the $ARG4^{null}$ strain. Transformations were performed as described above (see

§9.1.4). Cells were grown in minimal medium without uracil (SD-URA) 2% galactose 16 hours at 30ºC with shaking to express the recombinant genes. Growth in SD-URA without arginine (SD-ARG-URA) was determined as a marker of functional complementation, since it is possible only in the presence of a residual ASL activity. As shown in figure 44, human *ASL* efficiently complements the deleted strain.

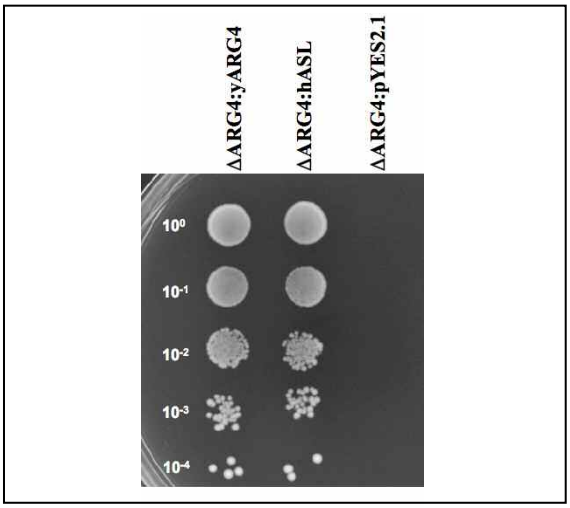

Fig.44 The human *ASL* gene restores the growth in SD-ARG-URA in ARG4Δ yeast. Cells grown in SD-URA 2% galactose were inoculated into SD-ARG-URA agar plates. The initial suspension at 1 U OD 660nm/mL was diluted 1/10 four times. Ten µL of cells solutions were spotted onto SD-ARG plates which were incubated at 30ºC for three days.

The *hASL*-pYES2.1 construct was then mutagenised using the Stratagene kit according to the manufacturer's protocol, in order to insert each one of the missense mutations previously identified in the cohort of patients. We obtained twelve different expression vectors, which were used to transform the ARG4^{null} strain. We tested the ability of the resulting transformants to grow in SD-ARG-URA to verify whether mutant constructs cause a decrease in ASL enzymatic activity.

In figure 45, yeast cells were grown in SD-ARG-URA containing 2% galactose, in order to induce the *GAL* promoter and overexpress the ASL protein. Based on different growth in the presence of the inductor, we found that the twelve missense mutations can be distinguished in three different classes:

1. Class 1: Mutations that virtually abolish ASL enzymatic activity (no growth in SD-ARG-URA) Q286R, R236W, R113Q, R182Q, E73K.
2. Class 2: Mutations that strongly reduce ASL enzymatic activity (some growth in SD-ARG-URA) D31N, R186Q, R297Q.
3. Class 3: Mutations with a relatively high residual activity (normal growth in SD-ARG-URA) V178M, M382R, V335L, R456W.

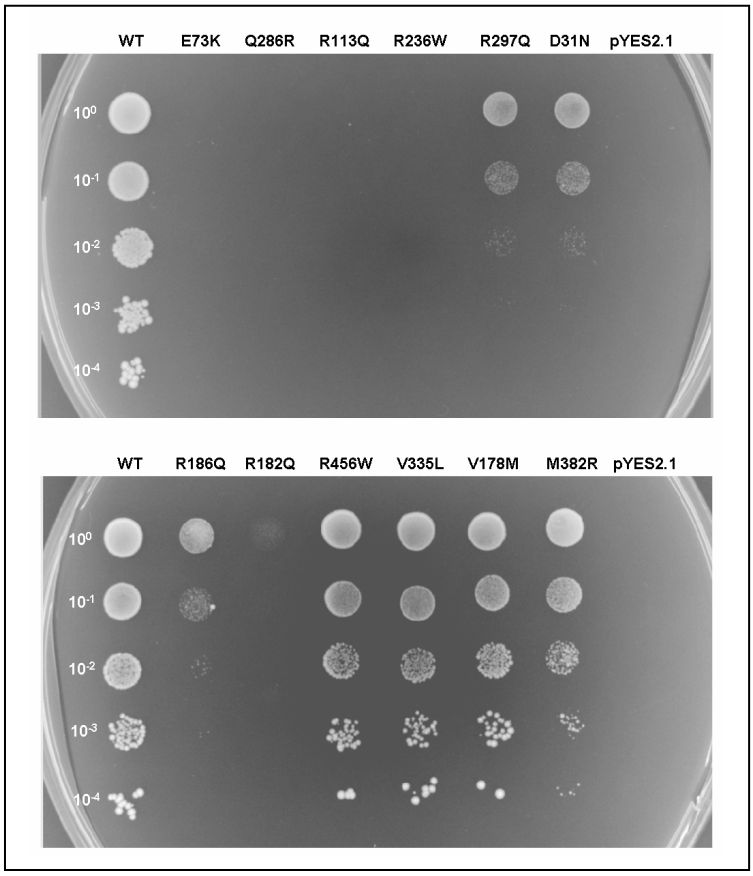

Fig.45 Functional complementation of ΔARG4 yeast strain transformed with the different mutated ASL constructs. Cells grown in SD-URA 2% galactose were inoculated into SD-ARG-URA agar plates. The initial suspension at 1 U OD 660nm/mL was diluted 1/10 four times. Ten µL of cells solutions were spotted onto SD-ARG plates, which were incubated at 30ºC for three days. WT = ΔARG4 transformed with wild-type *hASL*; pYES2.1 = ΔARG4 transformed with the empty vector.

Truncating mutations should be considered among class 1 mutations.

Mutations of the second and third classes were tested in SD-ARG-URA with reduced levels of the inducer: we used raffinose 2% as carbon source, which does not affect the *GAL* promoter, and supplemented the medium with 0,01% galactose, in order to modulate protein expression.

These conditions virtually abolish the growth of strains transformed with constructs carrying Class 2 mutations (R297Q, D31N and R186Q) and M382R mutation, whereas the others retained growth in SD-ARG-URA (fig.46), although at lower levels than the wild-type human protein.

For theses mutations (R456W, V335L and V178M), we measured ASL enzymatic activity of the strains transformed with the corresponding mutant allele. We used the protocol described by Barbosa et al (1991a), modified as follows: yeast cultures were

grown in minimal medium with galactose 2% until exponential phase (OD 0,8); cells were harvested and mechanically lyzed using MagnaLyzer instrument (Roche Diagnostic, Almere, The Netherlands). ASL activity was assayed by measuring ornithine levels using a Jeol JLC 500/V amino acid analyzer as above (13.3.2.1) and is expressed as percentage of activity of the deleted strain transformed with *hASL* (Table 12).

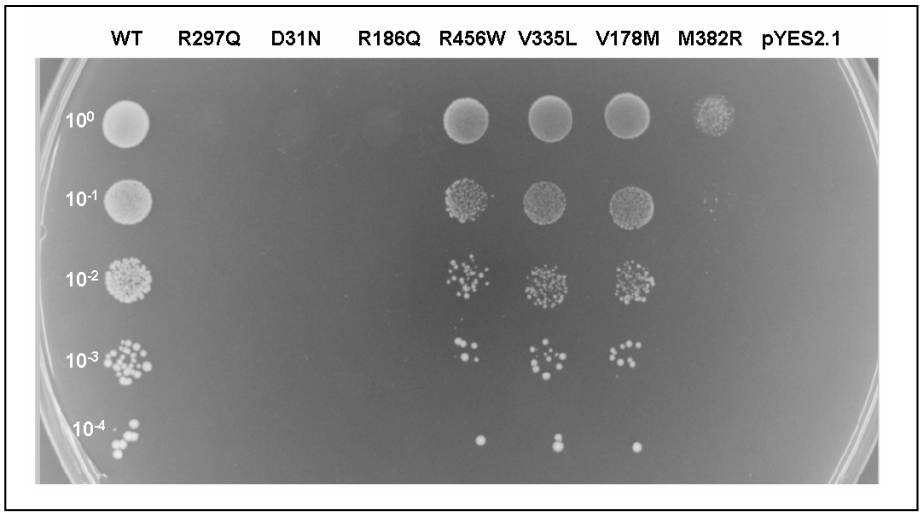

Fig.46 Functional complementation of ΔARG4 yeast strain transformed with ASL constructs carrying class 2 or class 3 mutations, in presence of reduced levels of inducer. Cells grown in SD-URA 2% raffinose were inoculated into SD-ARG-URA agar plates, containing 2% raffinose and 0,01% galactose. The initial suspension at 1 U OD 660nm/mL was diluted 1/10 four times. Ten µL of cells solutions were spotted onto plates, which were incubated at 30ºC for three days. Letter codes as in fig.45.

Table 12. ASL activity of strains transformed with mutant alleles
*ASL activity is expressed as a percentage of ΔARG4:hASL (117.79 nmol/hr/mg protein).

Strain	**ASL activity***
ΔARG4:pYES2.1	<5%
ΔARG4:hASL R456W	<5%
ΔARG4:hASL V335L	22%
ΔARG4:hASL V178M	25%

Mutant ASL proteins display a reduced enzymatic activity compared to the human wild-type protein: R456W shows an activity inferior to 5%, whereas V335L and V178M present an activity which is respectively 22% and 25% of the wild-type protein. The datum for the V335L is in accordance with biochemical measurements in patients' erythrocytes.

Biochemical determination of ASL activity in cell lysates has a limited sensitivity. In previous studies there was a poor correlation between direct biochemical measurements of ASL activity and ^{14}C-citrulline uptake studies (Kleijer et al. 2002). The apparent absence of residual activity in fibroblasts was explained invoking the lability of the mutant ASL in patients, which may lead to complete deterioration of the enzyme in a cell homogenate, while in vivo a steady state level of residual activity may remain owing to new synthesis of ASL monomers (Kleijer et al. 2002).

However, a low residual activity, undetected by the biochemical assay (as for the R456W mutation) is sufficient to overcome arginine auxotrophy, as demonstrated by growth data (fig.45 and 46). This indicates that functional complementation is much more sensitive to predict the effect of ASL mutated proteins than direct biochemical measurements.

We then performed a functional intragenic complementation assay to verify if these mutations could complement each other when present in a heterozygous state. We transformed both the opposite mating types (*Mat a* and *Mat* α) ΔARG4 strains (see table I in appendix II) with each *hASL* gene construct carrying one of the twelve missense mutations. We mated the transformants and tested their growth in the absence of arginine and uracil in a SD lacking methionine and lysine (for which the *Mat a* and the *Mat* α strains are respectively auxotrophic) (Fig.47).

Growth in the absence of arginine was observed in the diploid strains carrying one of the following alleles: R182Q and Q286R. As previously reported by Walker et al (1997), we confirm that Q286R is a frequent complementing allele, and describe a novel allele with even higher complementing activity (R182Q).

13.4 Genotype-phenotype correlations

Our series of patients displayed both the neonatal onset and the late onset form. The correlation between the residual ASL activity (observed as yeast growth in SD-ARG) and the clinical phenotype is only partial. Patients with the severe phenotype can harbor mutations of any class; on the other hand, none of the patients with the mild phenotype had two Class 1 mutations, indicating that residual ASL activity is necessary, but not sufficient, to ensure a milder phenotype in the patients.

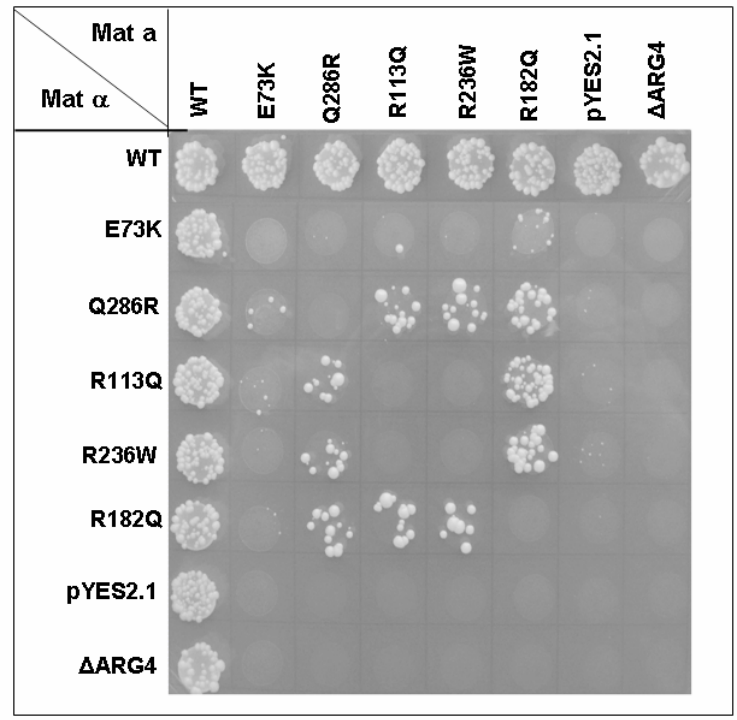

Fig.47 Intragenic complementation of ΔARG4 yeast strain with ASL mutated constructs. Cells grown in SD-URA 2% galactose were inoculated into SD-ARG-URA agar plates, diluting the initial suspension at 1 U OD 660nm/mL. Ten µL of cells solutions from *Mat a* and *Mat α* cultures were spotted onto plates, which were incubated at 30°C for three days. Letter codes as in fig.45.

As mentioned earlier, previous studies have found a poor correlation between ASL residual activity and clinical phenotype. However, these studies are influenced by several confounding factors:

a) Biochemical methods (either direct assays on patients tissues, or studies on purified recombinant proteins) are not very sensitive. Moreover, mutant enzymes are often labile, and tissue (or cell) homogenation may disrupt the tetrameric structure of the protein (Kleijer et al. 2002).

b) Patients are often compound heterozygotes for different mutations, and direct measurements cannot discriminate the role of individual alleles.

c) The results of more accurate tests, as radiolabelled citrulline uptake in fibroblasts, are affected by the genetic background of the patient

Our yeast system proved to be a useful model to establish the pathogenicity of *ASL* mutations and allows to study the effect of individual alleles, independently of the genetic background of the patient. Analysis of growth in arginine-free medium is simple, sensitive, and overcomes the problems inherent to classical biochemical

assays. Conceptually, it is similar to the indirect assay of radiolabelled citrulline uptake in fibroblasts, since both rely on an in vivo system.

The factors which determine clinical heterogeneity in our patients remain elusive.

Intragenic complementation does not appear to play a major role in our cohort because it can explain the milder phenotype only in Patient 11, who is a compound heterozygous for R297Q (a class 2 mutation) and R182Q (a class 1 mutation with high complementing activity). In the other kindreds with the milder form of the disease, this phenomenon cannot occur: patients were either homozygous for a missense mutation (D31N) or compound heterozygous for a missense (V335L; V178M) and a frameshift mutation.

The V335L mutation was found in a patient with a relatively high residual ASL activity in erythrocytes (about 9% of controls). The yeast strain transformed with the mutant allele had 22% activity compared to the wild-type human allele, indicating that this substitution is less detrimental for enzyme function.

Yeast expressing the V178M also had high residual ASL activity, and grew relatively well in raffinose. This mutation was initially reported in the homozygous state associated to a mild phenotype (Kleijer et al. 2002). In our series we found this mutation in two patients, one with the severe form, and one with the late-onset disease, in both cases in compound heterozygosity with two different mutations. Curiously it was associated with a class 1 frameshift mutation (c.839del_G) in patient 12 , who had the milder phenotype, and with a class 2 mutation (R186Q) in patient 4 who instead presented with the neonatal form. One possible explanation is that *ASL* expression levels in vivo may vary among different patients, albeit harboring the same mutation. These findings underscore the importance of other aspects (genetic modifiers and/or environmental factors) in determining the phenotype in patients (Lanpher et al. 2006).

Seizures were a common finding in our cohort, affecting most of patients with the neonatal presentation (who developed an epileptic syndrome that required continuous therapy with anticonvulsant drugs) and were the presenting symptom also in one of the patients with the late onset form.

Hepatic involvement is also found in most patients with the neonatal presentation. Patients displayed hepatomegaly, hypertransaminasemia, and reduced prothrombin time, but none had jaundice or signs of severe portal hypertension. In Patient 9, liver fibrosis was documented by a liver biopsy that also showed lipid and glycogen

accumulation, we believe that these two features are related to the particular dietary regimen. Interestingly, the six patients with the late-onset form have normal liver function. This finding suggests that hepatopathy is not common in patients with the milder form. Finally, it should be noted that in our series, patients with neonatal onset display progression of both neurological and hepatic manifestations despite adequate metabolic control.

Only two of the neonatal onset patients have normal liver function (Patients 4 and 7) and in both residual ASL activity was very low. Patient 7 was diagnosed and treated very early and at present he has only very mild psychomotor retardation. However, follow-up is too short and development of hepatic involvement or epilepsy later in the course of the disease is still possible. Patient 4 is 24 years old and, despite severe cerebral involvement, he still has normal liver function interestingly he is a compound heterozygous for the class 3 V178M mutation (see above).

14. CONCLUSIONS

Molecular genetic studies are not essential for the diagnosis of ASAuria because analysis of ammonia, and argininosuccinic acid in plasma, is considered adequate for a reliable diagnosis of the defect (Brusilov and Horwich, 2001). Determination of ASL activity in cultured fibroblasts or erythrocytes can be used to confirm the diagnosis; however, this technique is not widely available, and in the case of skin fibroblast, it is time consuming and requires a skin biopsy, an invasive procedure for young patients.

Reports on *ASL* mutations are scarce in the literature and only 32 mutations have been described thus far. In this work, we report 21 novel nucleotide changes (20 mutations and 1 neutral polymorphism) in the *ASL* gene found in a cohort of Italian patients. This is the only comprehensive mutation analysis in a cohort of patients with homogenous ethnical background.

Our genomic DNA-based approach has proved itself to be reliable, with a detection rate of 100% in our cohort of patients. Moreover, we described a novel pseudogene, which is crucial to perform genomic DNA-based mutation studies.

The functional hybrid minigene assay allows analyzing the pathogenicity of splice site mutations; furthermore, this novel approach could be easily adapted to the study of other metabolic disorders.

To test the pathogenicity of mutations in the argininosuccinate lyase (ASL) gene, we developed a functional complementation assay, using *S.cerevisiae* as experimental model. We found three different types of missense mutations, based on the ability to functionally complement the yeast null mutant strain. We believe that these differences reflect the residual enzymatic activity of the corresponding mutant alleles.

By generating heterozygous diploid strains, we proved intragenic complementation and found a new high activity complementing allele, R182Q, together with Q286R.

Genetic analysis should play an important role for prenatal diagnosis of ASAuria. Although measurement of ASL activity in chorionic villi is a reliable and sensitive method (Kleijer et al. 2002), it is complex and available only in very few laboratories worldwide. On the contrary, direct genetic analysis is feasible, fast, and specific and can be regarded as the method of choice for prenatal diagnosis. Therefore, we stress the importance of mutation screening in patients with ASAuria, in order to confirm

the clinical diagnosis and to provide adequate prenatal counseling to the future pregnancies of their families.

APPENDIX I

A CASE OF PELIZAEUS-MERZBACHER DISEASE

Pelizaeus-Merzbacher disease (PMD, MIM #312080) is a hypomyelinating disorder of the CNS, characterized by absence of myelin formation and severe neurological involvement with nystagmus, progressive spasticity, ataxia, and developmental delay (Inoue 2005). The magnetic resonance imaging (MRI) picture is characteristic, showing a uniformly increased intensity of the white matter signal on T2-weighted images. It is an X-linked recessive disorder caused by mutation in the *PLP1* gene. Point mutations, deletions and duplications of the entire *PLP1* gene have been associated with the disease.

The PMD-like disorder (PMDL, MIM #311601) presents with overlapping clinical features, but it is inherited as an autosomal recessive trait and is caused by mutations in the *GJA12* gene on chromosome 1q412 (Uhlenberg et al 2004). The *GJA12* gene codes for a 439-amino-acid gap junction protein (also known as connexin 46.6 or connexin 47), which is highly expressed in oligodendrocytes. At least, another yet unidentified gene is involved in PMLD (Uhlenberg et al 2004; Menichella et al 2003).

We studied a 5-year-old Pakistani girl with an unremarkable family history and whose parents denied consaguineity, who displayed clinical and neuroradiological features of PMD. She was diagnosed with nystagmus since age 3 months. MRI performed at 1 year of age showed diffuse hypomyelination, confirmed by a second MRI at 4 years. Neurologic examination revealed nystagmus, truncal hypotonia, lower limb spasticity, and dysarthric speech. EMG and peripheral nerve conduction studies were normal. Standard karyotype and analysis of the *PLP1* gene were normal, suggesting the possibility of an autosomal recessive disorder. Sequencing of the *GJA12* gene showed a homozygous 34-bp deletion within the coding region of the gene [c. 914_947del] (fig. 48A and B). The mutation alters the reading frame of the transcript from codon [p.P305fsX459]. Both parents were carriers of the deletion, which was absent in normal controls (fig.48C). The mutation was associated in both alleles with a neutral polymorphism [c. 285 G>A; p. 95 L>L]. The presence of the mutation was excluded in 100 control subjects (200 alleles). The novel homozygous 34-bp deletion in the

GJA12 gene alters the reading frame of the mRNA. The predicted mutant protein is 19 amino acids longer than the wild-type polypeptide.

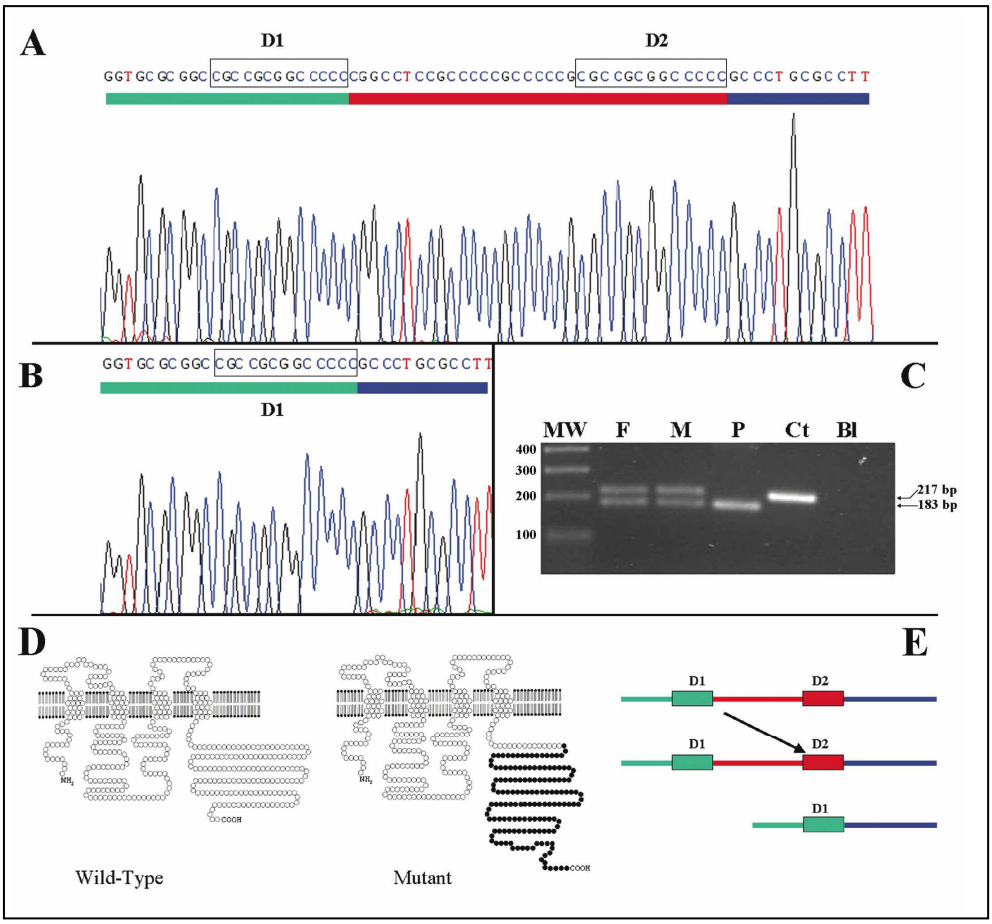

Fig.48: Sequence of the normal (A) and of the patient's (B) *GJA12* gene with the homozygous 34 nt deletion. The duplicated CGCCGCGGCCCCC sequences are boxed and marked D1 and D2. Underlined in red the deleted sequence, while in green and in blue the upstream and downstream regions. C) PCR fragments encompassing the deleted fragment in the patient (P), her father (F), her mother (M), and a normal control subject (Ct); MW= molecular markers, Bl= blank control. D) Schematic representation of the predicted mutated protein. In black the abnormal amino acids on the C-terminus of the mutant protein. E) Proposed molecular mechanism of the deletion: forward slippage of DNA polymerase mediated by D1 and D2 repeats during replication. Color codes as in A and B.

We believe that the mutation is pathogenic because the whole C-terminal domain, form codon 305, is completely altered (fig.48D). The heterozygous parents had a normal neurological examination, and there was no history of neurological disease in other family members. These data suggest that this novel *GJA12* mutation causes a "loss of function" of the Gja12 protein. Expression studies are needed to clarify this issue. The deleted sequence is flanked by a 13-nt CGCCGCGGCCCCC duplicated sequence. The deletion was probably caused by replication slippage, one common

causative mutational mechanism for deletions due to slipped mispairing of direct repeat sequences in proximity to one another (Chen et al. 2005) (fig.48E). The deletion was associated in both alleles with a neutral polymorphism [c. 285 G>A] suggesting a common ancestor, although the parents denied consanguinity.

This is only the third report of *GJA12* mutations associated with PMLD. Our data confirm that the clinical phenotype of patients with *GJA12* defects is quite homogeneous compared with that of *PLP1* mutations, which display ample phenotypic variability (Cailloux et al. 2000); however, we found no distinctive features that could help differentiate PMD and PMLD on clinical or neuroradiological bases. The distinction is based essentially on molecular genetic results.

Molecular analysis of *GJA12* is a simple procedure and is indicated in all patients with a PMD/PMLD phenotype without PLP mutations. However, we believe that female subjects and patients with consanguineous parents should probably be initially tested for mutations in this gene. The molecular diagnosis is important for appropriate counseling and prenatal diagnosis, and because confirmation of the clinical diagnosis avoids further unnecessary diagnostic procedures.

APPENDIX II

Summary of the *Escherichia coli*, *Saccharomyces cerevisiae* and *Caenorhabditis elegans* strains used in this study.

Strain	**Genotype**	**Source of reference**
E.coli DH5alpha	F- φ80lacZΔM15 Δ(lacZYA-argF) U169 recA1 endA1 hsdR17(rk-, mk+) gal- phoA supE44 λ- thi-1 gyrA96 relA1	Invitrogen
E.coli XL1blue	recA1 endA1 gyrA96 thi-1 hsdR17 supE44 relA1 lac [F´ proAB lacIqZΔM15 Tn10 (Tetr)]	Stratagene
E. coli HT115(DE3)	(F-, *mcrA*, *mcrB*, IN(*rrnD-rrnE*)1, lambda-, *rnc14::Tn10* (DE3 lysogen:*lacUV5* promoter-T7 polymerase)	*Caenorhabditis* Genetic Center, USA
E.coli OP50	(ura)	Brenner 1974
S.cerevisiae BY4741	Mat a; his3Δ1; leu2Δ0; met15Δ0; ura3Δ0	Euroscarf
S.cerevisiae Y05416 BY4741 Δ*coq2*	Mat a; his3Δ1; leu2Δ0; met15Δ0; ura3Δ0; YNR041c::kanMX4	Euroscarf
S.cerevisiae Y03563 BY4741 Δ*coq4*	Mat a; his3Δ1; leu2Δ0; met15Δ0; ura3Δ0; YDR204w::kanMX4	Euroscarf
S.cerevisiae Y06510 BY4741 Δ*coq5*	Mat a; his3Δ1; leu2Δ0; met15Δ0; ura3Δ0; YML110c::kanMX4	Euroscarf
S.cerevisiae Y00981 BY4741 Δ*arg4*	Mat a; his3Δ1; leu2Δ0; met15Δ0; ura3Δ0; YHR018c::kanMX4	Euroscarf
S.cerevisiae Y10981 BY4742 Δ*arg4*	Mat α; his3Δ1; leu2Δ0; lys2Δ0; ura3Δ0; YHR018c::kanMX4	Euroscarf
S.cerevisiae Y30981 BY4743 Δ*arg4*	Mat a/α; his3Δ1/his3Δ1; leu2Δ0/leu2Δ0; lys2Δ0/LYS2; MET15/met15Δ0; ura3D0/ura3Δ0; YHR018c::kanMX4/YHR018c::kanMX4	Euroscarf
C.elegans N2 Bristol	Wild-type strain	*Caenorhabditis* Genetic Center, USA
C. elegans DH26	*fer-15* (b26) II. Temperature sensitive. Spermatogenesis defective. Sterile at 25 ºC.	*Caenorhabditis* Genetic Center, USA
*C.*elegans NL2099	r*rf-3* (pk1426) II. Increased sensitivity to RNAi when compared to WT animals.	*Caenorhabditis* Genetic Center, USA

Abu-Abed M, Turner MA, Valle´e F, Simpson A, Slingsby C, Howell PL. (1997) Structural comparison of the enzymatically active and inactive forms of delta crystallin and the role of histidine 91. Biochemistry 36:14012–14022.

Adams PL, Lightowlers RN, Turnbull DM (1997) Molecular analysis of cytochrome c oxidase deficiency in Leigh's syndrome. Ann. Neurol. 41: 268–270.

Aeby A, Sznajer Y, Cavé H, Rebuffat E, Van Coster R, Rigal O, Van Bogaert P. (2007) Cardiofaciocutaneous (CFC) syndrome associated with muscular coenzyme Q10 deficiency. J Inherit Metab Dis. 30:827.

Allan JD, Cusworth DC, Dent CE, Wilson VK (1958) A disease, probably hereditary, characterised by severe mental deficiency and a constant gross abnormality of amino acid metabolism. Lancet I:182–187.

Al-Sayed M, Alahmed S, Alsmadi O, Khalil H, Rashed MS, Imtiaz F, Meyer BF. (2005) Identification of a common novel mutation in Saudi patients with argininosuccinic aciduria. J Inherit Metab Dis 28:877–883.

Antonicka H, Leary SC, Guercin GH, Agar JN, Horvath R, Kennaway NG (2003a) Mutations in COX10 result in a defect in mitochondrial heme A biosynthesis and account for multiple, early-onset clinical phenotypes associated with isolated COX deficiency. Hum. Mol. Genet. 12: 2693–2702.

Antonicka H, Mattman A, Carlson CG, Glerum DM, Hoffbuhr KC, Leary SC, Kennaway NG, Shoubridge EA (2003b) Mutations in COX15 produce a defect in the mitochondrial heme biosynthetic pathway, causing early-onset fatal hypertrophic cardiomyopathy. Am. J. Hum. Genet. 72: 101–114.

Appelgarth D, Davidson A, Perry L, Podon S, Chrichton J, Flandwick D (1975) Argininosuccinic acidemia in a healthy individual detected by a urine screening program. Clin Chem 21:950–951.

Arnesano F, Balatri E, Banci L, Bertini I, Winge DR. (2005) Folding studies of Cox17 reveal an important interplay of cysteine oxidation and copper binding. Structure. 13:713-22.

Artuch, R., Brea-Calvo, G., Briones, P., Aracil, A., Galvan, M., Espinos, C., Corral, J., Volpini, V., Ribes, A. and Andreu, A.L. et al. (2006) Cerebellar ataxia with coenzyme Q10 deficiency: Diagnosis and follow-up after coenzyme Q10 supplementation. J. Neurol. Sci, 246, 153–158.

Baba, S.W., Belogrudov, G.I., Lee, J.C., Lee, P.T., Strahan, J., Shepherd, J.N., Clarke, C.F. (2004). Yeast coq5 C-methyltransferase is required for stability of other polypeptides involved in coenzyme q biosynthesis. J. Biol. Chem. 279, 10052–10059.

Babcock GT and Wikstrom M. (1992) Oxygen activation and the conservation of energy in cell respiration. Nature 356: 301–309.

Baker NA, Sept D, Joseph S, Holst MJ, McCammon JA. (2001). Electrostatics of nanosystems: application to microtubules and the ribosome. Proc Natl Acad Sci USA 98:10037–10041.

Balamurugan K, Schaffner W. (2006) Copper homeostasis in eukaryotes: teetering on a tightrope. Biochim Biophys Acta. 1763:737-46.

Barbosa P, Wistow GJ, Cialkowski M, Piatigorsky J, O'Brien WE (1991a) Expression of duck lens delta-crystallin cDNAs in yeast and bacterial hosts. Delta 2-crystallin is an active argininosuccinate lyase. J Biol Chem 266: 22319–22322.

Barbosa P, Cialkowski M, O'Brien WE. (1991b) Analysis of naturally occurring and site-directed mutations in the argininosuccinate lyase gene. J Biol Chem 266:5286–5290.

Barros MH, Johnson A, Tzagoloff A. (2004) COX23, a homologue of COX17, is required for cytochrome oxidase assembly. J Biol Chem. 2004 279:31943-7.

Barros MH, Johnson A, Gin P, Marbois BN, Clarke CF, Tzagoloff A. (2005) The Saccharomyces cerevisiae COQ10 gene encodes a START domain protein required for function of coenzyme Q in respiration. J Biol Chem. 280:42627-35.

Bastone A, Diomede L, Parini R, Carnevale F, Salmona M. (1990) Determination of argininosuccinate lyase and arginase activities with an amino acid analyzer. Anal Biochem 191:384–389.

Beadle GW. (1950) Biochemical aspects of genetics. Fed Proc.92:512-6.

Beers J, Glerum DM, Tzagoloff A (1997) Purification, characterization, and localization of yeast Cox17p, a mitochondrial copper shuttle. J Biol Chem. 272:33191-6.

Belogrudov, G.I., Lee, P.T., Jonassen, T., Hsu, A.Y., Gin, P., Clarke, C.F. (2001). Yeast Coq4 encodes a mitochondrial protein required for coenzyme Q synthesis. Arch. Biochem. Biophys. 392, 48–58.

Bernardi P, Scorrano L, Colonna R, Petronilli V, Di Lisa F. (1999) Mitochondria and cell death. Mechanistic aspects and methodological issues. Eur J Biochem 264, 687-701.

Boitier E, Degoul F, Desguerre I, Charpentier C, Francois D, Ponsot G, Diry M, Rustin P, Marsac C (1998) A case of mitochondrial encephalomyopathy associated with a muscle coenzyme Q10 deficiency. J Neurol Sci 156:41–46.

Boyd D, Beckwith J. (1990) The role of charged amino acids in the localization of secreted and membrane proteins. Cell.62:1031-3.

Brandt U. and Trumpower B. (1994) The protonmotive Q cycle in mitochondria and bacteria. Crit. Rev. Biochem. Mol. Biol. 29:165–197

Brenner S. (1974) The genetics of Caenorhabditis elegans. Genetics. 77:71-94.

Brusilov SW and Horwich AL (2001) Urea cycle enzymes. In Scriver CR, Beaudet AL, Shy WS and Valle D editors. The Molecular and Metabolic Bases of Inherited Diseases Vol 2, 8th edition. New York: McGraw-Hill. p 1909–1964.

Cailloux F, Gauthier-Barichard F, Mimault C, Isabelle V, Courtois V, Giraud G, Dastugue B, Boespflug-Tanguy O (2000) Genotype-phenotype correlation in inherited brain myelination defects due to proteolipid protein gene mutations. Clinical European Network on Brain Dysmyelinating Disease. Eur J Hum Genet 8:837-45

Carlson CG, Barrientos A, Tzagoloff A, Glerum DM (2003) COX16 encodes a novel protein required for the assembly of cytochrome oxidase in Saccharomyces cerevisiae. J Biol Chem. 278:3770-5.

Cartegni L, Shern LC, Krainer AR. (2002) Listening to silence and understanding nonsense: exonic mutations that affect splicing. Nat Rev Genet 3:285–298.

Chen JM, Chuzhanova N, Stenson PD, Ferec C, Cooper DN (2005) Meta-analysis of gross insertions causing human genetic disease: novel mutational mechanisms and the role of replication slippage. Hum Mutat 25:207-21.

Chinnery PF, Turnbull DM (2001) Epidemiology and treatment of mitochondrial disorders. Am J Med Genet 106:94-101.

Claros MG. (1995) MitoProt, a Macintosh application for studying mitochondrial proteins. Comput Appl Biosci.11:441-7.

Collins FS. (1990) Identifying human disease genes by positional cloning. Harvey Lect. 86:149-64.

Dalakas MC, Illa I, Pezeshkpour GH, Laukaitis JP, Cohen B, Griffin JL. (1990) Mitochondrial myopathy caused by long-term zidovudine therapy. N Engl J Med. 322:1098-105.

Dillin A, Hsu AL, Arantes-Oliveira N, Lehrer-Graiwer J, Hsin H, Fraser AG, Kamath RS, Ahringer J, Kenyon C. (2002) Rates of behavior and aging specified by mitochondrial function during development. Science. 298:2398-401.

DiMauro S, Servidei S, Zeviani M, DiRocco M, DeVivo DC, DiDonato S, Uziel G, Berry K, Hoganson G, Johnsen SD. (1987) Cytochrome c oxidase deficiency in Leigh syndrome. Ann Neurol.22:498-506.

DiMauro S and De Vivo DC (1996) Genetic heterogeneity in Leigh syndrome. Ann. Neurol. 40: 5–7.

DiMauro S. (2004a) Mitochondrial diseases. Biochim Biophys Acta. 1658:80-8.

DiMauro S, Tay S, Mancuso M (2004b) Mitochondrial encephalomyopathies: diagnostic approach. Ann.N.Y.acad.Sci. 1011:217-231.

DiMauro S, Quinzii C, Hirano M (2007) Mutations in coenzyme Q10 biosynthetic genes. J Clin Invest. 117:587-9.

Dolezal P, Likic V, Tachezy J, Lithgow T. (2006) Evolution of the molecular machines for protein import into mitochondria. Science. 313:314-8.

Echtay KS, Winkler E, Klingenberg M. (2000) Coenzyme Q is an obligatory cofactor for uncoupling protein function. Nature. 408:609-13.

Echtay KS, Roussel D, St-Pierre J, Jekabsons MB, Cadenas S, Stuart JA, Harper JA, Roebuck SJ, Morrison A, Pickering S, Clapham JC, Brand MD (2002) Superoxide activates mitochondrias uncoupling proteins. Nature 415, 96-9.

Fontaine E, Ichas F, Bernardi P. (1998) A ubiquinone-binding site regulates the mitochondrial permeability transition pore. J Biol Chem. 273:25734-40.

Forsgren, M., Attersand, A., Lake, S., Grunler, J., Swiezewska, E., Dallner, G., Climent, I. (2004). Isolation and functional expression of human COQ2, a gene encoding a polyprenyl transferase involved in the synthesis of CoQ. Biochem. J. 382, 519–526.

Gaisne M, Bonnefoy N. (2006) The COX18 gene, involved in mitochondrial biogenesis, is functionally conserved and tightly regulated in humans and fission yeast. FEMS Yeast Res. 6:869-82.

Garesse R, Vallejo CG (2001) Animal mitochondrial biogenesis and function: a regulatory cross-talk between two genomes. Gene 263, 1-16.

Garrod AE, Clarke JW. (1907) A New Case of Alkaptonuria. Biochem J. 2:217-20.

Gibson QH. (1948) The reduction of methaemoglobin in red blood cells and studies on the cause of idiopathic methaemoglobinaemia. Biochem J. 42:13-23.

Gietz RD, Woods RA. (2006) Yeast transformation by the LiAc/SS Carrier DNA/PEG method. Methods Mol Biol. 313:107-20.

Gin P. and Clarke C.F. (2005) Genetic Evidence for a Multi-subunit Complex in Coenzyme Q Biosynthesis in Yeast and the Role of the Coq1 Hexaprenyl Diphosphate Synthase. JBC 280:2676–2681.

Glerum DM, Yanamura W, Capaldi RA, Robinson BH (1988). Characterization of cytochrome c oxidase mutants in human fibroblasts. FEBS Lett. 236: 100–104.

Glerum DM, Shtanko A, Tzagoloff A (1996) Characterization of COX17, a yeast gene involved in copper metabolism and assembly of cytochrome oxidase. J. Biol. Chem. 271:14504–14509.

Glerum, D.M., and Tzagoloff, A. (1997). Submitochondrial distributions and stabilities of subunits 4, 5, and 6 of yeast cytochrome oxidase in assembly defective mutants. FEBS Lett. 412:410– 414.

Grad LI, Sayles LC, Lemire BD. (2005) Introduction of an additional pathway for lactate oxidation in the treatment of lactic acidosis and mitochondrial dysfunction in Caenorhabditis elegans. Proc Natl Acad Sci U S A.102:18367-72.

Herrmann JM, Neupert W, Stuart RA (1997) Insertion into the mitochondrial inner membrane of a polytopic protein, the nuclearencoded Oxa1p. EMBO J.16:2217–2226.

Hill HZ, Goodman SI.(1974) Detection of inborn errors of metabolism. III. Defects in urea cycle metabolism. Clin Genet. 6:79-81.

Hirokawa T, Boon-Chieng S, Mitaku S. (1998) SOSUI: classification and secondary structure prediction system for membrane proteins. Bioinformatics 14:378-9.

Hiser L, Di Valentin M, Hamer AG, Hosler JP. (2000) Cox11p is required for stable formation of the Cu(B) and magnesium centers of cytochrome c oxidase. J Biol Chem. 275:619-23.

Horng YC, Cobine PA, Maxfield AB, Carr HS, Winge DR. (2004) Specific copper transfer from the Cox17 metallochaperone to both Sco1 and Cox11 in the assembly of yeast cytochrome C oxidase. J Biol Chem. 279:35334-40.

Howell PL, Turner MA, Christodoulou J, Walker DC, Craig HJ, Simard LR, Ploder L, McInnes RR. (1998) Intragenic complementation at the argininosuccinate lyase locus: reconstruction of the active site. J Inherit Metab Dis 21 (Suppl 1):72-85.

Indiveri C., Tonazzi A. and Palmieri F. (1992) Identification and purification of the ornithine/citrulline carrier from rat liver mitochondria. Eur. J. Biochem. 207: 449–454.

Inoue K (2005) PLP1-related inherited dysmyelinating disorders: Pelizaeus-Merzbacher disease and spastic paraplegia type 2. Neurogenetics 6: 1-16

Jaksch M, Horvath R, Horn N, Auer DP, Macmillan C, Peters J (2001). Homozygosity (E140K) in SCO2 causes delayed infantile onset of cardiomyopathy and neuropathy. Neurology 57: 1440–1446

Johnstone IL. (1999) Molecular biology. In: C. elegans—A Practical Approach. Edited by Hope, I.A. Oxford University Press, London.

Jonassen, T., Clarke, C.F. (2000). Isolation and functional expression of human COQ3, a gene encoding a methyltransferase required for ubiquinone biosynthesis. J. Biol. Chem. 275, 12381–12387.

Jones, M.E. (1980) Pyrimidine nucleotide biosynthesis in animals: genes, enzymes, and regulation of UMP biosynthesis. Annu. Rev. Biochem., 49,253–279.

Kadenbach B, Jarausch J, Hartmann R, Merle P (1983) Separation of mammalian cytochrome c oxidase into 13 polypeptides by a sodium dodecyl sulfate-gel electrophoretic procedure. Anal Biochem 129:517-21.

Kalen A, Appelkvist EL, Chojnacki T, Dallner G (1990) Nonaprenyl- 4-hydroxybenzoate transferase, an enzyme involved in ubiquinone biosynthesis, in the endoplasmic reticulum-Golgi system of rat liver. J Biol Chem 265:1158–1164.

Kaletta T, Hengartner MO. (2006) Finding function in novel targets: C. elegans as a model organism. Nat Rev Drug Discov. 5:387-98.

Kamath R.S., Martinez-Campos M., Zipperlen P., Fraser A.G., and Ahringer J. (2001). Effectiveness of specific RNA-mediated interference through ingested double-stranded RNA in Caenorhabditis elegans. Genome Biol, 2:

Katz, J.E., Dlakic, M., Clarke, S. (2003). Automated identification of putative methyltransferases from genomic open reading frames. Mol. Cell. Proteomics 2:525–540.

Kleijer WJ, Garritsen VH, Linnebank M, Mooyer P, Huijmans JG, Mustonen A, Simola KO, Arslan-Kirchner M, Battini R, Briones P, Cardo E, Mandel H, Tschiedel E, Wanders RJ, Koch HG. (2002) Clinical, enzymatic, and molecular genetic characterization of a biochemical variant type of argininosuccinic aciduria: prenatal and postnatal diagnosis in five unrelated families. J Inherit Metab Dis 25:399–410.

Lalani SR, Vladutiu GD, Plunkett K, Lotze TE, Adesina AM, Scaglia F. (2005) Isolated mitochondrial myopathy associated with muscle coenzyme Q10 deficiency. Arch Neurol. 62:317-20.

Lamperti C, Naini A, Hirano M, De Vivo DC, Bertini E, Servidei S, Valeriani M, Lynch D, Banwell B, Berg M, Dubrovsky T, Chiriboga C, Angelini C, Pegoraro E, DiMauro S (2003) Cerebellar ataxia and coenzyme Q10 deficiency. Neurology 60:1206–1208.

Lane P. and Gross S. S. (1999) Cell signaling by nitric oxide. Semin. Nephrol. 19: 215–229.

Lanpher B, Brunetti-Pierri N, Lee B. (2006) Inborn errors of metabolism: the flux from Mendelian to complex diseases. Nat Rev Genet 7:449–460.

Larsen PL and Clarke CF. (2002). Extension of life-span in Caenorhabditis elegans by a diet lacking coenzyme Q. Science, 295: 120-3.

Levy HL, Coulombe JT, Shih VE (1980) Newborn urine screening. In: Bickel H, Guthrie R, Hammersen G (eds) Neonatal screening for inborn errors of metabolism. Springer, Berlin Heidelberg New York, pp 89–103.

Lewis J.A. and Fleming J.T. (1995). Basic culture methods. Methods Cell Biol, 48:3-29.

Linnebank M, Homberger A, Rapp B, et al (2000) Two novel mutations (E86A, R113W) in argininosuccinate lyase deficiency and evidence for highly variable splicing of the human argininosuccinate lyase gene. J Inherit Metab Dis 23: 308 312.

Linnebank M, Tschiedel E, Häberle J, Linnebank A, Willenbring H, Kleijer WJ, Koch HG. (2002) Argininosuccinate lyase (ASL) deficiency: mutation analysis in 27 patients and a complete structure of the human ASL gene. Hum Genet 111:350–359.

Littarru GP and Tiano L. (2007) Bioenergetic and antioxidant properties of coenzyme Q10: recent developments. Mol Biotechnol. 37:31-7.

López LC, Schuelke M, Quinzii CM, Kanki T, Rodenburg RJ, Naini A, Dimauro S, Hirano M.(2006) Leigh syndrome with nephropathy and CoQ10 deficiency due to decaprenyl diphosphate synthase subunit 2 (PDSS2) mutations. Am J Hum Genet. 79:1125-9.

López-Martín JM, Salviati L, Trevisson E, Montini G, DiMauro S, Quinzii C, Hirano M, Rodriguez-Hernandez A, Cordero MD, Sánchez-Alcázar JA, Santos-Ocaña C, Navas P (2007). Missense mutation of the COQ2 gene causes defects of bioenergetics and de novo pyrimidine synthesis. Hum Mol Genet. 16:1091-7.

Maher AD, Kuchel PW, Ortega F, de Atauri P, Centelles J, Cascante M. (2003) Mathematical modelling of the urea cycle. A numerical investigation into substrate channelling. Eur J Biochem. 270:3953-61.

Marbois, B., Gin, P., Faull, K.F., Poon, W.W., Lee, P.T., Strahan, J., Shepherd, J.N. and Clarke, C.F. (2005) Coq3 and Coq4 define a polypeptide complex in yeast mitochondria for the biosynthesis of coenzyme Q. J. Biol. Chem. 280:20231–20238.

Mattatall NR, Jazairi J, Hill BC. (2000) Characterization of YpmQ, an accessory protein required for the expression of cytochrome c oxidase in Bacillus subtilis. J Biol Chem. 275:28802-9.

McCurdy PR. (1971) Use of genetic linkage for the detection of female carriers of hemophilia. N Engl J Med. 285:218-9.

McEwen JE, Ko C, Kloeckner-Gruissem B, Poyton RO (1986) Nuclear functions required for cytochrome c oxidase biogenesis in Saccharomyces cerevisiae. Characterization of mutants in 34 complementation groups. J Biol Chem 261: 11872–11879,

McInnes RR, Shih V, Chilton S. (1984) Interallelic complementation in an inborn error of metabolism: genetic heterogeneity in argininosuccinato lyase deficiency. Proc Nat. Acad Sci USA 81: 4480-4484.

Menichella DM, Goodenough DA, Sirkowski E, Scherer SS, Paul DL (2003) Connexins are critical for normal myelination in the CNS. J Neurosci 23:5963-73

Michel H, Behr J, Harrenga A, Kannt A. (1998) Cytochrome c oxidase: structure and spectroscopy. Annu Rev Biophys Biomol Struct 27:329-56.

Mignone F, Grillo G, Licciulli F, Iacono M, Liuni S, Kersey PJ, Duarte J, Saccone C, Pesole G (2005) UTRdb and UTRsite: a collection of sequences and regulatory motifs of the untranslated regions of eukaryotic mRNAs. Nucleic Acids Res. 33:D141-6.

Milenkovic D, Muller J, Stojanovski D, Pfanner N, Chacinska A (2007) Diverse mechanisms and machineries for import of mitochondrial proteins. Biol Chem 388, 891-897.

Mollet J, Giurgea I, Schlemmer D, Dallner G, Chretien D, Delahodde A, Bacq D, de Lonlay P, Munnich A, Rötig A. (2007) Prenyldiphosphate synthase, subunit 1 (PDSS1) and OH-benzoate polyprenyltransferase (COQ2) mutations in ubiquinone deficiency and oxidative phosphorylation disorders. J Clin Invest. 117:765-72.

Mootha VK, Lepage P, Miller K, Bunkenborg J, Reich M, Hjerrild M (2003) Identification of a gene causing human cytochrome c oxidase deficiency by integrative genomics. Proc. Natl. Acad. Sci. U.S.A. 100: 605–610.

Msall M, Batshaw ML, Suss R, Brusilow SW, Mellits ED. (1984) Neurologic outcome in children with inborn errors of urea synthesis. Outcome of urea-cycle enzymopathies. N Engl J Med. 310:1500-5.

Muller FL, Lustgarten MS, Jang Y, Richardson A, Van Remmen H. (2007) Trends in oxidative aging theories. Free Radic Biol Med. 43:477-503.

Munnich A, Rustin P (2001) Clinical spectrum and diagnostic of mitochondrial disorders. Am J Med Gen Semin 106:4-17.

Musumeci O, Naini A, Slonim AE, Skavin N, Hadjigeorgiou GL, Kravwiecki N Weissman BM, Tsao CY, Mendell JR, Shanske S, De Vivo DC, Hirano M, DiMauro S (2001) Familial cerebellar ataxia with muscle coenzyme Q10 deficiency. Neurology 56:849–855.

Naylor SL, Klebe RJ, Shows TB (1978) Argininosuccinic aciduria: assignment of the argininosuccinate lyase gene to the pter→q22 region of human chromosome 7 by bioautographie. Proc Natl Acad Sci USA 75:6159–6162.

Nijtmans LG, Taanman JW, Muijsers AO, Speijer D, and Van den Bogert C. (1998) Assembly of cytochrome-c oxidase in cultured human cells. Eur J Biochem 254: 389–394.

Nobrega MP, Bandeira SC, Beers J, Tzagoloff A (2002) Characterization of COX19, a widely distributed gene required for expression of mitochondrial cytochrome oxidase. J. Biol. Chem. 277:40206– 40211.

O'Brien WE, McInnes RR, Kalumuck K, Adcock M (1986) Cloning and sequence analysis of cDNA for human argininosuccinate lyase. Proc Natl Acad Sci USA 83:7211–7215.

Ogasahara S, Engel AG, Frens D, Mack D. (1989) Muscle coenzyme Q deficiency in familial mitochondrial encephalomyopathy. Proc Natl Acad Sci U S A. 86:2379-82.

Padilla S, Jonassen T, Jiménez-Hidalgo MA, Fernández-Ayala DJ, López-Lluch G, Marbois B, Navas P, Clarke CF, Santos-Ocaña C. (2004) Demethoxy-Q, an intermediate of coenzyme Q biosynthesis, fails to support respiration in Saccharomyces cerevisiae and lacks antioxidant activity. J Biol Chem. 279:25995-6004.

Pagano MA, Andrzejewska M, Ruzzene M, Sarno S, Cesaro L, Bain J, Elliott M, Meggio F, Kazimierczuk Z, Pinna LA. (2004) Optimization of protein kinase CK2 inhibitors derived from 4,5,6,7-tetrabromobenzimidazole. J Med Chem 47:6239–6247.

Papadopoulou LC, Sue CM, Davidson M, Tanji K, Nishino I, Sadlock J, Selby J, Glerum DM, Van Coster R, Lyon G, Scalais E, Lebel R, Kaplan P, Shanske S, De Vivo DC, Bonilla E, Hirano M, DiMauro S, Schon EA (1999) Fatal infantile cardioencephalomyopathy with COX deficiency and mutations in SCO2, a human COX assembly gene. Nat Genet 23:333–337.

Paulus H. (1983) The evolutionary history of the ornithine cycle as a determinant of its structure and regulation. Curr. Top. Cell Regul. 22: 177–200.

Petruzzella V, Tiranti V, Fernandez P, Ianna P, Carrozzo R, Zeviani M. (1998) Identification and characterization of human cDNAs specific to BCS1, PET112, SCO1, COX15, and COX11, five genes involved in the formation and function of the mitochondrial respiratory chain. Genomics. 54:494-504.

Piatigorsky J, O'Brien WE, Norman BL, Kalumuck K, Wistow GJ, Borras T, Nickerson JM, Wawrousek EF (1988) Gene sharing by delta-crystallin and argininosuccinate lyase. Proc Natl Acad Sci USA 85:3479–3483.

Preuss M, Ott M, Funes S, Luirink J, Herrmann JM (2005) Evolution of mitochondrial oxa proteins from bacterial YidC. Inherited and acquired functions of a conserved protein insertion machinery. J Biol Chem. 280:13004-11.

Quinzii CM, Kattah AG, Naini A, Akman HO, Mootha VK, DiMauro S, Hirano M (2005) Coenzyme Q deficiency and cerebellar ataxia associated with an aprataxin mutation. Neurology 64:539–541.

Quinzii C, Naini A, Salviati L, Trevisson E, Navas P, DiMauro S, Hirano M (2006) A mutation in para-hydroxybenzoatepolyprenyl transferase (COQ2) causes primary coenzyme Q10 deficiency. Am J Hum Genet 78:345–349.

Rae TD, Schmidt PJ, Pufahl RA, Culotta VC, O'Halloran TV. (1999) Undetectable intracellular free copper: the requirement of a copper chaperone for superoxide dismutase. Science. 284:805-8.

Rahman S, Hargreaves I, Clayton P, Heales S (2001) Neonatal presentation of coenzyme Q10 deficiency. J Pediatr 139:456–458.

Raijman L. (1974) Citrulline synthesis in rat tissues and liver content of carbamoyl phosphate and ornithine. Biochem. J. 138: 225–232.

Rea SL, Ventura N, Johnson TE. (2007) Relationship between mitochondrial electron transport chain dysfunction, development, and life extension in Caenorhabditis elegans. PLoS Biol.5:e259.

Rep M, and Grivell LA. (1996) The role of protein degradation in mitochondrial function and biogenesis. Curr. Genet. 30: 367–380

Rezzonico R, Burger D, Dayer JM (1998) Direct contact between T lymphocytes and human dermal fibroblasts or synoviocytes down-regulates types I and III collagen production via cell-associated cytokines. J Biol Chem. 273:18720-8.

Rigby K, Zhang L, Cobine PA, George GN, Winge DR. (2007) Characterization of the cytochrome c oxidase assembly factor Cox19 of Saccharomyces cerevisiae. J Biol Chem. 282:10233-42.

Rizzuto R, Pinton P, Brini M, Chiesa A, Filippin L, Pozzan T (1999) Mitochondria as biosensors of calcium microdomains. Cell Calcium. 1999 26, 193-9.

Robinson BH (2000) Human cytochrome oxidase deficiency. Pediatr Res.48:581-5.

Robinson BH, De Meirleir L, Glerum M, Sherwood G, Becker L. (1987) Clinical presentation of mitochondrial respiratory chain defects in NADH-coenzyme Q reductase and cytochrome oxidase: clues to pathogenesis of Leigh disease. J. Pediatr. 110: 216–222.

Rotig A, Appelkvist EL, Geromel V, Chretien D, Kadhom N, Edery P, Lebideau M, Dallner G, Munnich A, Ernster L, Rustin P (2000) Quinone-responsive multiple respiratory-chain dysfunction due to widespread coenzyme Q10 deficiency. Lancet 356:391–395.

Sääf A, Monné M, de Gier JW, von Heijne G. (1998) Membrane topology of the 60-kDa Oxa1p homologue from Escherichia coli. J Biol Chem. 273:30415-8.

Saiki R, Nagata A, Kainou T, Matsuda H, Kawamukai M. (2005) Characterization of solanesyl and decaprenyl diphosphate synthases in mice and humans. FEBS J. 272:5606-22.

Salviati L, Sacconi S, Rasalan MM, Kronn DF, Braun A, Canoll P, Davidson M, Shanske, Bonilla E, Hays AP, Schon EA, DiMauro S. (2002a) Cytochrome c oxidase deficiency due to a novel SCO2 mutation mimics Werdnig-Hoffmann disease. Arch. Neurol. 59:862-5.

Salviati L, Hernandez-Rosa E, Walker WF, Sacconi S, DiMauro S, Schon EA, Davidson MM. (2002b) Copper supplementation restores cytochrome c oxidase activity in cultured cells from patients with SCO2 mutations. Biochem J. 363:321-7.

Salviati L, Freehauf C, Sacconi S, DiMauro S, Thoma J, Tsai AC. (2004). Novel SURF1 mutation in a child with subacute encephalopathy and without the radiological features of Leigh Syndrome. Am J Med Genet A 128:195–198.

Salviati L, Sacconi S, Murer L, Zacchello G, Franceschini L, Laverda AM, Basso G, Quinzii C, Angelini C, Hirano M, Naini AB, Navas P, DiMauro S, Montini G (2005) Infantile encephalomyopathy and nephropathy with CoQ10 deficiency: a CoQ10-responsive condition. Neurology 65:606–608.

Sampaleanu LM, Vallée F, Thompson GD, Howell PL. (2001) Three-dimensional structure of the argininosuccinate lyase frequently complementing allele Q286R. Biochemistry.40:15570-80.

Santos-Ocana C., Do T.Q., Padilla S., Navas P. and Clarke C. F. (2002) Uptake of exogenous coenzyme Q and transport to mitochondria is required for bc1 complex stability in yeast coq mutants. J. Biol. Chem. 277, 10973–10981.

Saracco SA, Fox TD (2002) Cox18p is required for export of the mitochondrially encoded Saccharomyces cerevisiae Cox2p C-tail and interacts with Pnt1p and Mss2p in the inner membrane. Mol Biol Cell. 13:1122-31.

Scaglia F, Carter S, O'Brien WE, Lee B. (2004). Effect of alternative pathway therapy on branched chain amino acid metabolism in urea cycle disorder patients. Molecular Genetics and Metabolism 81: S79-S85.

Schon EA (2000) Mitochondrial genetics and disease, Trends Biochem Sci 25:555-560.

Searcy DG. (2003) Metabolic integration during the evolutionary origin of mitochondria. Cell Res. 13:229-38.

Shoubridge EA (2001). Cytochrome c oxidase deficiency. Am. J. Med. Genet. 106: 46–52.

Small I, Peeters N, Legeai F, Lurin C. (2004) Predotar: A tool for rapidly screening proteomes for N-terminal targeting sequences. Proteomics. 4:1581-90.

Souza RL, Green-Willms NS, Fox TD, Tzagoloff A, Nobrega FG (2000) Cloning and characterization of COX18, a Saccharomyces cerevisiae PET gene required for the assembly of cytochrome oxidase, J. Biol. Chem. 275:14898–14902.

Stiernagle, T. (1999). Maintenance of C. elegans. In: C. elegans—A Practical Approach. Edited by Hope, I. A. Oxford University Press, London.

Sulston J.E., Schierenberg E., White J.G., and Thomson J.N. (1983). The embryonic cell lineage of the nematode Caenorhabditis elegans. Dev Biol, 100: 64-119.

Szyrach G, Ott M, Bonnefoy N, Neupert W, Herrmann JM. (2003) Ribosome binding to the Oxa1 complex facilitates co-translational protein insertion in mitochondria. EMBO J. 22:6448-57.

Timmons L, Court DL, Fire A. (2001) Ingestion of bacterially expressed dsRNAs can produce specific and potent genetic interference in Caenorhabditis elegans. Gene. 263:103-12.

Timmons L. (2006) Delivery methods for RNA interference in C. elegans. Methods Mol Biol. 351:119-25.

Tiranti V, Hoertnagel K, Carrozzo R, Galimberti C, Munaro M, Granatiero M, Zelante L, Gasparini P, Marzella R, Rocchi M, Bayona-Bafaluy MP, Enriquez JA, Uziel G, Bertini E, Dionisi-Vici C, Franco B, Meitinger T, Zeviani M (1998) Mutations of SURF-1 in Leigh disease associated with cytochrome c oxidase deficiency. Am J Hum Genet 63:1609–1621.

Tran UC, Clarke CF. (2007) Endogenous synthesis of coenzyme Q in eukaryotes. Mitochondrion.7 Suppl:S62-71.

Trevisson E, Salviati L, Baldoin MC, Toldo I, Casarin A, Sacconi S, Cesaro L, Basso G, Burlina AB. (2007) Argininosuccinate lyase deficiency: mutational spectrum in Italian patients and identification of a novel ASL pseudogene. Hum Mutat. 28:694-702.

Tsang, W.Y., Sayles, L.C., Grad, L.I., Pilgrim, D.B. and Lemire, B.D. (2001) Mitochondrial respiratory chain deficiency in Caenorhabditis elegans results in developmental arrest and increased lifespan. J. Biol.Chem. 276:32240–32246.

Tsang, W.Y. and Lemire, B.D. (2002) Mitochondrial genome content is regulated during nematode development. Biochem. Biophys. Res. Commun., 291:8–16.

Tsang, W.Y. and Lemire, B.D. (2003) The role of mitochondria in the life of the nematode, Caenorhabditis elegans. Biochim. Biophys. Acta, 1638:91–105.

Tsukihara T, Aoyama H, Yamashita E, Tomizaki T, Yamaguchi H, Shinzawa-Itoh K, Nakashima R, Yaono R, and Yoshikawa S. (1995) Structures of metal sites of oxidized bovine heart cytochrome c oxidase at 2.8 A. Science 269: 1069–1074.

Turner MA, Simpson A, McInnes RR, Howell PL. (1997) Human argininosuccinate lyase: a structural basis for intragenic complementation. Proc Natl Acad Sci U S A. 94:9063-8.

Turunen M, Olsson J, Dallner G. (2004) Metabolism and function of coenzyme Q. Biochim Biophys Acta. 1660:171-99.

Tzagoloff A, Dieckmann CL. (1990) PET genes of Saccharomyces cerevisiae. Microbiol Rev 54:211-25.

Uhlenberg B, Schuelke M, Ruschendorf F, Ruf N, Kaindl AM, Henneke M, Thiele H, Stoltenburg-Didinger G, Aksu F, Topaloglu H, Nurnberg P, Hubner C, Weschke B, Gartner J (2004) Mutations in the gene encoding gap junction protein alpha 12 (connexin 46.6) cause Pelizaeus-Merzbacher-like disease. Am J Hum Genet 75:251-60.

Vajo, Z., King, L.M., Jonassen, T., Wilkin, D.J., Ho, N., Munnich, A., Clarke, C.F., Francomano, C.A. (1999). Conservation of the Caenorhabditis elegans timing gene

clk-1 from yeast to human: a gene required for ubiquinone biosynthesis with potential implications for aging. Mamm. Genome 10, 1000–1004.

Valentine JS, Wertz DL, Lyons TJ, Liou LL, Goto JJ, and Gralla EB. (1998) The dark side of dioxygen biochemistry. Curr Opin Chem Biol 2: 253–262.

Valnot I, Osmond S, Gigarel N, Mehaye B, Amiel J, Cormier-Daire V, Munnich A, Bonnefont JP, Rustin P, Rotig A (2000a) Mutations of the SCO1 gene in mitochondrial cytochrome c oxidase deficiency with neonatal-onset hepatic failure and encephalopathy. Am J Hum Genet 67:1104–1109.

Valnot I, von Kleist-Retzow JC, Barrientos A, Gorbatyuk M, Taanman JW, Mehaye B, Rustin P, Tzagoloff A, Munnich A, Rotig A (2000b) A mutation in the human heme A:farnesyltransferase gene (COX10) causes cytochrome c oxidase deficiency. Hum Mol Genet 9:1245–1249.

Van Coster R, Lombres A, De Vivo DC, Chi TL, Dodson WE, Rothman S, Orrechio EJ, Grover W, Berry GT, Schwartz JF, et al. (1991) Cytochrome c oxidase-associated Leigh syndrome: phenotypic features and pathogenetic speculations. J Neurol Sci. 104:97-111.

von Heijne G.(1989) Control of topology and mode of assembly of a polytopic membrane protein by positively charged residues. Nature. 341:456-8.

Walker DC, McCloskey DA, Simard LR, McInnes RR. (1990) Molecular analysis of human argininosuccinate Iyase: Mutant characterization and alternative splicing of the coding region. Proc Natl Acad Sci USA 87:9625-9629.

Walker DC, Christodoulou J, Craig HJ, Simard RL, Ploder L, Howell PL, McInnes RR. (1997) Intragenic complementation at the human argininosuccinate lyase locus. Identification of the major complementing alleles. J Biol Chem 7:6777–6783.

Widhalm K, Koch S, Scheibenreiter S, Knoll E, Colombo JP, Bachmann C, Thalhammer O. (1992) Long-term follow-up of 12 patients with the late-onset variant of argininosuccinic acid lyase deficiency: no impairment of intellectual and psychomotor development during therapy. Pediatrics 89:1182-4.

Woodsmall RM, Benson DA (1993) Information resources at the National Center for Biotechnology Information. Bull. Med. Libr. Assoc. 81:282–284.

Yoshida M, Muneyuki E, Hisabori T. (2001) ATP synthase--a marvellous rotary engine of the cell. Nat Rev Mol Cell Biol. 2:669-77.

Yu B and Howell PL (2000) Intragenic complementation and the structure and function of argininosuccinate lyase. Cell Mol Life Sci 57:1637–1651.

Yu B, Thompson GD, Yip P, Howell PL, Davidson AR. (2001) Mechanisms for intragenic complementation at the human argininosuccinate lyase locus. Biochemistry 40:15581-90.

Zeviani M, Corona P, Nijtmans L, Tiranti V (1999) Nuclear gene defects in mitochondrial disorders. Ital J Neurol Sci. 20:401-8.

Zeviani M, Di Donato S (2004) Mitochondrial disorders. Brain 127:2153-72.

Zhu Z, Yao J, Johns T, Fu K, De Bie I, Macmillan C, Cuthbert AP, Newbold RF, Wang J, Chevrette M, Brown GK, Brown RM, Shoubridge EA (1998) SURF1, encoding a factor involved in the biogenesis of cytochrome c oxidase, is mutated in Leigh syndrome. Nat Genet 20:337–343.

PUBLICATIONS

Sacconi S, Trevisson E, Pistollato F, Baldoin MC, Rezzonico R, Bourget I, Desnuelle C, Tenconi R, Basso G, DiMauro S, Salviati L. (2005) *hCOX18* and *hCOX19*: two human genes involved in cytochrome c oxidase assembly. Biochem Biophys Res Commun. 337:832-9.

Quinzii C, Naini A, Salviati L, Trevisson E, Navas P, Dimauro S, Hirano M. (2006) A mutation in para-hydroxybenzoate-polyprenyl transferase (COQ2) causes primary coenzyme Q10 deficiency. Am J Hum Genet. 78:345-9.

Martella M, Salviati L, Casarin A, Trevisson E, Opocher G, Polli R, Gross D, Murgia A. (2006) Molecular analysis of two uncharacterized sequence variants of the VHL gene. J Hum Genet. 51:964-8.

Salviati L, Trevisson E, Baldoin MC, Toldo I, Sartori S, Calderone M, Tenconi R, Laverda A. (2007) A novel deletion in the GJA12 gene causes Pelizaeus-Merzbacher-like disease. Neurogenetics 8:57-60.

Trevisson E, Salviati L, Baldoin MC, Toldo I, Casarin A, Sacconi S, Cesaro L, Basso G, Burlina AB. (2007) Argininosuccinate lyase deficiency: mutational spectrum in Italian patients and identification of a novel ASL pseudogene. Hum Mutat. 28:694-702.

López-Martín JM, Salviati L, Trevisson E, Montini G, DiMauro S, Quinzii C, Hirano M, Rodriguez-Hernandez A, Cordero MD, Sánchez-Alcázar JA, Santos-Ocaña C, Navas P. (2007) Missense mutation of the COQ2 gene causes defects of bioenergetics and de novo pyrimidine synthesis. Hum Mol Genet. 16:1091-7.

Dimmer KS, Navoni F, Casarin A, Trevisson E, Endele S, Winterpacht A, Salviati L, Scorrano L. (2008) LETM1, deleted in Wolf-Hirschhorn Syndrome is required for normal mitochondrial morphology and cellular viability. Hum Mol Genet. 17:201-14.

Sartori S, Burlina AB, Salviati L, Trevisson E, Toldo I, Laverda AM, Burlina AP. (2008) Increased level of N-acetylaspartylglutamate (NAAG) in the CSF of a patient with Pelizaeus-Merzbacher-like disease due to mutation in the GJA12 gene. Eur J Paediatr Neurol. In press.

Available online at www.sciencedirect.com
SCIENCE DIRECT
Biochemical and Biophysical Research Communications 337 (2005) 832–839
BBRC
www.elsevier.com/locate/ybbrc

hCOX18 and *hCOX19*: Two human genes involved in cytochrome *c* oxidase assembly

Sabrina Sacconi [a,1], Eva Trevisson [b,1], Francesca Pistollato [b], Maria Cristina Baldoin [b], Roger Rezzonico [a], Isabelle Bourget [a], Claude Desnuelle [a], Romano Tenconi [c], Giuseppe Basso [b], Salvatore DiMauro [d], Leonardo Salviati [c,*]

[a] *INSERM U638, Faculté de Médicine, Université de Nice, France*
[b] *Department of Pediatrics, University of Padova, Italy*
[c] *Servizio di Genetica Clinica ed Epidemiologica, Department of Pediatrics, University of Padova, Italy*
[d] *Department of Neurology, Columbia University, New York, NY, USA*

Received 16 September 2005
Available online 29 September 2005

Abstract

We identified the human homologues of *yCOX18* and *yCOX19*, two *Saccharomyces cerevisiae* genes involved in the biogenesis of mitochondrial respiratory chain complexes. In yeast, these two genes are required for the expression of cytochrome *c* oxidase: Cox18p catalyses the insertion of Cox2p COOH-tail into the mitochondrial inner membrane, and Cox19p is probably involved in metal transport to the intermembrane space. Both hCox18p and hCox19p present significant amino acid identity with the corresponding yeast polypeptides and reveal highly conserved functional domains. In addition, their subcellular localization is analogous to that of the yeast proteins. These data strongly suggest that the human gene products share similar functions with their yeast homologues. These two COX-assembly genes represent new candidates for mutational analysis in patients with isolated COX deficiency of unknown etiology.

Keywords: Cytochrome *c* oxidase; Respiratory chain; Metal chaperones; Mitochondria; COX-assembly genes; COX deficiency; Oxa1

Cytochrome *c* oxidase (COX), complex IV of the mitochondrial respiratory chain, is a multiheteromeric enzyme, located in the mitochondrial inner membrane (MIM). It comprises of 13 protein subunits and several prosthetic groups: two heme groups (*a* and *a*3), three copper ions, one zinc ion, and one magnesium ion. The biogenesis of COX is controlled by two distinct genomes: mitochondrial DNA (mtDNA), which encodes the three largest subunits that form the catalytic core of the enzyme, and nuclear DNA (nDNA), which encodes the 10 smaller subunits that have structural and regulatory functions [1]. The nDNA encodes also for a number of accessory proteins that are not structural components of the enzyme, but are required for the synthesis of the prosthetic groups, the transport and insertion of metal cofactors, and the correct assembly of the different polypeptides into the holoenzyme. These COX-assembly genes have been originally identified and characterized in *Saccharomyces cerevisiae* [2], and some of their human homologues have been subsequently identified.

In humans, isolated COX deficiency is a relatively common RC defect in infancy and childhood [3] that has been linked to both mtDNA and nDNA defects. However, mutations in the three mtDNA-encoded structural subunits are rare [4] and, although most isolated COX defects are inherited as autosomal recessive traits, no mutations have yet been found in any one of the 10 nDNA-encoded subunits [5,6]. After the discovery that mutations in *SURF1*, a COX-assembly gene, are associated with COX deficiency

* Corresponding author. Fax: +39 049 8211425.
E-mail address: leonardo.salviati@unipd.it (L. Salviati).
[1] These authors have contributed equally to this work.

0006-291X/$ - see front matter © 2005 Elsevier Inc. All rights reserved.
doi:10.1016/j.bbrc.2005.09.127

[7,8], researchers have focused their attention on assembly genes, and mutations have been described in several of them, including *SCO2*, *SCO1*, *COX10*, and *COX15*. Yet, the genetic defect remains elusive in many cases of isolated COX deficiency and other, as yet unidentified, genes must be involved. In yeast, at least 30 genes are required for COX biogenesis [2], but only less than 10 of their human counterparts are known. Hence, the importance of identifying and characterizing novel human COX-assembly genes.

Materials and methods

Identification of hCOX18 and hCOX19. The human gene sequences were identified through the "cyber-screening" method described by Petruzzella et al. [9]. In brief, the amino acidic sequences of the yeast proteins [10,11] were used as probes to identify human expressed sequences tags (EST) with significant homology to the yeast genes through the tBLASTn software (www.ncbi.nlm.nih.gov/blast) [12]. By aligning the obtained sequences and comparing them with those of human genomic DNA, it was possible to identify cDNA sequences that comprise the entire coding region of the two human genes and to establish their chromosomal localizations.

Multiple protein sequences were aligned using Multalin software (http://prodes.toulouse.inra.fr/multalin/multalin.html) [13]. The degrees of identity and similarity between the proteins were calculated using BLASTp software (www.ncbi.nlm.nih.gov/blast) as described [9].

The predicted subcellular localization of proteins was analysed with specific software: PREDOTAR (http://genoplante-info.infobiogen.fr/predotar/) [14], PSORT (http://psort.nibb.ac.jp/form.html) [15], and MITOPROT (http://ihg.gsf.de/ihg/mitoprot.html) [16].

Membrane topology was predicted as described [17].

CpG island and TATA box prediction were carried out with the GeneBuilder software (www.itba.mi.cnr.it/webgene) [18].

RNA extraction and RT-PCR amplification. Total RNA was extracted and purified from about 10^6 human cultured skin fibroblasts using the RNAzol Kit (Duotech) according to the manufacturer's protocols. Synthesis of total cDNA was carried out using SuperScript II kit for RT (Invitrogen), using random hexamers provided by the manufacturer. *hCOX18* and *hCOX19* cDNA fragments containing the entire coding regions of the genes were then amplified using suitable primer pairs and *Taq* DNA polymerase (Roche) according to the manufacturer's protocol. *hCOX19* was amplified using primers 1F and 472R. PCR conditions were 94 °C for 3 min, 35 cycles of 94 °C 1 min, 55 °C 1 min, 72 °C 1 min, and a final extension step of 7 min at 72 °C. *hCOX18* was amplified using a nested PCR protocol. The first step was carried out using primers −56F and 1287R with PCR conditions: 94 °C for 3 min, 30 cycles of 94 °C 1 min, 55 °C 1 min, 72 °C 1 min, and a final extension step of 7 min at 72 °C; the second step used primers −11F and 1152R, the same PCR conditions, but only 25 amplification cycles. Primer sequences are reported in Table 1.

Cloning. PCR fragments were cloned in pCR2.1TOPO (Invitrogen) using the TOPO TA-cloning kit, according to provided protocols. Colonies were analysed by PCR, using vector specific primers (M13R and M13F). Plasmid DNA was isolated from positive colonies using Plasmid MINI kit (Qiagen).

Sequence analysis of cDNA clones and DNA fragments was carried out on an ABI PRISM 310 Genetic Analyser (Applera, Foster City, CH, USA) by the Big Dye-Terminator Cycle Sequencing Ready Reaction Kit, using both Vector and internal gene specific primers.

Northern blot. Probes for Northern blot analysis were obtained by digestion of pCR2.1TOPO-COX19 with *Eco*RI, that yielded a 490 bp fragment containing the whole coding region of the hCOX19 gene and a portion of the 3′UTR. The COX18 probe was obtained by digestion of pCR2.1TOPO-COX18 with *Bam*HI, and *Xho*I that yielded a 1244 bp fragment. Probes were labelled with ^{32}P as described [19] and hybridized with a pre-made multiple-tissue Northern blot (Clontech), containing 2 μg per lane of poly(A)$^+$ RNA from eight human tissues, according to the manufacturer's protocol. Autoradiographs were quantified by densitometric scanning using a laser densitometer equipped with ImageQuant software (Molecular Dynamics).

The same blot was rehybridized with a β-actin probe (provided by the manufacturer) to monitor the quality and quantity of RNA samples.

Race. The 5′ and 3′ extremities of both transcripts were characterized by a rapid amplification of cDNA ends (RACE) protocol using the Gene Racer kit (Invitrogen) according to the manufacturer's guidelines.

In brief, for 5′ RACE total RNA was initially treated with DNAse to eliminate traces of genomic DNA from the RNA preparation. Then RNA was treated with calf intestinal phosphatase to dephosphorylate partially degraded mRNA. The 3-methyl-guanosine cap of full-length mRNA was then removed by treatment with tobacco acid phosphatase, and a synthetic RNA oligonucleotide provided by the manufacturer was ligated at the 5′ end of the mRNA. This procedure selects for full-length mRNA because partially degraded RNA molecules are not ligated to the synthetic oligonucleotide. Finally, the mRNA was retrotranscribed using the modified oligo(dT) nucleotides provided in the kit and aliquots of the reaction were used for PCR amplification of the transcript extremities.

PCR primers were designed in order to avoid repeated sequences present in the 3′UTR identified with the RepeatMasker [20] software (http://www.repeatmasker.org/). The amplification was carried out with a nested PCR protocol using the conditions recommended by the manufacturer.

hCOX18 5′ extremity was amplified using primers 500R and GeneRacer-5′ for the first step and primers 334R and GeneRacer-5′ nested for the second step. *hCOX19* 5′ extremity was amplified using primers 472R and GeneRacer-5′ for the first step, and primers 297R and GeneRacer-5′ nested for the second step. The 3′ extremity of *hCOX18* transcripts was amplified by three different reactions using primers 400F or 2317F or 2749F and GeneRacer-3′ for the first step, and 1268F or 2470F or 2839F and GeneRacer-3′ nested for the second step. The 3′ extremity of *hCOX19* was amplified with primers 3021F and GeneRacer-3′ for the first step, and 3256F or 3523F and GeneRacer-3′ nested for the second step.

The PCR products were cloned in pCR2.1TOPO and at least 10 clones were sequenced with the appropriate primers.

Generation of GFP-fusion proteins. A 263 bp *Sac*I–*Sca*I fragment from pCR2.1TOPO-hCOX18 was cloned in the pEGFPN1 vector (Clontech)

Table 1
Oligonucleotide used for amplification and sequencing of the two genes

Name	Sequence
COX18 −56F	5′-GGTGTATGTCCGCTGGATTG-3′
COX18 −11F	5′-GTGGTGCAGAAATGCTGTG-3′
COX18 400F	5′-CAAATCAGTTGGGGTGGTCC-3′
COX18 1268F	5′-CTCACAATACGGGGACTTCC-3′
COX18 2317F	5′-ACTCTGCCTTCTAGTTTCAGCTCTCA-3′
COX18 2470F	5′-CTAAGCTCAGGAAGGCTTAGGAGAA-3′
COX18 2749F	5′-AGGCAGAAATGTGTGTGCAGCTTAGG-3′
COX18 2839F	5′-CTTTGCCTTTGCCGTGTGTGTTACTG-3′
COX18 149R	5′-TGTACTGCAGAGACTGGTGC-3′
COX18 334R	5′-CCTTGGCCAGGATGTAGTGGTGGTA-3′
COX18 500R	5′-GGGTGGCAGTTACTCGCACATA-3′
COX18 632R	5′-CCACCAGTACCTAACAACTGTTCCTGA-3′
COX18 1002R	5′-TCATTTTCTTGAAATGAACTTGGTATT-3′
COX18 1152R	5′-GTGGCTCACGGATTACATC-3′
COX18 1287R	5′-GGAAGTCCCCGTATTGTGAG-3′
COX19 1F	5′-ATGTCGACCGCCATGAATTTC-3′
COX19 297R	5′-TCATTTTTTTGCCTCTGATTTTCC-3′
COX19 472R	5′-GTTCAATGCAGAAACACCCTCC-3′
COX19 3021F	5′-GGTCTTGGCCCTGATACCATTCTGT-3′
COX19 3256F	5′-GGATCACTTGAGCCAGAGGTTA-3′
COX19 3523F	5′-GTAATGGGCTGTAGCCCTCAGAAT-3′
COX19-GFP-SacF	5′-CTTTCTGACCTCATGTCGACCGCCATGA-3′
COX19-GFP-BamR	5′-CTTTCTGGATCCGTCCTGAGAGACCACTGA-3′

that had been digested with *Eco*RI, treated with Klenow enzyme (Roche) to fill in the 3′ overhangs, and then digested again with *Sac*I. Positive colonies were sequenced with suitable vector primers to confirm the correctness of the reading frame of the fusion gene.

The whole coding region of *hCOX19* lacking the termination codon was amplified from pCR2.1TOPO-hCOX19 with COX19-Sac-F and COX19-Bam-R primers that contained the recognition sequence for restriction endonucleases *Sac*I and *Bam*HI. The PCR product was digested with these two enzymes and cloned in pEGFPN1 digested in a similar way. Positive colonies were sequenced as above.

Expression of fusion proteins. Human HEK293 cells were grown on glass coverslips using DMEM (Invitrogen) supplemented with 5% fetal bovine serum (Invitrogen) until 70% confluent. At that point, they were transiently transfected with COX18-GFP or using the Effectene kit (Qiagen), according to the manufacturer's guidelines. After 48 h, cells were stained with Tetramethylrhodamine-methyl ester perchlorate (TMRM) (Molecular Probes) as described [21], and visualized using either a Zeiss fluorescent microscope or Nikon confocal microscope. COX19-GFP was co-transfected with a plasmid expressing red fluorescent protein linked to the mitochondrial importation sequence of COX VIII (mtRFP) [22] (gift of Dr. Luca Scorrano, VIMM, Padova, Italy).

Sequence submission. Sequences of the transcripts were submitted to the GenBank database with the following accession numbers:

COX18 transcript variant 1: AY957564,
COX18 transcript variant 2: AY957565,
COX19: AY957566.

Results

Identification of hCOX18 and hCOX19

Using yCox18p and yCox19p sequences as probes, we screened the GenBank database by the tBLASTn algorithm and found several human EST showing regions of homology with the yeast genes. We aligned these EST and obtained an initial contig, which was again used as a probe for the BLASTn software to identify EST overlapping with the 5′ or 3′ ends of our sequence. We repeated this operation until we obtained the complete coding region of the two genes. This information allowed us to design a set of oligonucleotides for the amplification by RT-PCR of the entire coding region of the two genes. Sequencing of the cloned PCR products confirmed our in silico predictions. We then aligned the obtained sequences with human genomic DNA sequences to determine the chromosomal localization of the two genes.

Structure of hCOX18

The gene *hCOX18* comprises a region of about 25 kb on chromosome 4q 21.1, lacks a TATA box, but its first exon is located on a CpG island. It contains seven exons, with the last one encoding only the 3′ untranslated region (3′UTR). The open reading frame (ORF) is 999 bp long and encodes a predicted 333 amino acid protein, with a predicted molecular weight of 37,105 Da. hCox18p shows 25% identity and 45% similarity with yCox18p. Fig. 1 shows hCox18p aligned with *S. cerevisiae* Cox18p and with proteins of other species identified with a similar procedure.

hCox18p has also discreet homology with another class of proteins (Fig. 1B), Oxa1p, which is located in the MIM, and is involved with the integration of both mtDNA- and nDNA-encoded proteins into the MIM [23].

We studied the predicted subcellular localization of Cox18p with three specific software (PREDOTAR,

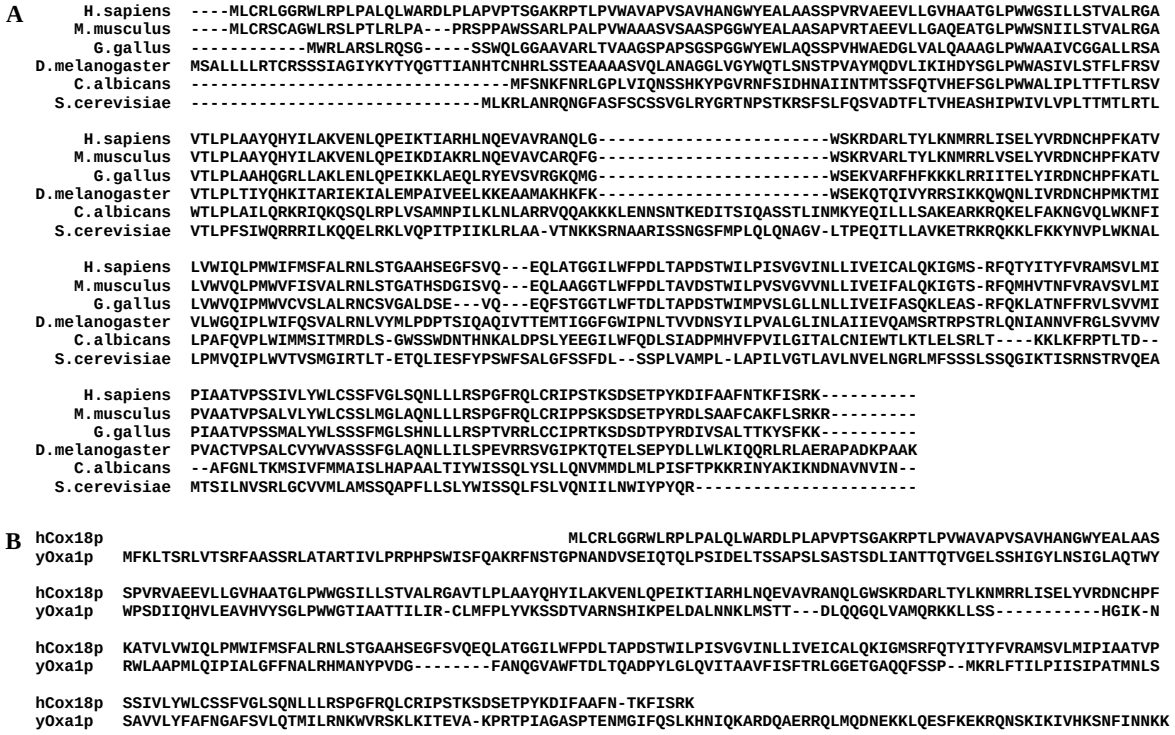

Fig. 1. (A) Alignment of hCox18p with Cox18 proteins form other species. (B) Alignment of hCox18p with yOxa1p.

PSORT, and MITOPROT) and all suggested a mitochondrial localization for the protein. yCox18p is predicted to contain four transmembrane domains [10], however in silico analysis produced conflicting results. For yCox18p three out of seven programs predicted a five transmembrane helixes model, three programs predicted a four helix model and one program predicted that it was a soluble protein. For hCox18p only one software predicted a five helix model, while the other programs favoured a four helix model. Prediction software gave consistent results on the first three transmembrane domains, but was discordant about fourth and fifth helixes, located at the C-terminus of the protein, that theoretically should be separated only by a short loop of two or three amino acids. We therefore aligned hCox18p with yOxa1p, whose transmembrane topology has been determined experimentally [24]. The first three transmembrane domains of yOxa1p match those predicted in hCox18p by computer analysis, while the fourth and fifth domains correspond to the fourth predicted domain of hCox18p. Fig. 2 depicts a possible model of hCox18 membrane topology based on these data.

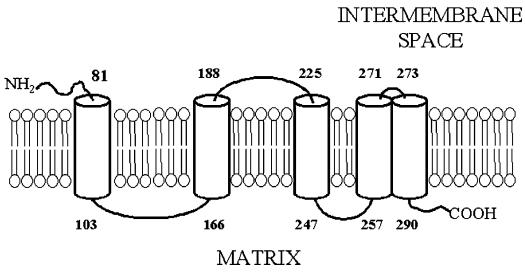

Fig. 2. Putative membrane topology of hCox18p. The numbers indicate the amino acid residues that limit the transmembrane segments.

Structure of hCOX19

The gene *hCOX19* comprises a region of about 12 kb on chromosome 7p22.3. It consists of three exons, and the coding region, 270 bp long, encodes a small protein of 90 amino acids with a predicted molecular weight of 10,387 Da. The protein product hCox19p has a greater homology with its yeast counterpart than hCox18p, 40% identity and 60% similarity with yCox19p (Fig. 3A).

hCox19p is a hydrophilic protein, without any region compatible with transmembrane domains. It does not appear to contain a mitochondrial importation signal: accordingly, all software employed by us predicted a cytosolic localization for hCox19p. The structure of hCox19p is similar to that of hCox17p [25], another protein involved in COX biogenesis that participates in copper transport into the mitochondrial intermembrane space (IMS) (Fig. 3B).

Gene expression and characterization of transcripts

We used the cloned cDNAs to synthesize ^{32}P labeled probes to explore by Northern blot analysis the pattern of tissue expression of the two genes and to gain information about the approximate size of the transcripts.

hCOX18 is expressed ubiquitously, with higher levels of expression in liver, heart, and pancreas. It is present predominantly as a transcript of approximately 3.5 kb (Fig. 4A), although the blot showed also some fainter signals corresponding to shorter transcripts.

We characterized these transcripts with a RACE protocol. Sequencing of the cloned RACE products indicated that the 5′UTR region extends 106 bp upstream of an

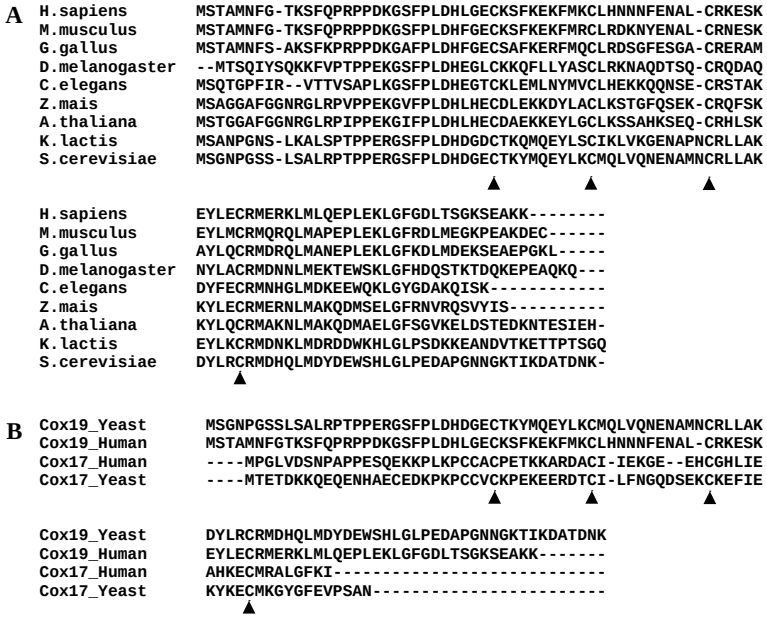

Fig. 3. (A) Alignment of hCox19p with Cox19 proteins form other species. (B) Alignment of hCox19, yCox19, hCox17, and yCox17. The arrowheads indicate the four conserved cysteins between Cox17 and Cox19 proteins.

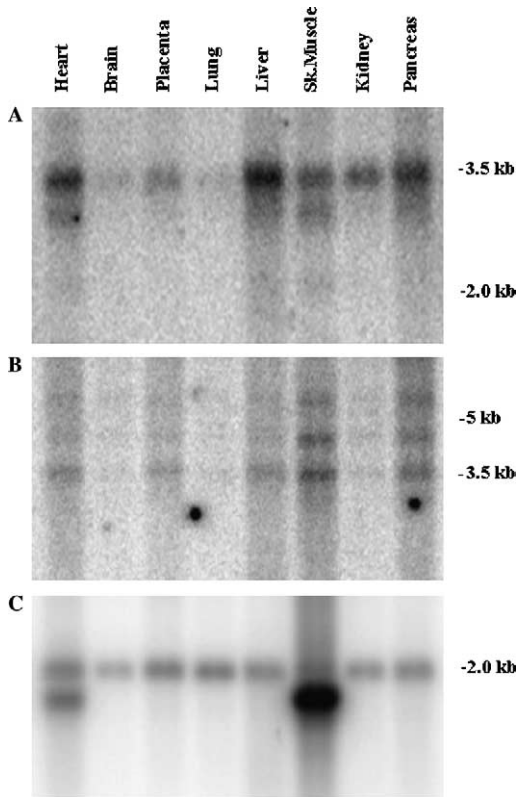

Fig. 4. Northern blot analysis of *hCOX18* and *hCOX19* expression. (A) Membrane hybridized with *hCOX18* probe and exposed for 3 days and visualized as described in text. (B) *hCOX19* probe, exposed for 4 days. (C) β-Actin probe, exposed for 2 h. Note that in heart and skeletal muscle two different transcripts of β-actin (1.8 and 2.0 kb long) are normally present.

ATG triplet at the beginning of the coding region. Interestingly, 7 out of 20 clones contained a shorter fragment that extended only 53 bases upstream of the ATG. We believe that they represent mRNA transcribed from a second transcription start site. To characterize the 3′ region, we used the approximate size information obtained from Northern blots to design specific primers on the 3′UTR of the gene. We confirmed the presence of a longer transcript of 3406 nt (with the exclusion of the the poly(A) sequence), GenBank Accession No. AY957564, and we identified a second shorter transcript, 2027 nt long, GenBank Accession No. AY957565. In both cDNAs, the poly(A) is preceded by a canonical AATAAA polyadenylation consensus. We could not identify any other in fibroblasts. When compared to β-actin (Fig. 4C), high levels of the *hCOX18* transcript were found in liver, heart, and pancreas.

hCOX19 is also expressed ubiquitously and is present in different transcripts, the smallest of which is of about 3.6 kb. Higher molecular weight transcripts are about 4.6 and 6 kb (Fig. 4B). *hCOX19* mRNA is most abundant in skeletal muscle. Both genes appear to be transcribed at very low levels when compared to β-actin.

We established by 5′RACE that the transcription origin is located 40 bp upstream to ATG triplet and that the transcript is 3602 nt long (with the exclusion of the poly(A) sequence), GenBank Accession No. AY957566. The 3′UTR region contains a second open reading frame that encodes a predicted 158 aa hypothetical protein. The latter, however, does not show homology with any known protein, and this ORF is not present in the murine *COX19* transcript.

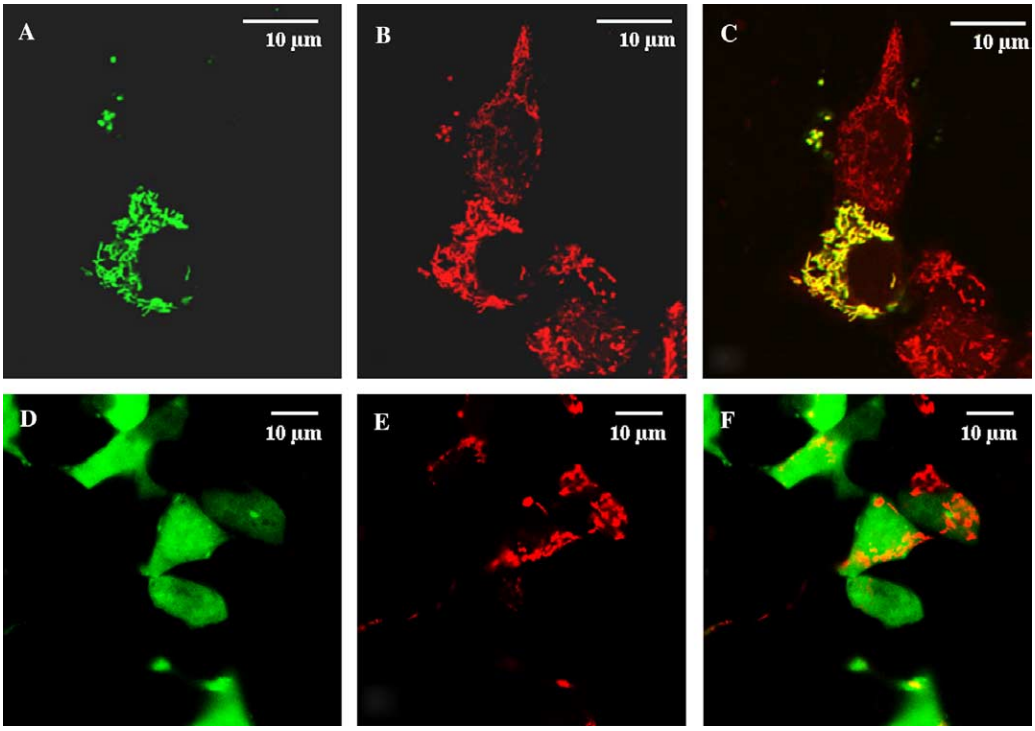

Fig. 5. Localization of COX18-GFP and COX19-GFP in HEK293 cells. (A) COX18-GFP, (B) TMRM, (C) Superimposition of the previous images, (D) COX19-GFP, (E) mtRFP, and (F) superimposition of the previous images.

We believe that this second ORF is not actually translated into protein.

Protein localization

To study the subcellular localization of hCox18p, we generated a COX18-GFP-fusion protein: we cloned a 5′-COX18 210 bp fragment, containing the putative mitochondrial importation signal sequence and the first conserved portion of the gene, into pEGFPN1. We used this construct to transfect human HEK293 cells. After transfection, cells were incubated with TMRM, a mitochondrial specific fluorescent stain that exploits the membrane potential of these organelles. The GFP fluorescence pattern (Fig. 5A) was compared with TMRM (Fig. 5B): as shown in Fig. 5C, there is perfect overlap between the two patterns, confirming that Cox18p is indeed a mitochondrial protein.

We repeated the experiment with a COX19-GFP-fusion protein. In the microscope, it is evident that COX19-GFP fluorescent pattern (Fig. 5D), unlike that of mtRFP (Fig. 5E), is diffuse, and resembles the fluorescence pattern of a purely cytosolic protein. This is in agreement with data obtained for yCox19p, for which mainly a cytosolic localization was described [11].

Discussion

The biogenesis of cytochrome *c* oxidase is a complex process controlled by two distinct genomes. mtDNA encodes the three large structural subunits with catalytic activity, while nDNA encodes the 10 smaller subunits with regulatory and structural functions. nDNA genes (COX-assembly genes) also encode numerous cofactors that are required for the correct assembly of the COX holoenzyme. They have been identified in mutant respiration-deficient yeast strains, and it is estimated that at least 30 genes are required for COX biosynthesis in *S. cerevisiae* [2]. In humans, the information is still incomplete and only about 10 COX-assembly genes have been identified and characterized thus far. Studies on cell lines exposed to inhibitors of protein synthesis have shown that COX assembly in mammalian cells requires three intermediates, S1, S2, and S3 (S4 being the mature enzyme), and that different genes are involved in the formation of each subcomplex [26].

We have identified and characterized two novel human COX-assembly genes, homologous to *yCOX18* and *yCOX19*.

yCox18p is a 316 amino acid protein, located in the mitochondrial inner membrane [10]. Its human homologue hCox18p consists of 333 amino acids and has a predicted molecular weight of 37,105 Da. We demonstrated that it is targeted to mitochondria, as is its yeast homologue.

hCox18p presents significant homology with proteins belonging to the Alb3/Oxa1/YidC family, which is very ancient phylogenetically and comprises both bacterial and eukaryotic proteins [27]. They mediate the correct membrane insertion of several classes of transmembrane proteins. Cox18p is similar to Oxa1p, a protein located in the mitochondrial inner membrane, which is found in yeast and in humans. In *S. cerevisiae*, Oxa1p is important for the insertion into MIM of several proteins, synthesized in the cytosol or in mitochondria [28,29], and its human counterpart is thought to play a similar role [9]. Cox18 proteins in humans and yeast differ from Oxa1 proteins because they lack the hydrophilic C-terminal domain that is thought to act as a ribosomal binding site[28,29]. This domain is important for efficient insertion of mtDNA-encoded proteins within the MIM. Oxa1p contains five transmembrane domains with the C-terminus located in the mitochondrial matrix [24]. Despite the contradictory data obtained from our computer analyses, we believe that Cox18 has a similar membrane topology. We favour a five helix model for hCox18 for two main reasons: because in all members of this family thus far characterized, including the bacterial proteins [30], the portion of the molecule with the translocase activity has five transmembrane domains, and because in a four helix model the positively charged C-terminus of the protein would be located in the IMS, thereby contradicting the so-called ''positive inside rule'' [31,32] of the MIM proteins. We believe that the closely spaced fourth and fifth transmembrane helixes (they appear to be separated only by a short loop of just two or three amino acids) are identified as a single transmembrane domain by topology prediction software. In fact, similar problems were reported with the computer analysis of bacterial and yOxa1p membrane topology [30].

Because yCox18p is required for the insertion into the MIM of the C-terminal tail of the mtDNA-encoded Cox2p subunit [33], hCox18p should be involved in the intermediate phase of COX assembly (formation of subcomplex S3). *COX18*^{null} yeast exhibits isolated COX deficiency with normal activities of other RC complexes [10], but it is not yet clear whether this protein is required for the insertion into the MIM of components of other mitochondrial metabolic pathways.

hCOX18 is expressed ubiquitously; when compared to β-actin expression, the highest expression was in liver. This suggests a possible role of *hCOX18* in the pathogenesis of those forms of COX deficiency associated with liver involvement.

RACE analysis of the 5′ region suggests the presence of two distinct transcription start sites, located 53 and 106 nucleotides upstream of the ATG. Multiple transcription start sites have been described in other genes with TATA-less promoters [34]. By 3′RACE, we characterized two types of transcripts, which differ only in the length of the 3′UTR. The 3406 nt long transcript is more abundant, whereas the shorter 2027 nt transcript is present at much lower levels. The 3′UTR is important for modulation of nucleo-cytoplasmic mRNA transport, translation efficiency, subcellular localization, and message stability [35]. Other COX-assembly genes, such as *hCOX11* and *hCOX15*, exhibit a similar phenomenon [9], but its physiological significance is still unclear.

hCox19p is a small 90 amino acid long protein lacking a mitochondrial targeting signal. The yeast protein is located mainly in the cytosol, although it has access to the IMS [11]. Our localization experiments confirmed a predominant cytosolic localization for hCox19p. We are aware that GFP may alter mitochondrial targeting, but our observations are in agreement with experimental data obtained in yeast. We will perform more detailed studies as soon as an anti-Cox19 antibody becomes available.

Expression analysis has shown that *hCOX19* is also ubiquitously expressed, and, again, multiple transcripts (3.6, 4.5, and 6 kb long) were detected, with the highest levels of expression, relative to β-actin, in muscle. This is in accordance with the high metabolic requirements of this tissue.

Although the exact function of Cox19p in yeast is still unknown, its structure is similar to that of Cox17p, a small soluble protein involved in copper transport to the MIM. In particular, both Cox19p and Cox17p share four highly conserved cystein residues making it likely that Cox19p is involved in metal transport [11]. The four cysteins are conserved also in the human protein, implying that these residues are of critical importance for the function of Cox19p and supporting the hypothesis that it acts as a copper chaperone.

Several proteins participate in copper metabolism. Cox17 and Cox23 are involved in the transport of copper from the cytosol to the IMS [36]. Copper is then transferred to Cox11, which inserts it into the CuB site on subunit Cox1p, but it is also transferred to the Sco1 and Sco2 proteins, which insert it into the CuA site on subunit Cox2p [37]. Cox17 and Cox23 share structural and functional properties, since *yCOX23* can complement $yCO17^{null}$ mutants [36]. To date, there are no data on the functional relationships between Cox19p and Cox17p or Cox23p. It should be noted, however, that the role of copper chaperone for Cox19p has been postulated only on the base of structural similarities with Cox17p, but there is no experimental evidence yet confirming this hypothesis. We cannot exclude the possibility that Cox19p might act as a chaperone for metals other than copper, such as zinc, another metal cofactor of COX.

Our experiments provide preliminary data on these two novel human genes and underscore the complexity of COX-assembly process in humans. *hCOX18* and *hCOX19* represent attractive candidates to be screened in patients with isolated COX deficiency but without mutations in other known COX-assembly genes.

Acknowledgments

This work was supported by Fondazione Città della Speranza and by EU contract 005151. Dr. Sacconi is supported by a fellowship from the European Neurological Society. We are grateful to Prof. Paolo Bernardi and his group for the assistance with fluorescent microscopy.

References

[1] H. Michel, J. Behr, A. Harrenga, A. Kannt, Cytochrome *c* oxidase: structure and spectroscopy, Annu. Rev. Biophys. Biomol. Struct. 27 (1998) 329–356.
[2] A. Tzagoloff, C.L. Dieckmann, PET genes of *Saccharomyces cerevisiae*, Microbiol. Rev. 54 (1990) 211–225.
[3] S. DiMauro, S. Servidei, M. Zeviani, M. Dirocco, D.C. Devivo, S. Didonato, G. Uziel, K. Berry, G. Hoganson, S.D. Johnsen, P.C. Johnson, Cytochrome *c* oxidase deficiency in Leigh syndrome, Ann. Neurol. 22 (1987) 498–506.
[4] S. Sacconi, L. Salviati, C.M. Sue, S. Shanske, M.M. Davidson, E. Bonilla, A.B. Naini, D.C. De Vivo, S. DiMauro, Mutation screening in patients with isolated cytochrome *c* oxidase deficiency, Pediatr. Res. 53 (2003) 224–230.
[5] P.L. Adams, R.N. Lightowlers, D.M. Turnbull, Molecular analysis of cytochrome *c* oxidase deficiency in Leigh's syndrome, Ann. Neurol. 41 (1997) 268–270.
[6] M. Jaksch, S. Hofmann, S. Kleinle, S. Liechti-Gallati, D.E. Pongratz, J. Muller-Hocker, K.B. Jedele, T. Meitinger, K.D. Gerbitz, A systematic mutation screen of 10 nuclear and 25 mitochondrial candidate genes in 21 patients with cytochrome *c* oxidase (COX) deficiency shows tRNA (Ser) (UCN) mutations in a subgroup with syndromal encephalopathy, J. Med. Genet. 35 (1998) 895–900.
[7] Z. Zhu, J. Yao, T. Johns, K. Fu, I. De Bie, C. Macmillan, A.P. Cuthbert, R.F. Newbold, J. Wang, M. Chevrette, G.K. Brown, R.M. Brown, E.A. Shoubridge, SURF1, encoding a factor involved in the biogenesis of cytochrome *c* oxidase, is mutated in Leigh Syndrome, Nat. Genet. 20 (1998) 337–343.
[8] V. Tiranti, K. Hoertnagel, R. Carrozzo, C. Galimberti, M. Munaro, M. Granatiero, L. Zelante, P. Gasparini, R. Marzella, M. Rocchi, M.P. Bayona-Bafaluy, J.A. Enriquez, G. Uziel, E. Bertini, C. Dionisi-Vici, B. Franco, T. Meitinger, M. Zeviani, Mutations of SURF-1 in Leigh disease associated with cytochrome *c* oxidase deficiency, Am. J. Hum. Genet. 63 (1998) 1609–1621.
[9] V. Petruzzella, V. Tiranti, P. Fernandez, P. Ianna, R. Carrozzo, M. Zeviani, Identification and characterization of human cDNAs specific to BCS1, PET112, SCO1, COX15, and COX11, five genes involved in the formation and function of the mitochondrial respiratory chain, Genomics 54 (1998) 494–504.
[10] R.L. Souza, N.S. Green-Willms, T.D. Fox, A. Tzagoloff, F.G. Nobrega, Cloning and characterization of COX18, a *Saccharomyces cerevisiae* PET gene required for the assembly of cytochrome oxidase, J. Biol. Chem. 275 (2000) 14898–14902.
[11] M.P. Nobrega, S.C. Bandeira, J. Beers, A. Tzagoloff, Characterization of COX19, a widely distributed gene required for expression of mitochondrial cytochrome oxidase, J. Biol. Chem. 277 (2002) 40206–40211.
[12] R.M. Woodsmall, D.A. Benson, Information resources at the National Center for Biotechnology Information, Bull. Med. Libr. Assoc. 81 (1993) 282–284.
[13] F. Corpet, Multiple sequence alignment with hierarchical clustering, Nucleic Acids Res. 16 (1988) 10881–10890.
[14] I. Small, N. Peeters, F. Legeai, C. Lurin, Predotar: a tool for rapidly screening proteomes for N-terminal targeting sequences, Proteomics 4 (2004) 1581–1590.
[15] K. Nakai, P. Horton, PSORT: a program for detecting sorting signals in proteins and predicting their subcellular localization, Trends Biochem. Sci. 24 (1999) 34–36.
[16] M.G. Claros, P. Vincens, Computational method to predict mitochondrially imported proteins and their targeting sequences, Eur. J. Biochem. 241 (1996) 779–786.
[17] J.K. Tie, C. Nicchitta, G. von Heijne, D.W. Stafford, Membrane topology mapping of vitamin k epoxide reductase by in vitro translation/cotranslocation, J. Biol. Chem. 280 (2005) 16410–16416.

[18] L. Milanesi, D. D'Angelo, I.B. Rogozin, GeneBuilder: interactive in silico prediction of gene structure, Bioinformatics 15 (1999) 612–621.
[19] R. Rezzonico, D. Burger, J.M. Dayer, J. Biol. Chem. 273 (1998) 18720–18728.
[20] J.A. Bedell, I. Korf, W. Gish, MaskerAid: a performance enhancement to RepeatMasker, Bioinformatics 16 (2000) 1040–1041.
[21] V. Petronilli, D. Penzo, L. Scorrano, P. Bernardi, F. Di Lisa, The mitochondrial permeability transition, release of cytochrome *c* and cell death. Correlation with the duration of pore openings in situ, J. Biol. Chem. 276 (2001) 12030–12034.
[22] S. Cipolat, O. Martins de Brito, B. Dal Zilio, L. Scorrano, OPA1 requires mitofusin 1 to promote mitochondrial fusion, Proc. Natl. Acad. Sci. USA 101 (2004) 15927–15932.
[23] M. Preuss, M. Ott, S. Funes, J. Luirink, J.M. Herrmann, Evolution of mitochondrial oxa proteins from bacterial YidC. Inherited and acquired functions of a conserved protein insertion machinery, J. Biol. Chem. 280 (2005) 13004–13011.
[24] J.M. Herrmann, W. Neupert, R.A. Stuart, Insertion into the mitochondrial inner membrane of a polytopic protein, the nuclear-encoded Oxa1p, EMBO J. 16 (1997) 2217–2226.
[25] D.M. Glerum, A. Shtanko, A. Tzagoloff, Characterization of COX17, a yeast gene involved in copper metabolism and assembly of cytochrome oxidase, J. Biol. Chem. 271 (1996) 14504–14509.
[26] L.G. Nijtmans, J.W. Taanman, A.O. Muijsers, D. Speijer, C. Van den Bogert, Assembly of cytochrome-*c* oxidase in cultured human cells, Eur. J. Biochem. 254 (1998) 389–394.
[27] A. Kuhn, R. Stuart, R. Henry, R.E. Dalbey, The Alb3/Oxa1/YidC protein family: membrane-localized chaperones facilitating membrane protein insertion? Trends Cell Biol. 13 (2003) 510–516.
[28] L. Jia, M. Dienhart, M. Schramp, M. McCauley, K. Hell, R.A. Stuart, Yeast Oxa1 interacts with mitochondrial ribosomes: the importance of the C-terminal region of Oxa1, EMBO J. 22 (2003) 6438–6447.
[29] G. Szyrach, M. Ott, N. Bonnefoy, W. Neupert, J.M. Herrmann, Ribosome binding to the Oxa1 complex facilitates co-translational protein insertion in mitochondria, EMBO J. 22 (2003) 6448–6457.
[30] A. Saaf, M. Monne, J.W. de Gier, G. von Heijne, Membrane topology of the 60-kDa Oxa1p homologue from *Escherichia coli*, J. Biol. Chem. 273 (1998) 30415–30418.
[31] G. von Heijne, Control of topology and mode of assembly of a polytopic membrane protein by positively charged residues, Nature 341 (1989) 456–458.
[32] D. Boyd, J. Beckwith, The role of charged amino acids in the localization of secreted and membrane proteins, Cell 62 (1990) 1031–1033.
[33] S.A. Saracco, T.D. Fox, Cox18p is required for export of the mitochondrially encoded *Saccharomyces cerevisiae* Cox2p C-tail and interacts with Pnt1p and Mss2p in the inner membrane, Mol. Biol. Cell 13 (2002) 1122–1131.
[34] J.R. Gum Jr., J.W. Hicks, S.C. Crawley, C.M. Dahl, S.C. Yang, A.M. Roberton, Y.S. Kim, Initiation of transcription of the MUC3A human intestinal mucin from a TATA-less promoter and comparison with the MUC3B amino terminus, J. Biol. Chem. 278 (2003) 49600–49609.
[35] F. Mignone, G. Grillo, F. Licciulli, M. Iacono, S. Liuni, P.J. Kersey, J. Duarte, C. Saccone, G. Pesole, UTRdb and UTRsite: a collection of sequences and regulatory motifs of the untranslated regions of eukaryotic mRNAs, Nucleic Acids Res. 33 (2005) D141–D146.
[36] M.H. Barros, A. Johnson, A. Tzagoloff, COX23, a homologue of COX17, is required for cytochrome oxidase assembly, J. Biol. Chem. 279 (2004) 31943–31947.
[37] Y.C. Horng, P.A. Cobine, A.B. Maxfield, H.S. Carr, D.R. Winge, Specific copper transfer from the Cox17 metallochaperone to both Sco1 and Cox11 in the assembly of yeast cytochrome *c* oxidase, J. Biol. Chem. 279 (2004) 35334–35340.

Report

A Mutation in *Para*-Hydroxybenzoate-Polyprenyl Transferase (*COQ2*) Causes Primary Coenzyme Q_{10} Deficiency

Catarina Quinzii,[1] Ali Naini,[1] Leonardo Salviati,[2] Eva Trevisson,[2] Plácido Navas,[3] Salvatore DiMauro,[1] and Michio Hirano[1]

[1]Department of Neurology, Columbia University College of Physicians and Surgeons, New York; [2]Servizio di Genetica Clinica ed Epidemiologica, Department of Pediatrics, University of Padova, Padova, Italy; and [3]Centro Andaluz de Biologia del Desarrollo, Universidad Pablo de Olavide, Seville, Spain

Ubiquinone (coenzyme Q_{10} or CoQ_{10}) is a lipid-soluble component of virtually all cell membranes, where it functions as a mobile electron and proton carrier. CoQ_{10} deficiency is inherited as an autosomal recessive trait and has been associated with three main clinical phenotypes: a predominantly myopathic form with central nervous system involvement, an infantile encephalomyopathy with renal dysfunction, and an ataxic form with cerebellar atrophy. In two siblings of consanguineous parents with the infantile form of CoQ_{10} deficiency, we identified a homozygous missense mutation in the *COQ2* gene, which encodes *para*-hydroxybenzoate-polyprenyl transferase. The A→G transition at nucleotide 890 changes a highly conserved tyrosine to cysteine at amino acid 297 within a predicted transmembrane domain. Radioisotope assays confirmed a severe defect of CoQ_{10} biosynthesis in the fibroblasts of one patient. This mutation in *COQ2* is the first molecular cause of primary CoQ_{10} deficiency.

In the mitochondrial respiratory chain, coenzyme Q_{10} (CoQ_{10}) (MIM 607426) is vital for the transport of electrons from complex I (NADH-ubiquinone oxidoreductase) and complex II (succinate-ubiquinone oxidoreductase) to complex III (ubiquinol-cytochrome *c* reductase) (Turunen et al. 2004). It is also an antioxidant (Kagan et al. 1990) and a membrane stabilizer (Turunen et al. 2004), and its oxidized form serves as a cofactor for uncoupling proteins in brown adipose tissue (Echtay et al. 2000). Increased levels of CoQ_{10} may protect cells from chemotherapy-induced oxidative stress (Brea-Calvo et al., in press).

Deficiency of CoQ_{10} has been associated with three major clinical phenotypes. A predominantly myopathic form is characterized by recurrent myoglobinuria and CNS involvement with seizures, ataxia, or mental retardation (Ogasahara et al. 1989; Sobreira et al. 1997; Boitier et al. 1998; Lalani et al. 2005). A second variant, described in three families, manifests as an infantile encephalomyopathy with renal involvement (Rötig et al. 2000; Rahman et al. 2001; Salviati et al. 2005). The third variant is dominated clinically by ataxia and cerebellar atrophy, with varying involvement of other regions of the CNS, peripheral nerve, and muscle (Musumeci et al. 2001; Lamperti et al. 2003). In three siblings with cerebellar ataxia and CoQ_{10} deficiency, we identified a homozygous stop codon mutation in the *APTX* gene (Quinzii et al. 2005), which is known to cause ataxia and oculomotor apraxia 1 (AOA1) (Date et al. 2001; Moreira et al. 2001). This finding supports the hypothesis that the ataxic form is a genetically heterogeneous entity in which deficiency of CoQ_{10} can be secondary. Patients with all three forms of CoQ_{10} deficiency have shown clinical improvements after initiating oral CoQ_{10} supplementation. Thus, early diagnosis is of critical importance in the management of these patients. The molecular bases for the CoQ_{10} deficiency in most of these patients remain to be identified and presumably involve defects of CoQ_{10} biosynthesis (fig. 1).

We reported a 33-mo-old boy with infantile encephalomyopathy, nephropathy, and deficiency of CoQ_{10} (Salviati et al. 2005). The disease appeared to be an autosomal recessive trait because the patient's parents were first cousins and his 9-mo-old sister with nephropathy also had CoQ_{10} deficiency in fibroblasts. The proband presented with proteinuria at age 12 mo; a renal biopsy revealed focal and segmental glomerulosclerosis. Neurological evaluation showed hypotonia, mild psy-

Received September 12, 2005; accepted for publication November 22, 2005; electronically published December 22, 2005.

Address for correspondence and reprints: Dr. Michio Hirano, Department of Neurology, Columbia University College of Physicians and Surgeons, 630 W. 168th Street, P&S 4–443, New York, NY 10032. E-mail: mh29@columbia.edu

Am. J. Hum. Genet. 2006;78:345–349. 0002-9297/2006/7802-0016$15.00

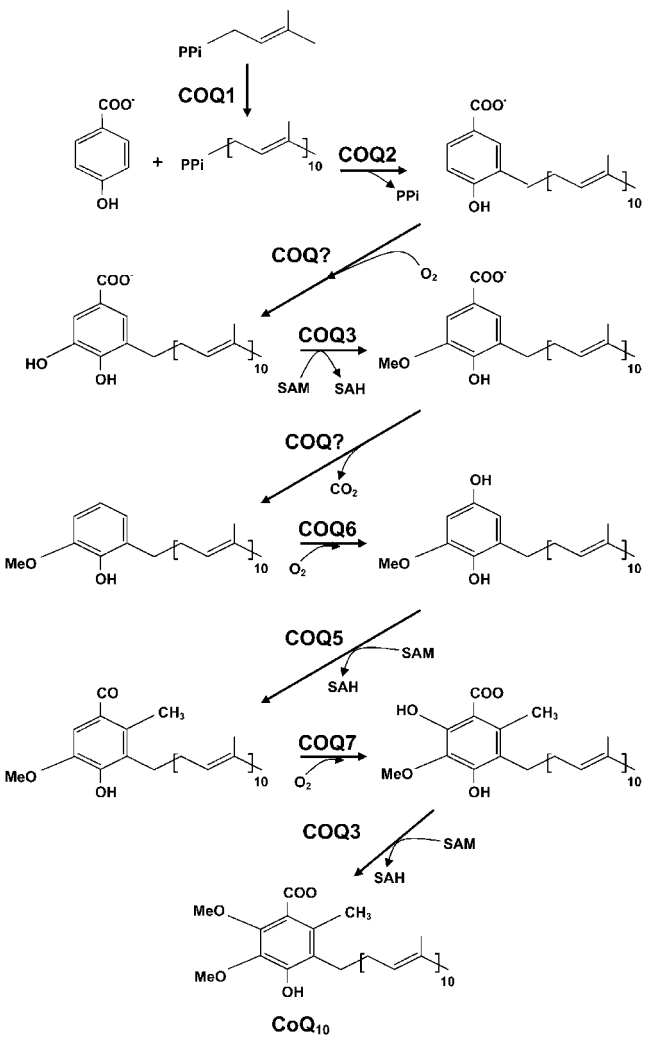

Figure 1 CoQ_{10} biosynthetic pathway with eight known biosynthetic enzymes denoted as COQ1–COQ8. COQ2, decaprenyl-4-hydroxybenzoate transferase, mediates the conjugation of the benzoquinone ring with the decaprenyl side chain.

chomotor delay, and optic atrophy. His renal function worsened. At age 18 mo, he developed frequent vomiting, and peritoneal dialysis was initiated. He developed psychomotor regression (loss of the ability to walk or stand unassisted), tremor, and new-onset status epilepticus with focal electroencephalogram abnormalities predominantly in the left occipital region. Brain magnetic resonance imaging showed cerebellar atrophy, mild diffuse cerebral atrophy, and stroke-like lesions in the left cingulate cortex and subcortical area. Blood and cerebrospinal fluid lactate levels were normal. At age 22 months, he developed right hemiplegia, myoclonus, and swallowing difficulties. A muscle biopsy revealed myofibers with excessive succinate dehydrogenase staining but no ragged-red fibers or cytochrome *c* oxidase–deficient fibers. Measurement of respiratory chain enzymes in muscle extracts showed decreased activities of complexes I + III (0.38 μmol/min/g fresh tissue; control mean $\pm$ SD = 1.02 $\pm$ 0.38) and II + III (0.22 μmol/min/g; control mean $\pm$ SD = 0.70 $\pm$ 0.23), whereas other complexes had normal activities. CoQ_{10} concentration in skeletal muscle of the proband was 12 μg/g fresh tissue (mean $\pm$ SD of 185 controls = 32.1 $\pm$ 6.7). In fibroblasts, CoQ_{10} levels were more severely reduced in both patients (proband = 19 ng/mg protein; sister = 18 ng/mg; mean $\pm$ SD of 15 controls = 105 $\pm$ 14). Activities of complexes II and III in the fibroblasts of both patients were decreased (23% and 22%, respectively, of controls), but the defect was corrected after the addition of 50 μM decylubiquinone. After the initiation of CoQ_{10} supplementation, the neurological manifestations of the boy improved dramatically.

We performed homozygosity mapping, using fluorescently labeled microsatellite markers (ABI Prism Linkage Mapping Set MD-10 [Applied Biosystems]) of chromosomal loci for the eight known human genes (*COQ1–COQ8)* encoding CoQ_{10} biosynthetic proteins. Three chromosomal loci revealed homozygosity in the affected individuals: chromosomes 14q24 (*COQ6*), 12q24 (*COQ5*), and 4q21 (*COQ2*). Primer sequences and PCR conditions for amplification of candidate genes are available from the author on request. Sequencing of the three candidate genes in the patients revealed only one nonsynonymous change: in *COQ2,* encoding *para*-hydroxybenzoate (PHB)–polyprenyl transferase (EC 2.5.1.39), we found a homozygous A→G transition at nucleotide 890, which is predicted to change amino acid 297 from tyrosine to cysteine in the third of six predicted transmembrane domains of the COQ2 protein (Forsgren et al. 2004) (fig. 2). The transition was heterozygous in both parents and absent in DNA from 100 healthy individuals tested by RFLP analysis using *Afl*II restriction endonuclease digestion of PCR-amplified DNA fragments. We also sequenced *COQ1,* to exclude a defect in transprenyl transferase. We did not identify any mutations in *COQ2* by sequencing genomic DNA in seven additional patients with CoQ_{10} deficiency in skeletal muscle (three with the predominantly myopathic form,

```
                                    C
                                    |
Human                VCLPLYFSGVMWTLIYDTIYAHQDKRDDVLIGLKSTAL
Mus musculus         VCLPLYFSGVMWTLIYDTIYAHQDKKDDALIGLKSTAL
S. cerevisiae        M-IPLYLSSYLWCMTYDTIYAHQDKKFDIKAGIKSTAL
S. pombe             VVAPLYLSTISWIVLYDTIYAHQDKRDDVKANIYSTAL
B. parapertussis     AAIAMWLGAVLWQVGYDSIYAYVDVRDDRSLGLHSTAT
P. falciparum        GFLPLSF----LTIIYDTIYAHQDKKDDIRLKLKSLAI
E. coli              SCWLMFLANILWAVAYDTQYAMVDRDDDVKIGIKSTAI
```

Figure 2 Evolutionary conservation of *COQ2*. Human amino acid 297 is normally tyrosine (Y). The A→G transition at nucleotide 890 changes amino acid 297 to cysteine.

two with severe ataxia, and two with infantile-onset encephalomyopathy).

To confirm that the patients had a defect of CoQ_{10} biosynthesis, we performed biochemical assays to measure incorporation of each of two radiolabeled substrates (fig. 1). For the first assay, fibroblasts from the proband and a control were plated in six separate wells of 24 × 6.5–mm plates (40,000 cells/well) and were cultured using Dulbecco's modified Eagle medium (DMEM) with 20% fetal calf serum (Nishigaki et al. 2003). After four days, the medium was replaced by fresh DMEM with 20% fetal calf serum and 0.1 μCi of ^{14}C-PHB (50 Ci/mol specific activity). After incubation for an additional 24 h, cells were washed twice with PBS and were detached from the bottom of the wells with the use of 0.5 ml of 1% SDS, followed by shaking for 10 min at room temperature (repeated once). The contents of each plate were combined (3 ml total), and 0.2 ml was saved for protein determination (Lowry et al. 1951). The remaining pooled suspensions were subjected to hexane extraction. CoQ_{10} was extracted after the addition of 4 ml hexane-ethanol (5/2 v/v) and was vortexed for 2 min. After centrifugation at 2,500 rpm at room temperature for 5 min, the upper phase was carefully transferred into a 20-ml glass scintillation vial (performed twice for each sample). The combined extract was evaporated under a gentle stream of N_2 gas, and the residue was dissolved in 0.15 ml of 1-propanol. An aliquot of 50 μl of the extract was directly injected into a high-performance liquid chromotography (HPLC) system with a C18 reversed-phase column and an electrochemical detector. The waste line of HPLC was connected to a fraction collector, which was programmed to collect 1.0 ml of fractions per minute. CoQ_{10} peak was identified by specific retention time determined after injection of a known amount of authentic CoQ_{10}. The amount of radioactivity in the collected fraction was determined in a Packard scintillation counter.

In the second COQ2 assay, enzymatic activity in fibroblast lysate was measured by a described method (Kalen et al. 1990), with modifications. The incubation mixture contained 250 nCi of ^{3}H-radiolabeled decaprenyl pyrophosphate (decaprenyl-PP) (20 Ci/mmol) solubilized in 25 μL of 1% Triton X-100, 50 mM potassium phosphate at pH 7.5, 10 mM $MgCl_2$, 5 mM ATP, 20 μM 4-hydroxybenzoic acid, and fibroblast lysate (~1 mg protein) in a total volume of 0.5 ml. After incubation at 37°C in a shaking water bath for 60 min, the reaction was stopped by the addition of 1 ml ethanol followed by 1 ml of 0.1-M SDS. Hexane extraction was performed as described above, and the residue was dissolved in 0.15 ml of 1-propanol. An aliquot of 50 μl was injected onto the HPLC. Fraction collection and radioactivity measurement were performed as described above.

In the first assay, after incubating fibroblasts from a control and patient 1 with ^{14}C-PHB, the level of radiolabeled CoQ_{10} in the patient's fibroblasts was ~22% of the control mean (patient = 338 decays per min/mg protein/h; control mean ± SD = 1,733 ± 747, n = 5) (table 1). In the second assay, homogenates from patient 1 and control fibroblasts incubated with ^{3}H-radiolabeled decaprenyl-PP revealed that COQ2 activity in the patient was only 36% relative to the control mean (patient = 48 pmol/mg protein/h; control mean ± SD = 130 ± 18, n = 5) (table 1). Unfortunately, the fibroblasts of the proband's sister did not replicate sufficiently to allow measurement of CoQ_{10} biosynthesis in her cells.

Cells synthesize CoQ_{10} de novo, starting with synthesis of the PHB ring and the polyisoprenyl tail, which anchors CoQ_{10} to membranes. The length of this tail varies among different organisms. In humans, the side chain is comprised of 10 isoprenyls producing CoQ_{10}, whereas rats predominantly generate CoQ_9. In yeast, mutations in any of the eight *COQ* genes block CoQ_{10} synthesis, and CoQ_{10}-deficient cells cannot grow on nonfermentable carbon sources because of respiratory chain dysfunction, despite the accumulation of the intermediate demethoxy-CoQ_{10} (Gin et al. 2003). These yeast strains are also more sensitive to oxidative stress. These results indicate that CoQ_{10} cannot be replaced by another molecule in the cell and suggest that human diseases due to primary CoQ_{10} deficiency may present as severe mitochondrial encephalomyopathies.

Although deficiency of CoQ_{10} in skeletal muscle was originally described in 1989 and has been reported in at least 35 patients, the pathogenic mechanisms had been undefined (Ogasahara et al. 1989; Sobreira et al. 1997; Boitier et al. 1998; Rötig et al. 2000; Di Giovanni et al. 2001; Musumeci et al. 2001; Rahman et al. 2001; Van Maldergem et al. 2002; Lamperti et al. 2003; Aure et al. 2004; Gironi et al. 2004; Lalani et al. 2005). The

Table 1

Biochemical Assays to Measure COQ2 Activity

Fibroblasts	CoQ_{10} Synthesis[a]	Percent of Control Mean
Assay 1[b]:		
Patient 1	388 DPM/mg protein/h	22
Control	1,733 ± 747 DPM/mg protein/h	100
Assay 2[c]:		
Patient 1	48 pmol/mg protein/h	36
Control	130 ± 18 pmol/mg protein/h	100

[a] In both assays, radiolabeled CoQ_{10} was isolated by HPLC and was quantitated in a scintillation counter. Controls are measured as means ± SDs (n = 5). DPM = decays per minute.

[b] Cultured cells were incubated for 24 h with 0.1 μCi ^{14}C-PHB (50 Ci/mol specific activity).

[c] Fibroblast homogenates were incubated with ^{3}H-radiolabeled decaprenyl-PP.

wide variety of clinical presentations associated with CoQ_{10} deficiency has suggested genetic heterogeneity, probably related to the many steps involved in the CoQ_{10} biosynthesis.

We have identified the first molecular cause of primary CoQ_{10} deficiency, a mutation in the gene encoding PHB-polyprenyl transferase (*COQ2*), the second enzyme in the biosynthetic pathway of CoQ_{10} (fig. 1). PHB-polyprenyl transferase mediates the conjugation of the benzoquinone ring with the decaprenyl side chain and, thus, plays a central role in the biosynthesis of CoQ_{10} (Forsgren et al. 2004).

The G→A mutation at nucleotide 890 of *COQ2* appears to exert a pathogenic effect by blocking ubiquinone synthesis. Evidence supporting pathogenicity includes: (1) the substitution of a well-conserved aromatic tyrosine amino acid by a polar uncharged cysteine in a predicted transmembrane domain of the protein, (2) absence of the mutation in 100 unrelated controls (200 alleles), and (3) the significantly decreased rate of CoQ_{10} synthesis, indicated by the reduced incorporation of radiolabeled PHB and decaprenyl-PP into CoQ_{10} in skin fibroblasts of the proband (23%–25% of control fibroblasts).

The pathogenic effects of CoQ_{10} deficiency in humans are uncertain. Lack of CoQ_{10} in mitochondria will disrupt the flow of reducing equivalents to respiratory chain complex III from complexes I and II, which, in turn, will lead to decreased ATP synthesis by oxidative phosphorylation. Respiratory chain defects typically cause encephalomyopathies due to the high energy requirements of these organs (DiMauro and Schon 2003); it is, therefore, not surprising that CoQ_{10} deficiency should also affect brain and muscle. In addition, because CoQ_{10} functions as an antioxidant, CoQ_{10} deficiency may preferentially affect postmitotic cells, such as neurons and muscle, which are particularly vulnerable to oxidative damage because they cannot replace dysfunctional cells. Furthermore, to function as an antioxidant, CoQ_{10} must be in the reduced form, but only 20% of the molecule is reduced in the brain (Naini et al. 2003). Brain vulnerability to oxidative stress has been demonstrated in neurodegenerative diseases, such as Friedreich ataxia (Puccio and Koenig 2002) and ataxia associated with deficiency of vitamin E (Yokota et al. 2001), which, like CoQ_{10}, is a lipid-soluble antioxidant in biological membranes. Finally, in *Schizosaccharomyces pombe* with defective PHB-polyprenyltransferase, there is also increased vulnerability to oxidative stress, which is demonstrated both by increased sensitivity to pro-oxidants like H_2O_2 and Cu^{2+} and by the ability of supplemental antioxidants (cysteine, glutathione, and α-tocopherol) to restore growth in glucose medium (Uchida et al. 2000).

Renal failure has been described in the infantile variant of CoQ_{10} deficiency and was present in our patients (Rötig et al. 2000). The vulnerability of the kidney is more difficult to explain, but lipid peroxidation and altered mitochondrial function have been implicated in congenital nephrotic syndrome and glomerular proteinuria (Neale et al. 1994; Holthofer et al. 1999).

This is the first report of a molecular defect causing primary human CoQ_{10} deficiency and the initial description of defects in human PHB-polyprenyl transferase. Further studies are needed to understand the pathogenesis of this disease, and the detection of mutations in *COQ2* in other patients will better define possible phenotypic variants in this condition. The availability of genetic testing will allow the initiation of early therapeutic intervention, even presymptomatically, in this otherwise life-threatening infantile encephalomyopathy responsive to CoQ_{10} supplementation.

Acknowledgments

We appreciate the generous cooperation of the patients and their relatives. The thoughtful comments of Dr. Eric Schon and excellent technical support of Ms. Saba Tadesse are acknowledged. The authors are supported by National Institutes of Health grant P01NS11766 and by grants from the Muscular Dystrophy Association and the Marriott Mitochondrial Disorder Clinical Research Fund.

Web Resources

The URL for data presented herein is as follows:

Online Mendelian Inheritance in Man (OMIM), http://www.ncbi.nlm.nih.gov/Omim/ (for CoQ_{10} deficiency)

References

Aure K, Benoist JF, Ogier de Baulny H, Romero NB, Rigal O, Lombes A (2004) Progression despite replacement of a myopathic form of coenzyme Q10 defect. Neurology 63:727–729

Boitier E, Degoul F, Desguerre I, Charpentier C, François D, Ponsot G, Diry M, Rustin P, Marsac C (1998) A case of mitochondrial encephalomyopathy associated with a muscle coenzyme Q_{10} deficiency. J Neurol Sci 156:41–46

Brea-Calvo G, Rodriguez-Hernandez A, Fernandez-Ayala DJM, Navas P, Sanchez-Alcazar JA. Chemotherapy induces an increase in coenzyme Q10 levels in cancer cell lines. Free Radic Biol Med (in press)

Date H, Onodera O, Tanaka H, Iwabuchi K, Uekawa K, Igarashi S, Koike R, Hiroi T, Yuasa T, Awaya Y, Sakai T, Takahashi T, Nagatomo H, Sekijima Y, Kawachi I, Takiyama Y, Nishizawa M, Fukuhara N, Saito K, Sugano S, Tsuji S (2001) Early-onset ataxia with ocular motor apraxia and hypoalbuminemia is caused by mutations in a new HIT superfamily gene. Nat Genet 29:184–188

Di Giovanni S, Mirabella M, Spinazzola A, Crociani P, Silvestri G, Broccolini A, Tonali P, Di Mauro S, Servidei S (2001) Coenzyme Q10 reverses pathological phenotype and reduces apoptosis in familial CoQ10 deficiency. Neurology 57:515–518

DiMauro S, Schon EA (2003) Mitochondrial respiratory-chain diseases. N Engl J Med 348:2656–2668

Echtay KS, Winkler E, Klingenberg M (2000) Coenzyme Q is an oblig-

atory cofactor for uncoupling protein function. Nature 408:609–613

Forsgren M, Attersand A, Lake S, Grunler J, Swiezewska E, Dallner G, Climent I (2004) Isolation and functional expression of human COQ2, a gene encoding a polyprenyl transferase involved in the synthesis of CoQ. Biochem J 382:519–526

Gin P, Hsu AY, Rothman SC, Jonassen T, Lee PT, Tzagoloff A, Clarke CF (2003) The Saccharomyces cerevisiae COQ6 gene encodes a mitochondrial flavin-dependent monooxygenase required for coenzyme Q biosynthesis. J Biol Chem 278:25308–25316

Gironi M, Lamperti C, Nemni R, Moggio M, Comi G, Guerini FR, Ferrante P, Canal N, Naini A, Bresolin N, DiMauro S (2004) Late-onset cerebellar ataxia with hypogonadism and muscle coenzyme Q10 deficiency. Neurology 62:818–820

Holthofer H, Kretzler M, Haltia A, Solin ML, Taanman JW, Schagger H, Kriz W, Kerjaschki D, Schlondorff D (1999) Altered gene expression and functions of mitochondria in human nephrotic syndrome. FASEB J 13:523–532

Kagan V, Serbinova E, Packer L (1990) Antioxidant effects of ubiquinones in microsomes and mitochondria are mediated by tocopherol recycling. Biochem Biophys Res Commun 169:851–857

Kalen A, Appelkvist EL, Chojnacki T, Dallner G (1990) Nonaprenyl-4-hydroxybenzoate transferase, an enzyme involved in ubiquinone biosynthesis, in the endoplasmic reticulum-Golgi system of rat liver. J Biol Chem 265:1158–1164

Lalani SR, Vladutiu GD, Plunkett K, Lotze TE, Adesina AM, Scaglia F (2005) Isolated mitochondrial myopathy associated with muscle coenzyme Q10 deficiency. Arch Neurol 62:317–320

Lamperti C, Naini A, Hirano M, De Vivo DC, Bertini E, Servidei S, Valeriani M, Lynch D, Banwell B, Berg M, Dubrovsky T, Chiriboga C, Angelini C, Pegoraro E, DiMauro S (2003) Cerebellar ataxia and coenzyme Q10 deficiency. Neurology 60:1206–1208

Lowry OH, Rosebrough NJ, Farr AL, Randall RJ (1951) Protein measurement with the Folin phenol reagent. J Biol Chem 193:265–275

Moreira MC, Barbot C, Tachi N, Kozuka N, Uchida E, Gibson T, Mendonca P, Costa M, Barros J, Yanagisawa T, Watanabe M, Ikeda Y, Aoki M, Nagata T, Coutinho P, Sequeiros J, Koenig M (2001) The gene mutated in ataxia-ocular apraxia 1 encodes the new HIT/Zn-finger protein aprataxin. Nat Genet 29:189–193

Musumeci O, Naini A, Slonim AE, Skavin N, Hadjigeorgiou GL, Krawiecki N, Weissman BM, Tsao CY, Mendell JR, Shanske S, De Vivo DC, Hirano M, DiMauro S (2001) Familial cerebellar ataxia with muscle coenzyme Q10 deficiency. Neurology 56:849–855

Naini A, Lewis VJ, Hirano M, DiMauro S (2003) Primary coenzyme Q_{10} deficiency and the brain. Biofactors 18:145–152

Neale TJ, Ojha PP, Exner M, Poczewski H, Ruger B, Witztum JL, Davis P, Kerjaschki D (1994) Proteinuria in passive Heymann nephritis is associated with lipid peroxidation and formation of adducts on type IV collagen. J Clin Invest 94:1577–1584

Nishigaki Y, Martí R, Copeland WC, Hirano M (2003) Site-specific mtDNA point mutations due to thymidine phosphorylase deficiency. J Clin Invest 111:1913–1921

Ogasahara S, Engel AG, Frens D, Mack D (1989) Muscle coenzyme Q deficiency in familial mitochondrial encephalomyopathy. Proc Natl Acad Sci USA 86:2379–2382

Puccio H, Koenig M (2002) Friedreich ataxia: a paradigm for mitochondrial diseases. Curr Opin Genet Dev 12:272–277

Quinzii CM, Kattah AG, Naini A, Akman HO, Mootha VK, DiMauro S, Hirano M (2005) Coenzyme Q deficiency and cerebellar ataxia associated with an *aprataxin* mutation. Neurology 64:539–541

Rahman S, Hargreaves I, Clayton P, Heales S (2001) Neonatal presentation of coenzyme Q10 deficiency. J Pediatr 139:456–458

Rötig A, Appelkvist EL, Geromel V, Chretien D, Kadhom N, Edery P, Lebideau M, Dallner G, Munnich A, Ernster L, Rustin P (2000) Quinone-responsive multiple respiratory-chain dysfunction due to widespread coenzyme Q10 deficiency. Lancet 356:391–395

Salviati L, Sacconi S, Murer L, Zaccello G, Franceschini L, Laverda AM, Basso G, Quinzii CM, Angelini C, Hirano M, Naini A, Navas P, DiMauro S, Montini G (2005) Infantile encephalomyopathy and nephropathy with CoQ10 deficiency: a CoQ10-responsive condition. Neurology 65:606–608

Sobreira C, Hirano M, Shanske S, Keller RK, Haller RG, Davidson E, Santorelli FM, Miranda AF, Bonilla E, Mojon DS, Barreira AA, King MP, DiMauro S (1997) Mitochondrial encephalomyopathy with coenzyme Q10 deficiency. Neurology 48:1238–1243

Turunen M, Olsson J, Dallner G (2004) Metabolism and function of coenzyme Q. Biochim Biophys Acta 1660:171–199

Uchida N, Suzuki K, Saiki R, Kainou T, Tanaka K, Matsuda H, Kawamukai M (2000) Phenotypes of fission yeast defective in ubiquinone production due to disruption of the gene for p-hydroxybenzoate polyprenyl diphosphate transferase. J Bacteriol 182:6933–6939

Van Maldergem L, Trijbels F, DiMauro S, Sindelar PJ, Musumeci O, Janssen A, Delberghe X, Martin JJ, Gillerot Y (2002) Coenzyme Q-responsive Leigh's encephalopathy in two sisters. Ann Neurol 52:750–754

Yokota T, Igarashi K, Uchihara T, Jishage K, Tomita H, Inaba A, Li Y, Arita M, Suzuki H, Mizusawa H, Arai H (2001) Delayed-onset ataxia in mice lacking alpha-tocopherol transfer protein: model for neuronal degeneration caused by chronic oxidative stress. Proc Natl Acad Sci USA 98:15185–15190

J Hum Genet (2006) 51:964–968
DOI 10.1007/s10038-006-0054-9

ORIGINAL ARTICLE

Molecular analysis of two uncharacterized sequence variants of the *VHL* gene

Maddalena Martella · Leonardo Salviati · Alberto Casarin · Eva Trevisson · Giuseppe Opocher · Roberta Polli · David Gross · Alessandra Murgia

Received: 30 June 2006 / Accepted: 30 July 2006 / Published online: 28 September 2006

Abstract Mutations in the *VHL* gene cause von Hippel–Lindau disease, a cancer predisposing syndrome characterized by a variety of benign and malignant neoplasms. We report the molecular characterization of two sequence variants of the *VHL* gene: a synonymous substitution c.462 A>C in exon 2 and a duplication of 11 bp in the promoter region (c.–65_–55dup11). The first variant is a pathogenic mutation because, although it does not change the sense of the affected codon, it causes skipping of exon 2 in the affected allele by altering the splicing consensus site at the 3′ end of exon 2. The 11 bp duplication represents a nonpathogenic variant. In fact, although it affects a critical region of the *VHL* promoter, it was found in healthy controls, and we show that carrier individuals express both *VHL* alleles at equimolar levels. Our data underline the importance of careful evaluation of the potential pathogenicity of sequence variants that may not belong to the obvious disease-causing mutation categories, or that affect relevant regulatory regions. mRNA analysis will be required to ultimately resolve this issue.

Keywords Duplication · mRNA · Polymorphism · Promoter · Silent mutation · VHL

Maddalena Martella and Leonardo Salviati contributed equally to this work.

M. Martella · A. Casarin · E. Trevisson · R. Polli · A. Murgia (✉)
Department of Pediatrics, University of Padova,
Via Giustiniani 3, 35128 Padua, Italy
e-mail: alessandra.murgia@unipd.it

L. Salviati
Servizio di Genetica Clinica ed Epidemiologica,
Department of Pediatrics, University of Padova,
Padua, Italy

G. Opocher
Department of Medical and Surgical Sciences,
University of Padua, Padua, Italy

D. Gross
Department of Medicine,
Hadassah University Hospital, Jerusalem, Israel

Introduction

The *VHL* gene (GenBank NM_000551) is a tumor suppressor gene located on chromosome 3p25 that encodes a 213 aa protein belonging to the ubiquitin ligase family. Mutations in *VHL* cause von Hippel–Lindau disease (MIM 193300), a dominantly inherited familial cancer syndrome predisposing to a variety of malignant and benign neoplasms, including retinal, cerebellar, and spinal hemangioblastoma, clear cell renal carcinoma and pheochromocytoma (Maher et al. 1991).

The disease is typically manifest after the second decade of life, although earlier onset is frequent. Penetrance is virtually complete by 60 years of age.

To date, missense, nonsense and frameshift mutations have been associated with the disease, as well as large-scale deletions and intronic mutations that alter mRNA splicing (Maher et al. 1991; Kaelin and Maher 1998); the pathogenicity of some sequence variants of the *VHL* gene is, however, still difficult to establish.

In this work we describe the molecular characterization of two such variants: a synonymous substitution

in exon 2, and the duplication of 11 nucleotides in the promoter region.

Materials and methods

Patient 1 is a 43-year-old woman who was diagnosed with von Hippel–Lindau disease because of the presence of a retinal angioma and a cerebellar hemangioblastoma. We performed a complete molecular analysis of the *VHL* gene on genomic DNA of the proband and her asymptomatic 44-year-old brother and 31-year-old sister. The male individual tested negative while the sister was found to harbor the same alteration as in the proband. A magnetic resonance scan in this latter subject revealed the presence of a spinal hemangioblastoma.

Patient 2 is a 40-year-old male affected by cerebellar hemangioblastoma and renal oncocytoma. Patient 3 is a 12-year-old boy affected by isolated hemangioblastoma of the central nervous system. Patient 4 is a 16-year-old girl referred to our center for VHL testing due to an isolated retinal angioma. Family history in these latter three patients was unremarkable.

Signed informed consent prior to VHL molecular analysis was obtained from each tested individual.

Genomic DNA analysis

Genomic DNA was extracted from peripheral blood lymphocytes using standard protocols. VHL gene dosage was evaluated by quantitative Southern blot or real-time quantitative PCR analysis, as described (Stolle et al. 1998; Casarin et al. 2006). The coding region of the *VHL* gene was studied by direct sequencing as described (Murgia et al. 2000). PCR fragments obtained using primers 1AF (5′ GAAATACAGTAACGAGTTGGCCTAGC 3′) and 1AR (5′ ACCTCGGCCTCGTCCCAGT 3′) containing the identified –65_–55dup11 variant were separated on a 2.5% agarose gel. Individual bands were excised and DNA was recovered using a Qiaquick Gel extraction kit (Qiagen, Hilden Germany). The purified amplicon with the 11 bp insertion was cloned with a TOPO TA Cloning kit (Invitrogen, Carlsbad, CA) and sequenced using T7 primers according to the supplier's protocol as previously described (Salviati et al. 2004).

mRNA analysis

Total mRNA was extracted from peripheral blood lymphocytes using RNA-Bee (TEL-TEST, Friendswood, TX) according to the manufacturer's protocol. cDNA was synthesized using a Superscript II kit (Invitrogen) and random hexamers, according to the manufacturer's protocol, and then amplified using primers 1CF (5′ GTGCTGCGCTCGGTGAACTC 3′) and 3R (5′ CAAGACTCATCAGTACCATCAAAA GCTG 3′). PCR conditions were as follows: 94°C 12 min; (94°C, 1 min; 63°C, 1 min; 72°C, 1 min) 40 cycles; 72°C, 10 min. PCR products were separated on a 10% acrylamide gel and visualized by silver staining. An aliquot of the PCR products was also separated in a 2% agarose gel. Bands were excised, purified as above, then sequenced using both amplification primers, and primer 2ex F (5′ AGGTCACCTTTGGCTCTTCAGA 3′) specific for the full-length *VHL* transcript.

PCR-RFLP analysis

The c.462 A > C variant was studied by means of a nested PCR protocol. An aliquot of the cDNA fragment, amplified with primers 1CF and 3R, and a genomic amplicon were re-amplified with primers P154Pmis F (5′ GACAGCCTATTTTTTGCCAATAT CACACTGGC 3′) and either 3R (cDNA) or 2R (genomic DNA). A mismatched nucleotide in primer P154Pmis F creates a *Hae*III site in the mutant allele. PCR conditions were: 94°C, 12 min; (94°C, 1 min; 63°C, 1 min; 72°C, 1 min) 15 cycles; 72°C, 7 min. PCR fragments digested by *Hae*III (Roche, Basel, Switzerland), were separated on a 12% acrylamide gel, and visualized by silver staining. The c.1149 A/G polymorphism was assayed as described (Gläsker et al. 2001).

Results

PCR–SSCP and direct sequencing of the *VHL* gene of patient 1 showed a heterozygous A>C nucleotide change at position c.462 of exon 2 (Fig. 1a). This substitution does not alter the sense of the corresponding codon (CCA>CCC, Pro>Pro). It was previously listed as a variant of unknown biological significance although predicted in silico to possibly disturb the splicing process of the gene (Olschwang et al. 1998). The mutation was present in the affected sister and absent in unaffected family members, as well as in 100 healthy controls. We detected no other nucleotide change in the affected individuals, and quantitative evaluation of the *VHL* gene dosage was also normal, excluding the possible presence of deletions undetected by conventional PCR techniques.

This substitution, however, affects the AG splicing consensus site at the 3′ end of exon 2. In order to demonstrate the presence of a splicing alteration, we

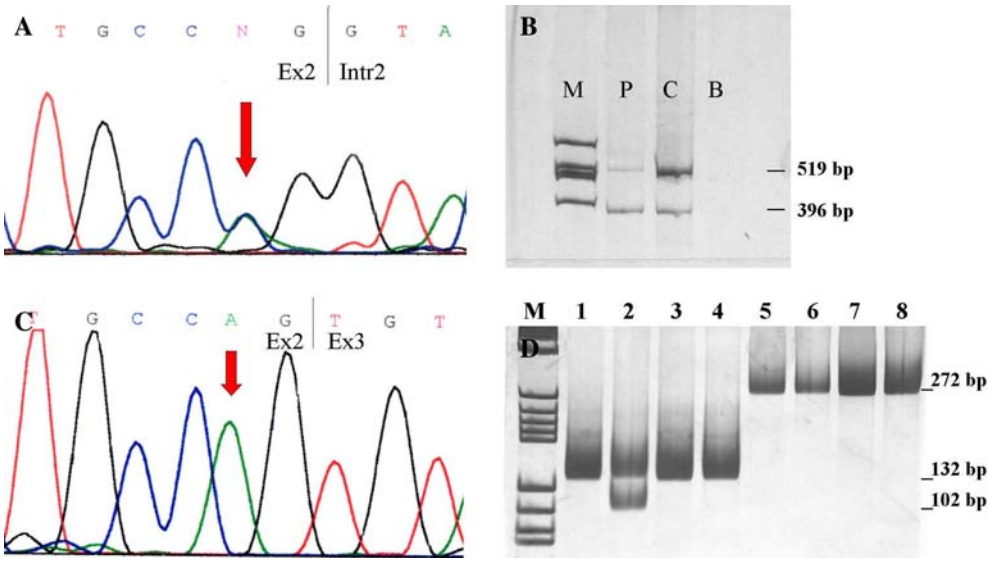

Fig. 1 **a** Sequence of *VHL* exon 2 from genomic DNA of patient 1; the *arrow* indicates nt c.462. **b** *VHL* cDNA fragments amplified by RT-PCR. Lanes: *M* Molecular weight marker (pBR322/*Hae*III), *P* proband, *C* normal control, *B* blank. **c** Sequence of *VHL* exon 2 from cDNA of patient 1; the *arrow* indicates nt c.462. **d** PCR–RFLP analysis (by *Hae* III digestion) of *VHL* exon 2 products amplified from genomic DNA and cDNA. Lanes: *M* Molecular weight marker (pBR322/*Hae*III);*1*, *2* undigested and digested genomic DNA of patient 1; *3*, *4* undigested and digested genomic DNA of negative control sample; *5*, *6* undigested and digested cDNA of patient 1; *7*, *8* undigested and digested cDNA of negative control sample

amplified *VHL* cDNA from the patient's peripheral blood lymphocytes. Two different transcripts of the *VHL* gene are normally present: a full-length transcript comprising exons 1, 2 and 3, and a shorter one, comprising only exons 1 and 3, the physiological significance of which is still unknown (Latif et al. 1993). The patient expressed both mRNAs and no abnormal transcripts were noted; however, the relative abundance of the full length form was apparently reduced in comparison to controls (Fig. 1b). Furthermore, sequencing of the PCR fragment demonstrated that the full-length transcript in the affected subject derived only from the wild-type allele (Fig. 1c). To confirm these data, and increase our sensitivity in detecting even small amounts of the mutant allele, we performed PCR–RFLP analysis of the mutation in both genomic and cDNA. The mutant allele was found in genomic DNA, while it was totally absent from the cDNA (Fig. 1d), indicating that the full length *VHL* transcript was expressed only from the wild type allele.

Molecular analysis of the *VHL* gene in patients 2, 3, and 4 did not detect pathogenic mutations in the coding region of the gene or in intron–exon boundaries, but revealed the presence of a duplication of 11 bp in the promoter region (c.–65_–55dup11) (Fig. 2a–c). Quantitative Southern blot/real-time quantitative PCR analyses were normal in these three patients, who had all inherited the duplication from a nonsymptomatic

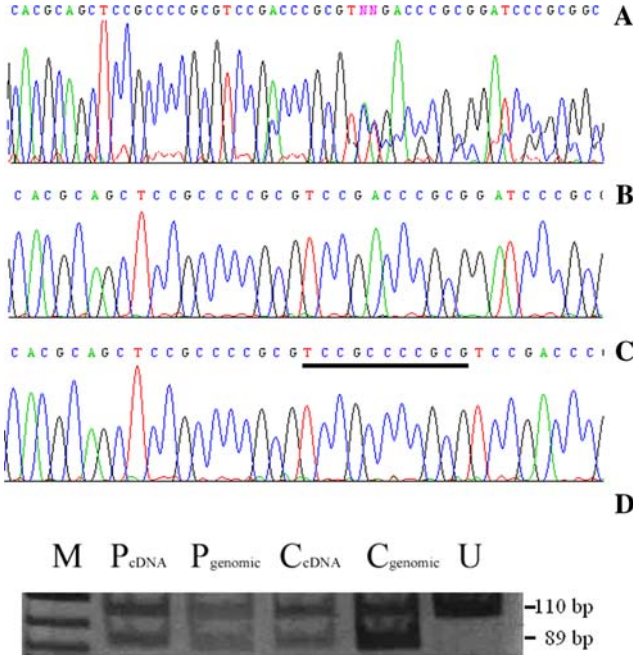

Fig. 2 **a** Sequence analysis of the *VHL* promoter region in patient 4. **b** Cloned wild-type allele. **c** Cloned duplicated allele; the 11 duplicated nucleotides are *underlined*. **d** PCR-RFLP analysis (by *Acc*I digestion) of the *VHL* c.1149 A/G polymorphism on cDNA and genomic DNA. Lanes: *M* Molecular weight marker (pBR322/*Hae*III), *P* patient 4, *C* control heterozygous individual, *U* uncut fragment

parent. Two siblings of patient 2, aged over 40 and also carriers of the same variant, underwent a thorough clinical evaluation, which was judged as negative. This variant was found in 1/100 control individuals.

Nevertheless, the 11 bp duplication is located within the promoter region of the *VHL* gene, in the vicinity of the main transcription initiation site (Kuzmin et al. 1995), and within the putative binding site of several transcription factors (Zatyka et al. 2002). We therefore investigated the possibility that the variant could alter transcription of the gene from the affected allele.

Patient 4 was informative for a known polymorphic variant on the 3′UTR of the *VHL* gene (c.1149 A/G). As in the characterization of the mutation in patient 1, we took advantage of the presence of a sequence variant to discriminate expression of individual *VHL* alleles using a PCR–RFLP assay. Although not precisely quantitative, this approach showed that both alleles were expressed in apparently equimolar amounts (Fig. 2d) suggesting that the 11 bp duplication has no effect on expression of the affected allele.

Discussion

It is often difficult to establish pathogenicity of novel sequence variants discovered during mutational analysis in affected individuals. We have utilised a simple strategy to study the effect of two sequence variants on the pattern of transcription of the*VHL* gene.

Our data show that c.462 A > C is a pathogenic mutation affecting splicing of the *VHL* transcript. Several sequences within exons are recognized by the spliceosomal machinery, in particular, the last two nucleotides at the 3′ end of exons are essential in the splice donor consensus sequence (Cartegni et al. 2002). This mutation does not change the sense of the codon involved (both CCA and CCC encode proline), but it disrupts the splicing consensus at the 3′ end of exon 2. The affected mRNA cannot undergo correct maturation, and in fact, in our patient, full-length transcripts encoding active VHL protein derive only from the wild type allele. The consequences of this mutation on mRNA maturation are particularly severe; some splice-site mutations still allow the synthesis of small amounts of the normal transcript from the mutated allele (Moller et al. 2000), while in our case this seems to be completely abolished.

The second variant, in contrast, appears as a neutral polymorphism. Despite the fact that the duplication involves a critical region of the *VHL* promoter, it does not seem to have any appreciable impact on transcription of the affected allele. Although a subtle difference in the amount of the two transcripts cannot be excluded, our data indicate apparently equivalent levels of expression from both alleles. A strong argument in support of our hypothesis is the presence of the same variant in healthy relatives of our patients as well as in 1/100 control individuals.

Definition of the pathogenicity of a sequence variant is crucial in providing genetic counselling to probands and their families, as well as for their clinical management. We were in fact able to detect the presence of a spinal hemangioblastoma in the clinically asymptomatic sister of patient 1, who was also found to be carrier of the c.462 A>C mutation. On the other hand, we informed the relatives of individuals carrying the 11 bp duplication, that this is highly unlikely to be a pathogenic variant and is therefore not related to the tumors identified in the patients. It is interesting to note that the frequency of this variant has been found to be similar in the general population as in individuals referred to us for VHL-related tumors (1/100 vs 3/270).

We would like to draw attention to the importance of considering the potential pathogenic effects of sequence variants that may not belong to the obvious disease-causing mutation categories. Nucleotide variants within exonic sequences, even though not causing amino acid substitutions, may prove relevant for the proper function of splicing mechanisms; conversely, not all alterations in critical regulatory regions of a gene result in abnormal gene expression.

References

Cartegni L, Chew SL, Krainer AR (2002) Listening to silence and understanding nonsense: exonic mutations that affect splicing. Nat Rev Genet 3:285–298

Casarin A, Martella M, Polli R, Leonardi E, Anesi L, Murgia A (2006) Molecular characterization of large VHL deletions by quantitative real-time PCR: the hypothesis of an Alu-mediated mechanism underlying VHL gene rearrangements. Mol Diagn Ther 10:243–249

Gläsker S, Bender BU, Apel TW, van Velthoven V, Mulligan LM, Zentnerb J, Neumann HPH (2001) Reconsideration of biallelic inactivation of the VHL tumour suppressor gene in hemangioblastomas of the central nervous system. J Neurol Neurosurg Psychiatr 70:644–648

Kaelin WG, Maher ER (1998) The VHL tumour-suppressor gene paradigm. Trends Genet 14:423–426

Kuzmin I, Duh FM, Latif F, Geil L, Zbar B, Lerman MI (1995) Identification of the promoter of the human von Hippel–Lindau disease tumor suppressor gene. Oncogene 10:2185–2194

Latif F, Tory K, Gnarra J, Yao M, Duh F-M, Orcutt ML, Stackhouse T, Kuzmin I, Modi W, Geil L, Schmidt L, Zhou F, Li H, Wei MH, Chen F, Glenn G, Choyke P, Walther MM, Weng Y, Duan D-SR, Dean M, Glavac D, Richards FM,

Crossey PA, Ferguson-Smith MA, Le Paslier D, Chumakov I, Cohen D, Chinault AC, Maher ER, Linehan WM, Zbar B, Lerman MI (1993) Identification of the von Hippel-Lindau disease tumor suppressor gene. Science 260:1317–1320

Maher ER, Iselius L, Yates JRW, Littler M, Benjamin C, Harris R, Sampson J, Williams A, Ferguson-Smith MA, Morton N (1991) Von Hippel-Lindau disease: a genetic study. J Med Genet 28:443–447

Moller LB, Tumer Z, Lund C, Petersen C, Cole T, Hanusch R, Seidel J, Jensen LR, Horn N (2000) Similar splice-site mutations of the ATP7A gene lead to different phenotypes: classical Menkes disease or occipital horn syndrome. Am J Hum Genet 66:1211–1220

Murgia A, Martella M, Vinanzi C, Polli R, Perilongo G, Opocher G (2000) Somatic mosaicism in von Hippel–Lindau Disease. Hum Mutat 15:114

Olschwang S, Richard S, Boisson C, Giraud S, Laurent-Puig P, Resche F, Thomas G (1998) Germline mutation profile of the VHL gene in von Hippel–Lindau disease and in sporadic hemangioblastoma. Hum Mutat 12:424–430

Salviati L, Freehauf C, Sacconi S, DiMauro S, Thoma J, Tsai AC (2004) Novel *SURF1* mutation in a child with subacute encephalopathy and without the radiological features of Leigh Syndrome. Am J Med Genet A 128:195–198

Stolle C, Glenn G, Zbar B, Humphrey JS, Choyke P, Walther M, Pack S, Hurley K, Andrey C, Klausner R, Linehan WM (1998) Improved detection of germline mutations in the von Hippel–Lindau disease tumor suppressor gene. Hum Mutat 12:417–423

Zatyka M, Morrissey C, Kuzmin I, Lerman MI, Latif F, Richards FM, Maher ER (2002) Genetic and functional analysis of the von Hippel–Lindau (VHL) tumour suppressor gene promoter. J Med Genet 39:463–472

Neurogenetics (2007) 8:57–60
DOI 10.1007/s10048-006-0065-x

SHORT COMMUNICATION

A novel deletion in the *GJA12* gene causes Pelizaeus–Merzbacher-like disease

Leonardo Salviati · Eva Trevisson · Maria Cristina Baldoin · Irene Toldo · Stefano Sartori · Milena Calderone · Romano Tenconi · AnnaMaria Laverda

Received: 20 July 2006 / Accepted: 1 September 2006 / Published online: 10 October 2006

Abstract Pelizaeus–Merzbacher disease (PMD) and Pelizaeus–Merzbacher-like disease (PMLD) are hypomyelinating disorders of the central nervous system with a very similar phenotype. PMD is an X-linked disorder caused by mutations in *PLP1*. PMLD is an autosomal recessive condition caused by mutations in *GJA12*. We report a 5-year-old girl with a complex neurological syndrome and severe hypomyelination on brain magnetic resonance imaging. She harbored a homozygous 34-bp deletion in the coding region of *GJA12*. There are no distinctive features for the differential diagnosis of PMD/PMLD. *GJA12* should be analyzed in all patients without *PLP1* mutations but should also be considered the initial genetic test in women and in patients with consanguineous parents.

Keywords Connexin 46.6 · Pelizaeus–Merzbacher disease · Autosomal recessive · PLP1 · Differential diagnosis

Introduction

Pelizaeus–Merzbacher disease (PMD-MIM312080) and Pelizaeus–Merzbacher-like disease (PMLD-MIM311601) are hypomyelinating disorders of the central nervous system (CNS) in which myelin is not formed properly [1, 2]. They are characterized by a virtually identical clinical phenotype: nystagmus, progressive spasticity, ataxia, and development delay. The magnetic resonance imaging (MRI) picture is characteristic, showing a uniformly increased intensity of the white matter signal on T2-weighted images. PMD is an X-linked recessive disorder caused by mutations in the *PLP1* gene [1], whereas PMLD is an autosomal recessive disorder caused by mutations in *GJA12* on chromosome 1q41 [2, 3]. At least, another yet unidentified gene is involved in PMLD [2, 3]. The *GJA12* gene codes for a 439-amino-acid gap junction protein (also known as connexin 46.6 or connexin 47) highly expressed in oligodendrocytes [4].

Case report

We studied a 5-year-old girl with an unremarkable family history. The parents were of Pakistani origin and denied consanguinity. Pregnancy and perinatal periods were uneventful. At 3 months of age, she developed horizontal and rotatory nystagmus. Brain computed tomography was normal. At the age of 1 year, she was noticed to have truncal hypotonia with hypertonus in the lower limbs, severe motor impairment, and ataxia. Funduscopic examination revealed optic atrophy.

At the age of 5 years, neurological examination was essentially unchanged: She was unable to walk or stand unassisted, truncal hypotonia was still evident, and she had severe lower limb spasticity. She also had ataxia and dysarthric speech. Cognitive functions were relatively spared: She could speak a few words and understand simple phrases. The verbal intelligence quotient (IQ) was

L. Salviati (✉) · E. Trevisson · M. C. Baldoin · R. Tenconi
Clinical Genetics, Department of Pediatrics, University of Padova,
Via Giustiniani 3,
35128 Padua, Italy
e-mail: leonardo.salviati@unipd.it

I. Toldo · S. Sartori · A. Laverda
Department of Pediatrics, University of Padova,
Padua, Italy

M. Calderone
Neuroradiology Unit, Azienda Ospedaliera Padova,
Padua, Italy

50, performance IQ was 53, and total IQ was 50 according to the Wechsler preschool and primary scale of intelligence [5]. Cerebrospinal fluid examination, electroretinogram, electromyogram, and peripheral nerve conduction studies were normal. Visually evoked potentials showed mildly prolonged responses, whereas brainstem auditory-evoked responses were markedly altered: Wave I had normal amplitude and latency, but subsequent waves were absent. Electroencephalograph was characterized by intermittent slow waves (2–3 Hz) over the temporal regions; however, the patient never experienced clinical seizures.

Brain MRI showed, on T2-weighted images, hyperintensity of the subcortical white matter, centrum semiovale, internal capsule, cerebellar peduncles, pyramidal tracts, and brainstem consistent with diffuse hypomyelination (Fig. 1).

Chromosomal analysis was normal. *PLP1* gene analysis by direct sequencing and real-time quantitative polymerase chain reaction (PCR) was carried out at another institution and was reported negative.

Materials and methods

The single coding exon of *GJA12* (GenBank accession number: NM_020435) was amplified from genomic DNA using primers 156F (5′-GTTTAAGGCGGTAAGCTCCA-3′) and 1545R (5′-TCTGGCTCCTAGGCCTCTCT-3′) and Expand High Fidelity PCR System (Roche) in the presence of 10% dimethylsulfoxide. PCR conditions were as follows: 94°C for 3 min, 35 cycles of 94°C for 1 min, 55°C for 1 min, 72°C for 1 min and 45 s, and a final extension step of 7 min at 72°C. The fragment was directly sequenced on both strands with internal primers 136F (5′-CGTCATT GACTGTGTAAGCAGA-3′), 523F (5′-GAGGAGGCGTG CACTAAGG-3′), 839F (5′-TGCTCAACCTCTGTGA GATG-3′), 642R (5′-CACGTACACGCGCATCAG-3′), 1056R (5′-GTTTGCCAGGTTCTGGTCAT-3′), and 1413R (5′-GGCTAAGGAGAAGGCTGAGG-3′) using the ABI PRISM 3100 automated sequencer (Applied Biosystems). The presence of the deletion was confirmed by a second PCR performed with primers 839F and 1056R in the same conditions as above except for a 30-s extension.

Nomenclature of mutations and polymorphisms follows the guidelines proposed by den Dunnen and Antonarakis [6].

Results

The MRI findings in the patient were compatible with a diagnosis of PMD/PMLD [7]. The normal karyotype and the absence of *PLP1* alterations suggested the possibility of an autosomal recessive disorder.

Sequencing of the *GJA12* gene showed a homozygous 34-bp deletion within the coding region of the gene [c. 914_947del] (Fig. 2a and b). The mutation alters the reading frame of the transcript from codon 305 [p. P305fsX459]. Both parents were carriers of the deletion, which was absent in normal controls (Fig. 2c). The mutation was associated in both alleles with a neutral polymorphism [c. 285 G>A; p. 95 L>L]. The presence of the mutation was excluded in 100 control subjects (200 alleles).

Discussion

It is still impossible to distinguish PMD and PMLD exclusively on the basis of clinical and neuroradiological findings [2, 3]. The distinction is based essentially on molecular genetic results. Our patient displayed a clinical picture similar to the patients with *GJA12* mutations reported by Bugiani et al. [3], with the onset of nystagmus in the first months of life, a progression of neurological

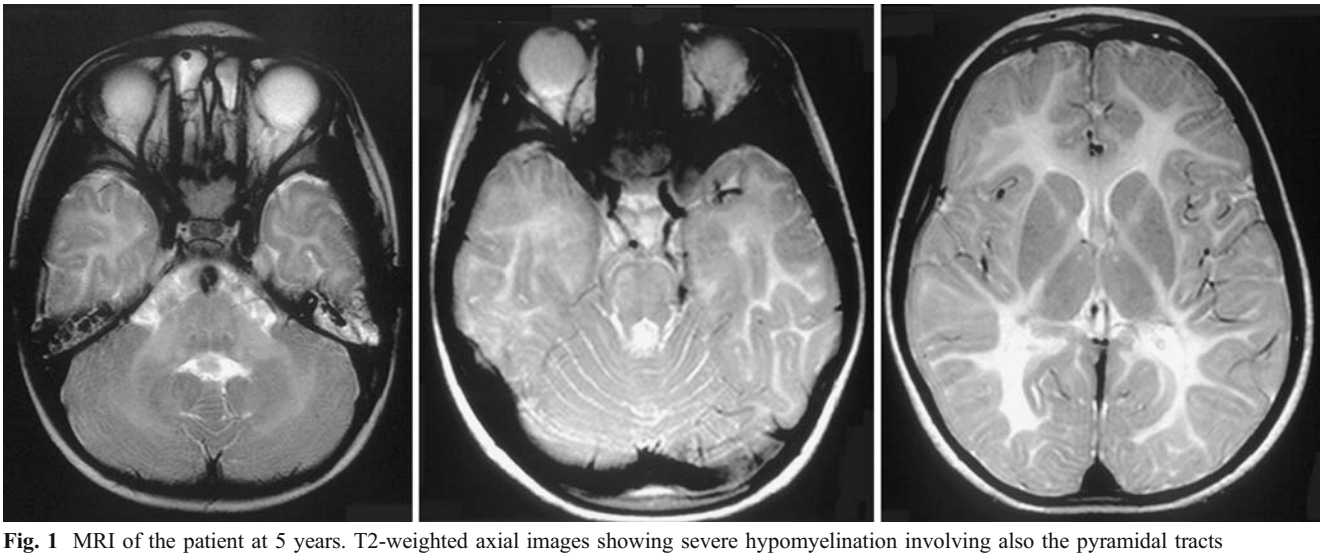

Fig. 1 MRI of the patient at 5 years. T2-weighted axial images showing severe hypomyelination involving also the pyramidal tracts

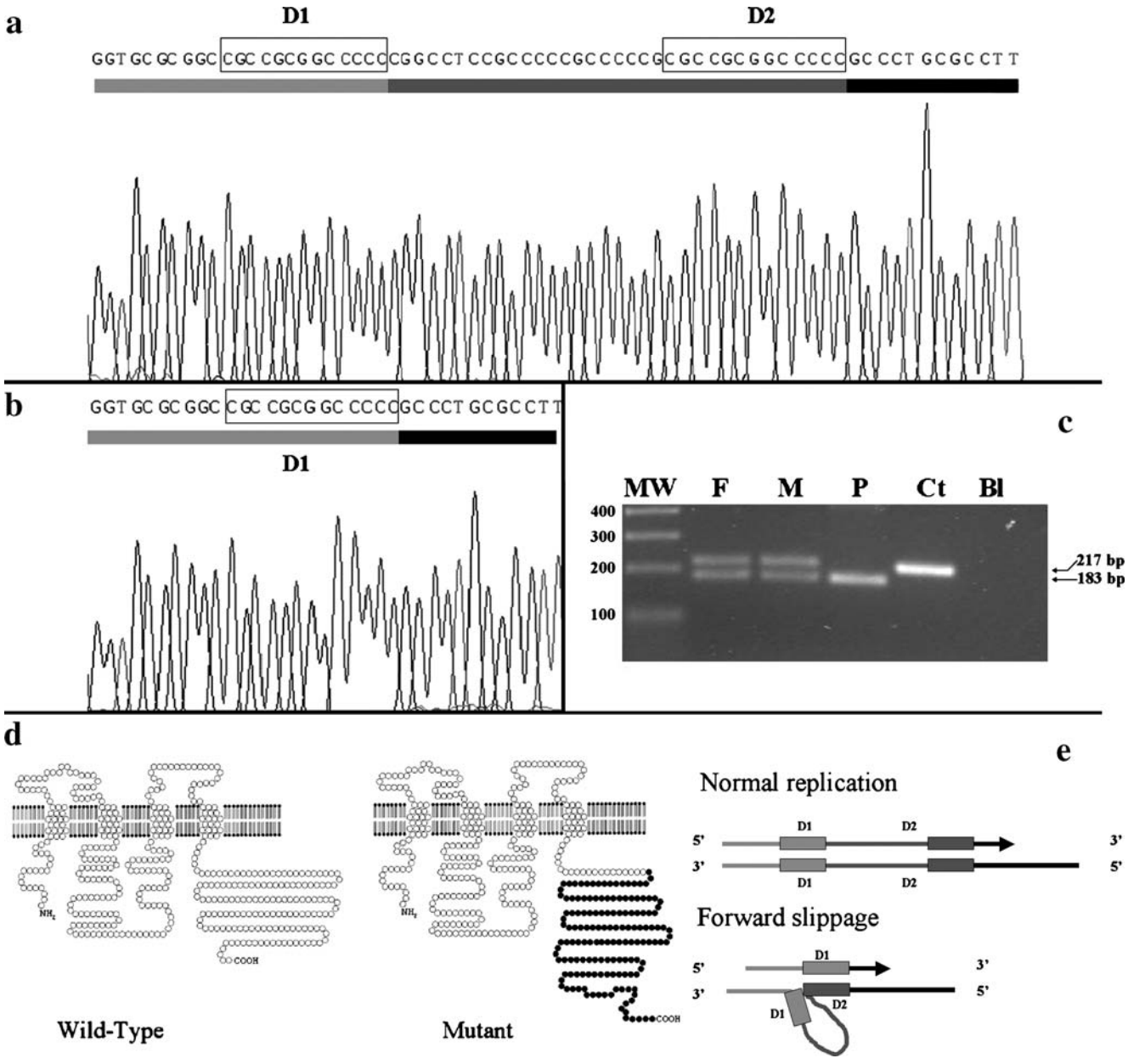

Fig. 2 Sequence of the normal (**a**) and of the patient's (**b**) *GJA12* gene with the homozygous 34-nt deletion. The duplicated CGCCG CGGCCCCC sequences are *boxed* and marked *D1* and *D2*. *Underlined in dark gray* are the deleted sequence, whereas in *light gray* and in *black* are the upstream and downstream regions, respectively. **c** PCR fragments encompassing the deleted fragment in the patient (*P*), her father (*F*), her mother (*M*), and a normal control subject (*Ct*); *MW* molecular size markers, *Bl* blank control. **d** Schematic representation of the predicted mutated protein. In *black* are the abnormal amino acids on the C-terminus of the mutant protein. **e** Proposed molecular mechanism of the deletion: forward slippage of DNA polymerase mediated by the D1 and D2 repeats during DNA replication. Color codes as in **a** and **b**

symptoms during the first year, a slow evolution afterwards, and a relative sparing of cognitive functions. She did not have signs of peripheral neuropathy or seizures as some of the patients reported by Uhlenberg et al. [2], although these features may appear at a later stage of the disease. MRI displayed the typical features of PMD/PMLD with diffuse CNS hypomyelination. Pyramidal tracts were severely affected in our patient, indicating that the sparing of these structures is not a distinctive feature of *GJA12* mutations as hypothesized by Bugiani et al. [3]. Electrophysiological studies showed a pattern of alterations similar to other PMD cases [8], revealing a marked alteration of CNS components, whereas peripheral structures appeared normal.

Molecular analysis revealed a novel homozygous 34-bp deletion in the *GJA12* gene, which alters the reading frame of the mRNA. The predicted mutant protein is 19 amino acids longer than the wild-type polypeptide. We believe that the mutation is pathogenic because the whole C-terminal

domain, form codon 305, is completely altered (Fig. 2d). The heterozygous parents had a normal neurological examination, and there was no history of neurological disease in other family members. These data suggest that this novel *GJA12* mutation causes a "loss of function" of the Gja12 protein and not a toxic polypeptide, as it has been suggested for other *GJA12* mutations [2]. Expression studies are needed to clarify this issue.

The deleted sequence is flanked by a 13-nt CGCCGCGGCCCCC duplicated sequence. We believe that the deletion was probably caused by replication slippage, one common causative mutational mechanism for deletions due to slipped mispairing of direct repeat sequences in proximity to one another [9, 10] (Fig. 2e). The deletion was associated in both alleles with a neutral polymorphism [c. 285 G>A] suggesting a common ancestor, although the parents denied consanguinity.

This is only the third report of *GJA12* mutations associated with PMLD. Our data confirm that the clinical phenotype of patients with *GJA12* defects is quite homogeneous compared with that of *PLP1* mutations, which display ample phenotypic variability [11]; however, we found no distinctive features that could help differentiate PMD and PMLD on a clinical basis.

Molecular analysis of *GJA12* is a simple procedure and is indicated in all patients with a PMD/PMLD phenotype without *PLP1* mutations. However, we believe that female subjects and patients with consanguineous parents should probably be initially tested for mutations in this gene. The molecular diagnosis is important for appropriate counseling and prenatal diagnosis, and because confirmation of the clinical diagnosis avoids further unnecessary diagnostic procedures.

Acknowledgement Dr. Salviati is supported by a grant from the Association Française contre les Myopathies (AFM).

References

1. Inoue K (2005) PLP1-related inherited dysmyelinating disorders: Pelizaeus–Merzbacher disease and spastic paraplegia type 2. Neurogenetics 6:1–16
2. Uhlenberg B, Schuelke M, Ruschendorf F, Ruf N, Kaindl AM, Henneke M, Thiele H, Stoltenburg-Didinger G, Aksu F, Topaloglu H, Nurnberg P, Hubner C, Weschke B, Gartner J (2004) Mutations in the gene encoding gap junction protein alpha 12 (connexin 46.6) cause Pelizaeus–Merzbacher-like disease. Am J Hum Genet 75:251–260
3. Bugiani M, Al Shahwan S, Lamantea E, Bizzi A, Bakhsh E, Moroni I, Balestrini MR, Uziel G, Zeviani M (2006) GJA12 mutations in children with recessive hypomyelinating leukoencephalopathy. Neurology 67:273–279
4. Menichella DM, Goodenough DA, Sirkowski E, Scherer SS, Paul DL (2003) Connexins are critical for normal myelination in the CNS. J Neurosci 23:5963–5973
5. Wechsler D (1973) Wechsler preschool and primary scale of intelligence. Organizzazioni Speciali, Florence
6. den Dunnen JT, Antonarakis SE (2001) Nomenclature for the description of human sequence variations. Hum Genet 109:121–124
7. Plecko B, Stockler-Ipsiroglu S, Gruber S, Mlynarik V, Moser E, Simbrunner J, Ebner F, Bernert G, Harrer G, Gal A, Prayer D (2003) Degree of hypomyelination and magnetic resonance spectroscopy findings in patients with Pelizaeus Merzbacher phenotype. Neuropediatrics 34:127–136
8. Nezu A (1995) Neurophysiological study in Pelizaeus–Merzbacher disease. Brain Develop 17:175–181
9. Streisinger G, Okada Y, Emrich J, Newton J, Tsugita A, Terzaghi E, Inouye M (1966) Frameshift mutations and the genetic code. Cold Spring Harbor Symp Quant Biol 31:77–84
10. Chen JM, Chuzhanova N, Stenson PD, Ferec C, Cooper DN (2005) Meta-analysis of gross insertions causing human genetic disease: novel mutational mechanisms and the role of replication slippage. Hum Mutat 25:207–221
11. Cailloux F, Gauthier-Barichard F, Mimault C, Isabelle V, Courtois V, Giraud G, Dastugue B, Boespflug-Tanguy O (2000) Genotype–phenotype correlation in inherited brain myelination defects due to proteolipid protein gene mutations. Clinical European network on brain dysmyelinating disease. Eur J Hum Genet 8:837–845

RESEARCH ARTICLE

Argininosuccinate Lyase Deficiency: Mutational Spectrum in Italian Patients and Identification of a Novel *ASL* Pseudogene

Eva Trevisson,[1] Leonardo Salviati,[2]* Maria Cristina Baldoin,[1] Irene Toldo,[1] Alberto Casarin,[1] Sabrina Sacconi,[3] Luca Cesaro,[4] Giuseppe Basso,[5] and Alberto B. Burlina[6]

[1]Department of Pediatrics, University of Padova, Padova, Italy; [2]Clinical Genetics, Department of Pediatrics, University of Padova, Padova, Italy; [3]Fédération des Maladies Neuromusculaires, Centre Hospitalier Universitaire (CHU) de Nice and Institut Nationale de la Santé et de la Recherche Médicale (INSERM) U638, Nice, France; [4]Department of Biochemistry, University of Padova, Padova, Italy; [5]Pediatric Oncology Laboratory, Department of Pediatrics, University of Padova, Padova, Italy; [6]Division of Metabolic Disorders, Department of Pediatrics, University of Padova, Padova, Italy

Communicated by William Sly

Argininosuccinic aciduria (ASAuria) is an inborn error of metabolism caused by mutations in the argininosuccinate lyase (*ASL*) gene, which leads to the accumulation of argininosuccinic acid (ASA) in body fluids and severe hyperammonemia. A severe neonatal form and a milder late-onset variant are described. We report a novel *ASL* pseudogene located in the centromeric region of chromosome 7, 14 novel mutations in the *ASL* gene, and a novel intronic polymorphism found in a cohort of Italian patients. Our approach relied exclusively on genomic DNA analysis. We found seven missense mutations, two nonsense, three small insertions/deletions, and two splicing mutations. Only two patients harbored previously described mutations, and among the novel variants only two were present in more than one kindred. The pathogenicity of the splicing mutations was demonstrated by a functional splicing assay that employed a hybrid minigene. We also performed molecular modeling using the reported three-dimensional structure of ASL to predict the functional consequences of the missense mutations. There was no genotype–phenotype correlation. Patients with neonatal onset display developmental delay and seizures despite adequate metabolic control. Moreover, hepatomegaly, fibrosis, and abnormal liver function tests are common complications in these patients, but not in patients with the late infancy form. We stress the importance of mutation analysis in patients with ASAuria, to confirm the clinical diagnosis, and to perform DNA-based prenatal diagnosis in future pregnancies of these families. Hum Mutat 0, 1–9, 2007. © 2007 Wiley-Liss, Inc.

KEY WORDS: urea cycle defects; argininosuccinic aciduria; argininosuccinate lyase; ASL; ASA; ASAuria; hybrid minigene

INTRODUCTION

Argininosuccinic aciduria (ASAuria; MIM# 207900) is a rare autosomal recessive disorder of the urea cycle, caused by deficiency of argininosuccinate lyase (ASL; EC 4.3.2.1; MIM# 608310), which leads to the accumulation of argininosuccinic acid (ASA) in body fluids and severe hyperammonemia.

Patients with ASAuria may present at any age, but onset is typically in the neonatal period or in late infancy. Patients with onset in the first days of life present with poor feeding, vomiting, tachypnea, lethargy, and seizures, with subsequent progression to coma and death, if untreated. Hepatomegaly is common later in the course of the disease. Patients with onset in late infancy present with less severe symptoms, which include vomiting, failure to thrive, irritability, behavioral problems, or psychomotor retardation. The diagnosis is made by measuring plasma levels of ammonia, ASA, and its anhydrides. Plasma amino acid analysis, measured by automated quantitative column chromatography, provides sufficient information to make a confident diagnosis of ASAuria [Brusilov and Horwich, 2001]. The analysis is definitive and unambiguous, and assays of ASL enzyme activity in erythrocytes or cultured fibroblasts are usually not required [Brusilov and Horwich, 2001].

The human *ASL* gene is approximately 17 kb in length, is comprised of 17 exons (the first, exon 0, codes only for the

The Supplementary Material referred to in this article can be accessed at http://www.interscience.wiley.com/jpages/1059-7794/suppmat.

Received 17 July 2006; accepted revised manuscript 12 January 2007.

*Correspondence to: Leonardo Salviati, MD, PhD, Clinical Genetics, Department of Pediatrics, University of Padova, Via Giustiniani 3, 35128 Padova, Italy. E-mail: leonardo.salviati@unipd.it

Grant sponsor: Association Française contre les Myopathies (AFM); Grant sponsor: Centro Regionale Malattie Metaboliche Ereditarie, Regione Veneto.

Eva Trevisson and Leonardo Salviati are co-first authors.

DOI 10.1002/humu.20498
Published online in Wiley InterScience (www.interscience.wiley.com).

5′UTR), and is located on chromosome 7cen–q11.2. The presence of another partial sequence on chromosome 22 was assumed to be a pseudogene [O'Brien et al., 1986; Linnebank et al., 2002]. The gene encodes for a 464–amino acid protein that catalyzes the degradation of argininosuccinate to fumarate and arginine.

The *ASL* gene was cloned 20 years ago [O'Brien et al., 1986], but the number of reported mutations is still quite small. The aim of our work was to analyze the mutational spectrum of *ASL* in a cohort of Italian patients with ASAuria, employing a diagnostic test that relies exclusively on genomic DNA.

MATERIALS AND METHODS

Patients

We studied 12 patients from 10 different kindreds. Clinical features are summarized in Table 1. The diagnosis of ASAuria was based on both clinical and biochemical criteria, and was established by the quantification of plasma ASA by amino acid chromatography, levels of serum ammonia, and determination of urinary orotic acid, during the acute phase of the disease.

Bioinformatic Analysis

The genomic sequence of the *ASL* gene was derived form contig NT_007758.11. Analysis of *ASL* pseudogenes was performed using the BLASTN software (www.ncbi.nlm.nih.gov/BLAST). Genomic sequences used as probes in the BLAST algorithm were analyzed for the presence of common repeated sequences using the RepeatMasker software (www.repeatmasker.org). The sequence of the *ASL* cDNA used is GenBank accession NM_001024943.1.

The sequence of the *ASL* pseudogene has been submitted to the GenBank database (Accession# DQ679421). Mutation data were submitted to the HGMD database (www.hgmd.cf.ac.uk/ac/gene.php?gene = ASL).

DNA Studies

Genomic DNA was extracted from peripheral blood leukocytes using the Puregene kit (Gentra, Minneapolis, MN; www.gentra.com).

The entire coding region of the *ASL* gene was amplified from genomic DNA by a protocol modified from the one reported by Linnebank et al., [2002], using standard Taq DNA polymerase (Roche, Basel, Switzerland; www.roche.com). PCR fragments longer than 600 bp were amplified using the Expand High Fidelity PCR System (Roche). Primer pairs and PCR conditions are available in Supplementary Table S1 (available online at http://www.interscience.wiley.com/jpages/1059-7794/suppmat).

PCR fragments were purified with the Microcon YM-100 kit (Millipore, Billerica, MA; www.millipore.com) and sequenced using the BigDye Cycle Reaction System v3.1 kit (Applied Biosystems, Foster City, CA; www.appliedbiosystems.com) and the ABI PRISM 3100 automated sequencer (Applied Biosystems). The presence of mutations was confirmed on a second PCR product. Fragments containing insertions/deletions were subcloned in the pCRIITOPO vector (Invitrogen, Carlsbad, CA; www.invitrogen.com) and individual colonies were sequenced as described [Salviati et al., 2004].

The presence of each point mutation was validated by a specific PCR-RFLP assay (Supplementary Table S2). After amplification, PCR products were digested overnight with the appropriate restriction nuclease. Fragments were separated on standard agarose gels. For mutations that did not alter natural restriction sites, we designed appropriate mismatched PCR primers in order to create novel nuclease recognition sequences in the mutant alleles.

TABLE 1. Clinical Features of Patients Included in the Study

Patient	Subtype	Age at diagnosis	Presenting symptoms	Laboratory tests at diagnosis[a]	Outcome (age)	Liver function
1	Neonatal onset	5d	Coma, hyperammonemia	NH_3 = 850 μg/dL; ASA > 1000 μmol/L	Alive (3 y), MR, epilepsy	Hepatomegaly, hypertransaminasemia
2	Neonatal onset	6d	Coma, hyperammonemia	NH_3 = 1200 μg/dL; ASA > 1000 μmol/L	Dead (10 y), MR, epilepsy	Hepatomegaly, hypertransaminasemia, reduced PT
3	Neonatal onset	4d	Coma, hyperammonemia	NH_3 = 2000 μg/dL; ASA > 700 μmol/L	Alive (9 y), MR, epilepsy	Hepatomegaly, hypertransaminasemia, reduced PT
4	Neonatal onset	7d	Coma, hyperammonemia	NH_3 = 1800 μg/dL; ASA > 1000 μmol/L	Alive (15 y), vegetative status, epilepsy	Normal
5a	Late onset	4y	MR	NH_3 = 120 μg/dL; ASA > 300 μmol/L	Alive (24 y), MR	Normal
5b	Late onset	2y	MR	NH_3 = 90 μg/dL; ASA > 300 μmol/L	Alive (21 y), MR	Normal
6	Neonatal onset	2d	Coma, hyperammonemia	NH_3 = 950 μg/dL; ASA > 1200 μmol/L	Alive (9 y), MR	Hepatomegaly, hypertransaminasemia, reduced PT
7	Neonatal onset	2d	Lethargy, hyperammonemia	NH_3 = 450 μg/dL; ASA > 600 μmol/L	Alive (2 y), mild psychomotor retardation	Normal
8a	Late onset	3y	Seizures	NH_3 = 120 μg/dL; ASA > 300 μmol/L	Alive (5 y), epilepsy	Normal
8b	Late onset	6mo	Failure to thrive, vomiting	NH_3 = 60 μg/dL; ASA > 300 μmol/L	Alive (21 mo)	Normal
9	Neonatal onset	6d	Coma, hyperammonemia	NH_3 = 2000 μg/dL; ASA > 1000 μmol/L	Alive (18 y), MR, epilepsy	Hepatic fibrosis, hypertransaminasemia, reduced PT
10	Neonatal onset	7d	Coma, hyperammonemia	NH_3 = 400 μg/dL; ASA > 500 μmol/L	Alive (1 y); clinical data NA	NA

[a]NH_3 normal value 20–70 μg/dL.
mo, months; d, days; y, years; MR, mental retardation; PT, prothrombin time; NA, not available; ASA, argininosuccinic acid.

Nomenclature of *ASL* exons follows the one proposed by Linnebank et al., [2002]. Mutation nomenclature follows journal guidelines (www.hgvs.org/mutnomen) and is based on GenBank NM_001024943.1 with +1 as the A of the ATG initiation codon (codon+1).

Minigene Construction

The two hybrid minigene constructs were generated using as a backbone the pEGFP-N1 vector (Clontech, Mountain View, CA; www.clontech.com) with the 5′ region of the human *COQ2* gene [Forsgren et al., 2004] (nt 1–366) cloned in the BglII-PstI sites (pEGFP-COQ2). This construct was selected because it had convenient restriction sites. Both minigenes comprised the exon adjacent to the mutation, and part of the upstream and downstream exons fused with the COQ2-GFP gene.

To generate the exon 5-6-7 minigene, the wild type and mutated genomic DNA from the patient was amplified using primers MG6A-MG6B and MG6C-MG6D (each primer contained an appropriate restriction site for subsequent cloning). Primer MG6A contained also a mismatch to abolish the natural SacI site present in exon 5. The 96-bp MG6A-MG6B fragment (comprising the last 41 nt of exon 5 and the first 50 nt of intron 5) was cloned in pEGFP-COQ2 cut with SacI and PstI. The resulting plasmid was then cut with PstI and BamHI and ligated with the 285-bp MG6C-MG6D fragment (comprising the last 58 nt of intron 5, exon 6, intron 6, and the first 67 nt of exon 7) digested with the same nucleases.

The exon 8-9-10 minigene was generated by amplifying from genomic DNA a 1,514-bp fragment using primers MG9A and MG9B. This fragment (comprising the last 31 nt of exon 8, intron 8, exon 9, intron 9, and the first 42 nt of exon 10) was cut with SacI and ApaI and cloned in pEGFP-COQ2 cut similarly. In both cases the resulting inserts (if correctly spliced) were designed to be in-frame with COQ2 and GFP. The correctness of plasmid clones was confirmed by direct sequencing. The structure of both hybrid minigene constructs is depicted in Figure 1.

Minigene Expression Analysis

A total of 0.4 μg of each wild type and mutant minigene plasmid constructs was transfected into 3×10^5 HeLa cells using Effectene reagent (Qiagen, Valencia, CA; www.qiagen.com); RNA was extracted after 48 hr using the Trizol kit (Invitrogen) and retrotranscribed using the Superscript III kit (Invitrogen). cDNA was amplified with primers specific for sequences in the flanking *COQ2* and *GFP* sequences (COQ2F and GFPR) in order to avoid interference from endogenous *ASL* mRNA. cDNA was also amplified with primers specific for the exon adjacent to the intronic mutation to be tested.

Pseudogene Expression Analysis

Expression of the *ψASL2* pseudogene was analyzed by RT-PCR using primers psASL2F 5′-ACTCATTGGCTGTGTGGATG-3′ and psASL2R 5′-AGGAATGGGCCCAGGGTG-3′ that are specific for *ψASL2* (the nucleotides unique to *ψASL2* are underlined), and amplify a 66-bp fragment corresponding to a portion of *ψASL2* homologous to *ASL* exon 3. A control amplification was conducted on genomic DNA.

Determination of ASL Activity in Erythrocytes

ASL activity in healthy controls and patients erythrocyte lysates was determined using the method of Bastone et al., [1990], which measures the production of ornithine, using a Jeol JLC 500/V amino acid analyzer (Jeol Ltd., Tokyo, Japan). A total of 10 normal controls were analyzed. Activity is expressed as nmol/hr/mg

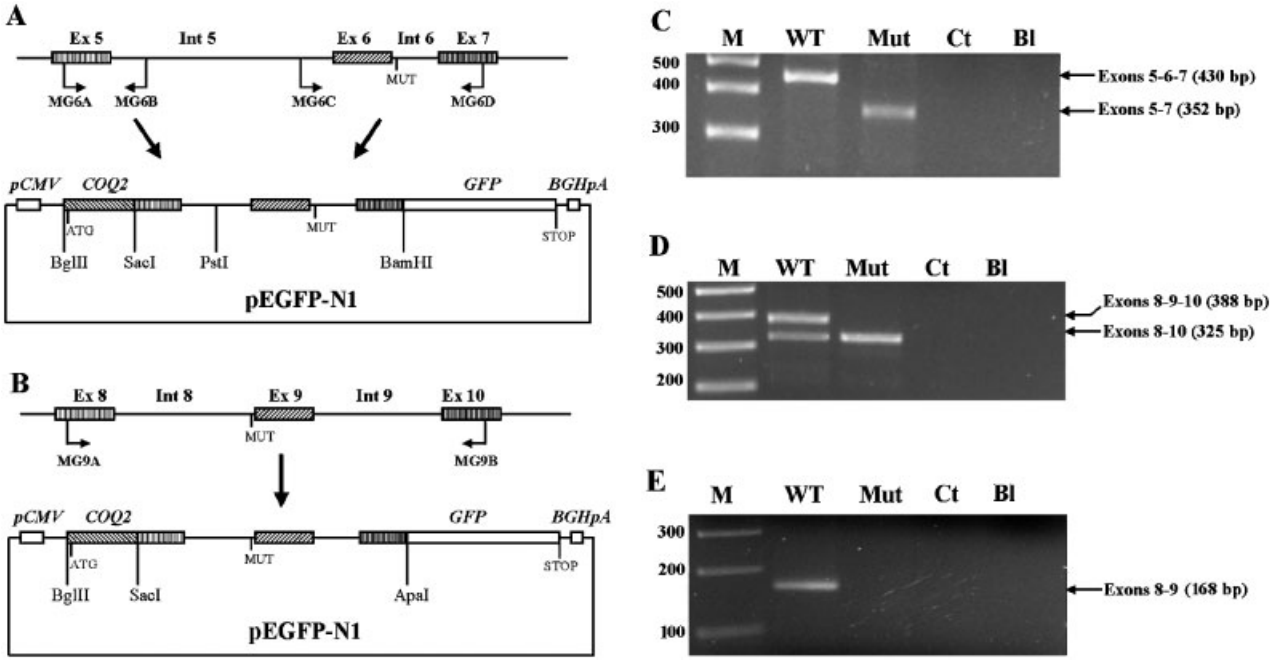

FIGURE 1. **A, B:** Schematic representation of the minigene constructs. Genomic DNA was amplified and products were cloned into the pEGFP-N1 vector containing the 5′ sequence of the human *COQ2* gene (see Materials and Methods for details). pCMV = CMV promoter, BGHpA = bovine growth hormone polyadenylation signal sequence, MUT indicates the position of the mutation to be tested. **C:** RT-PCR analysis of the exon 5-6-7 minigene expressed in HeLa cells using vector specific primers. M = 1 kb plus (Invitrogen) molecular marker, WT = wild-type construct, Mut = mutant construct, Ct = control cell line transfected with pEGFP-N1, Bl = blank control. **D:** RT-PCR analysis of the exon 8-9-10 minigene expressed in HeLa cells using vector specific primers. Letter codes are as in C. **E:** RT-PCR analysis of the exon 8-9-10 minigene expressed in HeLa cells using primers specific for exon 9. Letter codes are as in C.

hemoglobin. All samples were processed immediately after collection. In two patients ASL activity had been previously determined in Dr. W.J. Kleijer's laboratory (Department of Clinical Genetics, Erasmus University Medical Center, Rotterdam, The Netherlands) by [^{14}C]citrulline incorporation in primary skin fibroblasts.

Molecular Modeling

All images were generated by using Pymol (DeLano Scientific LLC; Palo Alto, CA; http://pymol.sourceforge.net) as reported previously [Pagano et al., 2004]. The structures utilized as templates for modeling were the human ASL protein (Protein Data Bank [pdb] code 1AOS; www.rcsb.org/pdb/home/home.do) and Duck Delta Crystallin (pdb code 1TJW), an ortholog of ASL, which is the only one crystallized as a tetramer with its substrate. The Duck Delta Crystallin protein contains two additional amino acids on the N-terminus (residues 5 and 6), therefore the numbering of residues differs by two units compared to the human protein (i.e., histidine 89 in the human protein corresponds to histidine 91 in the Duck Delta Crystallin).

The Biopolymer module of InsightII (Accelrys Software, Inc., San Diego, CA; www.accelrys.com) was used to analyze the R186Q, V335L, and R456W mutations. An energy minimization of the mutant protein was performed until the energy minimum was reached. The calculation of the electrostatic surface charges was performed with the APBS software [Baker et al., 2001] and visualized by using Pymol.

RESULTS

Identification of a Second *ASL* Pseudogene

When testing the PCR primer pair 5′-CTCTTGGCTGCTGAT GCCTG-3′ and 5′-AATGCTCAAAGTGGCCCTGG-3′, designed in *ASL* intron 2 and intron 3, we realized, after cloning of the PCR product, that amplification had yielded two different fragments of the same size. One corresponded to the correct *ASL* exon 3 and its intronic boundaries, while the other displayed multiple single-nucleotide changes compared to the reported *ASL* sequence, a result compatible with the simultaneous amplification of a gene and its pseudogene. We performed a BLAST search against the whole human genome using as probe the genomic sequence surrounding *ASL* exon 3, and retrieved three different sequences: *ASL* exon 3 (100% identity), the reported *ASL* pseudogene on chromosome 22—*ψASL1*—(90% identity), and a third sequence (90% identity), which however showed 100% identity with the second PCR fragment we had obtained. We have denominated this locus *ψASL2*. The *ψASL2* region comprises 561 nucleotides and is located on chromosome 7 about 3 Mb upstream of the *ASL* gene (nucleotides 589296–589857 of genomic sequence NT_007758.11), close to the centromere. The corresponding *ASL* region includes part of intron 2, exon 3, and part of intron 3. As opposed to *ψASL1*, which appears to be actively transcribed [Linnebank et al., 2002], we found no evidence of expressed sequence tags (ESTs) transcribed from the *ψASL2* locus, and we failed to detect any *ψASL2* expression by RT-PCR in primary fibroblasts, peripheral blood cells, and HeLa cells (data not shown).

We repeated a similar bioinformatic analysis for the entire *ASL* gene and we did not detect other pseudogenes. The sequence of *ψASL2* was submitted to Genbank (Accession♯ DQ679421).

Mutation Analysis in Patients

The entire coding region of the *ASL* gene was amplified and sequenced in all patients. We detected pathogenic mutations in all

TABLE 2. Mutations and ASL Activity in Patients*

Patient	Mutations	Location	Predicted effect on protein	ASL activity (% of controls)[a]
1	c.857A>G[b]	Exon 11	p.Q286R[b]	<5%
	c.857A>G[b]	Exon 11	p.Q286R[b]	
2	c.524+2T>G	Intron 6	p.E150_S175del[c]	ND
	c.1145T>G	Exon 15	p.M382R	
3	c.524+2T>G	Intron 6	p.E150_S175del[c]	<5%
	c.637C>T	Exon 8	p.R213X	
4	c.532G>A[d]	Exon 7	p.V178M[d]	<2% (in fibroblasts)
	c.557G>A	Exon 7	p.R186Q	
5a[e]	c.91G>A	Exon 2	p.D31N	ND
	c.91G>A	Exon 2	p.D31N	
5b[e]	c.91G>A	Exon 2	p.D31N	ND
	c.91G>A	Exon 2	p.D31N	
6	c.584_585delAT	Exon 8	p.N195fsX233	<5%
	c.656-1G>A	Intron 8	p.E219_V239del ‡	
7	c.338G>A	Exon 4	p.R113Q	<5%
	c.706C>T	Exon 9	p.R236W	
8a[e]	c.551_552delCT	Exon 7	p.S184X	ND
	c.1003G>T	Exon 13	p.V335L	
8b[e]	c.551_552delCT	Exon 7	p.S184X	9%
	c.1003G>T	Exon 13	p.V335L	
9	c.551_552delCT	Exon 7	p.S184X	<5%
	c.793_795delACCinsT	Exon 10	p.T265X	<2% (in fibroblasts)
10	c.544C>T	Exon 7	p.R182X	ND
	c.1366C>T	Exon 16	p.R456W	

*The reference *ASL* cDNA sequence used was GenBank accession NM_001024943.1. For DNA numbering, +1 is the A of the ATG initiation codon (codon+1).
[a]ASL activity in erythrocytes is expressed as a percentage of normal controls (7.7 ±1.2 nmol/hr/mg hemoglobin). In Patient 9, activity was determined both in skin fibroblasts and erythrocytes, while in Patient 4 activity was determined only in fibroblasts (courtesy of Dr. W.J. Kleijer).
[b]Mutation previously reported by Barbosa et al. [1991], Sampaleanu et al. [2001], Walker et al. [1997], and Linnebank et al. [2002].
[c]Predicted effect on protein according to minigene functional assay.
[d]Mutation previously reported by Kleijer et al. [2002] and Linnebank et al. [2002].
[e]Patients with late onset phenotype.
ND, not determined.

kindreds (Table 2). Homozygous mutations were detected in two kindreds, while all other patients were compound heterozygotes. We found a total of 16 mutations, only two of which were previously reported: Q286R and V178M [Barbosa et al., 1991; Walker et al., 1997; Sampaleanu et al., 2001; Kleijer et al., 2002; Linnebank et al., 2002]. Among the 14 novel mutations we found 11 single-nucleotide changes (seven missense, two nonsense, and two splicing) and three small insertion/deletions. Only the c.524+2 T>G and the c.549_550delCT mutations were found in two different kindreds. The presence of the mutations was confirmed in the parents DNA. All novel missense mutations were validated by PCR-RFLP analysis, they affect highly conserved residues of the protein (Fig. 2), and were absent in 100 control alleles.

We also found a novel intronic sequence variant located in intron 1 of the gene (c.12+105C>T). T in position +105 was present in 13 out of 20 alleles (four homozygous and five heterozygous) while 7 out of 20 alleles carried the C nucleotide (4 T/T, 40%; 5 T/C, 50%; and 1 C/C, 10%). Allelic frequencies are similar to those found in 100 healthy controls (41% T/T, 46% T/C, and 13% C/C), which correspond to the Hardy-Weinberg equilibrium.

Biochemical Analysis

ASL activity was measured in erythrocytes from 10 healthy control subjects (7.7 ± 1.2 nmol/hr/mg hemoglobin) and from six patients (Table 2). It was very low (<5% of controls) in all patients, except in Patient 8b, who had a relatively higher residual activity (about 9% of controls) and displayed the late-onset phenotype. In Patient 9, *ASL* activity had previously been measured in fibroblasts with a similar result. In Patient 4, activity has been determined only in fibroblasts and was also low (<2% of controls).

Molecular Modeling

To explore the possible consequences of individual missense mutations, we have analyzed the three-dimensional structure of the enzyme. ASL is active as a homotetramer (Fig. 3A) and each monomer is composed of three principal domains. Aspartate 31, arginine 113, and arginine 236 are conserved throughout evolution (Fig. 2), are located within the active site of the enzyme, and interact with the substrate (Fig. 3B). Arginine 113 interacts also with histidine 89, which is directly involved in the catalytic process [Abu-Abed et al., 1997; Sampaleanu et al., 2001]. Mutations in these highly conserved residues are likely to have a severe impact on the catalytic function of the protein. Interestingly, a different mutation at codon 113 has already been reported (R113W) [Linnebank et al., 2000].

Arginine 186, together with arginine 182 and histidine 252, forms a positively-charged pocket on the surface of the protein, which interacts with the negatively-charged aspartate 237 residue located on the adjacent monomer (Fig. 4A). We calculated the distribution of surface charges in the wild-type protein, and in the protein modeled with the R186Q mutation. As seen in Figure 4B and C, the presence of a glutamine at position 186 completely alters charge distribution, abolishing the positively-charged pocket essential for the interaction with aspartate 237. As the catalytic site is formed by three different monomers [Sampaleanu et al., 2001], it is likely that a faulty interaction between monomers impairs the catalytic properties of the mutated enzyme. Moreover, aspartate 237 is in contact with arginine 236, which, as was discussed above, is part of the catalytic site.

Valine 335 is located in one of the five alpha-helical segments that form a helical bundle within the central domain of the protein, which is critical for the association of monomers. As seen in Figure 3C, the larger steric hindrance of leucine displaces the alpha helix and probably impairs the correct folding of the enzyme. Valine is conserved in higher eukaryotes, while lower organisms have threonine or cysteine in this position, both residues with a smaller steric hindrance than leucine (Fig. 2).

Methionine 382 is located on the third domain of the protein (Fig. 3A). Analysis of ASL structure did not provide us with an obvious explanation for the pathogenicity of the M382R mutation. Methionine 382 is conserved in higher eukaryotes, while simpler organisms have a valine in this position (Fig. 2). It is possible that the substitution of a hydrophobic amino acid with a positively-

D31N

Patient	ASIAY**N**RHLWEVD
H.sapiens	ASIAY**D**RHLWEVD
M.musculus	SSISY**D**RHLWNVD
X.laevis	CSVNY**D**QRMWSAD
C.reinhardtii	ESLPF**D**KRLWAED
S.cerevisiae	ASLPY**D**YKMYKAD
B.subtilis	ASISF**D**QNLVAED

R113Q

Patient	HTGRS**Q**NDQVVTD
H.sapiens	HTGRS**R**NDQVVTD
M.musculus	HTGRS**R**NDQVVTD
X.laevis	HTGRS**R**NDQVVTD
C.reinhardtii	HTGRS**R**NDQVATD
S.cerevisiae	HTGRS**R**NDQVVTD
B.subtilis	HTGRS**R**NDQVATD

R186Q

Patient	TRDSE**Q**LLEVRKR
H.sapiens	TRDSE**R**LLEVRKR
M.musculus	TRDSE**R**LLEVQKR
X.laevis	SRDAE**R**LGEVKKR
C.reinhardtii	QRDDM**R**LRDLLPR
S.cerevisiae	TEDYK**R**LGQILHR
B.subtilis	ERDKE**R**FQDSMKR

R236W

Patient	DATSE**W**DFVAEFL
H.sapiens	DATSE**R**DFVAEFL
M.musculus	DATSE**R**DFVAEFL
X.laevis	DATSE**R**DFIAEFL
C.reinhardtii	DAVSD**R**DFVIETV
S.cerevisiae	VAVSD**R**DFIVELM
B.subtilis	DGVSD**R**DFILEFL

V335L

Patient	EAVFE**L**SDTMSAV
H.sapiens	EAVFE**V**SDTMSAV
M.musculus	EAVFE**V**SDTMIAV
X.laevis	EAMFD**V**YDTVCAV
C.reinhardtii	ELLFD**T**VDTVHDV
S.cerevisiae	EPLFD**C**LTTVEHS
B.subtilis	EGMFD**T**VKTVEGS

M382R

Patient	LVRKG**R**PFRQAHE
H.sapiens	LVRKG**M**PFRQAHE
M.musculus	LVRKG**M**PFRQAHE
X.laevis	LVRKG**M**PFRQAHG
C.reinhardtii	LVRKGVPFRETHH
S.cerevisiae	LVRKGVPFRETHH
B.subtilis	LAKKG**M**PFREAHE

R456W

Patient	QIRQV**W**ALLQAQQ
H.sapiens	QIRQV**R**ALLQAQQ
M.musculus	QIRQVRALLQAQE
X.laevis	QIEQLRTWMKTHR
C.reinhardtii	QVQKMRTYLAAEG
S.cerevisiae	QLDNLKSQLN
B.subtilis	ALEKAKACVAAGV

FIGURE 2. **Alignment of the regions encompassing the seven missense mutations in various species.**

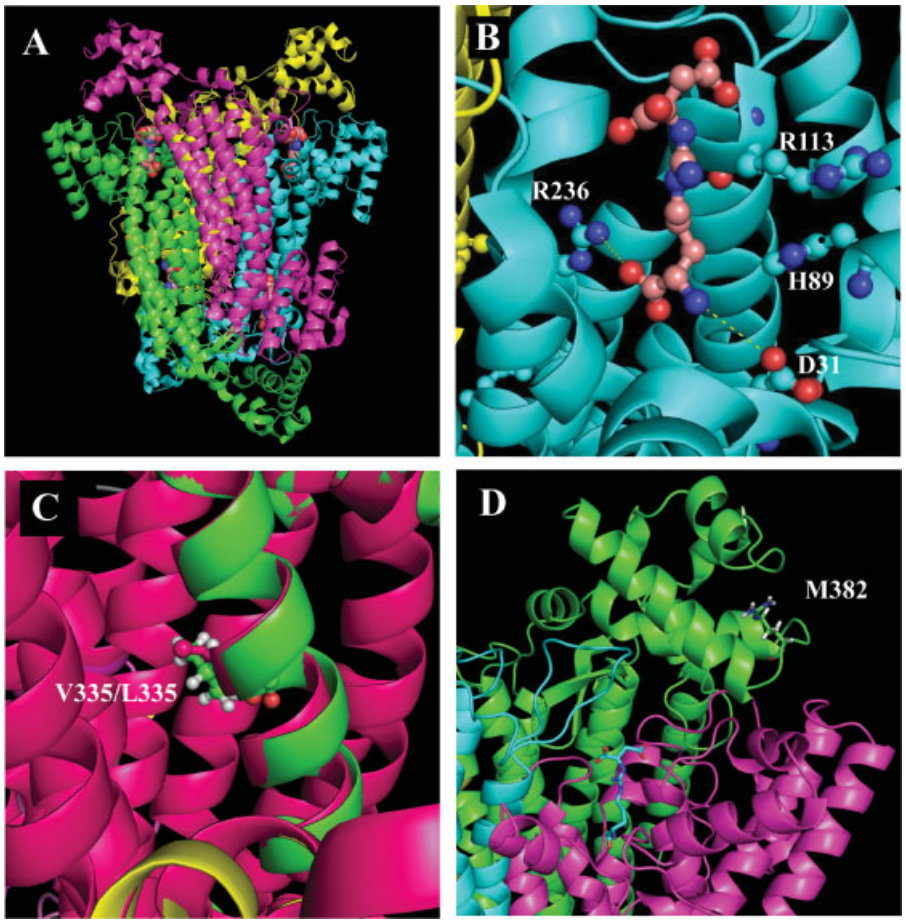

FIGURE 3. **Analysis of the effect of missense mutations on the structure of ASL. A: Representation of the active ASL tetramer. Individual monomers have different colors. B: Active site of the enzyme with aspartate 31, arginine 113, and arginine 236, and the ASA substrate. Arginine 113 interacts with histidine 89, which is actively involved in the catalytic process. C: Superimposition of the normal structure (magenta) with the calculated structure of the subunit carrying the V335L mutation (green). D: Representation of methionine 382 in the third domain of the enzyme.**

charged arginine alters the stability of this domain, however more detailed structural and functional analyses are needed to clarify this issue.

The last mutation R456W involves a conserved arginine in the terminal alpha helix of the protein. It is conserved in all higher eukaryotes, while in lower organisms is replaced by lysine, another basic amino acid with a similar size (Fig. 2). Substitution with tryptophan is predicted to cause a displacement of this alpha helix (Fig. 4D and F) and to shift the position of glutamine 454. This residue is important for dimerization because it forms a hydrophobic pocket that tightly interacts with leucine 227 located on the adjacent subunit (Fig. 4E) Both these amino acids are also highly conserved. Modeling data suggest that this interaction is impaired in the mutated protein (Fig. 4F).

Analysis of Splice-Site Mutations

To prove the pathogenicity of the two intronic mutations detected in our patients, we developed a functional splicing assay since no patients' RNA was available for our studies.

Both mutations affect nucleotides (positions +2 and −1 in respect to the corresponding exon) that are critical for exon recognition by the spliceosomal machinery [Cartegni et al., 2002]. RT-PCR analysis of mRNA expressed by the exon 5-6-7 minigenes transfected into HeLa cells revealed that the wild-type transcripts are correctly spliced, while transcripts carrying the c.524+2T>G mutation display skipping of exon 6 (Fig. 1C). Amplification with primers specific for exon 6 confirmed the complete exon 6 skipping in the mutated minigene (not shown).

The same experiment was repeated for the exon 8-9-10 minigene. In this case the splicing of the hybrid minigene was less efficient, showing some degree of exon skipping also in the wild-type minigene (Fig. 1D). It should be noted, however, that a variable degree of skipping occurs physiologically for various exons of the *ASL* transcript during maturation [Linnebank et al, 2000]. Nevertheless, no transcripts containing exon 9 were expressed from the mutated construct (Fig. 1E). Skipping of either exon 6 or exon 9 maintains the reading frame of the transcript. Transfected cells were examined by fluorescent microscopy, but only faint fluorescence was detected for either wild-type and mutated minigenes (data not shown), indicating that expression levels of mature transcripts were low.

DISCUSSION

Although the first molecular defects in the *ASL* gene were described more than 15 years ago, the number of reported mutations is quite small compared to other urea cycle defects, like ornithine transcarbamoylase deficiency [Tuchman et al., 2002]. Molecular genetic studies are not essential for the diagnosis of

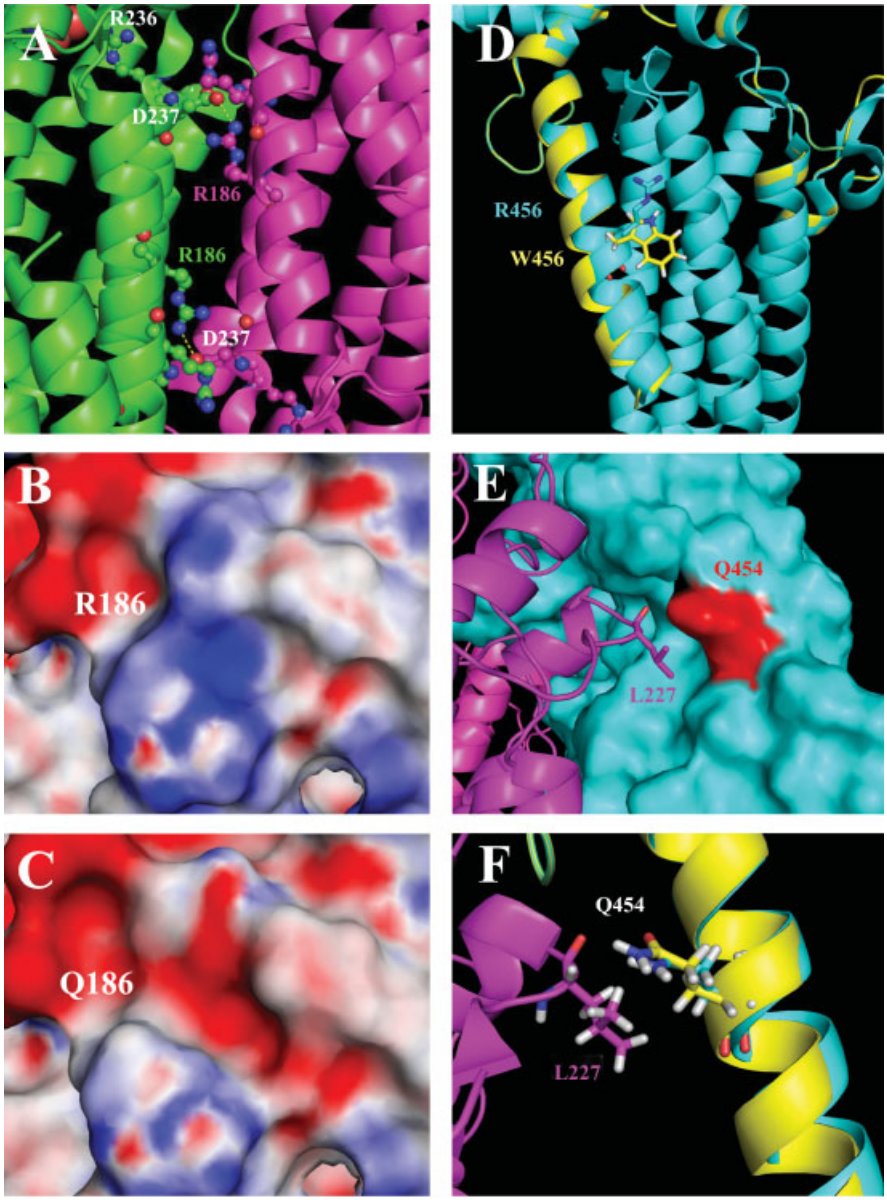

FIGURE 4. **Analysis of the effect of missense mutations on the structure of ASL. A: Representation of arginine 186 and aspartate 237 involved in the interaction of two adjacent subunits. B,C: Calculated surface charge surrounding residue 186 in the wild type (B) and in the protein with the R186Q mutation (C). In blue, the negatively charged regions; in red, the positively charged regions. D: Structure of the terminal domain in the wild-type protein (cyan) superimposed to the calculated structure of the R456W mutant (yellow). R456 and W456 are depicted. E: Interaction between glutamine 454 and leucine 227 on the adjacent monomer. F: Position of glutamine 454 in the wild type (cyan) and in the R456W mutant (yellow).**

ASAuria because analysis of ammonia, and argininosuccinic acid in plasma, is considered adequate for a reliable diagnosis of the defect [Brusilov and Horwich, 2001]. Determination of ASL activity in cultured fibroblasts or erythrocytes can be used to confirm the diagnosis; however, this technique is not widely available, and in the case of skin fibroblast, it is time consuming and requires a skin biopsy, an invasive procedure for young patients.

We performed mutation screening of the *ASL* gene in a cohort of Italian patients with hyperammonemia and elevated ASA levels. We developed a protocol based exclusively on genomic DNA analysis. All previous reports relied essentially on cDNA analysis, and genomic DNA was used to validate cDNA results [Walker et al., 1990; Barbosa et al., 1991; Linnebank et al., 2002, Kleijer et al., 2002]. The identification of the novel *ψASL2* pseudogene was critical to design specific primers that avoid the region of homology between *ASL*, *ψASL1*, and *ψASL2*. We believe that *ψASL2* was not detected by the bioinformatic analysis of Linnebank et al. [2002] probably because at the time information on centromeric regions was still largely incomplete. We did not find further bioinformatic or experimental evidence of other *ASL* pseudogenes.

We detected pathogenic mutations in all kindreds, for a total of 14 mutations, only two of which were previously described (V178M and Q286R). Previous studies have reported marked heterogeneity of *ASL* mutations in European patients [Linnebank et al., 2002], while Arabic patients have a common (Q354X) allele [Al-Sayed et al., 2005]. We did not find a common "Italian" mutation, most patients were compound heterozygous for different alleles, and the homozygous mutations were found in a family in

whom we suspect consanguinity (Q286R), and in another from Sardinia island (D31N), where a founder effect has been reported for many other genetic diseases.

Mutations were scattered throughout the gene; however, we confirm that exon 7 seems to be a mutational hotspot [Linnebank et al., 2002]; in fact, 4 of the 16 mutations we found were located in this region. Two mutations (R113Q and R182X) involve codons 113 and 182 that have been found affected by a different mutational event (R113W and R182Q) [Linnebank et al., 2000, 2002]. In all cases a transversion has occurred. However, analysis of the sequences flanking these codons did not reveal any peculiar motif that could explain the particular susceptibility of these codons to mutational events.

Of the 14 novel mutations, the three small insertions/deletions and the two nonsense mutations are predicted to cause premature stop codons. We believe their pathogenicity is obvious. Biochemical data are available only for four of the seven novel missense mutations, showing marked reduction of ASL activity in all four cases. Nevertheless all missense mutations were absent in 100 control alleles, affect highly conserved residues of the protein, and molecular modeling data (even though they represent only computer predictions) indicate that the involved amino acids are located in critical sites of the enzyme. Moreover, the D31N and the V335L mutations segregate with the phenotype in the two affected sibling pairs. Taken together, these data strongly argue in favor of the pathogenicity of these mutations.

We tested the effect of the two splicing mutations with a functional splicing assay. The transcripts from the mutant minigenes display aberrant splicing with exon skipping, and we could not detect the correctly spliced mRNA, which in contrast is expressed by the wild type constructs. In both cases exon skipping maintains the reading frame of the transcript and causes a deletion of 26 (exon 6) or 21 (exon 9) amino acids in critical regions of the protein. Even though we cannot be certain that our model exactly reproduces the in vivo situation, our data indicate that the two mutations have a severe effect on mRNA maturation; moreover, other reported splicing mutations in the *ASL* gene cause similar exon skipping [Linnebank et al., 2002].

Our series of patients displayed both the neonatal onset and the late infancy form. We found no obvious genotype–phenotype correlation. Intragenic complementation has been invoked to explain some of the cases with mild phenotypes [McInnes et al., 1984; Walker et al., 1997; Howell et al., 1998; Yu and Howell, 2000; Sampaleanu et al., 2001]. This is a phenomenon that occurs when a multimeric protein is formed from subunits produced by differently mutated alleles of the same gene. On complementation, a partially functional hybrid protein is produced from the two distinct types of mutant subunits, neither of which individually has appreciable enzymatic activity.

Intragenic complementation does not appear to play a role in the two kindreds with the milder form of the disease. In fact Patients 5a and 5b were homozygous for the D31N mutation, while Patients 8a and 8b were compound heterozygous for a missense (V335L) and a frameshift mutation. The patient with the V335L mutation had a relatively high residual ASL activity (about 9% of controls), suggesting that this substitution is less detrimental for enzyme function. However, in other studies correlation between residual activity and clinical severity is not well defined [McInnes et al., 1984; Walker et al., 1990, Kleijer et al., 2002].

Seizures were a common finding in our cohort of patients, 5 out of 7 patients with the neonatal presentation developed an epileptic syndrome that required continuous therapy with anticonvulsant drugs. Seizures were the presenting symptom also in one of the patients with the late onset form.

Hepatic involvement is found in 5 out of 7 patients with the neonatal presentation. Patients displayed hepatomegaly, hypertransaminasemia, and reduced prothrombin time, but none had jaundice or signs of severe portal hypertension. In Patient 9, liver fibrosis was documented by a liver biopsy that also showed lipid and glycogen accumulation, we believe that these two features are related to the particular dietary regimen. Interestingly, the four patients with the late-onset form have normal liver function. Liver involvement is not mentioned also in patients from Families B, C, D, and E reported by Kleijer et al., [2002], who were affected by the milder form. These findings suggest that hepatopathy is not common in patients with the milder form. Finally, it should be noted that in our series patients with neonatal onset display progression of both neurological and hepatic manifestations despite adequate metabolic control.

Only two of the neonatal onset patients have normal liver function (Patients 4 and 7). Patient 7 was diagnosed and treated very early (he was born in our Center) and at present he has only very mild psychomotor retardation. However, follow-up is too short and development of hepatic involvement or epilepsy later in the course of the disease is still possible. Patient 4 is 24 years old and, despite severe cerebral involvement, he still has normal liver function. He is a compound heterozygous for the V178M mutation, which was previously associated to a mild phenotype when present in the homozygous state [Kleijer et al., 2002]. Again, it is possible that this allele has a less detrimental effect on the enzyme, but this does not account for the severe cerebral phenotype. In both patients residual ASL activity was very low. It should be noted however that ASAuria is a highly pleomorphic disorder in which genetic modifiers and environmental factors may play an important role in influencing the clinical phenotype [Lanpher et al., 2006].

Our genomic DNA-based approach has proved itself to be reliable, with a detection rate of 100% in our cohort of patients. This approach has several advantages over cDNA analysis in terms of sample handling and availability, and it overcomes the possible mRNA degradation associated with some frameshift or splicing mutations [Linnebank et al., 2002]. The hybrid minigene assay integrates our method and allows to analyze the pathogenicity of splice site mutations.

Genetic analysis should play an important role for prenatal diagnosis of ASAuria. Although measurement of ASL activity in chorionic villi is a reliable and sensitive method [Kleijer et al., 2002], it is complex and available only in very few laboratories worldwide. On the contrary, direct genetic analysis is feasible, fast, and specific and can be regarded as the method of choice for prenatal diagnosis. Therefore, we strongly recommend mutation testing in patients with ASAuria, in order to provide adequate prenatal counseling to the future pregnancies of their families.

ACKNOWLEDGMENTS

This study was supported by grants from the Association Franç aise contre les Myopathies (AFM) (to L.S.) and Centro Regionale Malattie Metaboliche Ereditarie, Regione Veneto (to A.B.B.).

REFERENCES

Abu-Abed M, Turner MA, Vallée F, Simpson A, Slingsby C, Howell PL. 1997. Structural comparison of the enzymatically active and inactive forms of delta crystallin and the role of histidine 91. Biochemistry 36:14012–14022.

Al-Sayed M, Alahmed S, Alsmadi O, Khalil H, Rashed MS, Imtiaz F, Meyer BF. 2005. Identification of a common novel mutation in Saudi patients with argininosuccinic aciduria. J Inherit Metab Dis 28:877–883.

Baker NA, Sept D, Joseph S, Holst MJ, McCammon JA. 2001. Electrostatics of nanosystems: application to microtubules and the ribosome. Proc Natl Acad Sci USA 98:10037–10041.

Barbosa P, Cialkowski M, O'Brien WE. 1991. Analysis of naturally occurring and site-directed mutations in the argininosuccinate lyase gene. J Biol Chem 266:5286–5290.

Bastone A, Diomede L, Parini R, Carnevale F, Salmona M. 1990. Determination of argininosuccinate lyase and arginase activities with an amino acid analyzer. Anal Biochem 191:384–389.

Brusilov SW, Horwich AL. 2001. Urea cycle enzymes. In: Scriver CR, Beaudet AL, Sly WS, Valle D, editors. The metabolic and molecular bases of inherited disease, Vol 2, 8th edition. New York: McGraw-Hill. p 1909–1964.

Cartegni L, Shern LC, Krainer AR. 2002. Listening to silence and understanding nonsense: exonic mutations that affect splicing. Nat Rev Genet 3:285–298.

Forsgren M, Attersand A, Lake S, Grunler J, Swiezewska E, Dallner G, Climent I. 2004. Isolation and functional expression of human COQ2, a gene encoding a polyprenyl transferase involved in the synthesis of CoQ. Biochem J 382:519–526.

Howell PL, Turner MA, Christodoulou J, Walker DC, Craig HJ, Simard LR, Ploder L, McInnes RR. 1998. Intragenic complementation at the argininosuccinate lyase locus: reconstruction of the active site. J Inherit Metab Dis 21(Suppl 1):72–85.

Kleijer WJ, Garritsen VH, Linnebank M, Mooyer P, Huijmans JG, Mustonen A, Simola KO, Arslan-Kirchner M, Battini R, Briones P, Cardo E, Mandel H, Tschiedel E, Wanders RJ, Koch HG. 2002. Clinical, enzymatic, and molecular genetic characterization of a biochemical variant type of argininosuccinic aciduria: prenatal and postnatal diagnosis in five unrelated families. J Inherit Metab Dis 25: 399–410.

Lanpher B, Brunetti-Pierri N, Lee B. 2006. Inborn errors of metabolism: the flux from Mendelian to complex diseases. Nat Rev Genet 7: 449–460.

Linnebank M, Homberger A, Rapp B, Winter C, Marquardt T, Harms E, Koch HG. 2000. Two novel mutations (E86A R113W) in argininosuccinate lyase deficiency and evidence for highly variable splicing of the human argininosuccinate gene. J Inherit Metab Dis 23:308–312.

Linnebank M, Tschiedel E, Häberle J, Linnebank A, Willenbring H, Kleijer WJ, Koch HG. 2002. Argininosuccinate lyase (ASL) deficiency: mutation analysis in 27 patients and a complete structure of the human ASL gene. Hum Genet 111:350–359.

McInnes R, Shih V, Chilton S. 1984. Interallelic complementation in an inborn error of metabolism: genetic heterogeneity in argininosuccinate lyase deficiency. Proc Natl Acad Sci USA 81:4480–4484.

O'Brien WE, McInnes R, Kalumuck K, Adcock M. 1986. Cloning and sequence analysis of cDNA for human argininosuccinate lyase. Proc Natl Acad Sci USA 83:7211–7215.

Pagano MA, Andrzejewska M, Ruzzene M, Sarno S, Cesaro L, Bain J, Elliott M, Meggio F, Kazimierczuk Z, Pinna LA. 2004. Optimization of protein kinase CK2 inhibitors derived from 4,5,6,7-tetrabromobenzimidazole. J Med Chem 47:6239–6247.

Salviati L, Freehauf C, Sacconi S, DiMauro S, Thoma J, Tsai AC. 2004. Novel SURF1 mutation in a child with subacute encephalopathy and without the radiological features of Leigh Syndrome. Am J Med Genet A 128:195–198.

Sampaleanu LM, Vallée F, Thompson GD, Howell PL. 2001. Three-dimensional structure of the argininosuccinate lyase frequently complementing allele Q286R. Biochemistry 40:15570–15580.

Tuchman M, Jaleel N, Morizono H, Sheehy L, Lynch MG. 2002. Mutations and polymorphisms in the human ornithine transcarbamylase gene. Hum Mutat 19:93–107.

Walker DC, McCloskey DA, Simard LR, McInnes RR. 1990. Molecular analysis of human argininosuccinate lyase: Mutant characterization and alternative splicing of the coding region. Proc Natl Acad Sci USA 87: 9625–9629.

Walker DC, Christodoulou J, Craig HJ, Simard RL, Ploder L, Howell PL, McInnes RR. 1997. Intragenic complementation at the human argininosuccinate lyase locus. Identification of the major complementing alleles. J Biol Chem 7:6777–6783.

Yu B, Howell PL. 2000. Intragenic complementation and the structure and function of argininosuccinate lyase. Cell Mol Life Sci 57:1637–1651.

Human Molecular Genetics, 2007, Vol. 16, No. 9 ***1091–1097***
doi:10.1093/hmg/ddm058
Advance Access published on March 20, 2007

Missense mutation of the *COQ2* gene causes defects of bioenergetics and *de novo* pyrimidine synthesis

José M. López-Martín[1], Leonardo Salviati[2,*], Eva Trevisson[2], Giovanni Montini[3], Salvatore DiMauro[4], Catarina Quinzii[4], Michio Hirano[4], Angeles Rodriguez-Hernandez[1], Mario D. Cordero[1], José A. Sánchez-Alcázar[1], Carlos Santos-Ocaña[1] and Plácido Navas[1]

[1]Centro Andaluz de Biología del Desarrollo, Universidad Pablo de Olavide-CSIC, 41013 Sevilla, Spain, [2]Clinical Genetics, Department of Pediatrics, [3]Department of Pediatrics, University of Padova, 35128 Padova, Italy and [4]Department of Neurology, Columbia University College of Physicians and Surgeons, New York, NY 10032, USA

Received January 24, 2007; Revised February 28, 2007; Accepted March 10, 2007

Coenzyme Q_{10} (CoQ_{10}) deficiency has been associated with an increasing number of clinical phenotypes that respond to CoQ_{10} supplementation. In two siblings with encephalomyopathy, nephropathy and severe CoQ_{10} deficiency, a homozygous mutation was identified in the CoQ_{10} biosynthesis gene *COQ2*, encoding polyprenyl-*p*HB transferase. To confirm the pathogenicity of this mutation, we have demonstrated that human wild-type, but not mutant *COQ2*, functionally complements *COQ2* defective yeast. In addition, an equivalent mutation introduced in the yeast *COQ2* gene also decreases both CoQ_6 concentration and growth in respiratory-chain dependent medium. Polyprenyl-*p*HB transferase activity was 33–45% of controls in *COQ2* mutant fibroblasts. CoQ-dependent mitochondrial complexes activities were restored in deficient fibroblasts by CoQ_{10} supplementation, and growth rate was restored in these cells by either CoQ_{10} or uridine supplementation. This work is the first direct demonstration of the pathogenicity of a *COQ2* mutation involved in human disease, and establishes yeast as a useful model to study human CoQ_{10} deficiency. Moreover, we demonstrate that CoQ_{10} deficiency in addition to the bioenergetics defect also impairs *de novo* pyrimidine synthesis, which may contribute to the pathogenesis of the disease.

INTRODUCTION

Coenzyme Q_{10} (CoQ_{10}) is a vital molecule that transports electrons from mitochondrial respiratory chain complexes I and II to complex III (1). In addition, it functions as a cofactor for uncoupling proteins (2), as an antioxidant stabilizing plasma membrane and a regulator of the extracellularly-induced ceramide-dependent apoptotic pathway (1,3). CoQ_{10} also enhances survival of chemotherapy-treated cells (4) and is required for the stabilization of complex III in mitochondria (5). At least nine nuclear gene (*COQ*) products are involved in the CoQ biosynthesis complex pathway in yeast, which have homologous genes in all the species currently studied (6). This pathway and its regulation are still incompletely understood (1). CoQ_{10} deficiency (MIM 607426) has been associated with clinically heterogeneous diseases, which have been delineated into five major phenotypes: (i) an encephalomyopathic form (7,8), (ii) a predominantly ataxic form with cerebellar atrophy (9,10), (iii) a multisystem infantile variant with brain and renal disease (11,12), (iv) Leigh syndrome (13) and (v) isolated myopathy (14,15). It is anticipated that mutations in *COQ* genes or other components of the CoQ_{10} biosynthetic pathway are likely to cause these diverse syndromes (1).

We have recently demonstrated that two siblings with CoQ_{10} deficiency harbor a homozygous c.890 A>G mutation in the *COQ2* gene (MIM 609825) (16), which encodes polyprenyl-*p*-hydroxybenzoate transferase (17). This mutation changes amino acid 297 from tyrosine into cysteine, in a conserved *trans*-membrane domain (16). To demonstrate

*To whom correspondence should be addressed at: Clinical Genetics, Department of Pediatrics, University of Padova, Via Giustiniani 3, 35128 Padova, Italy. Tel: +39 0498213513; Fax: +39 0498211425; Email: leonardo.salviati@unipd.it

pathogenicity of this mutation, we performed functional complementation in *Saccharomyces cerevisiae* using the BY4741Δ*coq2* strain, which is unable to grow in non-fermentable carbon source. We have studied the role of CoQ_{10} supplementation on both respiratory chain complexes I + III and II + III and growth in deficient fibroblasts. Also, we have shown the requirement of uridine for maintaining growth of deficient fibroblasts demonstrating the dependence of these cells on pyrimidine biosynthesis.

RESULTS

Complementation of Δ*COQ2* yeast

Figure 1A compares the 5′-nucleotide sequences of the cloned cDNA and shows that the human gene contains four ATG initiation codons. The third ATG produces a transcript of similar length to the yeast gene. Wild-type human *COQ2* (h*COQ2*) and yeast *COQ2* (y*COQ2*) cDNA sequences were sub-cloned into the yeast expression vector pYES2.1-TOPO TA/V5-His with a GAL promoter, and transformed into BY4741Δ*coq2* strain, a null mutant strain for this gene. Increased growth in glycerol was observed when either homologous *yCOQ2* or heterologous third ATG-initiated *hCOQ2* was expressed in BY4741Δ*coq2* (Fig. 1B). Lower growth was observed with cDNA initiated at the first or second ATG, and no growth was detected with *hCOQ2* starting at the fourth ATG (Fig. 1B). The reported full-length *hCOQ2* has been cloned as a hybrid molecule: the 3′-sequence was obtained from mRNA while the 5′-sequence was amplified from genomic DNA due to difficulties in amplifying the 5′-region of the mRNA (17). Complementation of *COQ2* null yeast with this cDNA (initiating at the first ATG) induced ∼50% growth at 120 h compared with *yCOQ2* complementation (18), a similar growth rate as those we have obtained with first ATG *hCOQ2* (Fig. 1B).

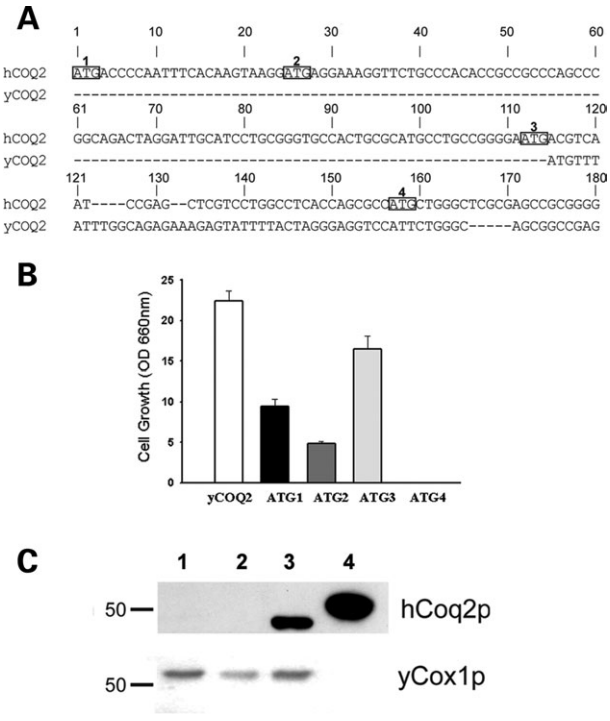

Figure 1. Human COQ2 starting at the 3rd ATG can replace yeast COQ2. (**A**) Comparison of 5′ end of human and yeast COQ2 gene showing the four initiation codons (ATG). The initiation ATG in yeast gene corresponds to the 3rd ATG in human gene. (**B**) Culture densities of *coq2* yeast strain transformed with clones of homologous yeast wild-type cDNA, and the heterologous human cDNAs starting from the four initiation codons. These cells were grown for 120 h in non-fermentable carbon source media (YPG). (**C**) Immunolocalization of human Coq2 peptide in mitochondria isolated from both wild-type (lane 1) and *coq2* (lane 2) yeast strains. Lane 3 corresponds to mitochondria isolated from BY4741 coq2:hCOQ2 (3rd ATG), and lane 4 corresponds to mitochondria isolated from HeLa cells. Localization was performed using a polyclonal antibody against the human protein (Agrisera, Sweden). The inferior panel shows the same membrane probed with an antibody against yCox1p (molecular probes), a protein with known mitochondrial localization.

Localization of hCoq2p in yeast mitochondria

To determine the localization of human Coq2p protein in yeast mitochondria, an immunoblot was developed with an antibody raised against the human Coq2 peptide (Fig. 1C). This protein was not detected in either wild-type yeast or *coq2* mutant strains, but it was detected in the mitochondria of both Δ*coq2:hCOQ2* and HeLa cells. The apparent molecular weight of Coq2p in HeLa cells is higher probably because of a different processing of the precursor polypeptide in yeast.

Complementation efficiency of mutated *COQ2*

To determine whether the mutation in *hCOQ2* gene (16) caused a loss of function of the encoded protein affecting both CoQ biosynthesis and respiration, we carried out complementation experiments transforming the yeast *yCOQ2* null mutant strain with cDNA cloned from patients, and the yeast gene engineered to harbor the c.783 A>G mutation (equivalent to *hCOQ2* c.890 A>G mutation). Cells expressing the mutant yeast gene displayed a lower growth rate than those expressing the wild-type gene (Fig. 2B), demonstrating that functional complementation is sufficiently sensitive to study the effect of a missense mutation in a CoQ biosynthetic gene. Also, transformation of BY4741 Δ*coq2* yeast strain with mutated *hCOQ2* showed a considerably lower respiration-dependent growth than with wild-type *hCOQ2*, which was, however, still significantly increased compared with the deleted strain (Fig. 2C).

Effect on CoQ biosynthesis

Growth results correlated with the content of Coenzyme Q_6 (CoQ_6) in the different transformed strains (Table 1). The expression of *yCOQ2* caused an accumulation of CoQ_6 in transformed yeasts in the range of the wild-type strain, and strains harboring *yCOQ2* (c.783 A>G) attained CoQ levels ∼59% of wild-type. These results demonstrate the deleterious effect of the mutation on the Coq2 protein, which, however, apparently retains some residual enzymatic activity. The expression of wild-type *hCOQ2* gene increased CoQ_6 levels to ∼64% of control, while expression of the mutated sequence

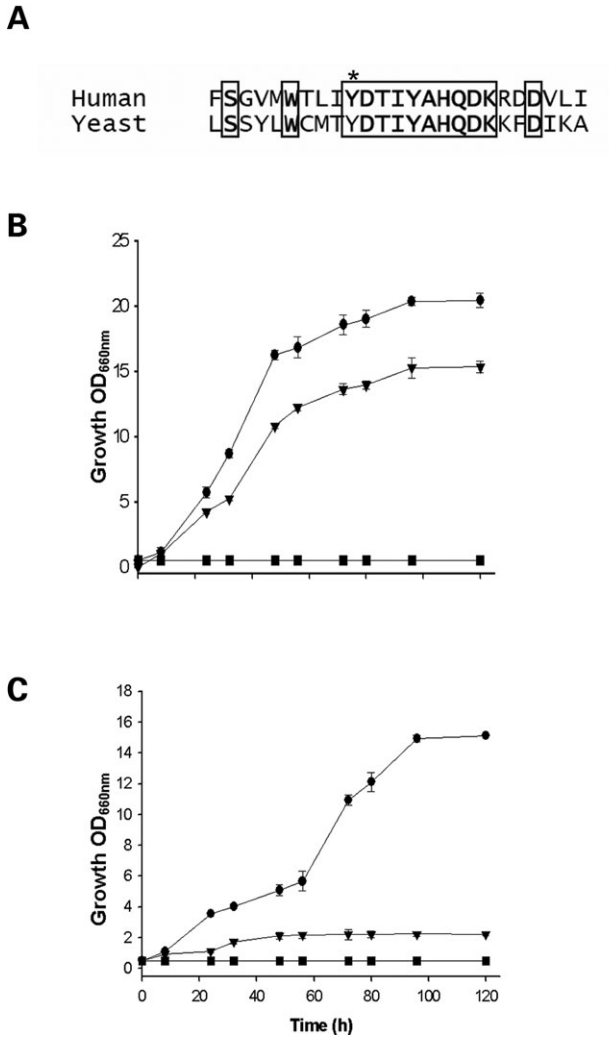

Figure 2. The c.890 A>G mutation decreases the rate of growth in transformed yeast strains. (**A**) Comparison of the sequences of human and yeast Coq2 proteins. The asterisk indicates the mutated Y>C residue. Conserved amino acids inside a frame. (**B**) Growth curves of the Δ*coq2* yeast strain (squares), and of this strain transformed with: wild-type *yCOQ2* (circles) or c.783 A>G mutated *yCOQ2* (triangles). (**C**) Growth of the Δ*coq2* yeast strain (squares) transformed with wild-type (circles) or mutant (triangles) *hCOQ2*.

produced CoQ_6 levels that were only 11% of transformed cells with the human wild-type allele.

Analysis of demetoxy-Q_6 (DMQ) levels, an intermediate of coenzyme Q biosynthesis, showed an increase of DMQ relative to CoQ6, in strains transformed with the mutated genes (Table 1), indicating an inhibition of the biosynthetic process also downstream of Coq2p.

COQ2 expression in patient's fibroblasts

We then analyzed the expression of *COQ2* in patient's fibroblasts by real-time-PCR (Fig. 3A). mRNA levels of this gene were significantly increased in patients harboring *COQ2* mutations (16) compared with controls and other CoQ_{10}-deficient fibroblasts isolated from ataxic patients, which do not harbor mutations in this gene (10). Furthermore, immunoblot analysis of Coq2p in fibroblasts demonstrated that cells from both P1 and P2 patients contained higher amount of protein than both control and P3 patient fibroblasts (Fig. 3B). We also measured polyprenyl-*p*HB transferase activity using a sensitive radioactive method (19). This activity was significantly lower in fibroblasts of patients with *hCOQ2* (c.890 A>G) gene (Fig. 3C) relative to controls and CoQ_{10}-deficient fibroblasts from ataxic patients (10). Increased expression of both mRNA and protein appears to be a compensatory mechanism for the enzymatic deficiency in the patient's fibroblasts.

Effect of CoQ_{10} on mitochondrial complexes activities

It has been shown that CoQ added to human cells reaches the inner mitochondrial membrane and acts on the respiratory chain (20). To demonstrate whether CoQ_{10} deficiency was responsible for mitochondria defects observed in CoQ_{10}-deficient patients (12), fibroblasts were incubated for 24 h with CoQ_{10}, and both complexes I + III and II + III activities were determined (Table 2). Both activities were significantly increased in deficient fibroblasts, which were not affected in control fibroblasts.

Effects of CoQ_{10} and uridine on fibroblasts growth rates

CoQ_{10} deficient fibroblasts showed slow rates of growth. To demonstrate that this phenotype was due to CoQ_{10} deficiency, cells (100 ± 20 cells/cm^2) were seeded and grown in a medium supplemented with serum-solubilized CoQ_{10}. Growth was significantly increased in deficient fibroblasts incubated with a supplement of CoQ_{10} (Fig. 4A). CoQ_{10} is required for the biosynthesis of pyrimidine nucleotides because it is an essential co-factor for dihydro-orotate dehydrogenase, an enzyme located in the inner mitochondrial membrane (21). To demonstrate that the deficiency of CoQ_{10} affects pyrimidine supply, and consequently cell growth, we incubated CoQ_{10}-deficient fibroblasts with uridine and observed that growth was also increased compared with both control and respiratory chain-deficient fibroblasts from a patient with mitochondrial encephalomyopathy without CoQ_{10} deficiency (Fig. 4B). No cumulative effect of uridine and CoQ_{10} was noted (data not shown).

DISCUSSION

Despite the fact that CoQ_{10} deficiency has been described more than 15 years ago, its genetic bases have remained elusive until this year, when mutations were identified in two genes involved in CoQ_{10} biosynthesis, *COQ2* and *PDSS2* (16,22). The product of *COQ2* catalyzes the transfer of *para*-hydroxybenzoate to the polyprenyl chain, one of the initial steps of CoQ biosynthesis. The aim of this work was to demonstrate the pathogenicity of the missense *COQ2* mutation found in our patients using a functional complementation approach in *S. cerevisiae*, and to analyze its consequences on the mitochondrial electron transport chain and cell proliferation.

Table 1. Content of CoQ_6 in yeast strains after 120 h growing in non-fermentable media (YPG)

Strain	Coenzyme Q_6 (ng/mg protein ± SD)	Demethoxy-Q_6 (ng/mg protein ± SD)	CoQ_6/DMQ_6 Ratio
BY4741	1448 ± 20	122 ± 10	11.86
BY4741 Δ*coq2*	ND	ND	—
BY4741 Δ*coq2*:hCOQ2	842 ± 12	73 ± 4	11.52
BY4741 Δ*coq2*:hCOQ2 (c.890 A>G)	92 ± 3	42 ± 9	2.19
BY4741 Δ*coq2*:yCOQ2	1309 ± 45	110 ± 18	11.90
BY4741 Δ*coq2*:yCOQ2 (c.783 A>G)	774 ± 70	230 ± 25	3.36

ND, non-detectable.

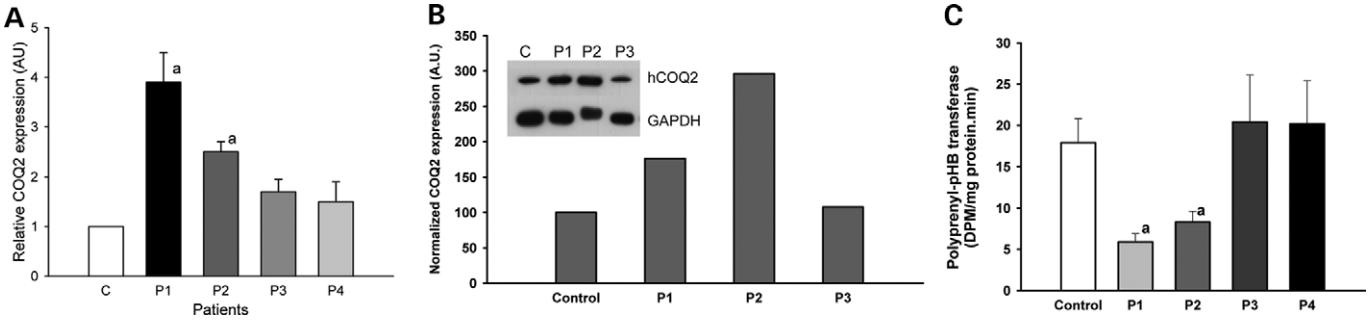

Figure 3. *COQ2* is over-expressed in fibroblasts of patients with mutation and Coq2p shows lower activity. (**A**) Expression of *COQ2* gene measured by real-time PCR in patients 1 (P1) and 2 (P2) harboring the c.890 A>G mutation, compared with fibroblasts from control and patients 3 and 4, who have CoQ_{10} deficiency but no *COQ2* mutation (10). a: Significant versus control ($P < 0.01$) and both P3 and P4 ($P < 0.05$). (**B**) Content of Coq2p in human fibroblasts. a: Significant versus both control and P3 ($P \leq 0.01$). Significant versus both control and P3 ($P < 0.05$). (**C**) Biochemical analysis of the polyprenyl-*p*HB transferase activity in mitochondria isolated from fibroblasts of the patients described earlier. a: Significant versus both control and P3 ($P < 0.01$).

Human *COQ2* contains four possible ATG codons on exon 1. The reported *hCOQ2* sequence starts from ATG number 1. We observed complementation with constructs initiating from each of the first three ATG, but not with ATG number 4 possibly because the sequence between the third to fourth ATGs contains a critical signal for mitochondrial importation in yeast (18).

The highest complementation efficiency was achieved with constructs initiating at the third ATG, this sequence is the most similar to the yeast mitochondrial importation presequence. However, analysis of *COQ2* genes in other mammalian species such as dog and rat revealed that they contain only one possible ATG initiation codon, which corresponds to the human fourth ATG. We are currently investigating the functional significance of the four ATG codons in human cells.

Both the mutated human *COQ2* gene and its yeast homolog engineered to harbor the corresponding mutation, failed to fully complement *COQ2* deficient yeast strain. Nevertheless, complementation studies clearly indicate that mutated proteins still retain some enzymatic activity because yeast can grow on non-fermentable substrates and accumulate some amount of CoQ_6, although at a significantly lower rate than the wild-type strains. Direct biochemical assays on patients P1 and P2 fibroblasts confirm the presence of residual enzymatic activity, which correlates with the amount of Coq2p detected by western blot. The residual Coq2 function is probably essential for embryogenesis, and may explain why the patients did not present symptoms of the disease until 1 year of age. In both patients P1 and P2, *COQ2* mRNA and Coq2 peptides are also hyper-expressed, suggesting that there is a feedback control mechanism regulating *COQ2* expression in cells.

Interestingly, yeast cells transformed with the mutated genes show accumulation of DMQ, an intermediate of coenzyme Q biosynthesis that is synthesized by reactions downstream of Coq2p. This apparent paradox can be explained by the fact that enzymes that catalyze coenzyme Q biosynthesis in yeast are thought to function in a multienzyme complex (20). In this case, the mutation in Coq2 proteins not only impairs enzymatic function of Coq2p, but probably affects the whole complex, interfering also with some of the downstream enzymatic steps.

In a second set of experiments, we analyzed the effect of *COQ2* deficiency in fibroblasts. We have previously shown that a CoQ_{10} analogue, decyl-ubiquinone, can rescue the complex II + III enzymatic defect *in vitro* (12). We have now checked the effect of ubiquinone supplementation *in vivo* on cell proliferation and mitochondrial complexes activities. Supplementation of human cells with different isoforms of CoQ shows that a small amount can reach inner mitochondrial membrane (23). Using this approach, we have shown that long-term incubation of deficient fibroblasts with CoQ_{10} increases significantly the activity of both complexes I + III and II + III. These results support the cause of mitochondrial dysfunction on the deficiency, and would explain the positive results observed after the treatment of deficient patients with CoQ_{10} (10,12).

We then analyzed if we could modulate the growth deficient phenotype in these cells. Surprisingly, the effect of uridine addition was even more pronounced than that of CoQ_{10}

Table 2. Effect of supplementation of CoQ_{10} on the CoQ-dependent mitochondrial complexes activities in human fibroblasts

Samples	Complex I + III (nmol/min/mg protein)		Complex II + III (nmol/min/mg protein)	
	No addition	10 μM CoQ_{10}	No addition	10 μM CoQ_{10}
Control	410 ± 36	445 ± 27	3.5 ± 0.23	3.8 ± 0.41
P1	248 ± 25	386 ± 44[a]	1.7 ± 0.02	3.6 ± 0.12[a]
P2	301 ± 37	480 ± 56[a]	1.9 ± 0.07	3.1 ± 0.15[a]

[a]Significant versus no addition.

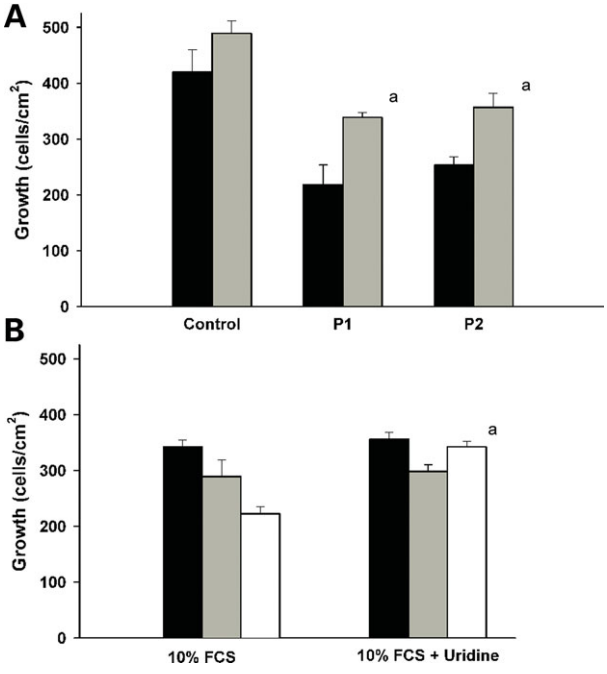

Figure 4. Growth of CoQ_{10} deficient fibroblasts can be restored by exogenous CoQ_{10} or uridine. (**A**) Addition of CoQ_{10} to culture media containing 20% FCS induced significant increases of growth of fibroblasts of patients harboring the *COQ2* mutation compared with control fibroblasts. Black bars: no CoQ_{10}. Grey bars: plus 10 μM CoQ_{10}. a: Significant versus no addition of CoQ10 ($P \leq 0.01$). (**B**) Growth of fibroblasts in media containing 10% FCS supplemented with 10 μM uridine. Black bars: control fibroblasts; grey bars: fibroblasts from a patient with mitochondrial respiratory chain deficiency but normal concentration of CoQ_{10}; white bars: fibroblasts harboring the *COQ2* mutation (patient 2). a: Significant versus no addition of uridine ($P < 0.05$).

suggesting that this phenotype is largely due to an insufficient supply of nucleotides rather than to an impairment of ATP production. We believe that the relative lower efficiency of CoQ_{10} in rescuing the defect in proliferation is probably due to a low efficiency of its incorporation in cells (1,23).

Taken together, our results demonstrate the pathogenicity of the *COQ2* mutation and that yeast is an optimal model to study the effects of mutations in *COQ* genes, because it is sensitive enough to unveil defects due to missense mutations. The high homology of yeast and human *COQ* genes may allow complementation studies to identify other human genes involved in CoQ_{10} deficiency. Moreover, we demonstrate that the pathogenesis of CoQ_{10} deficiency is related not only to a defect in bioenergetics, but also to an impairment of pyrimidine metabolism.

Table 3. Oligonucletides used in PCR amplifications

Primer name	Sequence 5′ → 3′
hCOQ2-Fext(ATG1)	5′-ATGACCCCAATTTCACAA-3′
hCOQ2-Rext(ATG1)	5′-ACTCAAGGCCATCTCAAA-3′
hCOQ2-Fext(ATG2)	5′-AAGGATGAGGAAAGGTTCTG-3′
hCOQ2-Rext(ATG2)	5′-TTGTATCAGATTTTGTATTCAAATC-3′
hCOQ2-Fext(ATG3)	5′-GAATGACGTCAATCCGA-3′
hCOQ2-Rext(ATG3)	5′-TGTAAAAAATGTATTAAAAATTC-3′
hCOQ2-Fext(ATG4)	5′-AGCTCGTCCTGGCCTCAC-3′
hCOQ2-Rext(ATG4)	5′-TGGGCAGAAGAATGTATCAACTA-3′
hCOQ2-Fint	5′-TTACAAGAACAGCCAATCGTC-3′
hCOQ2-Rint	5′-TGTCCTGATGGGCATAAATAGTG-3′
yCOQ2-Fext	5′-CAACTAATGTTTATTTGGCAGAG-3′
yCOQ2-Rext	5′-CTACAAGAATCCAAACAGTCTCA-3′
yMUTAG-F	5′-GTATGTTGGGTATTTTCGGTG-3′
yMUTAG-R	5′-CGTATATAGTATCG**C**AAGTCATACA-3′
hCOQ-RQ-F	5′-AGAACAGCCAATCGTTCCAATAGC-3′
hCOQ-RQ-R	5′-CCCAATTAAATGTCAAGCCCAAGG-3′

Bold-face character is the mismatched nucleotide used in site-directed mutagenesis.

MATERIALS AND METHODS

Fibroblast cultures

Fibroblasts from CoQ_{10} deficient patients (P1 and P2) (12,16), from patients with cerebellar ataxia and CoQ_{10} deficiency (10) and controls were plated in separate six-well plates (40 000 cells/well) and cultured using DMEM with 20% fetal calf serum (FCS). Also, HeLa cells were grown in a similar procedure. Supplemental CoQ_{10} pre-diluted in FCS was added to the plates at a final concentration of 10 μM.

Cloning of human and yeast *COQ2*

yCOQ2 was cloned into pGEM-T Easy (Promega) and in pYES2.1V5HisTOPO (Invitrogen) vectors using primers listed in Table 3. Initially, *hCOQ2* was cloned in a two-step protocol similarly to what has been described (17). pEGFPN1 was used as intermediate vector because of convenient cloning sites. The 5′ portion corresponding to each of the four ATG was amplified from genomic DNA and subcloned into pCRIITOPO (Invitrogen). The 3 portion was amplified from cDNA (both wild-type and patient's) and subcloned into the same vector. The fragments were then sequentially cloned into the PstI site of pEGFPN1. The full length cDNA was then cloned into pYES2.1V5HisTOPO.

Finally, the ATG3-hCOQ2 was directly cloned from reverse transcriptase (RT)-PCR amplified from total fibroblast RNA in

a single reaction in order to analyze patient samples. Site-directed mutagenesis of wild-type *yCOQ2* was carried out by PCR using primers yMUTAG-F and yMUTAG-R. All inserts were directly sequenced using standard protocols and the ABI-Prism 310 automated sequencer (Perkin Elmer).

Yeast complementation analysis

Yeast *coq2* mutants were transformed with the pYES2 vector containing the different versions of *hCOQ2*, and both wild-type and site-directed mutant yeast *COQ2* and the empty vector for complementation experiments. Growth rate in non-fermentable carbon source (YPG medium) was determined as a marker of functional complementation.

CoQ determination

CoQ_{10} was extracted after addition of 4 ml hexane-ethanol (5/2 v/v) and vortexed for 2 min. After centrifugation at 1000 *g* at room temperature for 5 min, the upper phase was carefully transferred into a 20-ml glass scintillation vial (performed twice for each sample). The combined extract was evaporated under a gentle stream of N_2 gas and the residue was dissolved in 0.1 ml of 1-propanol. An aliquot of 50 μl of the extract was directly injected into an HPLC system with a C18 reversed-phase column and an electrochemical detector.

Immunoblotting and real-time pcr

Western blotting was performed using standard methods, and a primary polyclonal antibody developed in hens against human Coq2 peptide, manufactured by Agrisera (Sweden), was used. The expression of *hCOQ2* in fibroblasts was analyzed by SYBR Green quantitative PCR using mRNA extracts and primers hCOQ-RQ-F and hCOQ-RQ-R. Actin was used as housekeeping control gene.

Polyprenyl-*p*HB transferase activity

The activity was assayed by measuring the incorporation of radioactive 4-hydroxybenzoate (*p*HB) into nonaprenyl-4-hydroxybenzoate. Isolated mitochondria (0.1–1 mg protein) were mixed with assay buffer (50 mM phosphate buffer, pH 7.5, 10 mM $MgCl_2$, 5 mM EGTA) containing 1 mM PMSF, 20 μg/ml each of the protease inhibitors chymostatin, leupeptin, antipain and pepstatin A, 5 μM solanesyl pyrophosphate solubilized in detergent solution (1% in water) and 10^5 DPM of [U-^{14}C]pHB. Sufficient volume of a 10% detergent stock solution was also added to the reaction medium to achieve a final detergent concentration of up to 1%. The following detergents were tested: Triton X-100, Chaps, sodium cholate, sodium deoxycholate, lysophosphatidyl choline and octylglucoside. After incubation for 30 min at 37°C with gentle stirring, the reaction was stopped by chilling samples to 4°C. Prenylated [U-^{14}C]pHB was separated by organic extraction with hexane and then measured using a liquid scintillation counter. Specific activity was expressed as DPM min^{-1}mg $protein^{-1}$.

Mitochondrial enzyme activities

Mitochondria-enriched fractions were obtained according to Fernández-Ayala *et al*. (23). and used to determine complex I + III and II + III activities. In both cases, mitochondria were incubated in 40 mM sodium phosphate buffer pH 7.5 plus 0.25 mM KCN and containing either 0.2 mM NADH or 5 mM succinate, and reduction of beef-heart cytochrome c (0.5 mM) was monitored spectrophotometrically at 550 nm for 5 min. To discriminate the rotenone-sensitive NADH-cytochrome c reductase activity (Complex I + III) from the rotenone-insensitive NADH-cytochrome c reductase activity due to the NADH-cytochrome b_5 reductase located in the outer mitochondrial membrane, 5 μM rotenone was added for the last 2 min of incubation.

Statistical analysis

All results are expressed as mean ± SEM. Serial measurements were analyzed by using two-way ANOVA with Tukey's *post-hoc* test using SigmaStat software from SPSS Science (Chicago, IL). The level of significance was set at $P < 0.05$.

ACKNOWLEDGEMENTS

This research was supported by European Union contract LSHB-CT-2004-005151. J.M.L. and M.D.C. are supported by the EU contract and A.R.H. is a fellow from the Spanish Instituto de Salud Carlos III.

Conflict of Interest statement. None declared.

REFERENCES

1. Turunen, M., Olsson, J. and Dallner, G. (2004) Metabolism and function of coenzyme Q. *Biochim. Biophys. Acta.*, **1660**, 171–199.
2. Echtay, K.S., Winkler, E. and Klingenberg, M. (2000) Coenzyme Q is an obligatory cofactor for uncoupling protein function. *Nature*, **408**, 609–613.
3. Navas, P. and Manuel Villalba, J. (2004) Regulation of ceramide signaling by plasma membrane coenzyme Q reductases. *Methods Enzymol.*, **378**, 200–206.
4. Brea-Calvo, G., Rodriguez-Hernandez, A., Fernández-Ayala, D.J.M., Navas, P. and Sanchez-Alcazar, J.A. (2006) Chemotherapy induces an increase in coenzyme Q10 levels in cancer cell lines. *Free Radic. Biol. Med.*, **40**, 1293–1302.
5. Santos-Ocana, C., Do, T.Q., Padilla, S., Navas, P. and Clarke, C.F. (2002) Uptake of exogenous coenzyme Q and transport to mitochondria is required for bc1 complex stability in yeast coq mutants. *J. Biol. Chem.*, **277**, 10973–10981.
6. Rodriguez-Aguilera, J.C., Gavilan, A., Asencio, C. and Navas, P. (2005) The role of ubiquinone in *Caenorhabditis elegans* longevity. *Ageing Res. Rev.*, **4**, 41–53.
7. Ogasahara, S., Engel, A.G., Frens, D. and Mack, D. (1989) Muscle coenzyme Q deficiency in familial mitochondrial encephalomyopathy. *Proc. Natl. Acad. Sci.*, **86**, 2379–2382.
8. Sobreira, C., Hirano, M., Shanske, S., Keller, R.K., Haller, R.G., Davidson, E., Santorelli, F.M., Miranda, A.F., Bonilla, E. and Mojon, D.S. *et al.* (1997) Mitochondrial encephalomyopathy with coenzyme Q10 deficiency. *Neurology*, **48**, 1238–1243.
9. Lamperti, C., Naini, A., Hirano, M., De Vivo, D.C., Bertini, E., Servidei, S., Valeriani, M., Lynch, D., Banwell, B. and Berg, M. *et al.* (2003) Cerebellar ataxia and coenzyme Q10 deficiency. *Neurology*, **60**, 1206–1208.

10. Artuch, R., Brea-Calvo, G., Briones, P., Aracil, A., Galvan, M., Espinos, C., Corral, J., Volpini, V., Ribes, A. and Andreu, A.L. *et al.* (2006) Cerebellar ataxia with coenzyme Q_{10} deficiency: Diagnosis and follow-up after coenzyme Q_{10} supplementation. *J. Neurol. Sci*, **246**, 153–158.
11. Rotig, A., Appelkvist, E.L., Geromel, V., Chretien, D., Kadhom, N., Edery, P., Lebideau, M., Dallner, G., Munnich, A., Ernster, L. and Rustin, P. (2000) Quinone-responsive multiple respiratory-chain dysfunction due to widespread coenzyme Q10 deficiency. *Lancet*, **356**, 391–395.
12. Salviati, L., Sacconi, S., Murer, L., Zacchello, G., Franceschini, L., Laverda, A.M., Basso, G., Quinzii, C., Angelini, C. and Hirano, M. *et al.* (2005) Infantile encephalomyopathy and nephropathy with CoQ10 deficiency: a CoQ10-responsive condition. *Neurology*, **65**, 606–608.
13. Van Maldergem, L., Trijbels, F., DiMauro, S., Sindelar, P.J., Musumeci, O., Janssen, A., Delberghe, X., Martin, J.J. and Gillerot, Y. (2002) Coenzyme Q-responsive Leigh's encephalopathy in two sisters. *Ann. Neurol.*, **52**, 750–754.
14. Lalani, S.R., Vladutiu, G.D., Plunkett, K., Lotze, T.E., Adesina, A.M. and Scaglia, F. (2005) Isolated mitochondrial myopathy associated with muscle coenzyme Q10 deficiency. *Arch. Neurol.*, **62**, 317–320.
15. Horvath, R., Schneiderat, P., Schoser, B.G., Gempel, K., Neuen-Jacob, E., Ploger, H., Muller-Hocker, J., Pongratz, D.E., Naini, A., DiMauro, S. and Lochmuller, H. (2006) Coenzyme Q10 deficiency and isolated myopathy. *Neurology*, **66**, 253–255.
16. Quinzii, C., Naini, A., Salviati, L., Trevisson, E., Navas, P., Dimauro, S. and Hirano, M. (2006) A mutation in para-hydroxybenzoate-polyprenyl transferase (COQ2) causes primary coenzyme Q10 deficiency. *Am. J. Hum. Genet.*, **78**, 345–349.
17. Forsgren, M., Attersand, A., Lake, S., Grunler, J., Swiezewska, E., Dallner, G. and Climent, I. (2004) Isolation and functional expression of human COQ2, a gene encoding a polyprenyl transferase involved in the synthesis of CoQ. *Biochem. J.*, **382**, 519–526.
18. Uchida, N., Suzuki, K., Saiki, R., Kainou, T., Tanaka, K., Matsuda, H. and Kawamukai, M. (2000) Phenotypes of fission yeast defective in ubiquinone production due to disruption of the gene for p-hydroxybenzoate polyprenyl diphosphate transferase. *J. Bacteriol.*, **182**, 6933–6939.
19. Burón, M.I., Herman, M.D., Alcain, F.J. and Villalba, J.M. (2006) Stimulation of polyprenyl 4-hydroxybenzoate transferase activity by sodium cholate and 3-[(cholamidopropyl)dimethylammonio]-1-propanesulfonate. *Anal. Biochem.*, **353**, 15–21.
20. Marbois, B., Gin, P., Faull, K.F., Poon, W.W., Lee, P.T., Strahan, J., Shepherd, J.N. and Clarke, C.F. (2005) Coq3 and Coq4 define a polypeptide complex in yeast mitochondria for the biosynthesis of coenzyme Q. *J. Biol. Chem.*, **280**, 20231–20238.
21. Jones, M.E. (1980) Pyrimidine nucleotide biosynthesis in animals: genes, enzymes, and regulation of UMP biosynthesis. *Annu. Rev. Biochem.*, **49**, 253–279.
22. Lopez, L.C., Schuelke, M., Quinzii, C.M., Kanki, T., Rodenburg, R.J., Naini, A., Dimauro, S. and Hirano, M. (2006) Leigh syndrome with nephropathy and CoQ10 deficiency due to decaprenyl diphosphate synthase subunit 2 (PDSS2) mutations. *Am. J. Hum. Genet.*, **79**, 1125–1129.
23. Fernández-Ayala, D.J.M., López-Lluch, G., García-Valdés, M., Arroyo, A. and Navas, P. (2005) Specificity of coenzyme Q10 for a balanced function of respiratory chain and endogenous ubiquinone biosynthesis in human cells. *Biochim. Biophys. Acta.*, **1706**, 174–183.

ELSEVIER

Official Journal of the European Paediatric Neurology Society

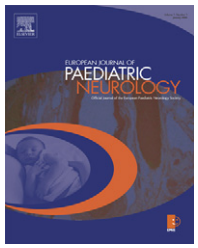

Case study

Increased level of N-acetylaspartylglutamate (NAAG) in the CSF of a patient with Pelizaeus-Merzbacher-like disease due to mutation in the *GJA12* gene

Stefano Sartori[a,*], *Alberto B. Burlina*[b], *Leonardo Salviati*[c], *Eva Trevisson*[c], *Irene Toldo*[a], *Anna Maria Laverda*[a], *Alessandro P. Burlina*[d]

[a]*Department of Pediatrics, University of Padua, Via Giustiniani, 3, 35128 Padova, Italy*
[b]*Metabolic Unit, Department of Pediatrics, University Hospital, Padua, Italy*
[c]*Clinical Genetics, Department of Pediatrics, University Hospital, Padua, Italy*
[d]*Department of Neuroscience, Neurological Clinic, University Hospital, Padua, Italy*

ARTICLE INFO

Article history:
Received 25 March 2007
Received in revised form
10 July 2007
Accepted 30 July 2007

Keywords:
GJA12
PLP1
Pelizaeus-Merzbacher disease
Pelizaeus-Merzbacher-like disease
NAAG

ABSTRACT

Autosomal recessive Pelizaeus-Merzbacher-like disease 1 (PMLD1) is a hypomyelinating disorder of the central nervous system (CNS) with virtually identical phenotype to Pelizaeus-Merzbacher disease (PMD). PMLD1 is caused by mutations in *GJA12* gene, PMD is due to mutations in *PLP1* gene.

Elevated levels of N-acetylaspartylglutamate (NAAG), the most abundant peptide neuromodulator in the human brain, have been recently reported in cerebral spinal fluid (CSF) of patients with PMD.

Using capillary electrophoresis, we analyzed for the first time, the CSF from a girl with PMLD1 and detected high concentrations of NAAG.

This finding confirms the hypothesis that NAAG may be involved in myelination-related processes and can be considered as a useful diagnostic marker not only for patients with the *PLP1* related disorder, but also in those with Pelizaeus-Merzbacher like hypomyelinating disease due to other defined genetic causes, such as PMLD1.

1. Introduction

Autosomal recessive Pelizaeus-Merzbacher-like disease 1 (PMLD1-MIM 608804) is a disorder of myelination characterized by diffuse and symmetrical hypomyelination in the brain, clinically undistinguishable from Pelizaeus-Merzbacher disease (PMD-MIM 312080). The phenotypes are virtually identical: nystagmus, impaired motor development, hypotonia, progressive spasticity, ataxia, choreoathetotic movements and development delay.[1] The MRI picture is characteristic, showing an uniformly increased intensity of the white matter signal in T2-weighted images, with inconstant high signal intensity in the internal capsule, optic radiation and proximal corona radiata in T1-weighted images. PMD is an X-linked recessive disorder caused by mutations in the *PLP1* gene encoding the most abundant protein of CNS myelin, while PMLD1 is an autosomal recessive disorder caused by mutations in *GJA12* that codes for a gap junction protein (also known as connexin 46.6 or connexin 47) which is highly expressed in oligodendrocytes.[2–4]

*Corresponding author. Tel.: +39 049 8218094; fax: +39 049 8213509.
E-mail address: stefano.sartori@unipd.it (S. Sartori).
1090-3798/$ - see front matter © 2007 European Paediatric Neurology Society. Published by Elsevier Ltd. All rights reserved.
doi:10.1016/j.ejpn.2007.07.011

Please cite this article as: Sartori S, et al. Increased level of N-acetylaspartylglutamate (NAAG) in the CSF of a patient with Pelizaeus-Merzbacher-like disease due to mutation in the *GJA12*.... *Eur J Paediat Neurol* (2007), doi:10.1016/j.ejpn.2007.07.011

N-acetylaspartylglutamate (NAAG) is the most abundant dipeptide in the mammalian central nervous system (CNS).[5] It is synthesized from *N*-acetylaspartate (NAA) and glutamate in neurones and is catabolized in the extracellular space by astrocyte-membrane bound NAAG dipeptidases.[6,7] In vivo proton magnetic resonance spectroscopy demonstrated that NAAG concentrations in the human brain are higher in white matter than those found in gray matter.[8] Furthermore, it has been reported that NAAG levels increase in white matter during childhood.[9]

High concentrations of NAAG have been detected in the cerebral spinal fluid (CSF) of patients with PMD, but also in patients with a genetically undefined hypomyelinating phenotype resembling PMD.[10–12]

2. Case study

A detailed clinical history and the molecular analysis of the patient have already been reported elsewhere.[4] She is a 5-year-old girl with a clinical, neuroradiological and electrophysiological picture highly suggestive of PMD. Duplication and coding region mutations in the *PLP1* gene were excluded by real-time PCR and direct sequencing, whereas she harbored a homozygous 34 bp deletion within the coding region of the *GJA12* gene [c. 914_947del].

We analyzed a CSF sample that had been previously collected and stored at −80 °C during an initial work-up performed—after obtaining parental informed consent—before the molecular diagnosis had been established. The amount of NAAG in the CSF was measured using a capillary electrophoresis system—Beckman Coulter P/ACE MDQ, according to Burlina et al. (1999).[11] Our detection limit for NAAG was 0.66 μmol/L, at a signal-to-noise ratio of approximately 10.

N-acetylaspartylglutamate concentration in the CSF of the patient was 50 μmol/L (normal value 0.73–12.68 μmol/L), similar to the values found in PMD,[10] whereas the NAA level was normal.

3. Discussion

In 2000, using capillary electrophoresis, Burlina et al.[10] reported the presence of high levels of NAAG, with normal NAA values, in the urine and CSF of patients with PMD. Subsequently, applying in vitro magnetic resonance spectroscopy, Wolf et al.[12] found strongly elevated NAAG in CSF of two unrelated girls with a hypomyelinating disorder resembling severe PMD, but without *PLP1* mutations. More recently, using capillary electrophoresis, high concentrations of NAAG and normal NAA levels were detected by Burlina et al.[11] in the CSF of seven patients with a phenotype virtually identical to PMD, but without *PLP1* mutations. Conversely, an elevation of NAAG in the CSF has never been reported in any other leukodistrophy,[11] except for Canavan disease,[13] where this finding is likely to be a consequence of the NAA mass action in the biosynthetic NAA–NAAG pathway, as recently demonstrated in the human neuroblastoma cell line where the addition of unlabeled NAA to the culture media resulted in a dose-dependent increase in NAAG synthesis from radiolabeled precursors.[6]

The increase of NAAG in the CSF in these patients does not have a clear explanation yet. Even though it has been hypothesized that the occurrence of axonal degeneration and neuronal loss might underlie the late-onset, progressive neurological deterioration of patients with PLP1 mutation,[14,15] it also possible the high level of NAAG is not secondary to neuronal damage or loss, since NAA values are still normal in the patients described by Burlina and Wolf. The increase in NAAG could rather be explained by a reduced function of the NAAG-degrading enzyme on the astrocyte membranes, secondary to the abnormal or severely reduced myelination.[12]

Our case is, to our knowledge, the first report of a patient with a genetically defined Pelizaeus-Merzbacher-like disease, caused by a mutation in the *GJA12* gene, showing increased levels of NAAG.

This finding confirms that the phenotype of *GJA12*-mutant patients is indistinguishable to PMD, not only for the clinical, electrophysiological and neuroradiological aspects but also for some biochemical features, namely NAA and NAAG levels.

Such phenotypic similarity allows us to hypothesize that, in spite of genetic heterogeneity, a common pathogenic process leads to the arrest of myelination in these diseases, supporting the idea that connexin 47 and *PLP1* are part of a well-orchestrated myelinogenic program.[3,16] The disruption of this program could alter the tricellular metabolic cycle (which includes NAA, NAAG and glutamate) operating between neurones, oligodendrocytes and atrocytes, causing elevated NAAG elevation, subsequently detectable in the CSF of these patients.[12,17] Interestingly, the recently reported possibility of in vivo differentiation of NAA from NAAG by in vivo magnetic resonance spectroscopy at 3 T,[18] will help to better understand the relationship between the biochemical findings and the molecular aspects and the role of *PLP1*, *GJA12* and other genes in the myelination process.

Further, although the link between altered NAAG and dysmyelination remains to be fully elucidated, our finding provides additional evidence for NAA and NAAG as having roles in axonal physiology, axon–glial interactions, and the production and maintenance of the myelin sheath, both in normal myelinogenesis and in dysmyelination, as pointed out recently by Moffet et al.[19]

In conclusion, we believe that the measurement of NAAG in the CSF can become a useful biochemical marker for the investigation of hypomyelinating disorders. It can address more precisely towards the diagnosis not only of PMD but also of Pelizaeus-Merzbacher like hypomyelinating disease due to other defined genetic causes, such as *GJA12*-related PMLD (PMLD1).

REFERENCES

1. Inoue K. PLP1-related inherited dysmyelinating disorders: Pelizaeus-Merzbacher disease and spastic paraplegia type 2. *Neurogenetics* 2005;6:1–16.
2. Uhlenberg B, Schuelke M, Ruschendorf F, et al. Mutations in the gene encoding gap junction protein alpha 12 (connexin

Please cite this article as: Sartori S, et al. Increased level of *N*-acetylaspartylglutamate (NAAG) in the CSF of a patient with Pelizaeus-Merzbacher-like disease due to mutation in the *GJA12*.... *Eur J Paediat Neurol* (2007), doi:10.1016/j.ejpn.2007.07.011

46.6) cause Pelizaeus-Merzbacher-like disease. *Am J Hum Genet* 2004;**75**:251–60.
3. Bugiani M, Al Shahwan S, Lamantea E, et al. GJA12 mutations in children with recessive hypomyelinating leukoencephalopathy. *Neurology* 2006;**67**:273–9.
4. Salviati L, Trevisson E, Baldoin, et al. A novel deletion in the *GJA12* gene causes Pelizaeus-Merzbacher-like disease. *Neurogenetics* 2007;**8**:57–60.
5. Neale JH, Bzdega T, Wroblewska B. *N*-acetylaspartylglutamate: the most abundant peptide neurotransmitter in the mammalian central nervous system. *J Neurochem* 2000;**75**:443–52.
6. Arun P, Madhavarao CN, Moffett JR, Namboodiri MAA. Regulation of *N*-acetylaspartate and *N*-acetylaspartylglutamate biosynthesis by protein kinase activators. *J Neurochem* 2006;**98**:2034–42.
7. Bzdega T, Crowe SL, Ramadan ER, et al. The cloning and characterization of a second brain enzyme with NAAG peptidase activity. *J Neurochem* 2004;**89**:627–35.
8. Pouwels PJW, Frahm J. Differential distribution of NAA and NAAG in human brain as determined by quantitative localized proton MRS. *NMR Biomed* 1997;**10**:73–8.
9. Pouwels PJW, Brockmann K, Kruse B, et al. Regional age dependence of human brain metabolites from infancy to adulthood as detected by quantitative localized proton MRS. *Pediatr Res* 1999;**46**:474–85.
10. Burlina AP, Ferrari V, Burlina AB, et al. Increased levels of *N*-acetylaspartylglutamate in CSF and urine of patients with Pelizaeus-Merzbacher disease. *J Inherit Metab Dis* 2000;**23**(Suppl. 1):213 [abstract].
11. Burlina AP, Ferrari V, Burlina AB, et al. *N*-Acetylaspartylglutamate (NAAG) in Pelizaeus-Merzbacher disease. *Adv Exp Med Biol* 2006;**576**:353–9.
12. Wolf NI, Willemsen MAAP, Engelke UF, et al. Severe hypomyelination associated with increased levels of *N*-acetylaspartylglutamate in CSF. *Neurology* 2004;**62**:1503–8.
13. Burlina AP, Ferrari V, Divry P, et al. *N*-acetylaspartylglutamate in Canavan disease: an adverse effector? *Eur J Pediatr* 1999;**158**:406–9.
14. Bonavita R, Schiffmann DF, Moore, et al. Evidence for neuroaxonal injury in patients with proteolipid protein gene mutatios. *Neurology* 2001;**56**:785–8.
15. Griffiths I, Klugmann M, Anderson T, et al. Axonal swelling and degeneration in mice lacking the major proteolipid of myelin. *Science* 1998;**280**:1610–3.
16. Menichella DM, Goodenough DA, Sirkowski E, et al. Connexin are critical for normal myelination in the CNS. *J Neurosci* 2003;**23**:5963–73.
17. Baslow MH, Guilfoyle DN. Functions of *N*-acetylaspartate and *N*-acetylaspartylglutamate in brain: evidence of a role in maintenance of higher brain integrative activities of information processing and cognition. *Adv Exp Med Biol* 2006;**576**:95–112.
18. Edden RA, Pomper MG, Barker PB. In vivo differentiation of *N*-acetyl aspartyl glutamate from *N*-acetyl aspartate at 3 Tesla. *Magn Reson Med* 2007;**57**(6):977–82.
19. Moffet JR, Ross B, Arun P, et al. *N*-Acetylaspartate in the CNS: from neurodiagnostic to neurobiology. *Prog Neurobiol* 2007;**81**:89–131.

Please cite this article as: Sartori S, et al. Increased level of *N*-acetylaspartylglutamate (NAAG) in the CSF of a patient with Pelizaeus-Merzbacher-like disease due to mutation in the *GJA12*.... *Eur J Paediat Neurol* (2007), doi:10.1016/j.ejpn.2007.07.011

Human Molecular Genetics, 2008, Vol. 17, No. 2 **201–214**
doi:10.1093/hmg/ddm297
Advance Access published on October 9 2007

LETM1, deleted in Wolf–Hirschhorn syndrome is required for normal mitochondrial morphology and cellular viability

Kai Stefan Dimmer[1], Francesca Navoni[1], Alberto Casarin[2], Eva Trevisson[2], Sabine Endele[3], Andreas Winterpacht[3], Leonardo Salviati[2] and Luca Scorrano[1,*]

[1]Dulbecco-Telethon Institute, Venetian Institute of Molecular Medicine, 35129 Padova, Italy, [2]Section of Human Genetics, Department of Paediatrics, University of Padova, 35121 Padova, Italy and [3]Institute of Human Genetics, University Hospital Erlangen, Friedrich-Alexander-University, 91054 Erlangen, Germany

Received August 22, 2007; Revised and Accepted October 7, 2007

Wolf–Hirschhorn syndrome (WHS) is a complex congenital syndrome caused by a monoallelic deletion of the short arm of chromosome 4. Seizures in WHS have been associated with deletion of *LETM1* gene. *LETM1* encodes for the human homologue of yeast Mdm38p, a mitochondria-shaping protein of unclear function. Here we show that human LETM1 is located in the inner membrane, exposed to the matrix and oligomerized in higher molecular weight complexes of unknown composition. Down-regulation of *LETM1* did not disrupt these complexes, but led to DRP1-independent fragmentation of the mitochondrial network. Fragmentation was not associated with changes in the levels of respiratory chain complexes, or with obvious or latent mitochondrial dysfunction, but was recovered by nigericin, which catalyzes the electroneutral exchange of K^+ against H^+. Down-regulation of *LETM1* caused 'necrosis-like' death, without activation of caspases and not inhibited by overexpression of Bcl-2. Primary fibroblasts from a WHS patient displayed reduced *LETM1* mRNA and protein, but mitochondrial morphology was surprisingly unaffected, raising the question of whether and how WHS patients counteract the consequences of monoallelic deletion of *LETM1*. *LETM1* highlights the relationship between mitochondrial ion homeostasis, integrity of the mitochondrial network and cell viability.

INTRODUCTION

Wolf–Hirschhorn syndrome (WHS; OMIM 194190) has an incidence of 1/50 000 and is characterized by severe growth retardation, loss of muscular tone, mental retardation, hypertelorism, microcephaly, dysgenic corpus callosum, speech problems and epilepsy. Seizures characterize the full WHS phenotype: they start during the first year of life and are a frequent cause of death (1). WHS is caused by the partial deletion of the short arm of one chromosome 4 involving chromosome region 4p16.3 (2). WHS is thought to be a contiguous gene deletion syndrome with an unknown number of genes contributing to the phenotype. A WHS critical region (WHSCR-1) has been defined to a 165 kb region encompassing several genes (3,4). The variety of combination of symptoms and the different severity in different patients reflects the diverse extents of the chromosomal deletion in individual patients. Seizures constitute the most life-threatening problem in WHS and have been initially associated with deletion of the $GABA_A$ receptor gene, which however maps proximal to the critical deletion region (WHSCR), specifically, 4p12–p13 (5). Recently, a novel gene, *LETM1*, <80 kb distal to the WHSCR-1, was cloned (6). *LETM1* has been found to lie within the newly proposed critical region WHSCR-2, and to be invariably associated with a complete clinical picture, including seizures (2). The idea that LETM1 could play a role in seizures of WHS patients was also substantiated by the finding that it possessed two putative Ca^{2+} binding EF hands (6), and that it was a mitochondrial protein (7), like its homologue in *Saccharomyces cerevisiae*, Mdm38p.

*To whom correspondence should be addressed at: Istituto Veneto di Medicina Molecolare, Via Orus 2, 35129 Padova, Italy. Tel: +39 0497923221; Fax: +39 0497923271; Email: lscorrano@dti.telethon.it

Mitochondria are crucial organelles for life and death of the cell. They produce most of the ATP, participate in Ca^{2+} signalling and integrate diverse apoptotic stimuli by releasing protein cofactors needed in the cytosol for activation of effector caspases (8,9). Mitochondrial shape changes, i.e. fission of the mitochondrial reticulum and cristae remodelling, are crucial to ensure apoptosis progression (10–13). Mitochondria recently attracted interest as players in the pathogenesis of seizures: mtDNA mutations result in mitochondrial dysfunction and seizures (14) and apoptosis follows seizures in the newborn (15). In this respect, haploinsufficiency of *LETM1* could be a central event in the pathogenesis of seizures associated to WHS.

Mdm38p, the yeast homologue of *LETM1*, was discovered in a genome-wide screening to be involved in the maintenance of mitochondrial morphology (16). Lack of Mdm38p leads to disruption of the subcortical mitochondrial network and apparent swelling of mitochondria. The molecular function of this protein is poorly understood. It has been suggested that Mdm38p is involved in mitochondrial K^+ homeostasis, by regulating, or by physically being a component of the long sought mitochondrial K^+/H^+ antiporter (17). Loss of the master regulator of mitochondrial K^+ homeostasis would cause an increase in mitochondrial K^+ levels, leading to an influx of water into the matrix that could explain the 'swollen' mitochondrial phenotype (18). Alternatively, Mdm38p has also been proposed to be involved in the export of proteins to the inner membrane and in the biogenesis of complexes III and IV. Mdm38p shares functional homology with the well-characterized Oxa1-complex, that is responsible for the insertion of mitochondrially encoded proteins. Mdm38p binds mitochondrial ribosomes and when this interaction is disrupted by its ablation, assembly and therefore steady-state levels of amounts of electron chain complexes were altered (19).

Function of *LETM1* is even less understood. It has been recently reported that ablation of *Letm1* in *Caenorhabditis elegans* is lethal at larval stage, while RNA interference (RNAi)-mediated down-regulation of its expression results in increased mortality. The mechanism by which this is exerted is unclear. In mammalian mitochondria, LETM1 is found in high molecular weight (MW) fractions, consistent with its tendency to homointeract. Its ablation causes derangement of mitochondrial morphology, with a 'swollen' appearance, similar to what is observed in yeast and in *C. elegans* (20). Taken together, these results suggest that LETM1 could participate in the regulation of mitochondrial volume. Nevertheless, they raise several questions: is the mitochondrial fragmentation caused by ablation of LETM1 direct, or is it orchestrated by the Drp1-dependent fission machinery? Do levels of LETM1 control mitochondrial respiratory chain complexes and function of the organelle? And finally, what is the consequence of LETM1 ablation on viability?

In order to address these questions and to gain insights into the function of LETM1, we studied the biochemical properties of LETM1 and the effects of its ablation on mitochondrial physiology, morphology and cellular viability. Our results indicate that LETM1 is located in the inner mitochondrial membrane, with the bulk of the protein facing the matrix, in a high MW oligomer. Ablation of LETM1 causes Drp1 independent mitochondrial fragmentation, while levels of the respiratory chain complexes, mitochondrial respiratory rates and membrane potential are unaffected. The changes in mitochondrial morphology can be pharmacologically reverted by the nigericin, which catalyzes the K^+/H^+ exchange across biological membranes. Unexpectedly, mitochondrial fragmentation by LETM1 results in caspase-independent, necrotic death. Taken together, our results suggest that LETM1 is a regulator of mitochondrial shape independently of the classical Drp1-dependent pathway, and its ablation results in loss of viability.

RESULTS

Subcellular and submitochondrial localization of LETM1

In silico analysis of the sequence of LETM1 does not provide information on the putative function of the protein, but gives clues on its cellular localization. LETM1 is conserved throughout eukaryotic organisms, and a classical mitochondrial presequence is predicted in LETM1, like in its homologue in yeast Mdm38p. Furthermore, LETM1 possesses, close to its N-terminus, a hydrophobic stretch long enough to span a membrane. Interestingly, this predicted transmembrane domain contains three conserved proline residues. Proteins which are imported and inserted into the inner mitochondrial membrane follow two distinct routes (21): they are laterally inserted into the membrane by the TIM23-complex, or they pursue the classical import pathway into the matrix and re-enter the inner membrane from inside mitochondria. Proline residues in the transmembrane domain are indicative of the latter and therefore suggest that the main C-terminal part of LETM1 is located in the matrix. We therefore examined the distribution of LETM1 in subcellular and submitochondrial fractions in HeLa cells. LETM1 was located only in a mitochondrial fraction, like the bona fide mitochondrial markers Tom20 and Opa1, and not in the microsomal and cytosolic fractions (Fig. 1A). Carbonate extraction experiment showed that LETM1 is an integral membrane protein (Fig. 1B). In order to verify the submitochondrial localization of this integral membrane protein, we performed a subfractionation of mitochondria followed by separation of individual compartments on a Percoll gradient. Albeit the outer mitochondrial membrane fraction was contaminated by a small amount of inner membrane, LETM1 was found in the inner mitochondrial membrane fraction and in smaller amount in the matrix (Fig. 1C). This could represent a slight contamination of the matrix fraction with components of the inner membrane, or it could suggest that LETM1 transits from the matrix before being inserted in the inner membrane. In order to understand orientation of LETM1 in the inner membrane, we turned to a protease accessibility assay. LETM1 was protected from cleavage by proteinase K (PK) as long as the inner membrane remained intact. This reactivity was shared by matrix proteins, like mitochondrial Hsp70; conversely, inner membrane proteins exposed to the intermembrane space (IMS), like Opa1, were readily digested when the outer face of the inner membrane was exposed to the protease by osmotically swelling mitochondria (Fig. 1D). In conclusion, our data suggest that C-terminal bulk of LETM1 is

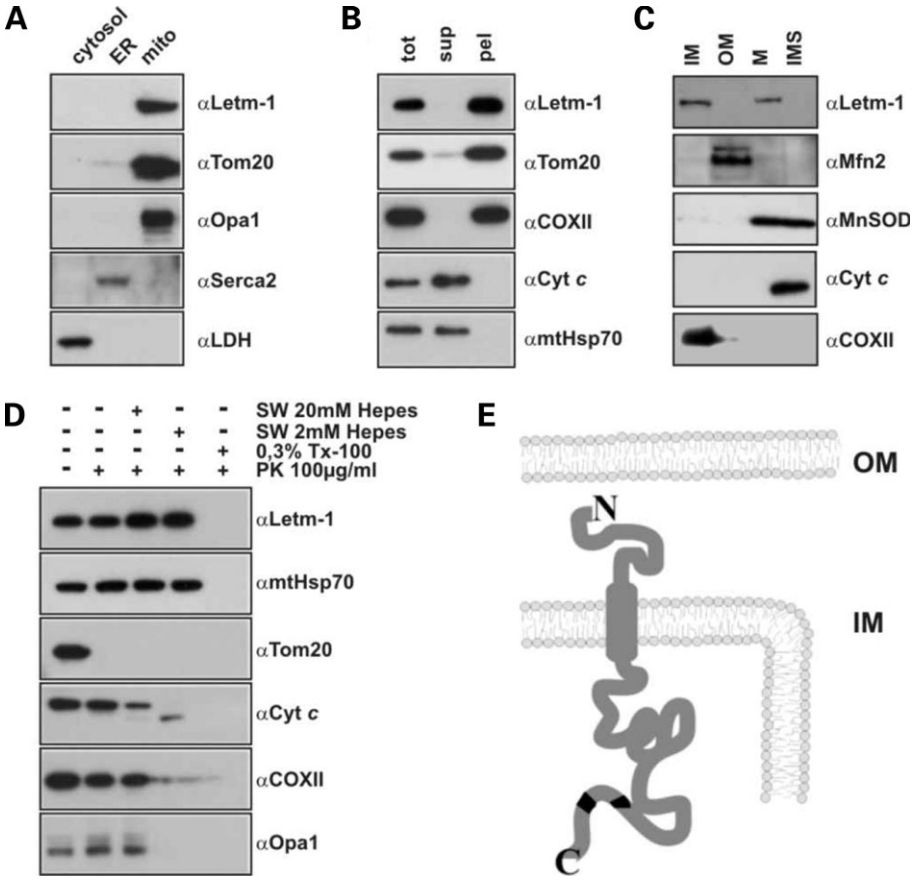

Figure 1. LETM1 is an inner mitochondrial membrane protein facing the matrix. (**A**) Subcellular fractions of HeLa cells were prepared and 10 μg of protein of each fraction was separated by SDS–PAGE and immunoblotted using the indicated antibodies. (**B**) Carbonate extraction. Purified mitochondria were incubated in 0.1 M Na_2CO_3 pH 11 for 30 min at 4°C. Soluble and membrane fractions were separated by centrifugation for 1 h, 4°C, 24 000*g* and equal amounts (10 μg) of proteins were separated by SDS–PAGE and immunoblotted using the indicated antibodies. (**C**) Submitochondrial fractionation was performed as described in material and methods and equal amounts (25 μg) of proteins from inner membrane (IM), outer membrane (OM), matrix (M) and intermembrane space (IMS) were separated by SDS–PAGE and immunoblotted using the indicated antibodies. Note that the LETM1 immunoreactive band in the matrix runs at a slightly higher molecular weight (MW) than the one in the inner membrane. (**D**) Proteinase K accessibility assay. Purified mitochondria (0.1 mg/ml) incubated in isolation buffer were treated as indicated in the figure and 10 μg of protein was separated by SDS–PAGE and immunoblotted using the indicated antibodies. SW, swelling. (**E**) Cartoon depicting the mitochondrial localization of LETM1.

likely to be protected from protease cleavage by the inner membrane, while cleavage of the small N-terminus is not detectable by size shift in SDS–PAGE. Thus, LETM1 likely is an integral inner membrane protein that faces the matrix (Fig. 1E).

LETM1 oligomerizes in higher MW complexes

The prototypical Na^+/H^+ antiporter possesses 12 alpha helices, while prediction of secondary structure of LETM1 indicated the existence of only one putative transmembrane domain. This structure is not suggestive of a direct role of LETM1 in ion exchange. Nevertheless, we decided to explore the possibility that in native conditions LETM1 assembles in higher MW complexes, which in principle could represent a suitable site for ion exchange across the inner membrane. To this end, we wished to analyze the organization of LETM1. First, we explored whether crosslinking of HeLa mitochondria with an amino-specific (disuccinimidyl suberate, DSS) or a thiol-specific (beta maleimido hexane, BMH) reagent yielded higher MW adducts, immunoreactive for LETM1. In BMH-treated mitochondria, two adducts which could correspond to a dimer (∼140 kDa) and a trimer (∼210 kDa) of LETM1 (∼70 kDa) were visible, while in the case of DSS we only observed the ∼210 kDa adduct (Fig. 2A). We further investigated LETM1 organization by blue native gel electrophoresis to confirm the higher MW LETM1 containing complexes suggested by crosslinking and to determine their size. Di-dodecyl maltoside (DDM) solubilized mitochondria showed three major higher MW complexes immunoreactive for LETM1, with an apparent size of ∼250, 500 and 650 kDa. Interestingly, the distribution of LETM1 in these complexes depended on the concentration of DDM: increasing DDM concentration led to a decreased LETM1 immunoreactivity in the 650 kDa complex, in favour of the 500 kDa one (Fig. 2B). Second dimension denaturing SDS–PAGE of the DDM solubilized complexes identified a smeared immunoreactivity for LETM1 in a MW range comprised between ∼220 and 850 kDa (Fig. 2D). In order to verify specificity of the complexes, we decided to monitor

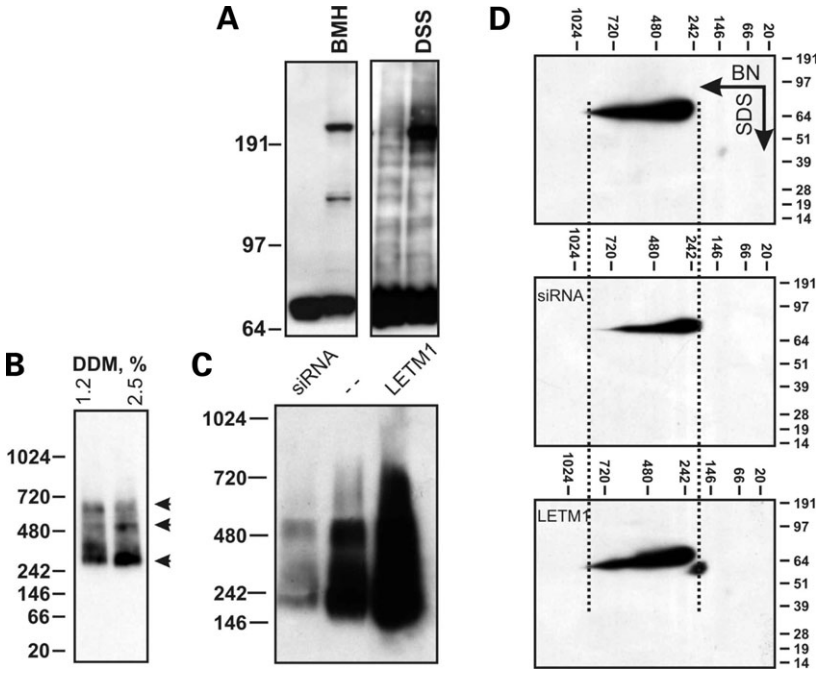

Figure 2. LETM1 is organized in higher MW complexes in the inner mitochondrial membrane. (**A**) Purified mitochondria were treated where indicated with 0.5 mM DSS or 0.5 mM BMH for 30 min, followed by centrifugation and TCA precipitation. Thirty μg of proteins in the pellets were separated by SDS–PAGE and immunoblotted using anti-LETM1 antibodies. (**B**) Purified HeLa mitochondria were incubated for 30 min at 4°C with the indicated concentrations (w/V) of DDM and 50 μg of proteins were separated by BN-PAGE and immunoblotted using anti-LETM1 antibodies. (**C**) HeLa cells were transfected with a scrambled siRNA (- -), with LETM1-specific siRNA (siRNA), or with pcDNA3.1-Letm1 (Letm1). After 24 h, mitochondria were isolated and solubilized using 2.5% DDM. BN-PAGE and immunoblotting was performed as in (B) (**D**) Experiment was performed as in (C). Following isolation of the complexes by BN-PAGE, lanes were excised and mounted on a second dimension SDS–PAGE as described in Materials and Methods. Proteins were separated and immunoblotted using an anti-LETM1 antibody.

them in mitochondria from cells where *LETM1* expression had been silenced by RNAi or where *LETM1* was overexpressed. In both cases, the three prominent LETM1 immunoreactive complexes were readily identifiable, suggesting that the existence of these complexes did not depend critically on the levels of LETM1. The second dimension analysis further confirmed this possibility and showed a lower MW LETM1-immunoreactive band accumulated outside from the LETM1-containing complexes in LETM1-overexpressing complexes (Fig. 2C and D). The appearance of this band, likely a degradation product, was also evident from immunoblotting of mitochondrial proteins from LETM1-overexpressing mitochondria separated by conventional SDS–PAGE (Fig. 3A). Taken together, these data indicate that LETM1 is part of at least three inner mitochondrial protein complexes of unknown composition. Moreover, they indicate that these complexes are maintained in mitochondria where *LETM1* is silenced or overexpressed, suggesting that levels of LETM1 are not essential for the correct assembly of the complexes. Finally, overexpression of LETM1 results in its degradation to a lower MW species by an unknown protease.

Levels of LETM1 regulate mitochondrial morphology

We next wished to verify whether mitochondrial morphology was affected by changes in the levels of LETM1. Following specific RNAi, LETM1 was efficiently reduced (Fig. 3A) to ~40% in comparison to cells transfected with a scrambled RNA, as determined by densitometry on five different experiments (not shown). When we analyzed mitochondrial morphology, we found that silencing of *LETM1* resulted in large, dot-like mitochondria that clustered in the perinuclear region (Fig. 3B and quantification in C). This phenotype was also observed in other cells such as the human osteosarcoma U2OS cell line (not shown). The pictures of mitochondria lacking LETM1 were reminiscent of what observed following overexpression of pro-fission proteins such as Fis1 (22) or ablation of pro-fusion ones like Opa1 (23). In both cases, inhibition of the Drp1-dependent fission machinery, by silencing or by using a dominant negative, $Drp1^{K38A}$ mutant recovers mitochondrial morphology (24,25). We therefore sought to determine whether the phenotype induced by down-regulation of *LETM1* was similarly complemented by ablation or inhibition of Drp1. Co-transfection of HeLa cells with siRNAs directed against *LETM1* and *Drp1* efficiently reduced expression of both proteins (Fig. 3D). In HeLa cells that normally show already elongated mitochondria, silencing of *Drp1* resulted in further elongation of the mitochondrial tubules (arrowhead in Fig. 3E). Nevertheless, co-silencing of *Drp1* did not recover the fragmented phenotype induced by reduction of LETM1 (Fig. 3E and quantification in F). Similarly, silencing of *LETM1* in cells expressing $DRP1^{K38A}$ resulted in mitochondrial fragmentation (Fig. 3F). Thus, adequate levels of LETM1 are essential to maintain mitochondrial morphology and blockage of the fission machinery does not recover the fragmented phenotype induced by silencing of

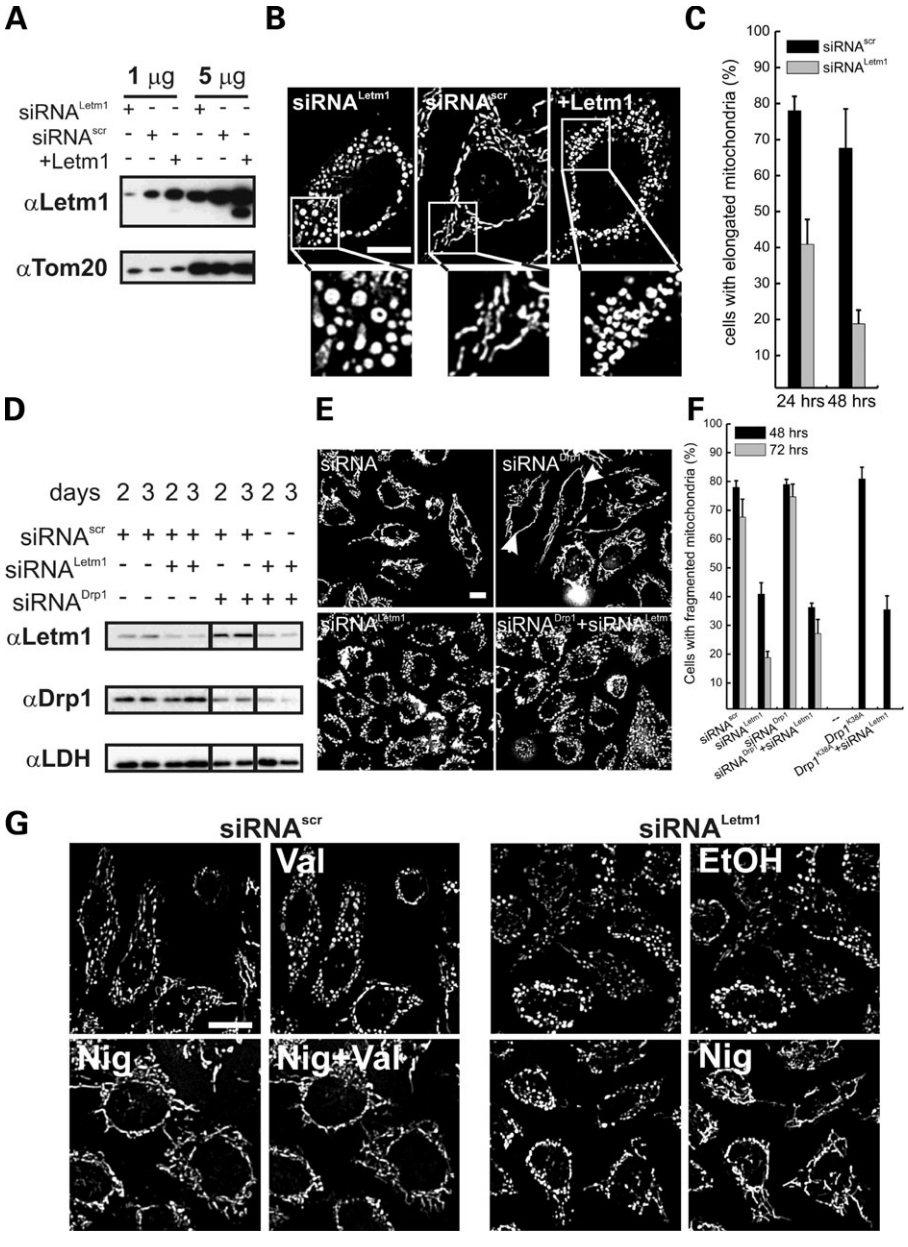

Figure 3. Lack of LETM1 causes Drp1-independent mitochondrial fragmentation. (**A**) HeLa cells were transfected with the indicated siRNA or with pcDNA3.1-Letm1 (+Letm1) and after 48 h mitochondria were isolated, lysed and the indicated amount of protein was separated by SDS–PAGE and immunobloted using the indicated antibodies. (**B**) Representative epifluorescence images of mitochondrial morphology. HeLa cells stably expressing mtRFP were transfected with the indicated siRNA; alternatively, HeLa cells were cotransfected with mtRFP and *LETM1* and after 48 h images were acquired and deconvolved as described. Bar, 10 μm. Boxed areas are enlarged 2.7×. (**C**) Quantitative analysis of mitochondrial shape changes. Experiments were performed as in (B) and morphometric analysis was performed in blind as described in Materials and Methods. Data represent mean ± SE of three independent experiments ($n > 400$ cells each condition). (**D**) HeLa cells were transfected with the indicated siRNA and after the indicated time lysed and the indicated amount of protein was separated by SDS–PAGE and immunobloted using the indicated antibodies. Black lines show irrelevant lanes that were eliminated from the picture of the blot. (**E**) Representative epifluorescence images of mitochondrial morphology. HeLa cells stably expressing mtRFP were transfected with the indicated siRNA and after 48 h images were acquired and deconvolved as described. Bar, 10 μm. Arrowheads point to cells with highly elongated mitochondria. (**F**) Quantitative analysis of mitochondrial shape changes. Experiments were performed as in (E) and morphometric analysis was performed in blind as described in Materials and Methods. Data represent mean ± SE of three independent experiments. In the right part of the graph, HeLa cells were cotransfected with mtRFP and the indicated siRNA and/or plasmid. After 24 h, mitochondrial morphology was evaluated as described in (E). Data represent mean ± SE of four independent experiments. (**G**) Nigericin restores mitochondrial morphology following down-regulation of *LETM1*. HeLa cells stably expressing mtRFP were transfected with the indicated siRNA and after 48 h images were acquired and deconvolved as described. Where indicated, cells were treated for 20 min with 2 μM nigericin (Nig), for 15 min with 1 μM valinomycin (Val) or for 20 min with 0.1%, V/V vehicle (EtOH). Bar, 20 μm. Images are representative frames from at least three independent real time mitochondrial morphology imaging experiments.

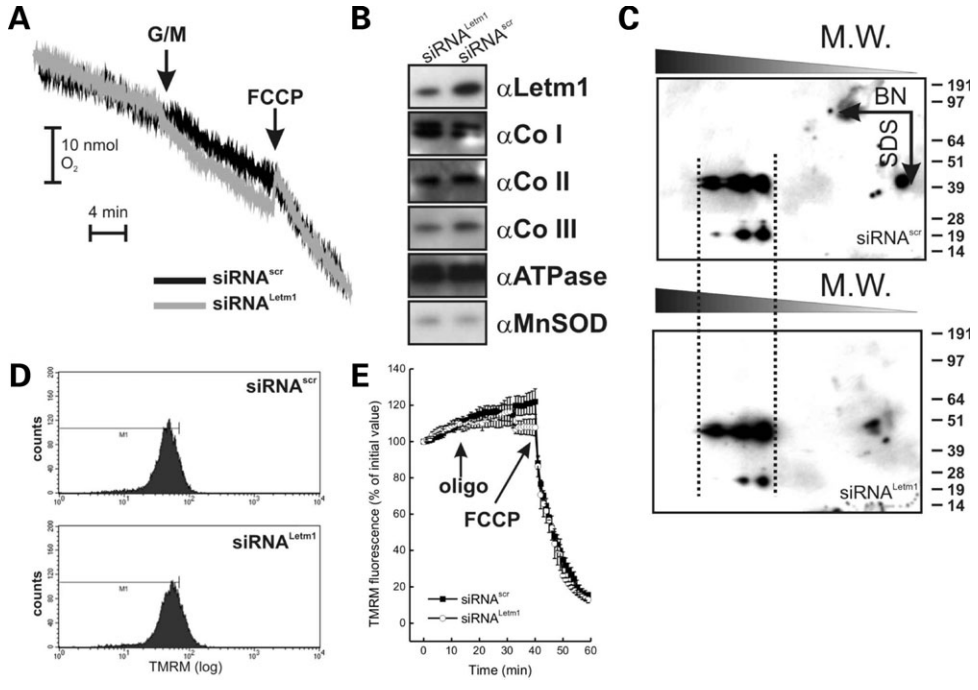

Figure 4. Effect of *LETM1* silencing on biogenesis of mitochondrial respiratory chain complexes and mitochondrial function. (**A**) Representative traces of respiration of mitochondria of the indicated genotype. HeLa cells were transfected with the indicated siRNA and after 48 h mitochondria were isolated and transferred into an oxygen electrode chamber containing experimental buffer (125 mM KCl, 10 mM Tris-MOPS, 10 μM EGTA-Tris, 1 mM Pi). Where indicated (arrows), 5 mM glutamate/2.5 mM malate (G/M) and 60 nM FCCP were added. (**B**) Levels of nuclear-encoded components of individual respiratory chain complexes. HeLa cells were transfected with the indicated siRNA and after 48 h mitochondria were isolated, lysed and equal amounts (10 μg) of proteins were separated by SDS–PAGE and immunoblotted using the indicated antibodies raised against the OXPHOS complexes. (**C**) Two-D, BN-, SDS–PAGE of mitochondria isolated from HeLa cells transfected with the indicated siRNA were performed as described in Figure 2D and immunoblotted using an anti-complex III antibody. (**D**) Flow cytometric analysis of TMRM uptake. HeLa cells transfected with the indicated siRNA after 48 h were stained with TMRM and uptake was determined by flow cytometry as described in Materials and Methods. (**E**) Quantitative analysis of TMRM fluorescence changes over mitochondrial regions in HeLa cells transfected as indicated. Twenty-four hours after transfection, cells. Data represent mean ± SE of five independent experiments. Where indicated (arrows), 1 μM oligomycin and 2 μM FCCP were added.

LETM1. This prompted us to address whether fragmentation could be counteracted by restoration of K^+/H^+ antiport by pharmacological means. To this end, we took advantage of the antibiotic nigericin, a well-characterized monocarboxylate polyether that catalyzes the exchange of one K^+ ion with one H^+ across biological membranes, including mitochondria (26) and that has been successfully employed to revert the mitochondrial phenotype of the Δ*mdm31* and *32 S. cerevisiae* strain (27). Pretreatment with nigericin counteracted mitochondrial fragmentation induced by the K^+ ionophore valinomycin and restored shape of the mitochondrial network in HeLa cells where *LETM1* was down-regulated by siRNA (Fig. 3G). In conclusion, these experiments point out to a relationship between LETM1, K^+ homeostasis and mitochondrial morphology.

Upon overexpression of *LETM1*, mitochondria also appeared fragmented, often organized in round, doughnut-like structures, smaller than the species observed following silencing of the protein (Fig. 3D). This morphology is often a sign of mitochondrial distress and is for example observed in cells treated with the ATPase inhibitor oligomycin, or with the uncoupler FCCP (not shown). Given that overexpression of *LETM1* results in the appearance of LETM1 band with faster mobility (probably caused by unspecific proteolysis, Figs 2D and 3A), we interpreted this morphology as an unspecific mitochondrial response to protein overload.

Silencing of *LETM1* does not impair mitochondrial function

Since mitochondrial fragmentation caused by the silencing of *LETM1* was not complemented by blockage of the fission pathway, we reasoned that it could represent the visual counterpart of an underlying mitochondrial dysfunction. This would furthermore be in agreement with both proposed functions of its yeast orthologue Mdm38p in K^+/H^+ antiport, or insertion of proteins into the inner membrane. We therefore decided to explore function of mitochondria lacking LETM1. Silencing of *LETM1* did not affect basal, as well as uncoupled respiration supported by the complex I substrate glutamate (Fig. 4A). In accordance to this, levels of complexes of the respiratory chain, as well as of the ATPase, were unaffected (Fig. 4B). Not only levels, but also assembly of respiratory complexes, like complex III, were unaltered, as indicated by two-dimensional blue native electrophoresis followed by SDS–PAGE (Fig. 4C). These data indicate that silencing of *LETM1* is not sufficient to influence levels of the respiratory chain components and their assembly into complexes. Nevertheless, they do not exclude the possibility that mitochondrial dysfunction occurs *in situ*. To verify this possibility, we measured the cellular uptake of the potentiometric dye tetramethyl rhodamine methyl ester (TMRM), that depends on the plasma and mitochondrial membrane

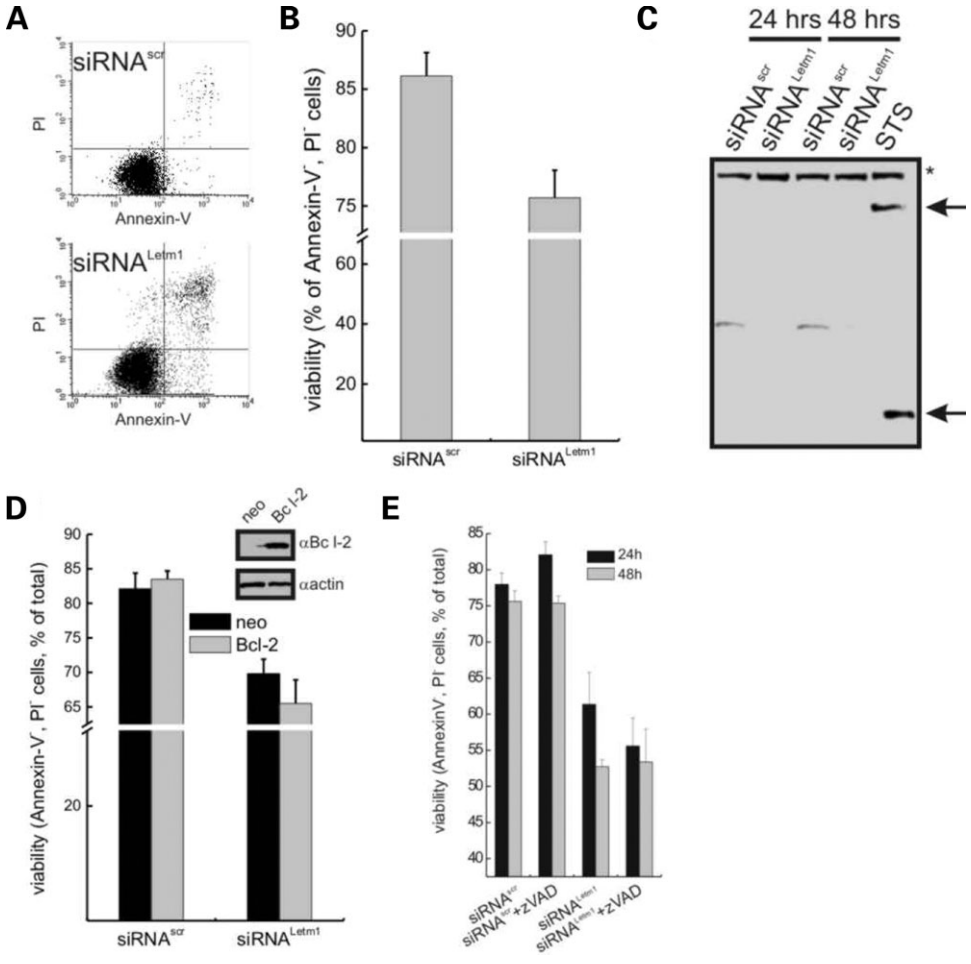

Figure 5. Loss of LETM1 causes caspase-independent, Bcl-2 insensitive cell death. (**A**) Representative dot plots of Annexin-V-FLUOS, PI staining of HeLa cells transfected for 24 h with the indicated siRNA. (**B**) Quantitative analysis of the effect of LETM1 reduction on viability. Experiments were as in (A). Data represent mean ± SE of three independent experiments. (**C**) Silencing of *LETM1* does not result in PARP cleavage. HeLa cells were transfected with the indicated siRNA, and after the indictaed times lysed and equal amounts (50 μg) of protein were separated by SDS–PAGE and immunoblotted with an anti-PARP antibody. Rightmost lane was loaded with 50 μg of proteins from untransfected HeLa cells treated for 12 h with 2 μM staurosporine (STS). Asterisk, uncleaved PARP; arrowheads, caspase cleaved PARP fragments. (**D**) Death caused by silencing of *LETM1* is not blocked by Bcl-2. HeLa cells of the indicated genotype were transfected with the indicated siRNA and after 24 h viability was measured. Inset shows levels of Bcl-2. Equal amounts (50 μg) of protein from cells of the indicated genotype were separated by SDS–PAGE and immunoblotted using the indicated antibodies. (**E**) Death caused by ablation of *LETM1* is not insensitive to inhibition of caspases. HeLa cells were transfected with the indicated siRNA and treated where indicated with 50 μM zVAD-fmk for the whole duration of the experiment. At the indicated times, cells were harvested and viability was determined. Data represent mean ± SE of four independent experiments.

potential. Flow cytometry showed that down-regulation of *LETM1* did not impair uptake of the dye even when cells were pretreated with 50 mM KCl to depolarize the plasma membrane and therefore to drive TMRM uptake only by mitochondrial membrane potential (Fig. 4D). *In situ*, membrane potential of dysfunctional mitochondria can be maintained by the proton pumping activity of the reversal of the ATPase. This latent mitochondrial dysfunction can be unveiled by oligomycin, a specific inhibitor of the ATPase (28). Real time imaging of TMRM fluorescence intensity in mitochondria showed that upon addition of oligomycin, mitochondrial membrane potential increased irrespective of LETM1 levels (Fig. 4E). In conclusion, mitochondrial function measured *in situ* and *in vitro* is unaffected by ablation of ∼60% of LETM1, raising the question of whether the residual LETM1 is sufficient to maintain the mitochondrial functions measured here.

Silencing of *LETM1* causes Bcl-2 insensitive, caspase-independent cell death

In order to understand the functional relevance of the mitochondrial fragmentation caused by silencing of LETM1, we explored if it was associated with changes in viability. Silencing of LETM1 in HeLa cells caused *per se* after 24 h an increase in AnnexinV/propidium iodide (PI) staining, indicative of their reduced viability (Fig. 5A and B). Interestingly, the percentage of single PI-positive cells increased from 2 to 8, suggesting that cells lacking this mitochondrial protein are more prone to necrosis. Furthermore, PARP cleavage, a sign of caspase activation, was undetectable in cells where *LETM1* was silenced, while it was prominent in cells treated with the apoptotic inducer staurosporine (Fig. 5C). We therefore decided to check if death was affected by two different strategies to inhibit apoptosis, at the mitochondrial as well

as at the post-mitochondrial level. We first turned to an HeLa cell line stably overexpressing the mitochondrial antiapoptotic protein Bcl-2 that blocks the release of cytochrome *c* and of other mitochondrial proapoptotic proteins (29). Overexpression of Bcl-2 was completely ineffective in blocking death caused by silencing of *LETM1* (Fig. 5D). Similarly, the addition of the pan-caspase inhibitor z-VAD had no effect whatsoever on the loss of viability induced by the loss of LETM1 (Fig. 5E). Taken together, these results show that silencing of *LETM1* triggers caspase-independent, Bcl-2 insensitive death.

Levels of LETM1 and mitochondrial morphology in cells from patients with severe WHS

In order to explore whether the down-regulation of *LETM1* by siRNA could be a faithful model of WHS, we established a lymphoblastoid cell line from a WHS patient with the full clinical phenotype. This patient suffered from seizures and had a cryptic terminal deletion 4p16.3 sizing 2.2–2.8 Mb, with breakpoint between the deleted cosmid probe LA04NC01-33c6 (MXD4) and the non-deleted cosmid probe LA04NC01-247f6 (SH3BP2) (not shown), encompassing both WHS-critical regions 1 and 2. Deletion of the *LETM1* gene was verified by fluorescence *in situ* hybridization (FISH) with cosmid LA04NC01-75b9, which includes the 5′end of the *LETM1* gene and was caused by the loss of the paternal allele, as shown by a microsatellite marker 182 Kb cetromeric to *LETM1* (Fig. 6B). The generated, transformed lymphoblastoid cell line was then probed for levels of LETM1 protein, which were unexpectedly unchanged (Fig. 6C). To address whether this was a cell-specific effect, possibly related to the transformation of the lymphoblastoid line, we decided to generate a primary fibroblasts from a different patient, also suffering from severe WHS. Real-time PCR analysis of genomic as well as of mRNA *LETM1* showed a clear ∼50% reduction (Fig. 6D). Evaluation of LETM1 by immunoblotting in the same sample revealed a corresponding reduction in the levels of the protein (Fig. 6F and densitometric analysis in E). It should be noted that a repeated analysis of LETM1 in these fibroblasts showed a certain degree of variability. Levels of LETM1 in WHS fibroblasts, assessed by densitometry following normalization for the cytosolic protein LDH, were on average 63.9 ± 12.1% of those detected in the age and sex matched control ($n = 5$, $P = 0.12$ in a two paired Student's *t*-test). Mitochondrial morphology, measured by loading fibroblasts with the potentiometric probe TMRM and assessed as previously described (23), was unexpectedly unaffected in the WHS sample (Fig. 6F and quantification in G).

DISCUSSION

Most of the proteins that regulate shape of mitochondria are associated to the outer mitochondrial membrane. Only a few ones [Opa1/Mgm1p (30,31), or Mdm31p, Mdm32p (32) and Mdm33p (33)] reside inside mitochondria. The control of mitochondrial morphology and dynamics from 'inside' mitochondria is therefore much less understood. Furthermore, although the processes that alter mitochondrial morphology during programmed cell death are well studied, we have scarce knowledge of how mitochondrial morphology is regulated during life of the cell and how this impacts on integrated cellular processes (34,35). In this respect, the yeast protein Mdm38p and its human homologue LETM1 are interesting candidates to integrate regulation 'from the inside' of mitochondrial shape changes to the normal life of the cell. Mdm38p is indeed supposed to be involved in ion homeostasis across (17), or insertion of respiratory chain components into (19), the inner membrane. Furthermore, deletion of *LETM1* is associated with epilepsy in WHS patients (2). Thus, knowledge of the function of LETM1 is not only crucial to clarify how morphology of the mitochondria can be influenced by ions and/or assembly of the respiratory chain complexes, but also to better understand pathogenesis of seizures in WHS.

LETM1, like its yeast homologue, is located in the inner mitochondrial membrane with its bulge C-terminal part facing the matrix. This is consistent with the presence of prolines in the only predicted transmembrane domain of this protein, which are highly suggestive of protein transit from the matrix, followed by re-insertion into the inner membrane (21). Accordingly, in subfractionation experiments of mitochondria we observed traces of LETM1 in the matrix compartment, albeit this could also represent a slight contamination of this subfraction with components of the inner membrane. This latter hypothesis is somehow reinforced by the lack of soluble LETM1 in the carbonate extratction experiment. The topology that we propose is in accordance with what observed for Mdm38p in yeast (17,19) and slightly different from what proposed for LETM1 (20). This discrepancy could be caused by the fact that in the latter experiments by Hasegawa and van der Bliek, digitonin instead of osmotic swelling was used to make IMS accessible to protease. Thus, it is possible that higher concentrations of digitonin caused a certain degree of solubilization of the inner membrane and leaving matrix proteins accessible to the action of protease. In accordance to this hypothesis, in the experiments by Hasegawa and van der Bliek (20) the susceptibility pattern of glutamate dehydrogenase seems to be superimposable to that of LETM1. Furthermore, both functions so far ascribed to LETM1 (participation to K^+ homeostasis or to protein export) are more likely to require a protein whose bulk is exposed to the matrix, rather than a protein facing the IMS. In conclusion, while our experiments favour the orientation of LETM1 proposed in Fig. 1E, the accurate mapping of LETM1 topology requires additional proofs using antibodies against different epitopes of the molecule.

Blue native electrophoresis indicated that once inserted in the inner membrane, LETM1 is retrieved in at least three higher MW complexes, with apparent MW of ∼250, 500 and 650 kDa. Furthermore, crosslinking with the thiol-selective reagent BMH identified an additional complex at ∼140 kDa. In a gel filtration approach, LETM1 was similarly found in a higher MW complex of a compatible ∼540 kDa size (20). Silencing or overexpression of LETM1 did not change the occurrence of the different complexes, suggesting that LETM1 does not have an essential scaffolding role. In other words, either the complexes are composed solely by

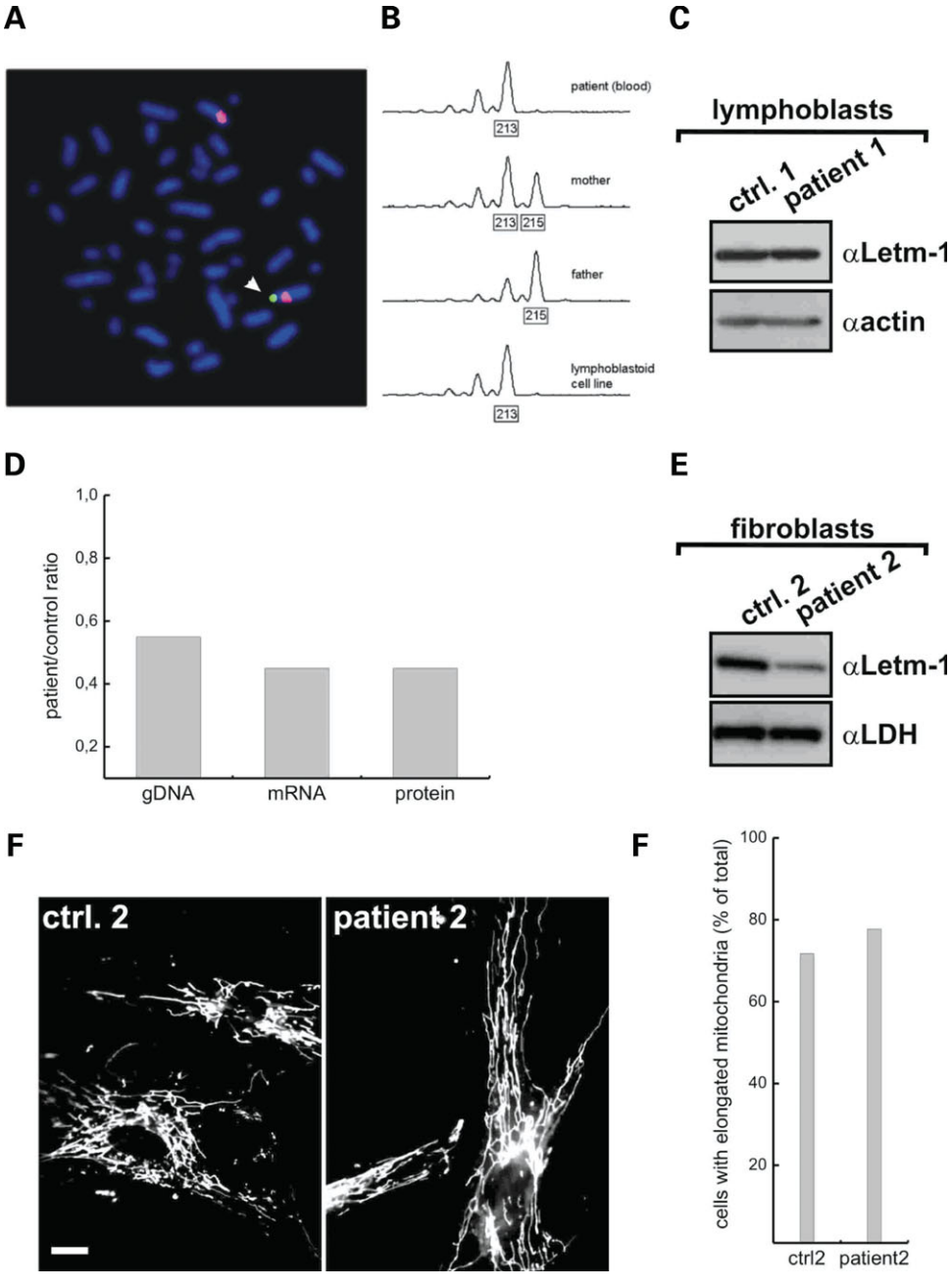

Figure 6. LETM1 levels and mitochondrial morphology in cells from two WHS patients. (**A**) FISH analysis with cosmid LA04NC01-75b9 (green) and a chromosome 4 specific centromere probe (red) indicating deletion of *LETM1* on one chromosome (arrow). (**B**) Analysis of microsatellite marker MS-27h9, representing a dinucleotide polymorphism 182 kb centromeric to *LETM1*. The patient (DNA from blood sample as well as the lymphoblastoid cell line) inherited a 213 bp allel from the heterozygous mother (215 and 213 bp alleles), but not the 215 bp allele from the homozygous father. (**C**) Levels of LETM1 in control (ctrl.) and WHS patient lymphoblasts. Cells were lysed and equal amounts of protein (10 μg) were separated by SDS–PAGE and immunoblotted using the indicated antibodies. Blots are representative of six different experiments. (**D**) Patient:control ratio of *LETM1* in genomic DNA (gDNA), messenger RNA (mRNA) and of LETM1 protein (determined on the same sample by densitometry following immunoblotting). *LETM1* levels in gDNA and mRNA were measured by RT-PCR as described (**E**) Levels of LETM1 in control (ctrl. 2) and WHS patient (patient 2) fibroblasts. Cells were lysed and equal amounts of protein (10 μg) were separated by SDS–PAGE and immunoblotted using the indicated antibodies. Blots correspond to the sample analyzed in panel (D). (**F**) Mitochondrial morphology in control (ctrl. 2) and WHS patient (patient 2) fibroblasts. Cells were loaded for 30 min with 20 nM TMRM and representative epifluorescence images were acquired as described in Materials and Methods. Bar, 15 μm. (**G**) Quantitative analysis of mitochondrial morphology control (ctrl. 2) and WHS patient (patient 2) fibroblasts. Experiments were as in (F). Total cell number was 106 (ctrl. 2) and 110 (patient 2) in two independent experiments.

LETM1 molecules that homo-oligomerize according to their ability to self interact (20), or their structural integrity does not depend on the presence of LETM1.

The loss of LETM1 results in striking morphological abnormalities of mitochondria, which appear fragmented and clustered in the perinuclear region. This was similar to the

morphologies observed following overexpression of pro-fission molecules like Fis1 or ablation of pro-fusion ones like Opa1 (22,23). Nevertheless, mitochondrial morphology was not recovered by ablation or inhibition of the fission pathway. This suggests that fragmentation of mitochondria lacking LETM1 does not require activation of the Drp1-dependent fission pathway, at a major variance from what observed in the case of overexpression of other pro-fission proteins (24) or ablation of pro-fusion ones (25). The unusual independence from Drp1 could imply that the fragmentation caused by silencing of *LETM1* is not caused by an unbalance in the fusion–fission equilibrium; rather, it could represent the morphological counterpart of a mitochondrial sufferance that follows the inhibition of a crucial function of ion homeostasis or protein export into the inner membrane. In particular, mitochondria with lower levels of LETM1 rounded up and seemed to be enlarged. The 'ring' shape observed following LETM1 overexpression could be the result of matrix shrinkage, followed by network fragmentation and ring-like closure of mitochondria to obtain a more stable structure. Alternatively, this morphology could represent a non-specific mitochondrial damage, supported by the retrieval in these mitochondria of proteolysis products of LETM1 that lie outside the complexes containing the native protein. On the other hand, the fragmented and enlarged morphology of mitochondria with less LETM1 was complemented by the antibiotic nigericin, which exchanges K^+ with protons and therefore can be considered a pharmacological K^+/H^+ antiporter. This evidence strongly supports a role for LETM1, like its yeast orthologue Mdm38p, in the regulation of the extrusion of K^+ from the mitochondrial matrix. If LETM1 is the antiporter, or it is one of its regulators, remain an open question. In principle, other ion exchangers display a much more complex structure, with 12 transmembrane helices. Conversely, the EF hands identified in LETM1 display a low affinity for divalent ions, suggesting that they could bind matricial Mg^{2+} rather than Ca^{2+} (6). It should be kept in mind that the K^+/H^+ antiporter is indeed directly regulated by matricial Mg^{2+} (36); and that the MW weight of LETM1 is compatible with the $\sim$80 kDa protein identified by Garlid and colleagues (37) as the putative antiporter. On the other hand, one would expect that mitochondria with impaired K^+ extrusion and deranged volume homeostasis would be dysfunctional, but all our attempts to unveil a dysfunction in mitochondria where *LETM1* was silenced failed. Respiration, membrane potential, steady-state levels of nuclear encoded, exported subunits of the respiratory chain were all apparently normal. Furthermore, we could not detect an interaction between LETM1 and ribosomal protein of mitochondria (not shown), as proposed for its yeast orthologue Mdm38p (19). We cannot exclude that the residual 40% of LETM1 protein can maintain mitochondrial function or protein export. In this case, mitochondrial shape would represent the most sensible indicator of mitochondrial damage. In conclusion, our morphological analysis supports a role for LETM1 in ion and therefore volume homeostasis across the inner membrane.

Ablation of Letm1 in *C. elegans* is lethal and yeast strains lacking Mdm38p display growth defects on non-fermentable carbon sources. Similarly, we could not generate clones where *LETM1* was stably ablated by RNAi (not shown) and transient down-regulation of the levels of the protein was associated with spontaneous death. The features of this death were indeed more 'necrotic', with permeabilization of the plasma membrane to PI. Interestingly, caspases were not activated and their inhibition did not counteract death; moreover, Bcl-2, which keeps in check release of cytochrome *c* from mitochondria (38) and is a primary inhibitor of most intrinsic apoptotic stimuli (39), did not prevent death that follows reduction in LETM1 levels. Cells can die by the so-called 'caspase-independent' mode of apoptosis, relying on the release of factors like AIF, Omi, EndoG that directly act at the nuclear level to exert DNA degradation. However, their release from mitochondria is similarly controlled by Bcl-2 (40). In this respect, it is unlikely that lack of LETM1 primes 'caspase-independent' apoptosis, since it is not blocked by Bcl-2. Failure of inhibition by Bcl-2 apparently rules out also the possibility that lack of LETM1 results in autophagy, also blocked by enforced expression of Bcl-2 (41).

We established two cell models, a transformed lymphoblast cell line and a primary fibroblast culture, derived from two different full clinical picture WHS patients. Genetic analysis revealed that in both samples one allele of *LETM1* was lacking, but in the case of the lymphoblasts the levels of the protein seemed unchanged as compared to an age- and sex-matched control lymphoblast line. A similar situation was observed by van der Bliek and colleagues in fibroblasts (20), opening the possibility that *LETM1* displays a monoallelic expression, and that its protein levels are therefore unaffected by the loss of a single allele. Although we have not investigated mono- or biallelic expression in humans, we could at least demonstrate biallelic expression of *Letm1* in various murine tissues (not shown), which strongly indicates a similar situation in human. We deepened our analysis by generating a second cellular model from a different WHS patient. In the case of this primary fibroblast culture, we could demonstrate a $\sim$50% reduction in the levels of *LETM1* gene, messenger and LETM1 protein. It should be stressed that the reduction in LETM1 protein levels appeared somehow variable. Thus, the results in lymphoblasts could be a consequence of the transformed nature of this cell line, or be ascribed to an even higher variability in this protein levels reduction. Irrespective of this, mitochondrial morphology in WHS fibroblasts was unexpectedly superimposable to that observed in the controls. This result opens the possibility that the striking phenotype of fragmentation of the organelle observed in HeLa cells depended on the efficient down-regulation observed following RNAi. In other words, there is a strict threshold of LETM1 levels that must be crossed in other to obtain a clear phenotype. Alternatively, there could be a yet uncharacterized effect of the other genes deleted in WHS (on mitochondrial morphology, which could compensate the fragmentation caused by the monoallelic loss of *LETM1*.

Whether LETM1 is still a good candidate for the pathogenesis of seizures in WHS remains an open question. So far, three different cell models from WHS patients [two described here and one in (20)] failed to display the same mitochondrial alterations observed by deleting the gene in yeast and *C. elegans*, or by down-regulating it in cultured mammalian cells. Nevertheless, no studies have been so far performed in neurons, which are known to critically depend on

mitochondrial function and dynamics (42,43). In conclusion, it appears that function of LETM1 should be investigated in neurons, and that a mouse model of *Letm1* ablation is required to understand the role of this protein in the CNS and in the pathogenesis of seizures.

MATERIALS AND METHODS

SDS–PAGE, western blotting and antibodies

Proteins were separated by 4–12% Tris-MOPS SDS–PAGE (NuPage, Invitrogen) transferred onto PVDF membranes (Millipore) and probed using the indicated antibodies. The following antibodies were used: monoclonal anti-LETM1 (1:500, Abnova, Taipei, Taiwan); polyclonal anti-LETM1 [1:1000 (6)]; polyclonal anti-Tom20 (1:2000, Santa Cruz Biotechnology), anti-Serca2 (1:500, Santa Cruz Biotechnology) antiGrp75 (mtHsp70, 1:500, Santa Cruz Biotechnology); monoclonal anti-Opa1 (1:500, BD Biosciences, Lexington, KY); monoclonal anti-cytochrome *c* (1:500, BD Biosciences); polyclonal anti-MnSOD (1:3000, Nventa Biopharmaceuticals, San Diego, CA); monoclonal anti-PARP (1:5000, Cell Signaling Technology, Danvers, MA); polyclonal anti-MnSOD (1:2000, Invitrogen, Novato, CA); polyclonal anti-LDH (1:1000, Rockland, Gilbertsville, PA) and polyclonal anti-Mfn2 (44) (1:200, a kind gift from Dr M. Rojo). Purified antibodies raised against isolated OXPHOS complexes were a kind gift by Dr L. Vergani and included: anti-complex I (polyclonal anti 51 kDa subunit); anti-complex II (polyclonal anti 70 kDa subunit); complex III (polyclonal anti bc1 (45)) and anti-ATPase (polyclonal anti-αβ subunit). All anti OXPHOS antibodies were used at a final dilution of 1:1000. Isotype matched, horse-radish peroxidase-conjugated secondary antibodies (Sigma) were used followed by detection by chemiluminescence (Amersham).

Molecular biology

Two siRNA against *LETM1* were synthesized from the following sequences 5′-GGA ACU GCC UGA AUG UUC Ctt-3′, and 5′-CAG AGA CUU CCA UAA UCA Att-3′ and were used in combination at a final concentration of 100 nM each. The scrambled control siRNA (5′-GUA GCA CGC GUA ACU GUC Utt-3′) was used at the same final concentration. All siRNA were obtained from Ambion (Huntington, UK).

The cDNA of LETM1 was cloned in the *Eco*RI, *Xho*I sites of pcDNA3 (Invitrogen, Carlsbad, CA). Constructs were confirmed by sequencing. Mitochondrially targeted red fluorescent protein (mtRFP) corresponded to pDsRed2-Mito and was from Clonetech (Mountain View, CA).

Quantitative analysis of *LETM1* gene dosage and expression

Genomic DNA and total RNA from cultured fibroblasts were extracted using standard methods and prepared for subsequent analysis. mRNA was retrotranscribed using Superscript II RT–PCR Kit and random hexameres (Invitrogen). Real-time quantitative PCR was performed using Power SYBR Green PCR Master Mix and a 7900 Genetic Analyzer (Applied Biosystems). Reaction conditions were standard (95°C 15 s, 60°C 30 s; 40 cycles). Oligonucleotides used in the reaction were 5′-GGGAGCGCAGGCAGTTT-3′ and 5′-ACAGCAACAGGCAGCAGAAA-3′ for genomic DNA and 5′-GGGCACAGGCGTGAGATG-3′ and 5′- CTGCATTCCAACTGCTC AGACT-3′ for mRNA. Results were normalized to the albumin gene to evaluate genomic DNA copy number, and to GUS for mRNA expression. Data were analyzed using the Delta/Delta CT method as previously reported (46).

Cell culture and transfection

Human primary fibroblasts were obtained at the Department of Pediatrics, University of Padova, from a 20 years old female patient during elective spinal surgery, with informed consent of the parents, her legal representatives. The diagnosis had been previously established by chromosomal analysis and 4p16 FISH. Control fibroblasts were obtained from an age- and sex-matched healthy donor by cutaneous biopsy.

Cells were cultured in Dulbecco's Modified Eagle's Medium (DMEM) (Gibco) supplemented with 10% fetal bovine serum (Gibco), 50 U/ml Penicillin, 50 μg/ml Streptomycin, 100 μM non-essential aminoacids (MEM, Gibco/Invitrogen) and 2 mM glutamine (Gibco).

A lymphoblastoid cell line was established from a female WHS patient at the Institute of Human Genetics, University Hospital Erlangen, with informed consent of the patient's legal representative. Deletion was verified by FISH as well as by microsatellite analysis. Microsatellite analysis was performed using fluorescently labelled primers 27h9-F: 5′-GAGACCAGCTTAGGTAACG-3′ and 27h9-R: 5′-GGCTG TGGTGAGTTGTTTG-3′ to amplify a polymorphic region at cosmid LA04NC01-27H9 (Acc. Z49237) (at ∼2.022 Mb). PCR products were electrophoresed using an ABI3100 sequencer and results were analyzed using genescan and genotyper software (Applied Biosystems).

HeLa cells stably expressing Bcl-2 ($HeLa^{Bcl-2}$) and their respective control carrying the empty vector ($HeLa^{neo}$) (47) were a kind gift from P. Bernardi (University of Padova). HeLa cells stably expressing mtRFP were generated by selection with the antibiotic G418 (500 μg/ml) followed by clonal selection by limiting dilution. Homogeneous expression of mtRFP was confirmed by flow cytometry and cells were grown in DMEM supplemented as above, plus G418 (500 μg/ml). Transfection of HeLa cells with siRNA and plasmid DNA was performed with Lipofectamine 2000 (Invitrogen) according to the manufacturer's protocol.

Mitochondrial isolation and subfractionation

Mitochondrial isolation from 10^9 HeLa cells was performed by standard differential centrifugation as previously described (48). To isolate the light membrane and the cytosolic fraction, the post-mitochondrial supernatant was spun twice for 30 min at 100 000*g* to separate pellet (light membranes) and supernatant (cytosol). Protein in separated fractions was determined by a BCA protein assay (Pierce).

Submitochondrial fractionation was performed according to Sottocasa *et al*. (49). Briefly, 50 mg of mitochondria were resuspended in 10 ml of 10 mM KH_2PO_4 using a Teflon

pestle. Mitochondria were left on ice for 5 min and spun at 8000*g* for 10 min. The supernatant was recovered and the pellet resuspended in 125 mM KCl, 10 mM Tris-MOPS pH 7.4, centrifuged again and the former with the latter supernatant constituted the IMS fraction. The pellet was resuspended in 10 ml of 10 mM KH_2PO_4 and 3.5 ml of a solution containing 1.8 M sucrose, 2 mM ATP, 2 mM $MgSO_4$ were added. After 5 min the sample was sonicated at 4 W for 20 min, laid on the top of 15 ml of a solution containing 1.18 M sucrose and spun for 2 h at 90 000*g*. After the centrifugation, an upper soluble clear layer corresponding to the matrix (M) fraction, a yellow interphase corresponding to the outer membrane (OM) and a brown pellet corresponding to the IM were collected.

Protease-accessibility assay

Mitochondria (0.1 mg/ml) resuspended in isolation buffer (IB, 0.2 M sucrose, 10 mM Tris-Mops pH 7.4, 0.1 mM EGTA-Tris) were treated with 100 μg/ml PK at 4°C for 30 min. Where indicated, hypotonic rupture of the OM was achieved by diluting the mitochondrial suspension 1:40 in 2 mM HEPES/KOH pH 7.4; Triton X-100 was added where indicated at a final concentration of 0.3% (V/V). PK was inactivated by incubation with 1 mM PMSF at 4°C for 5 min. The resulting samples were precipitated with 10% trichloroacetic acid (TCA), spun at 4°C, 18 000*g* for 30 min, and the pellet was washed with cold acetone, resuspended in 100 μl of NuPAGE loading buffer (Invitrogen) and a tenth (10 μg) was loaded on a gel.

Crosslinking and blue native gel electrophoresis

For crosslinking, mitochondria (0.1 mg/ml) were incubated in 20 mM HEPES/KOH pH 7.4, 125 mM KCl, 1 mM KPI and treated with 500 μM BMH for 30 min at room temperature, or with 500 μM DSS (Pierce) at 4°C for 30 min. Samples were TCA-precipitated as described above and 30 μg of protein was separated by SDS–PAGE and immunoblotted.

The blue native gel electrophoresis was performed using the NativePAGE™ Novex® Bis-TrisGel System (Invitrogen) according to manufacturer's protocol. The first dimension was separated on a 4–16% gradient NativePAGE Gel. Samples from isolated mitochondria were prepared with the NativePAGE™ Sample Prep Kit following the instructions of the manufacturer. For solubilization, DDM was used in two different final concentrations of 1.2 and 2.5% (w/V) and 50 μg of solubilized mitochondrial protein were separated. For the second dimension, a 4–12% Bis-Tris NuPAGE-Gel was used in the SDS–PAGE.

Imaging

For real-time imaging, cells seeded onto 24-mm round glass coverslips were transfected as indicated and after 48 h loaded with 10 nM TMRM (Molecular Probes) in the presence of 2 mg/ml cyclosporine H (Sigma), a P-glycoprotein inhibitor (30 min at 37°C). Subsequently cells were placed on the stage of an Olympus IX81 inverted microscope equipped with a CellR Imaging system. Sequential images of TMRM fluorescence were acquired every 60 s using exposure times of 30 ms with a 40×, 1.4 NA Plan Apo objective (Olympus), a 525 ± 20 excitation filter and an emission 570 LP filter. Images were stored for subsequent analysis, background subtraction and normalization which was performed exactly as described previously (13).

For confocal imaging of the mitochondrial network, 6×0^4 HeLa cells stably expressing mtRFP were seeded onto 24 mM-round glass coverslips and transfected as indicated. After 24–48 h cells were incubated in Hank's Balanced Salt Solution (HBSS) supplemented with 10 mM HEPES and coverslips were placed on the stage of a Nikon Eclipse TE300 inverted microscope equipped with a spinning-disk Perkin Elmer Ultraview LCI confocal system and a Orca ER 12-bit CCD camera (Hamamatsu). Cells were excited using the 543 nm line of the He-Ne laser (Perkin Elmer) with exposure times of 50 ms using a 60 × 1.4 NA Plan Apo objective (Nikon).

For epifluorescence imaging of the mitochondrial network, 6×0^4 HeLa cells stably expressing mtRFP were seeded onto 24 mM-round glass coverslips and transfected as indicated. After 24–48 h, cells were incubated in HBSS supplemented with 10 mM HEPES and coverslips were placed on the stage of a Olympus IX81 inverted microscope equipped with a CellR imaging system (Olympus). Cells were excited using the 525 ± 20 excitation filter and emitted light was collected using a 570 LP filter with exposure times of 50 ms using a 40 × 1.4 NA Plan Apo objective (Olympus). Where indicated, images were deconvolved using the convolution filter of the program ImageJ (NIH). Morphometric analysis was performed as described previously (23).

Flow cytometry

For evaluation of membrane potential, HeLa cells were grown in 6-well plates, transfected as indicated and after 48 h harvested. Cells were washed with PBS, resuspended in HBSS supplemented with 10 mM HEPES and loaded with 10 nM TMRM (Molecular Probes) in the presence of 2 mg/ml cyclosporine H, a P-glycoprotein inhibitor and 50 mM KCl (30 min at 37°C). Cells were then analyzed by flow cytometry using with a FACSCalibur cytometer (Becton-Dickinson).

For evaluation of apoptosis, 5×10^5 HeLa, $HeLa^{neo}$ or $HeLa^{Bcl2}$ cells were grown in 6-well plates and transfected with siRNA as indicated. After 24–48 h, cells were harvested and stained with PI and Annexin-V-FLUOS (Roche) according to manufacturer's protocol. Viability was measured by flow cytometry as the percentage Annexin-V, PI negative cells.

ACKNOWLEDGEMENTS

We wish to thank PD Dr Anita Rauch (Erlangen) for help with the patient and the fluorescence *in situ* hybridization.

Conflict of Interest statement. None declared.

FUNDING

L.S. is a Senior Telethon Scientist of the Dulbecco-Telethon Institute and this research was supported by Telethon Italy,

AIRC Italy, Compagnia di San Paolo, UMDF. K.S.D. is supported by a Long-Term Fellowship of the Federation of European Biochemical Societies (FEBS).

REFERENCES

1. Bergemann, A.D., Cole, F. and Hirschhorn, K. (2005) The etiology of Wolf–Hirschhorn syndrome. *Trends Genet.*, **21**, 188–195.
2. Zollino, M., Lecce, R., Fischetto, R., Murdolo, M., Faravelli, F., Selicorni, A., Butte, C., Memo, L., Capovilla, G. and Neri, G. (2003) Mapping the Wolf–Hirschhorn syndrome phenotype outside the currently accepted WHS critical region and defining a new critical region, WHSCR-2. *Am. J. Hum. Genet.*, **72**, 590–597.
3. Wright, T.J., Ricke, D.O., Denison, K., Abmayr, S., Cotter, P.D., Hirschhorn, K., Keinanen, M., McDonald-McGinn, D., Somer, M., Spinner, N. *et al.* (1997) A transcript map of the newly defined 165 kb Wolf–Hirschhorn syndrome critical region. *Hum. Mol. Genet.*, **6**, 317–324.
4. Wright, T.J., Costa, J.L., Naranjo, C., Francis-West, P. and Altherr, M.R. (1999) Comparative analysis of a novel gene from the Wolf–Hirschhorn/Pitt-Rogers-Danks syndrome critical region. *Genomics*, **59**, 203–212.
5. Buckle, V.J., Fujita, N., Ryder-Cook, A.S., Derry, J.M.J., Barnard, P.J., Lebo, R.V., Schofield, R., Seeburg, P.H., Bateson, A.N., Darlison, M.G. and Barnard, E.A. (1989) Chromosomal localization of GABAA receptor subunit genes: relationship to human genetic disease. *Neuron*, **3**, 647–654.
6. Endele, S., Fuhry, M., Pak, S.J., Zabel, B.U. and Winterpacht, A. (1999) LETM1, a novel gene encoding a putative EF-hand Ca(2+)-binding protein, flanks the Wolf–Hirschhorn syndrome (WHS) critical region and is deleted in most WHS patients. *Genomics*, **60**, 218–225.
7. Schlickum, S., Moghekar, A., Simpson, J.C., Steglich, C., O'Brien, R.J., Winterpacht, A. and Endele, S.U. (2004) LETM1, a gene deleted in Wolf–Hirschhorn syndrome, encodes an evolutionarily conserved mitochondrial protein. *Genomics*, **83**, 254–261.
8. Jouaville, L.S., Ichas, F., Holmuhamedov, E.L., Camacho, P. and Lechleiter, J.D. (1995) Synchronization of calcium waves by mitochondrial substrates in *Xenopus laevis* oocytes. *Nature*, **377**, 438–441.
9. Wang, X. (2001) The expanding role of mitochondria in apoptosis. *Genes Dev.*, **15**, 2922–2933.
10. Frank, S., Gaume, B., Bergmann-Leitner, E.S., Leitner, W.W., Robert, E.G., Catez, F., Smith, C.L. and Youle, R.J. (2001) The role of dynamin-related protein 1, a mediator of mitochondrial fission, in apoptosis. *Dev. Cell*, **1**, 515–525.
11. Scorrano, L., Ashiya, M., Buttle, K., Weiler, S., Oakes, S.A., Mannella, C.A. and Korsmeyer, S.J. (2002) A Distinct pathway remodels mitochondrial cristae and mobilizes cytochrome c during apoptosis. *Dev. Cell*, **2**, 55–67.
12. Cipolat, S., Rudka, T., Hartmann, D., Costa, V., Serneels, L., Craessaerts, K., Metzger, K., Frezza, C., Annaert, W., D'Adamio, L. *et al.* (2006) Mitochondrial rhomboid parl regulates cytochrome c release during apoptosis via opa1-dependent cristae remodeling. *Cell*, **126**, 163–175.
13. Frezza, C., Cipolat, S., Martins, d.B., Micaroni, M., Beznoussenko, G.V., Rudka, T., Bartoli, D., Polishuck, R.S., Danial, N.N., De Strooper, B. and Scorrano, L. (2006) OPA1 controls apoptotic cristae remodeling independently from mitochondrial fusion. *Cell*, **126**, 177–189.
14. DiMauro, S., Kulikova, R., Tanji, K., Bonilla, E. and Hirano, M. (1999) Mitochondrial genes for generalized epilepsies. *Adv. Neurol.*, **79**, 411–419.
15. Wasterlain, C.G., Niquet, J., Thompson, K.W., Baldwin, R., Liu, H., Sankar, R., Mazarati, A.M., Naylor, D., Katsumori, H., Suchomelova, L. and Shirasaka, Y. (2002) Seizure-induced neuronal death in the immature brain. *Prog. Brain Res.*, **135**, 335–353.
16. Dimmer, K.S., Fritz, S., Fuchs, F., Messerschmitt, M., Weinbach, N., Neupert, W. and Westermann, B. (2002) Genetic basis of mitochondrial function and morphology in *Saccharomyces cerevisiae*. *Mol. Biol. Cell*, **13**, 847–853.
17. Nowikovsky, K., Froschauer, E.M., Zsurka, G., Samaj, J., Reipert, S., Kolisek, M., Wiesenberger, G. and Schweyen, R.J. (2004) The LETM1/YOL027 gene family encodes a factor of the mitochondrial K+ homeostasis with a potential role in the Wolf–Hirschhorn syndrome. *J. Biol. Chem.*, **279**, 30307–30315.
18. Bernardi, P. (1999) Mitochondrial transport of cations: channels, exchangers and permeability transition. *Physiol. Rev.*, **79**, 1127–1155.
19. Frazier, A.E., Taylor, R.D., Mick, D.U., Warscheid, B., Stoepel, N., Meyer, H.E., Ryan, M.T., Guiard, B. and Rehling, P. (2006) Mdm38 interacts with ribosomes and is a component of the mitochondrial protein export machinery. *J. Cell Biol.*, **172**, 553–564.
20. Hasegawa, A. and van der Bliek, A.M. (2007) Inverse correlation between expression of the Wolfs Hirschhorn candidate gene Letm1 and mitochondrial volume in *C. elegans* and in mammalian cells. *Hum. Mol. Genet.*, **16**, 2061–2071.
21. Meier, S., Neupert, W. and Herrmann, J.M. (2005) Proline residues of transmembrane domains determine the sorting of inner membrane proteins in mitochondria. *J. Cell Biol.*, **170**, 881–888.
22. Alirol, E., James, D., Huber, D., Marchetto, A., Vergani, L., Martinou, J.C. and Scorrano, L. (2006) The mitochondrial fission protein hFis1 requires the endoplasmic reticulum gateway to induce apoptosis. *Mol. Biol. Cell*, **17**, 4593–4605.
23. Cipolat, S., de Brito, O.M., Dal Zilio, B. and Scorrano, L. (2004) OPA1 requires mitofusin 1 to promote mitochondrial fusion. *Proc. Natl. Acad. Sci. USA*, **101**, 15927–15932.
24. James, D.I., Parone, P.A., Mattenberger, Y. and Martinou, J.C. (2003) hFis1, a novel component of the mammalian mitochondrial fission machinery. *J. Biol. Chem.*, **278**, 36373–36379.
25. Sesaki, H., Southard, S.M., Yaffe, M.P. and Jensen, R.E. (2003) Mgm1p, a dynamin-related GTPase, is essential for fusion of the mitochondrial outer membrane. *Mol. Biol. Cell*, **14**, 2342–2356.
26. Scorrano, L., Petronilli, V. and Bernardi, P. (1997) On the voltage dependence of the mitochondrial permeability transition pore. A critical appraisal. *J. Biol. Chem.*, **272**, 12295–12299.
27. Kucejova, B., Kucej, M., Petrezselyova, S., Abelovska, L. and Tomaska, L. (2005) A Screen for Nigericin-resistant yeast mutants revealed genes controlling mitochondrial volume and mitochondrial cation homeostasis. *Genetics*, **171**, 517–526.
28. Irwin, W.A., Bergamin, N., Sabatelli, P., Reggiani, C., Megighian, A., Merlini, L., Braghetta, P., Columbaro, M., Volpin, D., Bressan, G.M. *et al.* (2003) Mitochondrial dysfunction and apoptosis in myopathic mice with collagen VI deficiency. *Nat. Genet.*, **35**, 367–371.
29. Danial, N.N. and Korsmeyer, S.J. (2004) Cell death: critical control points. *Cell*, **116**, 205–219.
30. Wong, E.D., Wagner, J.A., Gorsich, S.W., McCaffery, J.M., Shaw, J.M. and Nunnari, J. (2000) The dynamin-related GTPase, Mgm1p, is an intermembrane space protein required for maintenance of fusion competent mitochondria. *J. Cell Biol.*, **151**, 341–352.
31. Frezza, C., Cipolat, S., Martins, d.B., Micaroni, M., Beznoussenko, G.V., Rudka, T., Bartoli, D., Polishuck, R.S., Danial, N.N., De Strooper, B. and Scorrano, L. (2006) OPA1 controls apoptotic cristae remodeling independently from mitochondrial fusion. *Cell*, **126**, 177–189.
32. Dimmer, K.S., Jakobs, S., Vogel, F., Altmann, K. and Westermann, B. (2005) Mdm31 and Mdm32 are inner membrane proteins required for maintenance of mitochondrial shape and stability of mitochondrial DNA nucleoids in yeast. *J. Cell Biol.*, **168**, 103–115.
33. Messerschmitt, M., Jakobs, S., Vogel, F., Fritz, S., Dimmer, K.S., Neupert, W. and Westermann, B. (2003) The inner membrane protein Mdm33 controls mitochondrial morphology in yeast. *J. Cell Biol.*, **160**, 553–564.
34. Scorrano, L. (2005) Proteins that fuse and fragment mitochondria in apoptosis: con-fissing a deadly con-fusion? *J. Bioenerg. Biomembr.*, **37**, 165–170.
35. Dimmer, K.S. and Scorrano, L. (2006) (De)constructing mitochondria: what for? *Physiology (Bethesda)*, **21**, 233–241.
36. Nakashima, R.A., Dordick, R.S. and Garlid, K.D. (1982) On the relative roles of Ca2+ and Mg2+ in regulating the endogenous K+/H+ exchanger of rat liver mitochondria. *J. Biol. Chem.*, **257**, 12540–12545.
37. Martin, W.H., Beavis, A.D. and Garlid, K.D. (1984) Identification of an 82,000-dalton protein responsible for K+/H+ antiport in rat liver mitochondria. *J. Biol. Chem.*, **259**, 2062–2065.
38. Kluck, R.M., Bossy-Wetzel, E., Green, D.R. and Newmeyer, D.D. (1997) The release of cytochrome c from mitochondria: a primary site for Bcl-2 regulation of apoptosis. *Science*, **275**, 1132–1136.

39. Hockenbery, D., Nunez, G., Milliman, C., Schreiber, R.D. and Korsmeyer, S.J. (1990) Bcl-2 is an inner mitochondrial membrane protein that blocks programmed cell death. *Nature*, **348**, 334–336.
40. Donovan, M. and Cotter, T.G. (2004) Control of mitochondrial integrity by Bcl-2 family members and caspase-independent cell death. *Biochim. Biophys. Acta Mol. Cell Res.*, **1644**, 133–147.
41. Pattingre, S., Tassa, A., Qu, X., Garuti, R., Liang, X.H., Mizushima, N., Packer, M., Schneider, M.D. and Levine, B. (2005) Bcl-2 antiapoptotic proteins inhibit beclin 1-dependent autophagy. *Cell*, **122**, 927–939.
42. Kann, O. and Kovacs, R. (2007) Mitochondria and neuronal activity. *Am. J. Physiol. Cell Physiol.*, **292**, C641–C657.
43. Li, Z., Okamoto, K., Hayashi, Y. and Sheng, M. (2004) The importance of dendritic mitochondria in the morphogenesis and plasticity of spines and synapses. *Cell*, **119**, 873–887.
44. Rojo, M., Legros, F., Chateau, D. and Lombes, A. (2002) Membrane topology and mitochondrial targeting of mitofusins, ubiquitous mammalian homologs of the transmembrane GTPase Fzo. *J. Cell Sci.*, **115**, 1663–1674.
45. Petronilli, V., Penzo, D., Scorrano, L., Bernardi, P. and Di Lisa, F. (2001) The mitochondrial permeability transition, release of cytochrome c and cell death. Correlation with the duration of pore openings in situ. *J. Biol. Chem.*, **276**, 12030–12034.
46. Casarin, A., Martella, M., Polli, R., Leonardi, E., Anesi, L. and Murgia, A. (2006) Molecular characterization of large deletions in the von Hippel-Lindau (VHL) gene by quantitative real-time PCR: the hypothesis of an alu-mediated mechanism underlying VHL gene rearrangements. *Mol. Diagn. Ther.*, **10**, 243–249.
47. Milanesi, E., Costantini, P., Gambalunga, A., Colonna, R., Petronilli, V., Cabrelle, A., Semenzato, G., Cesura, A.M., Pinard, E. and Bernardi, P. (2006) The mitochondrial effects of small organic ligands of BCL-2: sensitization of BCL-2-overexpressing cells to apoptosis by a pyrimidine-2,4,6-trione derivative. *J. Biol Chem.*, **281**, 10066–10072.
48. Frezza, C., Cipolat, S. and Scorrano, L. (2007) Organelle isolation: functional mitochondria from mouse liver, muscle and cultured fibroblasts. *Nat. Protoc.*, **2**, 287–295.
49. Sottocasa, G.L., Kuylenstierna, B., Ernster, L. and Bergstrand, A. (1967) An electron-transport system associated with the outer membrane of liver mitochondria. A biochemical and morphological study. *J. Cell Biol.*, **32**, 415–438.

ACNOWLEDGEMENTS

This work is the result of a collaboration between the group in Padova and the groups at Columbia University, New York, Universidad Pablo de Olavide, Sevilla, and at the University of Nice, France.

In particular:

Giuseppe Basso, Leonardo Salviati, Alberto Burlina, Maria Cristina Baldoin, Mara Doimo, Alberto Casarin, Giovanna Casagrande, Vanessa Pertegato, Mauro Natale at the Dept. of Pediatrics, Oncohematology lab.

Geppo Sartori, Caterina Peggion, Elena Casanova, Luca Cesaro, at the Dept. of Biochemistry

Claude Desnuelle, Sabrina Sacconi, Roger Rezzonico, at the University of Nice

Placido Navas,. Juan-Carlos Rodriguez-Aguilera, Carlos Santos-Ocaña, Claudio Asencio, Gloria Brea Calvo, Sergio Sierra at the Centro Andaluz de Biologia del Desarrollo, Universidad Pablo de Olavide Seville

Salvatore DiMauro, Michio Hirano, and Catarina Quinzii, at the Dept. of Neurology

I would like to thank Prof. Basso for giving me the opportunity to work in his laboratory and for trusting in me.

I want to thank my supervisor, Dr Salviati because he has always guided my research with helpfulness and dedication, he has taught me to think in a scientific manner and he has enriched my work with many brilliant ideas.

A very important part of this work is based on the assistance, support and friendship of all the people of my laboratory; particularly I dedicate a special mention to Mara, Cristina, Alberto, Vanessa and Sara.

Finally, I am grateful to Prof. Navas for inviting me to visit his laboratory in Seville, to Prof. Rodriguez-Aguilera and Prof. Santos-Ocaña for their precious suggestions and to all the Spanish colleagues that I had the honor to work with.